

BOEING
STRESS
CORROSION
TESTING
OF HIGH STRENGTH
STEELS

FINAL REPORT

CONTRACT AF 33 616 7839 ASD-TDR 62-876
AERONAUTICAL SYSTEMS DIVISION
AIR FORCE SYSTEMS COMMAND
UNITED STATES AIR FORCE

**BLANK PAGES
IN THIS
DOCUMENT
WERE NOT
FILMED**

AIR FORCE MATERIALS LABORATORY

RESEARCH AND TECHNOLOGY DIVISION
AIR FORCE SYSTEMS COMMAND
UNITED STATES AIR FORCE
WRIGHT-PATTERSON AIR FORCE BASE, OHIO 45433

REPLY TO
ATTN OF

MAAE (Lt R. M. Dunco)

SUBJECT

Request for Report: ASD-TDR 62-876

10 SEP 1964

TO

U. S. Department of Commerce
Office of Technical Services
Attn: Mr. George K. Taylor
Washington 25, D. C.

1. Attached is a copy of subject report that you requested. This report has been published in limited quantities by the Contractor and is presently scheduled for reprinting and distribution in large quantities by the Air Force Materials Laboratory, Research and Technology Division, Air Force Systems Command.
2. Subject report is available as A. D. 603219.
3. In future correspondence with this office, please include your ZIP Code Number to facilitate mail handling.

Robert M. Dunco

ROBERT M. DUNCO, 1st Lt, USAF
Materials Engineering Branch
Materials Applications Div.

1 Atch
Report - ASD-TDR 62-876

AD 603 219

INVESTIGATION OF SUSCEPTIBILITY OF HIGH STRENGTH MARTENSITIC STEEL
ALLOYS TO STRESS CORROSION

TECHNICAL DOCUMENTARY REPORT NO. ASD-TDR-62-876
September 1962

Directorate of Materials and Processes
Aeronautical Systems Division
Air Force Systems Command
Wright-Patterson Air Force Base, Ohio

Project No. 7381, Task No. 738103

(Prepared under Contract No. AF 33(616)-7839 by The Boeing Company,
Transport Division, Renton, Washington; Gary A. Dreyer, Author)

FOREWORD

The program described in this report was conducted by the Metals Group, Materials and Process Unit, Structures Staff, The Boeing Company, Transport Division, Renton, Washington. The work was administered by the Applications Laboratory, Directorate of Materials and Processes, Aeronautical Systems Division. This work was conducted under Project No. 7381, "Materials Application", Task No. 738103, "Data Collection and Correlation." Project Engineer was Lt. W. F. Payne of the Applications Laboratory.

The investigation was initiated in March 1961, and concluded in July 1962. R. A. Davis of the Metals Group directed the technical aspects of the program under the supervision of M. A. Disotell, Supervisor of the Metals Group, F. N. Markey, Chief of the Materials and Process Unit and A. C. Larsen, Staff Engineer - Structures. Test work was carried out by G. A. Dreyer assisted by W. C. Gallagher, S. D. Dahlgren, and R. M. Hammett. All laboratory testing and optical microscope work was done in the Metals Laboratory, Transport Division.

Electron microscopy techniques for fractographic study were developed at the Boeing Scientific Research Laboratories under the guidance of Dr. Regis M. N. Pelloux.

ABSTRACT

The stress corrosion susceptibility of several high strength steels has been evaluated by alternate immersion testing in a 3.5 per cent salt solution. The variables studied were material, grain direction, heat treatment, stress level, surface preparation, protective coatings, and variations from holes and fasteners. The test materials were 4330M, 4340, 4340M, H-11, AM 350, and AM 355 steels. Notch tensile testing and x-ray diffraction measurements of residual surface stresses were also carried out.

PUBLICATION REVIEW

This technical documentary report has been reviewed and is approved

W. P. Conrardy
Chief, Materials Engineering Branch
Applications Laboratory
Directorate of Materials and Processes

TABLE OF CONTENTS

	PAGE
I. Introduction	1
II. Summary	2
III. Procedure	4
A. Specimen Configuration	4
1. Plate and Billet	4
2. Sheet	4
B. Literature Survey	4
C. Test Variables	5
1. Low Alloy Steels	5
2. Stainless Steels	7
D. Test Method	8
E. Fractography	9
IV. Results	10
A. Specimen Configuration	10
1. Plate and Billet	10
2. Sheet	10
B. Literature Survey	11
C. Test Variables	11
1. Low Alloy Steels	11
2. Stainless Steels	17
D. Test Method	18
E. Fractography	18
V. Discussion	19
A. General	19
B. Low Alloy Steels	20
C. Stainless Steels	27

	PAGE
VI. Conclusions	30
VII. Recommendations	32
VIII. References	33
Appendix I - Stress Corrosion Specimen Configuration	150
Appendix II - Round Notched Tensile Specimen Configuration	174
Appendix III - Literature Survey; The Nature of Stress Corrosion Cracking	178

LIST OF TABLES

TABLE		PAGE
I	Chemical Composition of 4330M Steels	34
II	Heat Treatment of 4330M (Billet L) and 4340 (Billet M) Specimens	35
III	Tensile Properties of 4330M (Billet L) and 4340 (Billet M)	36
IV	Chemical Composition of 4340 Steels	37
V	Heat Treatment of 4340 (Billets K and N)	38
VI	Chemically Milling, Electropolishing, Sand Blasting, Shot Peening, and Vapor Blasting Procedures	39
VII	Surface Grinding of Low Alloy Steels	40
VIII	Face Milling of Low Alloy Steels (32 RHR Finish)	41
IX	Face Milling of Low Alloy Steels (125 RHR Finish)	42
X	Chemical Composition of 4340M Steel	43
XI	Chemical Composition of H-11 Steel	44
XII	Heat Treatment of 4340 (Billet N, Martempered)	45
XIII	Heat Treatment of 4340M (Billet P)	46
XIV	Heat Treatment of 4330M (Billet R, Air Melt, Vacuum Melt)	47
XV	Heat Treatment of H-11 (Billet V)	48
XVI	Heat Treatment of H-11 Cubes (Billets U and V)	49
XVII	Cadmium Plating of 4340 Specimens	50
XVIII	Painting of 4340 Specimens	51
XIX	Preparation of Center Holes in 4340 Specimens	52
XX	Chemical Composition of AM 355	53
XXI	Heat Treatment of AM 355 to the SCT 850 Condition	54
XXII	Milling of AM 355 and AM 350	55
XXIII	Chemical Composition of AM 350	56
XXIV	Heat Treatment of AM 350 to the SCT 850, SCT 1050, and DA 850 Conditions (Billet Y)	57

LIST OF TABLES (Cont'd)

TABLE		PAGE
XXV	Testing Times of 4330M Specimens (Billet L)	58
XXVI	Testing Times of 4340 Specimens (Billet M)	59
XXVII	Testing Times of 4340 Shot Peened Specimens (Billet N)	61
XXVIII	Smooth Tensile Properties of 4340 (Billet N, Martempered)	62
XXIX	Notched Tensile Properties of 4340 (Billet N, Martempered)	63
XXX	Smooth Tensile Properties of 4340 (Billet K)	64
XXXI	Notched Tensile Properties of 4340 (Billet K)	65
XXXII	Testing Times of 4340 Specimens (Billet N, Martempered)	66
XXXIII	Testing Times of 4340 Specimens (Billet K)	68
XXXIV	Smooth Tensile Properties of 4340M (Billet P)	70
XXXV	Notched Tensile Properties of 4340M (Billet P)	71
XXXVI	Testing Times of 4340M Specimens (Billet P)	72
XXXVII	Smooth Tensile Properties of H-11 (Billet V)	74
XXXVIII	Notched Tensile Properties of H-11 (Billet V)	75
XXXIX	Testing Times of H-11 Specimens (Billet V)	76
XL	Smooth Tensile Properties of 4330M (Billet R)	78
XLI	Notched Tensile Properties of 4330M (Billet R)	79
XLII	Testing Times of 4330M Specimens (Billet R)	80
XLIII	Testing Times of Cadmium Plated or Painted Center Hole 4340 Specimens (Billet N)	82
XLIV	Smooth Tensile Properties of Air Melt (VNB) and Vacuum Melt (VVB) 4330M	84
XLV	Notched Tensile Properties of Air Melt (VNB) and Vacuum Melt (VVB) 4330M	85
XLVI	Testing Times of Air Melt and Vacuum Melt 4330M Specimens	86
XLVII	Testing Times of AM 355 Specimens	87
XLVIII	Tensile Properties of AM 355	88

LIST OF TABLES (Cont'd)

TABLE		PAGE
XLIX	Smooth Tensile Properties of AM 350 (Billet Y)	89
L	Notched Tensile Properties of AM 350 (Billet Y)	90
LI	Testing Times of AM 350 Specimens (Billet Y)	91
LII	Smooth Tensile Properties of AM 350 (Sheet Z)	92
LIII	Notched Tensile Properties of AM 350 (Sheet Z)	93
LIV	Testing Times of AM 350 Specimens (Sheet Z)	94
LV	Residual Surface Stress Levels in Surface Ground Low Alloy U-Bend Specimens	95
LVI	Average Times to Failure of Low Alloy Steels	96
LVII	Mode of Cracking in Low Alloy Steels	97
LVIII	Strain Gauge and Photostress Readings on Tapered Cantilevered Specimens	159
LIX	Strain Gauge Test Results From U-Bend Stress Corrosion Specimens of M300 Steel	160
LX	Corrosives Which Induce Stress Corrosion Cracking in Certain Metals	197

LIST OF ILLUSTRATIONS

FIGURE		Page
1	Cantilever Bend Specimen	98
2	Phelps-Loginow Specimen	98
3	Boeing U-Bend Specimen-Original Configuration	99
4a	Boeing U-Bend Specimen-Modified Configuration	99
4b	Schematic of Modified Boeing U-Bend Specimen	100
5	Boeing U-Bend Specimen with Center Hole	100
6	Billet Smooth Tensile Specimen (Round)	101
7	Billet Notched Tensile Specimen (Round)	101
8	Sheet Stress Corrosion Specimen	102
9	Sheet Stress Corrosion Test Jig	102
10	Sheet Smooth Tensile Specimen	103
11	Sheet Notched Tensile Specimen	103
12	U-Bend Specimen Locations in 4330M (Billet L) and 4340 (Billet M)	104
13	U-Bend Specimen Locations in 4340 (Billets K and N), 4340M (Billet P), 4330M (Billet R) and AM 350 (Billet Y)	105
14	Tensile Specimen Locations in 4340 (Billet K), 4340M (Billet P), 4330M (Billet R) and AM 350 (Billet Y)	106
15	Tensile Specimen Locations in 4340 (Billet N)	107
16	U-Bend Specimen Locations in H-11 (Billet V)	108
17	Tensile Specimen Locations in H-11 (Billet V)	109
18	U-Bend Specimen Locations in Vacuum Melt (VVB) and Air Melt (VNB) 4330M	110
19	Tensile Specimen Locations in Vacuum Melt and Air Melt 4330M	111
20	U-Bend Specimen Locations in AM 355 Billet	111
21	Stress Corrosion and Tensile Specimen Locations in AM 350 (Sheet Z)	112

LIST OF ILLUSTRATIONS (Cont'd)

FIGURE		PAGE
22	Stress Level as a Function of U-Bend Specimen Leg Deflection	113
23	Ferris Wheel - Alternate Immersion Testing Apparatus	114
24	Chemically Milled Surface	114
25	Electropolished Surface	115
26	Ground Surface	115
27	Face Milled (32 RHR) Surface	115
28	Face Milled (125 RHR) and Sand Blasted Surface	116
29	Face Milled (32 RHR) and Shot Peened Surface	116
30	Range of Failure Times of 4330M (Billet L) U-Bend Specimens After Receiving Various Surface Finishes	117
31	Range of Failure Times of 4340 U-Bend Specimens After Receiving Various Surface Finishes	118
32	Banding in Specimen UB (Billet U, H-11) After 1100°F Temper	119
33	Precipitation in Specimen UB (H-11) After 1100°F Temper	119
34	Precipitation in Specimen UA (H-11) After 1000°F Temper	120
35	Precipitation in Specimen VD (H-11, Billet V) After 1000°F Temper	120
36	Smooth Tensile Properties as a Function of Tempering Time at 1050°F AM 350 SCT 1050 Condition	121
37	Electrolytic Cell Arrangement Used in Hydrogen Embrittlement and Stress Corrosion Crack Shape Studies	122
38	Cracking in 4340M Specimen Anodic in 3% NaCl Solution	123
39	Cracking in 4340M Specimen Cathodic in 3% NaCl Solution	123
40	Cracking in 4340 Specimen Anodic in 3% NaCl Solution	124
41	Cracking in 4340 Specimen Cathodic in 0.125 N Na ₂ S Solution	124
42	Rust on 4340 (Billet M) Test Blocks	125
43	Fractured 4340 (Billet M) Surface Ground Specimens	125

LIST OF ILLUSTRATIONS (Cont'd)

FIGURE		PAGE
44	Fracture Faces of 4340 (Billet M) Surface Ground Specimens	126
45	Fracture Origin Width vs Time to Failure 4340 (Billet M) S	126
46	Range of Failure Times of Martempered 4340 (Billet N)	127
47	Range of Failure Times of 4340 (Billet K)	128
48	Range of Failure Times of 4340M (Billet P)	129
49	Range of Failure Times of H-11 (Billet V)	130
50	Range of Failure Times of 4330M (Billet R)	131
51	Fractured Air Melt (VNB) and Vacuum Melt (VVB) 4330M Specimens	132
52	Fracture Faces of Air Melt and Vacuum Melt 4330M Specimens	132
53	Fracture Origin of 4340 Specimen (Martempered 21N) Which Failed While Stressed but Before Testing	132
54	Electron Micrograph of Fracture Origin of 21N	133
55	Electron Micrograph of Hydrogen Embrittlement Failure	133
56	Electron Micrograph of Stress Corrosion Failure	134
57	Electron Micrograph of Fatigue Failure	134
58	Electron Micrograph of Ductile Fracture Failure	135
59	Electron Micrograph of Quench Crack Fracture Face	135
60	Fracture Faces of 4340 (Billet N Martempered) Specimen	136
61	Fracture Faces of 4340 (Billet K, Oil Quenched) Specimens	136
62	Fractured Painted and Plated 4340 Specimens	136
63	Fracture Faces of Painted and Cadmium Plated Specimens	137
64	Fractured 4340M (Billet P) High Strength Specimens	137
65	Fracture Faces of High Strength 4340M (Billet P) Specimens	137

LIST OF ILLUSTRATIONS (Cont'd)

FIGURE		PAGE
66	Fracture Faces of Low Strength 4340M (Billet P) Specimens	138
67	Fracture Faces of H-11 (Billet V) Specimens	138
68	Fracture Faces of 4330M (Billet R) Specimens	138
69	Cracking on Tension Surface of Failed H-11 (Billet V) Specimen	139
70	Stress Corrosion Cracking in 4340 Heat Treated to 240,000 psi Strength	139
71	Stress Corrosion Cracking in 4340M Heat Treated to 290,000 psi Strength	140
72	Stress Corrosion Cracking in 4330M Heat Treated to 227,000 psi Strength	140
73	Stress Corrosion Cracking in H-11 Heat Treated to 293,000 psi Strength	141
74	Inclusions Surrounded by Corrosion Products	141
75	Crack Originating from Inclusion Pit and Traveling Parallel to Fracture Face	142
76	Microstructure of 4340 (Billet K) Heat Treated to 174,000 psi Strength	142
77	Microstructure of 4330M (Billet R) Heat Treated to 188,000 psi Strength	143
78	Microstructure of H-11 (Billet V) Heat Treated to 235,000 psi Strength	143
79	Fracture Faces of AM 355 SCT 850 Plate Specimens	144
80	Microstructure of AM 355 Plate Near Fracture Origin	145
81	Microstructure of AM 355 Billet Material Heat Treated to the SCT 850 Condition Using Standard Procedure	145
82	Microstructure of AM 355 Billet Material Heat Treated to the SCT 850 Condition Using Modified Procedure	146
83	Fracture Face of AM 350 SCT 850 Specimen	144

LIST OF ILLUSTRATIONS (Cont'd)

FIGURE		PAGE
84	Microstructure of Failed AM 350 SCT 850 Specimen 3Y Near Fracture Origin	146
85	Tensile Fracture Face of AM 350 SCT 850 Specimen	147
86	Tensile Fracture Face of AM 350 SCT 1050 Specimen	147
87	Tensile Fracture Face of AM 350 DA 850 Specimen	148
88	Microstructure of AM 350 CRT 850 .060" Sheet in the Longitudinal Grain Direction	148
89	Microstructure of AM 350 CRT 850 .060" Sheet in the Transverse Grain Direction	149
90	Tapered Cantilevered Specimen	161
91	Variation in Longitudinal and Transverse Tensile Stresses in Tapered Cantilevered Specimen	161
92	Variation in Shear Stresses Through the Thickness of the Tapered Cantilevered Specimen	162
93	Location of Stress Readings on Tapered Cantilever Specimen	162
94	Photograph Under Polarized Light of Stressed Cantilever Specimen with Photostress	163
95	Deflection Variables in a Pin Loaded Column	163
96	Relationship Among P/P_{CR} , H/L and δ/L for Phelps-Loginow Specimen	164
97	Photograph Under Polarized Light of Stressed Phelps-Loginow Specimen	164
98	Photostress Readings from Stressed Phelps-Loginow Specimen	165
99	Simple Beam in Pure Bending	165
100	U-Type Stress Corrosion Specimen Showing Strain Gauge Locations	166
101	Variation in Longitudinal Bending Stress in Boeing U-Bend Specimen	166

LIST OF ILLUSTRATIONS (Cont'd)

FIGURE		PAGE
102	Photograph Under Polarized Light of Stressed Boeing U-Bend Specimen	167
103	Schematic of Modified Boeing U-Bend Assembly	167
104	Strain Gauge Locations on Modified Boeing U-Bend Specimen	168
105	Photostressed Boeing U-Bend Specimens With and Without Center Holes	168
106	Stress Distribution Parallel to the Longitudinal Axis of The U-Bend Specimen	169
107	Stress Distribution Transverse to the Longitudinal Axis of the U-Bend Specimen	170
108	Stress Variation Parallel to the Longitudinal Axis of U-Bend Specimen with Center Hole	171
109	Stress Variation Transverse to Longitudinal Axis of U-Bend Specimen with Center Hole	171
110	Stress Distribution in Stressed U-Bend Specimen with Bolt Through the Center Hole	172
111	Stress Distribution Parallel to Longitudinal Axis of U-Bend Specimen with Bolt Through the Center Hole	172
112	Stress Distribution Transverse to The Longitudinal Axis of U-Bend Specimen with Bolt Through Center Hole	173
113	Variation of Time to Fracture with Applied Stress For 18-8 Stainless Steel	200
114	Specimen Potential Curves for 18-8 Stainless Steel	201

I. INTRODUCTION

At the present time many structural components of both aircraft and missiles are fabricated from high strength low alloy martensitic steels. The service life of most of these components embodies a corrosive environment and possibly surface tensile stresses which may result from processing, installation, or applied loading. This service environment provides an ideal condition for the phenomenon of stress corrosion cracking to occur in unprotected steels. The present investigation was undertaken to elucidate, from the engineering viewpoint, the variables affecting stress corrosion cracking, and to study the metallurgical nature of this phenomenon in four commonly used martensitic low alloy steels and two semi-austenitic stainless steels.

The areas of study on this program were primarily concerned with material and processing variables. Forged block, which is comparable to many of the forgings used in Aero-Space applications, was used to ascertain the effect of grain direction on stress corrosion susceptibility. The method of surface preparation such as milling, grinding, chemical milling, electropolishing, shot peening, and sand blasting was investigated. Residual surface stress measurements were made utilizing an x-ray diffraction technique on each differently prepared surface. The effect of stress level during testing was evaluated.

The steels selected for study were 4330M, 4340, 4340M (300M), H-11, AM 350, AM 355. These materials were heat treated to various strength levels to determine which levels are most susceptible to stress corrosion cracking. The difference between air melted and vacuum melted material was evaluated. The effect of holes and fasteners which simulate aircraft construction was evaluated to ascertain the protection afforded by plated fasteners in unprotected holes.

The corrosive environment consisted of a 3.5 per cent salt (NaCl) water solution. A rotating ferris wheel arrangement immersed stressed specimens in the solution for 8 minutes each hour.

Correlations were attempted between stress corrosion susceptibility and notch sensitivity. Optical metallography and electron microscopy were used to investigate the mode of fracture of failed specimens.

Manuscript released by author August 1962 for publication as an ASD Technical Documentary Report.

II. SUMMARY

The stress corrosion cracking susceptibility of four low alloy steels and two semi-austenitic stainless steels has been evaluated by alternate immersion testing. Test materials were 4330M, 4340, 4340M, H-11, AM 350 and AM 355 billets, AM 350 sheet, and AM 355 plate. Selection of a test specimen for use with the billet and plate material was made on the basis of theoretical and experimental stress analyses. The specimen selected is a constant bending moment beam specimen. Sheet material was evaluated using a modified tensile specimen configuration stressed by axial loading.

The effect of surface preparation method was evaluated with short transverse specimens from 4330M and 4340 billets. The methods studied were electro-polishing, chemical milling, grinding, sand blasting, face milling, and shot peening. Ground specimens from the 4330M and the 4340 billets were used to evaluate grain direction effects. Ground specimens were used to evaluate heat treatment and stress level effects with 4330M, 4340, 4340M and H-11 steels. Specimens from AM 350 billet and AM 355 bar and plate were surface finished by milling with the specimens from AM 350 sheet left in the as-received cold rolled condition. Ground and drilled specimens of 4340 steel were used to evaluate the effect of holes and fasteners which simulate aircraft construction. Holes were drilled in these specimens after either cadmium plating or painting to ascertain the protection afforded by cadmium plated fasteners in unprotected holes. Specimens from two forgings of 4330M steel were used to assess the relative stress corrosion cracking tendencies of air melted and vacuum melted steel.

Supplementary information was obtained by measuring surface residual stresses with a non-destructive x-ray diffraction technique. Fractography and metallography studies were carried out by optical and electron microscopy techniques. Sharply notched tensile specimens were tested for each alloy and strength level to correlate notch sensitivity with stress corrosion cracking susceptibility.

The results of this investigation are as follows:

1. Electropolishing, chemical milling, and grinding provide the most stress corrosion susceptible surface finishes. Face milling, face milling and sand blasting, and face milling and shot peening provide the least stress corrosion susceptible surface finishes. Shot peening increases the compressive surface stresses and decreases the stress corrosion susceptibility of ground surfaces. Milled surfaces are less stress corrosion susceptible than shot peened and ground surfaces with the equivalent surface stresses.
2. The transverse grain directions of billet and bar material are more stress corrosion susceptible than the longitudinal grain direction.
3. Residual surface stresses of all finishing techniques were compressive.

4. Generally with the low alloy steels the stress corrosion susceptibility increases with increasing strength level and increasing test stress level.
5. The least stress corrosion susceptible steel chemistries at the various strength ranges were:

4340M	270,000 - 300,000 psi
4330M	240,000 - 260,000 psi
H-11	220,000 - 240,000 psi

Comparison of these steels, at common stress levels below 180,000 psi, showed H-11 to be the least stress corrosion susceptible.

6. In general AM 350 and AM 355 show less stress corrosion susceptibility than the low alloy steels. AM 355 plate specimens, however, were very stress corrosion susceptible.
7. Specimens from the longitudinal grain direction of a vacuum arc melted 4330M forging were slightly less stress corrosion susceptible than specimens from a similar air melted 4330M forging.
8. Painted specimens from the hole and fastener evaluation of simulated aircraft structure were less stress corrosion susceptible than cadmium plated specimens.
9. Fractographic and metallographic studies show that the low alloy steels fractured intergranularly at the low strength levels and by a combination of intergranular and transgranular cracking at the higher strength levels. Electron microscope fracture face studies indicate stress corrosion and hydrogen embrittlement fractures are similar.

III. PROCEDURE

A. Specimen Configuration

1. Plate and Billet

The evaluation of plate and billet material required a stress corrosion specimen configuration that would facilitate ease of fabrication and utilization. The specimen configuration originally proposed (1)* was a cantilever type, presented at the 1944 ASTM - AIME Conference (2) on stress corrosion and is shown in Figure 1. A second configuration, which had been used by Phelps and Loginow (3), was considered and is shown in Figure 2. These configurations, after experimental and theoretical stress analysis, were found to provide insufficient surface area of uniform stress when the specimen was loaded. A configuration was subsequently designed and utilized for all plate and billet stress corrosion testing. This latter design, known as the Boeing U-bend specimen, originally had the form shown in Figure 3 but was later modified to the principally-used shape shown in Figure 4.

To simulate aircraft structures, .250-inch center holes were drilled in the test section of some of the U-bend specimens. This form, shown in Figure 5, was experimentally stress analyzed both with and without a bolt inserted in the center holes.

Mechanical properties of the billet material were obtained using the smooth and notched tensile specimen configurations shown in Figures 6 and 7. A notch root radius of 0.001-inch was selected in order to evaluate fracture toughness.

2. Sheet

The sheet stress corrosion specimen and stressing jig are shown in Figures 8 and 9. Smooth and notched tensile specimen configurations are illustrated in Figures 10 and 11. The notched tensile configuration is the same as that used in a study of AM 350 sheet (4) under a separate Air Force contract at Michigan State University.

B. Literature Survey

A continued survey of the metallurgical literature was maintained during the tenure of this program. Particular attention was directed towards those publications dealing with the effects of various variables on stress corrosion cracking in steels.

- See References

C. Test Variables

1. Low Alloy Steels

a. Surface Preparation

A primary objective of this program was to determine the significant effects of various surface finishing techniques on stress corrosion cracking susceptibility. To accomplish this objective, U-bend specimens were removed from 433OM and 4340 billets. Specimen locations are shown in Figures 12 and 13. The specimens were heat treated to the 250,000 and 280,000 psi strength levels. Heat treatment, chemical composition and mechanical property data are shown in Tables I through V. Surface finishing was then carried out on heat treated specimens as follows with three specimens being prepared for each different condition:

- chemical milling
- electropolishing
- grinding
- face milling (32 RHR)*
- grinding (32 RHR) and shot peening**
- face milling and shot peening
- face milling and sand blasting

Detail finishing methods are included in Tables VI through IX.

The 433OM specimens were tested at a stress level of 90 per cent of the 0.2 per cent yield strength. This high stress level masked differences in susceptibility among the various finishing methods. For this reason the 4340 specimens were tested at a stress level of 75 per cent of the 0.2 per cent yield strength. With the 4340 specimens, unstressed control blocks were tested for each of the finishing techniques. One control block, with a surface ground finish, was placed in the test solution. The remaining control blocks were tested in the same manner as the corresponding stressed specimens.

Residual stress measurements were made on all specimens utilizing a nondestructive x-ray diffraction technique (5).

b. Grain Direction

After selection of grinding as a standard surface preparation technique, three specimens were removed from the long transverse and three from the longitudinal grain directions of the 433OM and 4340 billets. Specimen locations are shown in Figure 12. The 433OM specimens were stressed to 90 per cent of the 0.2 per cent yield strength to permit comparison with similarly stressed 433OM specimens from the short transverse grain direction. The 4340 specimens were stressed to 75 per cent of the 0.2 per cent yield strength for similar comparative purposes.

* RHR = Roughness Height Reading. All surface roughness measurements were made using a profilometer.
** No 433OM specimens were tested in this condition.

c. Heat Treatment and Test Stress Level

The effect of strength level on stress corrosion cracking susceptibility was determined for 4340, 4340M, 4330M and H-11 steels. All U-bend smooth and notched tensile specimens were removed from the short transverse grain direction of each billet. All specimen locations are shown in Figures 13 through 17.

Chemical compositions of the steels are given in Tables I, IV, X, XI. Detailed heat treatment details are included in Tables V, XIII, XIV and XV. In addition to the standard tempering procedures, specimens of 4340 steel were martempered to strength ranges of 180,000 to 200,000, 220,000 to 240,000 and 260,000 to 280,000 psi (Table XII).

The heat treated U-bend specimens were finished by surface grinding and subsequently retempered at 50°F below the original tempering temperature. The light oxide scale caused by retempering was removed by vapor blasting.

Surface roughness and x-ray back reflection residual surface stress measurements were made.

Test stress levels of 50, 75 and 90 per cent of the yield strength were used for each alloy and strength level.

In addition, a metallographic study of 3" cubes of two H-11 steels was carried out to determine if any precipitation differences could be detected between oil quenching and air quenching. Chemistries and heat treatments of these materials are given in Tables XI and XVI.

d. Holes and Fasteners

The effect of the stress field about a center hole was evaluated using twenty-seven 4340 short transverse U-bend specimens heat treated to 275,000 psi ultimate strength, surface ground, tempered, and vapor blasted. Eighteen specimens were then cadmium plated and nine were painted. After coating the surfaces, .250-inch diameter holes were drilled, reamed, and honed in the center of each specimen (Figure 5). This method of preparing the holes is the same as that used on critical aircraft components.

Heat treating details are given in Table V and cadmium plating, painting, and hole drilling procedures are listed in Tables XVII, XVIII and XIX.

Cadmium plated bolts were placed in the center holes of half the cadmium plated and all the painted specimens. The bolts, washers, and nut combinations used with each specimen are listed below:

Bolt NAS 1104-4W
Washer MS 2002C4
Washer MS 200024
Nut AN 314-4R

The torque on each bolt was 60 inch-lb.

The center holes of the remaining nine cadmium plated U-bend specimens were left empty. All specimens were stressed until the loading at the edge of the bolt hole was 90, 75 or 50 per cent of the 0.2 per cent yield strength. The desired stress level at the hole edge was obtained by multiplying the gross area stress by 2.30, the stress concentration factor.

e. Air Melt versus Vacuum Melt

In order to determine the effect of air melting and vacuum melting on stress corrosion susceptibility, specimens were cut from identical forgings of 4330M representing the two conditions. Because of size limitations it was not possible to remove U-bend specimens from the transverse grain directions of the two forgings. Therefore, the U-bend, smooth tensile, and notched tensile specimens were removed from the longitudinal grain direction and heat treated to the previously determined most susceptible heat treat strength level (225,000 psi). Following heat treatment all specimens were surface ground, retempered, and vapor blasted. Surface roughnesses of all specimens were determined. Residual surface stress measurements were made using the x-ray back reflection technique.

Three U-bend specimens from each group were stressed to 90 per cent of the 0.2 per cent yield strength level (170,000 psi). A 90 per cent stress level was selected since previous data indicated that this was necessary in order to obtain failures within the 1,000 hour test period.

Chemistries of the air melt (VNB) and vacuum melt (VVB) steels are given in Table I, and heat treat procedures in Table XIV. Specimen locations in the forgings are shown in Figures 18 and 19.

2. Stainless Steels

a. AM 355

During the evaluation of the original Boeing U-bend specimen configuration, three specimens of AM 355 were prepared from .313 inch plate. These specimens were heat treated to the SCT 850 condition using standard procedures and milled to final dimensions. All specimens were stressed to 90 per cent of the 0.2 per cent yield strength (160,000 psi) and tested. Since the times to failure were unexpectedly short, U-bend specimens were cut from a billet of AM 355 and heat treated to the SCT 850 condition using both a standard and a modified procedure. These latter specimens were milled (32 RHR) to final dimensions but were only stressed to 75 per cent of the 0.2 per cent yield strength (120,000 psi) prior to testing.

Mechanical properties were determined from small tensile coupons removed from the tested specimens. Surface roughnesses of all specimens were measured. Residual surface stresses were determined using the x-ray back reflection technique.

Chemical compositions of the AM 355 steels are given in Table XX, heat treat and milling procedures are listed in Tables XXI and XXII. Specimen locations in the AM 355 billet are shown in Figure 20.

b. AM 350

The relative stress corrosion susceptibilities of AM 350 in various heat treat conditions was evaluated using both billet and sheet materials.

U-bend and the corresponding smooth and notched tensile specimens were removed from the short transverse grain direction of an AM 350 billet and heat treated to the DA 850, SCT 850 and SCT 1050 condition. Heat treatment to the DA 850 and SCT 850 conditions was accomplished using standard procedures. The tempering times for the SCT 1050 condition were determined from tensile coupons which were tempered from 1/2 to 3 hours. All U-bend specimens were milled to final dimensions.

Transverse stress corrosion and tensile specimens were fabricated from 0.060-inch sheet of AM 350 in the CRT 850 condition. The surfaces of the stress corrosion sheet specimens were left in the as-received condition.

The surface roughness of all AM 350 stress corrosion specimens was determined. X-ray residual stress measurements were made on selected specimens.

All billet and sheet stress corrosion specimens were stressed to 90, 75 or 50 per cent of the 0.2 per cent yield strength.

Chemical composition of the AM 350 billet and sheet is given in Table XXIII. Heat treatments of the billet specimens are shown in Table XXIV. Surface milling was done according to the procedure shown in Table XXII. Original locations of the specimens in the billet and sheet are shown in Figures 13, 14 and 21.

D. Test Method

The stress level in the U-bend specimens was controlled by the amount of bending. This is illustrated in Figures 3 and 4. The amount of loading in all U-bend specimens, except those having a center hole, was determined using strain gauges attached to the tension surface. The applied stress level in those specimens having a center hole was estimated by measuring the amount of leg deflection since strain gauges could not be placed on the cadmium plate or paint. Figure 22 shows a plot of leg deflection versus stress level.

Sheet stress corrosion specimens were stressed by applying an axial tension load. The loading jig is shown in Figure 9. The stress level in all sheet specimens was attained using strain gauges.

When a constant applied stress level had been obtained (24 to 48 hours after loading) in the loaded stress corrosion specimens, the strain gauges were removed using acetone as the solvent. The possibility of hydrogen charging the specimens by the acetone was checked using a hydrogen detection gauge (6). No free hydrogen ions were detected in the acetone used for strain gauge removal.

All surfaces, except for the test areas, of the blocks used in the surface finish evaluation were coated with red glyptal.* Each stressed U-bend specimen, except for those removed from the AM 355 plate, was coated with red glyptal enamel, leaving a 2" x 1" center test section. The AM 355 plate specimens were protected with clear glyptal lacquer cement. The AM 350 sheet stress corrosion specimens were coated, after stressing the desired amount and removing the strain gauges, with red glyptal except for a 2" x .3" center section test area.

The stress corrosion test apparatus consisted of a ferris wheel 4' in diameter and 1.5' wide, a tank to contain the test solution, driving motor, and clamps or fasteners to attach the specimens to the ferris wheel. The ferris wheel and tank arrangement are shown in Figure 23. Stressed specimens were attached to steel slats along the rim of the ferris wheel and alternately immersed for 8 minutes per hour in the 3.5 per cent NaCl solution in the tank at the ferris wheel base. The salt solution was changed every 3 to 5 days.

All stress corrosion specimens were left on the ferris wheel until failure occurred or until 1,000 hours had transpired. This 1,000 hour test period was selected on the basis of preliminary data which indicated that the majority of failures would occur within that time. A specimen was considered to have failed when complete fracture had occurred or the fractured test sections were held together by only a small section of metal. Actual growth of cracks was not observed on any specimens.

E. Fractography

The advent of an electron microscope technique for studying fracture faces at high magnifications prompted continued study in this area with the present work. In order to set up standards for comparative purposes, two stage fax film carbon replicas were made from fracture faces of several steel specimens broken under known conditions. The conditions studied were fatigue, tensile, hydrogen embrittlement and quench cracks in 4340 and 4330M steel specimens heat treated to various high strength levels.

Replicas were made from the fracture faces of appropriate stress corrosion specimens to compare this mode of cracking to that of the standards.

* General Electric Lacquer Cement

IV. RESULTS

A. Specimen Configuration

1. Plate and Billet

Theoretical and experimental stress analyses of the plate and billet stress corrosion specimen configurations are included in Appendix I.

The analysis of the tapered cantilevered specimen showed that only along the specimen center line are there constant longitudinal bending stresses. As the specimen edges are approached the longitudinal stresses become distorted because of the taper of the specimen. High biaxial stresses are generated in the transverse direction because of the high width to thickness ratio of the specimen. These biaxial stresses vary since the width to thickness ratio varies along the length of the specimen.

The main drawback to the Phelps-Loginow specimen is the lack of a large area having a constant stress. The stresses were found to vary from the midpoint of a stressed specimen along both the longitudinal and transverse axis. When values were selected from the Phelps-Loginow report to obtain a level just below the yield point, the specimen was found to be yielded after completing the experimental stress analysis.

When the Boeing U-bend configuration is utilized, essentially only unidirectional stresses were generated along the longitudinal axis. This area of unidirectional stresses extends to within 1.50 inches of the ends of the specimen. Only unidirectional stresses are produced since the width to thickness ratio of less than 5 causes the specimen to behave strictly as a beam and not as a plate.

The maximum stresses in a loaded U-bend specimen at the edges of a 0.250 inch center hole are approximately 2.30 times the gross area stress. The maximum stress in a loaded U-bend specimen with a bolt and washer installed is at the edge of the washer and is approximately 1.40 times the gross area stress. At the same location in a specimen with no bolt installed the stress was approximately 1.15 times the gross area stress.

The mechanical properties are given in tabular form and are referenced throughout the body of the report. The round circumferentially notched tensile specimens did not provide suitable fracture toughness information. A detailed discussion of specimen geometry limitations is presented in Appendix II.

2. Sheet

The sheet stress corrosion specimen did provide a large center section area of uniform stress. After the specimen was loaded no relaxation occurred after the initial 24 to 48 hour period following stressing.

Mechanical properties of the AM 350 sheet material are discussed in the section under stainless steels.

B. Literature Survey

A comprehensive literature survey is contained in Appendix III.

C. Test Variables

1. Low Alloy Steels

a. Surface preparation

Testing times of alternate immersion testing in the 3.5 per cent salt solution are shown in Tables XXV through XXVII for the 4330M and 4340 steels. The characteristically large scatter of stress corrosion test results is evident.

Although the 90 per cent stress level used with the 4330M specimens has masked differences among the various finishing techniques, one significant fact is evident. Shot peening decreases the stress corrosion susceptibility.

Though the stress level of 90 per cent of the yield strength was too severe to suitably evaluate the relative susceptibilities of the various surface finishing techniques using 4330M, the stress level of 75 per cent of the yield strength was successfully used with the 4340 specimens.

The surface conditions resulting from the various surface preparation procedures are shown in Figures 24 through 29. Electropolishing, chemical milling, and grinding produced those surfaces most susceptible to stress corrosion failure. Face milling, shot peening, and sand blasting provided surfaces with less stress corrosion susceptibility.

Untempered martensite was formed on those surfaces which had been face milled. The amount and distribution of untempered martensite on these surfaces depended on the particular milling procedures used. Face milling to a nominal surface roughness of 32 RHR caused the formation of a uniform layer over the entire surface, whereas face milling to a surface roughness of 125 RHR caused untempered martensite formation only at the tips of the cutter ridges.

A general observation regarding the relative stress corrosion susceptibilities of the various surface finishing procedures is evident. Those surface finishing techniques which remove a surface layer but do not deform the surface, such as electropolishing and chemical milling provide the most stress corrosion susceptible finishes. Ground surfaces, which have nicks and gouges produced during machining, are nearly as susceptible as those surfaces produced by electropolishing or chemical milling. Surface finishing procedures which flow or compressively deform the surface metal, such as face milling and shot peening decrease the stress corrosion susceptibility.

The relative stress corrosion susceptibilities of the various surface finishes evaluated in this program are, with the most susceptible first;

- electropolishing, chemical milling
- grinding
- grinding and shot peening
- face milling (32 RHR), face milling (125 RHR) and sand blasting, face milling (32 RHR) and shot peening

A graphical depiction of the 4330M and 4340 data is given in Figures 30 and 31.

Comparison of the surfaces of the control blocks and U-bend specimens having similar surface finishes showed that stress has no effect on the type of rust formation.

The fracture origins of the 4330M specimen tested during the surface finish evaluation were perpendicular to the tension surfaces, but the remainder of the fracture faces were extremely rough and had no particular geometrical relationship with those tension surfaces. The 4340 fracture faces, including origins, were perpendicular to the tension surfaces. A correlation could be made between the size of the fracture origins of the electropolished, chemical milled, and ground 4340 specimens and the time to failure. This correlation could not be made from the 4340 specimens that had been face milled, face milled and sand blasted, and face milled and shot peened.

b. Grain Direction

Results of 4330M and 4340 long transverse and longitudinal testing are tabulated in Tables XXV through XXVI. With the 4330M steel at a test stress level of 90 per cent of the yield strength the long transverse specimens had a slightly lower stress corrosion susceptibility than short transverse specimens. Longitudinal specimens, however, show a dramatic improvement in cracking resistance of ten fold over the short transverse specimens. With the 4340 material, stressed to 75 per cent of the yield strength, the longitudinal grain direction showed considerably more resistance to cracking than either of the transverse directions. No significant difference was observed between short transverse and long transverse specimen failure times.

c. Heat Treatment and Test Stress Level

The prior billet location of the tensile coupons in the billets of 4340, 4340M and 4330M had no effect on the mechanical properties. However, the yield strengths of the H-11 specimens were very dependent upon prior billet locations. At the higher tempering temperatures this dependence on the H-11 yield strengths disappeared. Reduction-in-area values indicate that H-11 is quite brittle when tempered at 800°F, which is below the secondary hardness peak.

It was not possible to determine suitable fracture toughness values of the various heats of the low alloy steels because of net section yielding that occurred in the notched specimens. However, the ratio of the notched to unnotched ultimate strength did provide a good

indication of the susceptibilities of the 4340, 4340M and H-11 specimens to stress corrosion failure. Generally, when considering a particular steel, the lower this ratio for a given heat treat strength the earlier the failure. The only instance where this did not strictly hold was when comparing 4330M heat treated to 227,000 and 250,000 psi strengths.

The fracture faces of the 4340, H-11 and lower strength 4340M specimens were perpendicular to the tension faces. Though the fracture origins of the 4330M and high strength 4340M specimens were perpendicular to the tension surfaces the remainder of the fracture faces were extremely rough and had large fracture lips. The majority of fractures originated at the corners of the stress corrosion specimens.

All the origins on the fracture faces of the specimens that failed during testing were outlined by rust rings. There was no rust present on those 4340 specimens which failed while stressed but before testing. These latter specimens are discussed in the following subsection. No correlation could be made between the size of the fracture origin, as outlined by the rust ring, and the time to failure.

The mode of fracture in the highest strength levels was a combination of intergranular plus transgranular cracking. The cracking in the lower strength specimens was solely intergranular.

(1) 4340

The smooth and notched tensile properties of the martempered and oil quenched 4340 specimens are given in Tables XXVIII, XXIX, XXX and XXXI.

Five specimens, four martempered and one oil quenched, failed while stressed but before testing. The martempered specimens had been heat treated to a strength of 269,000 psi while the oil quenched specimen had a heat treat strength of 240,000 psi. Three of the martempered specimens and the oil quenched specimen had been stressed to 90 per cent of the 0.2 per cent yield strengths, (200,000 and 190,000 psi respectively). The remaining martempered specimen was stressed to 75 per cent of yield (170,000 psi). Hydrogen embrittlement was suspected as the cause of failure of these specimens.

The martempered specimens, from the 269,000 and 244,000 psi strength levels, that had been stressed to 90 and 75 per cent of the 0.2 per cent yield strengths failed shortly after testing was initiated. An average time to failure could not be estimated for those specimens stressed to the 90 per cent level because of the many pretest failures and the widely diverging test times to failure. An approximate time to failure of the specimens stressed to the 75 per cent level ranged from 126 minutes for the 269,000 psi strength specimens to 250 minutes for the 244,000 psi strength specimens. Though all the high strength

martempered specimens failed during testing an approximate time to failure of those specimens stressed to the 50 per cent level was not estimated because of the extremely wide variance in fracture periods.

The oil quenched specimens from the 275,000 and 240,000 psi strength levels failed in an average time of 200 minutes after being stressed to 90 per cent of the yield strengths. Failure times of both steels increased to 500 minutes when stressed to the 75 per cent level. All specimens, from these two strength levels, that had been stressed to the 50 per cent level did not fail during testing so an average failure time could not be determined.

Only one specimen from the lower strength martempered and oil quenched groups failed during testing.

The failure times of the martempered and oil quenched 4340 specimens are given in Tables XXXII and XXXIII.

(2) 4340M

All the specimens from the four heat treat levels (297,000, 290,000, 250,000, 224,000 psi) failed during test when stressed to 90 and 75 per cent of the 0.2 per cent yield strengths. The average times to failure varied from temper to temper with specimens heat treated to 297,000 and 250,000 psi strengths and stressed to the same percentage of the yield strength failing before comparable specimens from the other two heat treat groups. Only one U-bend specimen failed in test after being stressed to 50 per cent of the 0.2 per cent yield strength.

Tensile properties are given in Tables XXXIV and XXXV.

Testing times of all 4340M specimens are given in Table XXXVI.

(3) H-11

(a) Effect of Tempering Temperature

Triple tempering at 600°F, 800°F and 1000°F for the same time period produced ultimate tensile strengths that were between 290,000 and 310,000 psi. Tempering at 1100°F provided a strength of 235,000 psi.

Specimens tempered at 600°F and 800°F were the most stress corrosion susceptible. The average failure times of specimens which had been stressed to 90 per cent of the 0.2 per cent yield strength were 174 and 126 minutes respectively. Those specimens which had been tempered at

1000°F and stressed to the 90 per cent level failed in an average time of 800 minutes. All the 600°, 800° and 1000°F tempered U-bend specimens failed, at all stress levels, the majority long before the 1,000 hour test period had elapsed. Only one of the lower strength U-bend specimens (1100°F temper) failed during alternate immersion testing.

Tensile properties are given in Tables XXXVII and XXXVIII.

Testing times of all H-11 U-bend specimens are given in Table XXXIX.

(b) Air cooling versus Oil Quenching

No metallographic difference was noted between steel cubes, from the same billet, which had been oil quenched or air cooled or between sections removed from the edge and center of the same 3-inch cube.

However, examination showed that a large amount of banding (Figure 32) can be present in conventionally heat treated H-11 steel. This banding, which was observable only in the longitudinal grain direction, was composed of light and dark etching areas. Within the bands there appeared to be a great deal of precipitation along apparent austenite grain boundaries. The amount of banding and apparent grain boundary precipitation depended on the tempering temperature and also the particular billet of H-11 steel (Figures 33, 34 and 35).

Specimens (1" cubes) from two billets, representing the billet edges and center were austenitized at 1850°, 1875° and 1900°F for one hour, and triple tempered at 1000°F for 4 + 4 + 4 hours. The amount of banding and apparent grain boundary precipitation decreased with increasing austenitizing temperature and was not visible in the 1900°F specimens.

(4) 4330M

The most stress corrosion susceptible U-bend specimens were those heat treated to the 227,000 psi strength range. Failures in this group were limited to specimens which had been stressed to 90 and 75 per cent of the 0.2 per cent yield strength.

The specimens from the 202,000 psi group which had been stressed to 90 per cent of the yield strength had average failure times that were twice the 227,000 psi group.

Fractures in the 250,000 psi group (highest strength level) occurred outside the 2" x 1" test area. However, these specimens, which were stressed to the 90 per cent level, did not fail until after a test period nearly twice that of the comparable 227,000 psi specimens.

There were no failures in the 188,000 psi group.

Tensile results are given in Tables XL and XLI.

Testing times of the 4330M billet specimens are given in Table XLII.

d. Holes and Fasteners

Failure of the cadmium plated specimens with and without center hole bolts began after 84 and 90 hours of testing. Ten of these specimens, five from each group, failed during the 1,000 hour test period. Six of the ten failures originated at the center hole or the edge of the center bolt washers. Two failures originated at the specimen corners. The remaining two failures, both in specimens with center bolts, occurred outside the test area. Of the eight fractures that occurred in the test area, three did not pass through the center hole. The fracture origins on four of the eight fracture faces were not outlined by rust rings, as was common on previous fracture faces. Hydrogen embrittlement was suspected as contributing to the cause of failure of the latter four specimens.

Only two painted specimens failed, of which one fractured outside the test area. The other failure (after 210 hours of testing) originated at the interface between the center bolt washer and enamel coating. This latter fracture passed through the center hole.

All failures occurred in cadmium plated or painted specimens which had been stressed to either 90 or 75 per cent of the 0.2 per cent yield strength. No failures occurred at the 50 per cent stress level.

No separation could be made between the relative susceptibilities of the two groups of cadmium plated specimens. However, the cadmium plated specimens were more prone to failure than those that had been painted.

Testing times of the cadmium plated or painted specimens is given in Table XLIII.

e. Air Melt versus Vacuum Melt

Longitudinal testing indicated that vacuum melted 4330M material was slightly more resistant to cracking. Air melted specimens all failed between 480 and 655 hours of testing; vacuum melted, between 625 and 840 hours of testing. Microstructural studies showed that both air melted and vacuum melted specimens fractured by a combination of intergranular and transgranular cracking.

Detail testing and mechanical property data are included in Tables XLIV, XLV and XLVI

2. Stainless Steels

a. AM 355

The three U-bend specimens which were prepared (SCT 850 condition) from the .313-inch plate failed between 7.5 and 48 hours. The fracture origins were located at the corner of the tension surfaces. All three fracture faces made an approximate 45° angle with the tension surfaces. Cracking was intergranular.

Small smooth tensile specimens removed from the legs of AM 355 plate specimen 3 showed that though the ultimate and yield values were satisfactory, the reduction in area values were quite low for the longitudinal grain direction.

The second set of AM 355 U-bend specimens cut from a 6" x 6" x 8" billet and heat treated using both modified and standard procedures to the SCT 850 condition successfully passed the 1,000 hour evaluation. No failures occurred within 1500 hours of additional testing. Tensile specimens cut from these U-bend specimens had much higher reduction in area values than those manufactured from plate.

Testing times and tensile properties of the AM 355 specimens are given in Tables XLVII and XLVIII.

b. AM 350

The tempering time of 1/2 hour at 1050°F was selected for all U-bend specimens in the SCT 1050 condition. This tempering time provided an ultimate strength in the 160,000 to 180,000 psi strength range (Figure 36).

There was little variation in ultimate and yield strengths across the billet but reduction in area values were very dependent on prior billet position. Those specimens removed from near the billet edges had much higher reduction in area values than those from the billet center. Smooth and notched tensile data is given in Tables XLIX and L.

One U-bend specimen, in the SCT 850 condition, failed after being tested for 310 hours. None of the remaining AM 350 billet specimens failed (Table LI).

Smooth and notched tensile properties across the AM 350 CRT 850 sheet are given in Tables LII and LIII. There were no failures in any of the sheet specimens stressed to 90, 75 or 50 per cent of the 0.2 per cent yield strength (Table LIV).

D. Test Method

The stress level in loaded stress corrosion specimens was checked over a period of one month. A constant stress level was obtained in all specimens 24 to 48 hours after initially loading. An additional check was made on U-bend specimens which had not failed during testing. In all cases, the amount of leg deflection was the same just prior to testing and after test completion.

The method of testing with the alternate immersion Ferris Wheel arrangement was suitable for evaluating the variables in this program. Stressing of specimens was easily carried out. Delineating the test area with glyptal provided no galvanic acceleration of corrosive attack as evidenced by the random nature of cracking within the test sections. Examination of specimens for cracking was readily carried out.

E. Fractography

Electron microscopic examination of fracture face replicas showed that characteristic differences could be detected between various fracture modes. Fine dimples characteristic of a local shearing fracture were evident with the tensile mode of separation. Fatigue fractures were typified by very flat surfaces and repetitive striations. Hydrogen embrittlement and quench cracks were intergranular with respect to the prior austenite grain boundaries.

Replicas made from stress corrosion specimen fractures showed intergranular cracking to be predominant with the low alloy steels. Stainless steel fracture faces were too irregular for suitable replicas to be made.

There is a marked similarity among stress corrosion, hydrogen embrittlement, and quench cracking modes. All show the block-type intergranular structure on the fracture faces. These blocks were approximately the same size as the prior austenitic grains. With the stress corrosion fracture surfaces, however, there is some evidence of very localized pitting. A lacy network was found on several of the grain faces of the stress corrosion fractures.

V. DISCUSSION

A. General

One of the most complicating factors involved in the study of stress corrosion fracture in steel is a precise identification of the problem. What stress corrosion is and how it can be separated from hydrogen embrittlement has been the main subject of numerous investigations. An idea of the scope of many of the more recent experiments in this area can be gained from the literature survey in Appendix III.

One suggested way of separating the phenomena of stress corrosion and hydrogen embrittlement in steel is the use of metallography for crack shape studies. This approach has been used with some success at The Boeing Company.

Specimens of 4340M and 4340 steels .020" x 1" x 2.50" were stressed in a phenolic jig of the Phelps-Loginow configuration (Figure 2) and made either the cathode or anode in a 3 per cent NaCl solution. A schematic diagram of the circuit is shown in Figure 37. When the specimen was made the anode chlorine ions would be attracted and any cracking would be due to stress corrosion. When the polarity was reversed hydrogen embrittlement would cause the specimen failure.

Examples of the two types of cracking produced in a 3 per cent NaCl solution (6 ma/in² current density) are shown in Figures 38 and 39. When cracking takes the forms shown in these pictures identification of the reason for fracture is quite easy. Here the stress corrosion cracking in 4340M is shown to be typified by wide cracks in which the sides do not match and the crack tips are rounded. The hydrogen embrittlement cracks are narrow, with matching sides and sharp tips.

However, when the metals and solutions were changed, the types of fractures were more difficult to separate on the basis of crack shape. For example, specimens of 4340 in 3 per cent NaCl and 0.125N Na₂S produced similar types of cracks when made the anode (Figure 40) and the cathode (Figure 41) in a direct current circuit. These latter pictures illustrate that there are cracks which do not have an appearance definitely characteristic of solely stress corrosion or hydrogen embrittlement cracking.

Since there was some question as to the means of identifying hydrogen embrittlement and stress corrosion failures the following criteria was adopted during the investigation of the 4330M, 4340M, 4340, H-11, AM 350 and AM 355 steels. The (U-bend specimen) fracture origins which were outlined by rust areas were assumed to have been caused by stress corrosion. In those instances where there was no rust outlining the fracture origins hydrogen embrittlement was suspected as a cause of failure. This is discussed in more detail in the following section.

B. Low Alloy Steels

The method of surface finishing does have a very noticeable effect on the stress corrosion susceptibility of a particular steel. The use of such methods of surface preparation as face milling and shot peening may provide a compressive stress field which extends to a greater depth below the surface than the stress field produced by surface grinding. This greater depth of surface compressive stresses due to face milling and shot peening would in turn increase the resistance to crack formation during testing. Of these two methods of causing high surface compressive stresses, face milling provides the greatest protection, indicating a greater depth of surface deformation than that produced by shot peening. Face milling decreased the stress corrosion susceptibility by a factor greater than 10 (as compared to a ground surface) while the decrease due to shot peening was about 2 (Tables XXVI and XXVII, Figures 30 and 31).

The formation of untempered martensite on the surface during face milling apparently is not as detrimental as when this microconstituent is present in drilled holes. This could be due to differences in geometry - where the stress center caused by the hole greatly accentuates any notch effect due to the cracking of untempered martensite. When a uniformly stressed specimen, such as the Boeing U-bend configuration, is utilized, there is no stress center created by specimen design and the only surface irregularities that would be present are the face milled ridges, inclusions, and cracked untempered martensite.

Sand blasting does increase the compressive stresses but the magnitude of stress corrosion protection provided by this method is not precisely known. Grinding did cause the formation of compressive stresses on the surface but this was largely offset by either a possibly shallower depth of deformation (as compared to face milling), or by the small parallel ridges or nicks (Figure 26) formed during surface preparation which acted as small stress raisers and traps for corrosive solution.

Electropolishing or chemically milling did not mechanically deform the surface. What resistance the material had to stress corrosion cracking was inherent in the metal except for what changes introduced by possible hydrogen charging during surface preparation.

The rust that formed on the 4340 blocks on the ferris wheel was the same as that on the comparable U-bend specimens. The stress level or type of surface finish did not affect the amount or type of rust. Only the amount of time of alternate immersion determined the quantity of red rust formation (Table XXVI). A thick black rust covered the exposed surface of the block (32 RHR ground finish) which had been left lying in the 3.5 per cent NaCl solution for 1,000 hours without alternate immersing (Figure 42).

The fracture faces of all failed 4340 U-bend specimens were perpendicular to the tension surface (Figure 43). In some instances there was the appearance of a thin lip of metal along the junction formed by the tension surface and fracture faces. Immediately after failure the fracture origins were clearly outlined as shown in Figure 44. However, if the failed specimens were not removed from the ferris wheel before passing through the NaCl solution the recently exposed fracture face was corroded and the sharp outline of the origin was obliterated.

The size of the fracture origin increased with increase in time to failure of the ground, electropolished, and chemical milled surfaces (Figure 45). No correlation could be made between size of the fracture origins and the time to failure of the face milled, face milled and shot peened, and face milled and sand blasted specimens. This was due to the obliteration of the origins by the corrosive media during the long period before final failure and the formation of cracks in the tension surface which were parallel to the fracture face. These parallel cracks also contained origins so that even though the specimen fractured in only one place the effect of the parallel cracks in changing the effective cross sectional area and thereby the effective stress cannot be ignored. This parallel cracking was not noted on the surface ground, electropolished, and chemically milled surfaces of the 4340 (Billet M) specimens.

A direct correlation could not be made between the surface roughness or compressive stresses and time to failure. However, when comparing specimens which had been surface finished using the same procedure (i.e., grinding, face milling, etc.), the apparent trend was a longer time to failure the rougher the surface and higher the compressive surface stresses.

Though chemical milling and electropolishing produced the most stress corrosion sensitive surfaces of the six surface finishing procedures tested, there was some question as to the amount of hydrogen absorption that occurred during surface preparation.

Grinding was selected as the final finishing procedure because this method is commonly used in industry and produced a sensitive stress corrosion surface without the hydrogen absorption problem of electropolishing and chemically milling.

After the final temper, the magnitude of the compressive residual surface stresses in the surface ground 4330M, 4340, 4340M, and H-11 U-bend specimens ranged between 20,000 to 80,000 psi. Vapor blasting increased these compressive stresses to between 70,000 and 170,000 psi (Table LV). The surface roughness of the U-bend specimens was the same before and after vapor blasting. Microstructural examination could reveal no difference (other than the oxide layer) between surfaces representing the before vapor blasting and after vapor blasting conditions.

The resultant surface stresses after stressing a U-bend specimen could not be determined by adding the residual surface stresses in the unstressed condition to the applied tensile stress. For example, when a specimen of 4340M steel, which had a residual compressive stress of 80,000 psi, was stressed to 170,000 psi tension as measured by a strain gauge the resultant stress as measured by x-ray diffraction was not 90,000 psi tension but rather 20,000 psi compression. Even when the limiting accuracy ($\pm 20,000$ psi) of the x-ray residual stress measurements are taken into consideration there is still a minimum gap between the two values of 70,000 psi. This disparity, which was also noted on other specimens, has not been satisfactorily explained. One possible reason for the disagreement may be that some portions of the surfaces, such as peaks or asperities (which deflect the x-ray beam), may not be stressed as much as the remainder of the surface.

The erratic nature of the H-11 tensile data could be explained by incomplete homogenization during austenitizing. This was illustrated by the microstructures of the H-11 steel cubes which were austenitized at gradually increasing temperatures until the banding and apparent grain boundary precipitation disappeared. This indicates that either the austenitizing temperature or time has to be increased in order to obtain complete homogenization.

It had been hoped that some type of relationship could be determined that would relate the tear resistance (using the stress intensity parameter, K_{Ic}) and the time to stress corrosion fractures. However, the ultimate strengths of the notched specimens (nominal .001" root radius) in many instances exceeded the yield strengths (net section yielding) of the corresponding smooth tensile specimens. When this was the case, it was only possible to calculate a K_{Ic} value for which the material was known to exceed. The K_{Ic} values were calculated using the smooth tensile yield strengths rather than the notched ultimate strengths for the parameter σ_m .

This K_{Ic} data which was calculated using the notched ultimate strengths was very limited and very little can be said concerning the relative tear resistant properties. Comparison of the applicable 4340 (Billet K, Tables XXXI and XXXII) and H-11 (Billet V, Tables XXXVIII and XXXIX) data indicates that there is an increase in the resistance to stress corrosion failure with increasing K_{Ic} values.

A round notched tensile configuration was designed that theoretically would provide accurate quantitative data on the tear resistance (Appendix II). However, the time limitations of the program did not permit the manufacture and testing of any specimens of this configuration.

An indication of the stress corrosion susceptibility is given by the ratio of the notched to smooth ultimate strengths. A notched to smooth ratio of less than 1.0 indicated that the material (low alloy steel) would fail in less than 100 hours when stressed to 90 per cent of the 0.2 per cent yield strength. This relationship held true, with extended failure times, for those specimens stressed to 75 per cent of the yield strengths. The ratio was not as selective of the specimens that failed after being stressed to the lowest (50 per cent yield strength) level.

There was a significant difference in the times to failure between the 4340 specimens which were martempered and those oil quenched. Comparison of the two methods indicates that martempering and tempering to a given strength range results in a lower notched to smooth ratio and a decreased time to failure. (Figures 46 and 47).

The failures of the 4340M specimens were easily predictable on the basis of the notched to unnotched ratio. This steel (from the only vacuum melt billet in the program) showed the best correlation of all the low alloy steels, between this ratio and the times to failure. This agreement between the various heat treat strengths of the 4340M specimens and the ratio is illustrated in Figure 48.

There also may be a tie between time to failure and impact properties since tempering at 400° and 800°F produces the 4340M structures least resistant to impact (7). U-bend specimens tempered at these temperatures were the first to fail.

Though the H-11 smooth and notched tensile data was somewhat erratic, the ratios that were determined (Table XXXVIII) show the same correlation (between this ratio and time to failure) that was indicated by the other steels (Figure 49). While tempering H-11 at 600°, 800° or 1000°F does place this material in the same heat treat strength range (290,000 - 310,000 psi) the material tempered at 1000°F had the greatest resistance to stress corrosion fracture. This increase in resistance may be due to the formation of alloy carbides during tempering to the secondary hardness peak or to the decrease in the amount of retained austenite. The amount of retained austenite has been reported as high as 3 per cent immediately after quenching from the austenitizing temperature. This retained austenite did not disappear until after being tempered at 1000°F (8).

The only instance where the notched to unnotched ratio could not be directly correlated with the time to failure occurred when testing specimens from the 4330M billet which had been heat treated to 227,000 and 250,000 psi strengths (600° and 400°F tempers). Though the ratios of the two groups were nearly the same (1.12 to 1.09) those specimens at the 227,000 psi strength level failed in less than one-half the time required for failure of the specimens heat treated to 250,000 psi.

Even though the notched to smooth ratios of the two 4330M billet heat treat strengths were nearly the same there has been reported a noticeable difference in the impact properties (9). Those specimens which were tempered at 600°F and had the lowest impact values were the first to fail.

The sensitivity or the ability of the notched to unnotched ratio to predict the susceptibility to stress corrosion was dependent on the material under study. Only in a roughly quantitative way could the ratios of one steel be compared to another. Generally speaking, the lower this ratio the earlier the specimen failed due to stress corrosion fracture. There were no failures in any of the low alloy billet specimens having a notched to unnotched ratio greater than 1.20.

The average times to failure of the various low alloy steel billet specimens and comparison of the various heat treat strengths is given in Table LVI. The best steels, from a least stress corrosion susceptible viewpoint, at the various strength levels are:

270,000 - 300,000 psi	4340M (600°F temper)
240,000 - 260,000 psi	4330M (400°F temper)
220,000 - 240,000 psi	H-11 (1100°F temper)

When the above steels were stressed to levels below 180,000 psi, H-11 proved to be the least stress corrosion susceptible.

Vacuum melt steel appears to be slightly more resistant than air melt steel to stress corrosion fracture. This is demonstrated in Table XLIV, XLV and XLVI which show that the vacuum melt 4330M was less susceptible when the air melt and vacuum melt smooth and notched tensile properties were the same. The fractures of the 4330M air melt material all originated at the leading edge of the tension surface whereas the origins in the vacuum melt specimens were located at either the leading or the trailing edges (Figures 51 and 52). The odd appearance of the air melt fractures was traced to the conglomeration of sulfide inclusions on that side of the U-bend specimen which was closest to the center of the forging. This specimen side, closest to the forging center (Figure 18), was the side of the U-bend specimen which was first to enter the 3.5 per cent NaCl solution (the corner between this side and the tension surface was known as the leading edge). The presence of the sulfide inclusions was particularly significant since inclusion of this type cause the greatest decrease in reduction in area values (10).

The majority of fractures in the low alloy billet specimens originated at the trailing edge of the tension surface. This was due to the accumulation and concentration of solution at the trailing edge during the time just after the specimen came out of the tank solution until that specimen reached the top of the ferris wheel. The remaining fracture origins were approximately equally divided between the leading edge and center of the tension surface. Many of the fractures originating at the leading edges occurred in specimens which had been covered with a rust coating. This coating roughened the surface and could have prevented much of the solution from traveling across the specimen surface during the movement of the ferris wheel. This in turn would have increased the concentration of solution near the leading edge, increasing the likelihood of failure there.

Fractographic examination did not reveal any rust rings or corroded areas on the faces of the 4340 specimens (4 martempered and 1 oil quenched) which failed while stressed but before testing in 3.5 per cent NaCl. The main characteristic of the failure origin, which was delineated by the chevron markings, was the lack of any rust on the fracture faces and the appearance of "spikes" near the center of these fracture origins. An example of these spikes is given in Figure 53. The presence of these spikes was noted in the origin areas of all the specimens which had failed before testing. Spikes were also observed at the origins of U-bend specimens which had failed due to stress corrosion fracture after very short immersion times (of only a few hours). These spikes may have been present on all stress corrosion specimens but the presence of the rust coating prevented detailed study of many of the origins.

An electron micrograph of a replica taken from the origin area of a specimen (21N) that had failed while in the stressed condition but before stress corrosion testing is given in Figure 54. For comparison purposes electron micrographs of typical fracture faces caused by hydrogen embrittlement, stress corrosion, fatigue, ductile failure, and quench cracks are shown which illustrate the characteristic appearance of each.

The close relationship between stress corrosion and hydrogen embrittlement is shown in Figures 55 and 56. In both instances the failures were intergranular in nature. The only noticeable difference between the two modes of fracture was the appearance of a few ductile regions about the hydrogen embrittlement origin.

Typical striations appeared after fatigue failure (Figure 57), while the ductile fracture face (Figure 58) was composed of equiaxed dimples. The quench crack failure was entirely intergranular (Figure 59) (11).

Because of the similarity in appearance of the hydrogen embrittlement failure and that of specimen 21N and because of the lack of rust rings around the origin area of this specimen and those that had failed in a like manner, hydrogen embrittlement was suspected as the cause of these premature fractures.

The four martempered 4340 specimens had been tempered at 450°F to obtain a strength within the normal high strength range of 260,000 to 280,000 psi. Material heat treated in this manner has impact properties which meet normal aircraft specifications. However, the single oil quenched specimen (18K) was tempered at 600°F which placed it within the 220,000 - 240,000 psi heat treat strengths (9) the early failure of specimen 18K may be related to the low impact strength. Why the martempered specimens failed in the supposedly high impact strength range and not in the lower impact levels is not completely understood.

The fracture faces of the 4340 U-bend specimens (oil quenched and martempered) which had failed after placing on the ferris wheel were very similar in appearance. These fracture faces were perpendicular to the tension surface with only a thin lip of metal evident at the tension edge. The origins were usually outlined by a semicircular area of rust and the texture (appearance of the surface) of each origin and the remainder of the fracture face was the same (Figures 60 and 61).

The cadmium plated 4340 U-bend specimens with the center hole were much more susceptible to failure than those specimens which had been painted. Though the majority of fracture origins were indicated by rust rings there were some origins very similar in appearance to the stressed (uncoated) 4340 specimens that failed on the shelf. These latter failures indicate that the sacrificial removal of cadmium during the corrosion process hydrogen may be liberated which enters the steel and causes failure. The origins of failure could be located at any spot such as the edge of the specimen, edge of the center hole, or (when a center bolt is used) the interface between the washer and cadmium plate. This is illustrated in Figures 62 and 63.

The fracture of the 4340 painted specimen in the test area (one specimen failed outside the test area) originated at the interface between the paint and cadmium plated washer. The paint had been chipped off and a small local cell had been set up between this point and the cadmium plated washer. This caused the formation of a pit until fracture occurred. The appearance of a typical fracture face and the origin point on the tension surface are illustrated in Figures 62 and 63.

Those fracture faces which resulted from the failures of 4340M U-bend specimens could be generally classified into two groups. The first group, representing the higher strength levels (above 290,000 psi strength) was typified by a rough fracture face having a large fracture lip. There was a difference between the texture (or appearance) of each fracture origin and the remainder of the fracture face (Figures 64 and 65).

The lower strength 4340M and high strength H-11 U-bend specimens were represented by fracture faces perpendicular to the tension surface. The fracture origins were outlined by semicircular rust areas and the texture was the same over the entire fracture surface (Figures 66 and 67).

Many of the origins of the 4340M and H-11 fracture faces were composed of the semicircular area of rust, surrounded by discolored areas (Figures 65 and 66). These latter areas were always the texture of the remaining portion of the fracture faces. Fractured specimens having this appearance were said to have double or triple (multiple) origins. (This is not the same as having failure due to the formation of many separate origins at the same time).

These multiple origins were believed to have resulted from a combination of the mechanical and chemical effects. Since the original load on the tension surface of a stressed U-bend specimen was constant, any corrosion crack which formed perpendicular to the longitudinal axis of the specimen would increase the stress by decreasing the effective surface area. When the stress exceeded the ultimate strength plastic deformation occurred (lowering the stress or load per cross section area) and a fresh area around the crack would be exposed to the corrosive media. The corrosive media would discolor the fresh area and attack the bottom of the crack until the ultimate strength was again exceeded. Fracture would again occur forming another fresh face at the bottom of the crack or causing complete failure of the specimen.

The fracture faces of the 4330M U-bend specimens were typified by large origin areas which could either be located at a tension edge or at the center of the tension surface. The texture of the fracture origin and the remainder of the fracture face were different. Though the fracture origins were perpendicular to the tension surface the remainder of the fracture faces were irregularly shaped with fracture lips along the tension surface (Figure 68).

The failure outside the test area of all the 4330M (Billet R) specimens from the 250,000 psi strength group which had been stressed to 90 per cent of the 0.2 per cent yield strength was traced to an unusually large concentration of sulfide inclusions in the area where the fractures occurred. The failures all originated at the edges of the tension surfaces. It is at these corners, where the maintenance of a glyptal coating is most difficult, that the effect of the localized cell at a bare spot could be most detrimental when combined with the presence of inclusions. As previously mentioned, the presence of sulfide inclusions causes the greatest decrease in ductility of any of the common inclusions observed in steel.

It was possible to relate the size of the fracture origin to the time to failure of only the 4340 (Billet M) electropolished, chemically milled and surface ground specimens. The data from the remaining low alloy specimens did not follow any definite trend. There was no way of determining the crack growth rate from calculations based on the size of the origin. The size of the origin did not necessarily increase with increased time to failure. One major factor, complicating the determination of any relationship between origin size and time to failure, is the effect of secondary cracks, parallel to the fracture face, which formed during the same period as the crack causing failure. (The face milled 4340 Billet M specimens also developed this secondary cracking). The appearance of these secondary cracks after removal of the

tension surface rust layer is illustrated in Figure 69. Breaking open such cracks revealed fracture faces similar to those that were produced by the failure of the U-bend specimens. Thus, the fracture notch, formed during testing is not the only notch on the surface. The presence of many notches, of relatively the same size, could greatly change the stress distribution across the tension surface. This would then cause the growth of a failure origin of different dimensions than would be necessary if only one notch center were involved.

The fracture times of the 4340, 4330M, 4340M and H-11 stress corrosion specimens showed no correlation with the billet positions.

It was difficult to etch low alloy steels in a manner that will satisfactorily reveal the grain boundaries. This was more evident in the specimens which were heat treated to the higher strengths. At the lower strength levels there was evidence of some carbide precipitation outlining the grain boundaries.

The mode of cracking appeared to depend on the heat treat strength. In the higher strength levels of the 4340, 4340M, 4330M and H-11 steels there was a combination of intergranular and a limited amount of transgranular cracking (Figures 70, 71, 72 and 73). At the lower levels the cracking was intergranular in nature (Table LVII).

The type of cracking in the 4330M, 4340 and H-11 steels was not related to the textures of the fracture faces. However, there was a combination of intergranular plus transgranular cracking in those failed 4340M specimens in which the textures of the fracture origins differed from the remainder of the fracture faces. If the appearance of the entire 4340M fracture faces were the same the cracking was solely intergranular.

Many of the cracks that developed in the tension faces of the U-bend specimens originated at the interface between a surface inclusion and the surrounding metal. Rust pits on the surface of a U-bend specimen were often composed on an inclusion and its corrosion products (Figure 74). A crack running from such a pit is shown in Figure 75.

Short cracks running transverse to the fracture face were found in the majority of the failed specimens. These cracks usually were not in the fracture origin area but they did initiate from the fracture edge of the tension surface (Figure 69).

In addition to the microstructures which represent the U-bend specimens that failed, there are micrographs shown in Figures 76, 77 and 78 of the 4340, 4330M and H-11 steels which successfully passed the 1,000 hour test.

C. Stainless Steel

Though the ultimate and yield strengths of the AM 355 SCT 850 specimens (longitudinal grain direction) from the plate and billet were within the desired strength ranges, there were wide differences in the reduction in area values. The AM 355 plate material had an average reduction in area value of 3.0 per cent while the billet specimens had an average value in excess of 40.0 per cent. This may explain why the U-bend plate specimens failed in such short times while the billet specimens were intact after 2,500 hours of testing.

The locations of the fracture origins on the AM 355 fracture faces are shown in Figure 79.

The microstructure at a stress corrosion fracture (specimen 3) from the AM 355 SCT 850 plate is shown in Figure 80. Here the intergranular nature of the stress corrosion fracture can be easily noted. There was a large difference between the microstructures of the plate and billet (Figure 81) specimens that had been heat treated to the SCT 850 condition using standard procedure. Heat treating billet specimens to the SCT 850 condition using both standard and modified (Figure 82) procedures caused the precipitation of larger number of carbides within the grains than was present in the grains of the plate specimens.

Based on the trends shown by the low alloy steels, the low notched to un-notched ratio of the AM 350 SCT 850 material indicated early failure. The DA 850 and SCT 1050 ratios were greater than 1.0 and no early failures were expected.

Since there was only one failure from among the 27 U-bend AM 350 specimens (short transverse grain direction) representing the DA 850, SCT 850 and SCT 1050 conditions the separation of these heat treatments on the basis of stress corrosion susceptibility was not possible. However, the failure of one AM 350 specimen in the SCT 850 condition (notched to smooth ratio .82) may indicate the subsequent failure of specimens in this SCT 850 condition after an extended testing time.

The fracture face of the AM 350 SCT 850 specimen had a much different appearance than the failed AM 355 SCT 850 specimens. In the latter instance the fractures made a near 45° angle with the tension surface and the fracture faces had a layered appearance (Figure 79). The fracture of the AM 350 specimen was perpendicular to the tension surface. There were no fracture lips, similar to those noted on the low alloy steel specimen, along the tension edge of the fracture face of the AM 350 specimen (Figure 83).

Figure 84 shows the microstructure, at the tension surface, of the fracture origin. The failure in this instance was intergranular in nature and is very similar in appearance to the fracture edge of the AM 350 tensile specimen shown in Figure 85.

The lone AM 350 SCT 850 specimen (3Y) that failed was from that part of the billet that had an average reduction in area of only 8 per cent (Table LI, Figures 13 and 14). This is considerably lower than the 17+ and 30+ per cent reduction in area values of the DA 850 and SCT 1050 conditions and could be a partial explanation for the SCT 850 failure.

As in the case of the low alloy steels the K_{Ic} values that were obtained from notched tensile testing AM 350 in the SCT 850, SCT 1050 and DA 850 conditions could not be used to quantitatively estimate the tear resistance properties. All minimum K_{Ic} values were calculated using as the value of σ_y the smooth tensile yield strengths.

The microstructures of AM 350 in the SCT 850 and SCT 1050 conditions were very similar (Figures 85 and 86). The main difference was the appearance of sub-grain boundaries within the delta ferrite of the SCT 1050 materials.

AM 350 in the DA 850 condition is shown in Figure 87.

The AM 350 CRT 850 sheet had an ultimate strength (in the transverse grain direction) of 200,000 psi and an average elongation of 20 per cent. The average notched to unnotched ratio was 0.776 (Table LV) which is considerably below the ratio of 0.98 reported (12) for similar AM 350 material; however, the difference may be due to the testing of different grain directions. The microstructure was characterized by long stringers of delta ferrite passing through the matrix material (Figures 88 and 89).

There were no AM 350 CRT 850 failures during the 1,000 hours of alternate immersion testing.

VI. CONCLUSIONS

- 1) Use of the Boeing U-bend configuration provides a simple method of evaluating the relative stress corrosion susceptibility of plate and billet material.
- 2) The relative susceptibilities to stress corrosion fracture of the 7 finishing procedures evaluated are, with the most susceptible first:
 - a. electropolishing, chemical milling
 - b. grinding
 - c. grinding and shot peening
 - d. face milling,
face milling and sand blasting, face milling and shot peening
- 3) The highest surface compressive stresses were induced by shot peening or sand blasting after face milling.
- 4) During face milling portions of the surfaces were heated above the A_1 temperature and untempered martensite formed at these spots.
- 5) There is the possibility that hydrogen embrittlement contributed to the rapid failure of specimens surface finished by chemical milling and electropolishing.
- 6) The longitudinal grain direction is much more stress corrosion fracture resistant than the long transverse or short transverse grain directions.
- 7) The presence of inclusions at the surface of a stressed specimen is significant. At these points there is the possibility of stress concentration effects and the chemical interaction of corrosive medium, steel, and inclusion.
- 8) Some of the cracking which appears on the tension face of specimens after failure originates in areas composed of an inclusion and its corrosion products.
- 9) There is a certain amount of cracking transverse to the fracture face of failed U-bend specimens. This amount of transverse cracking apparently increases with increasing stress level.
- 10) Vapor honing after grinding increases the compressive stresses by 40,000 to 100,000 psi.
- 11) Martempered 4340 in the 220,000 - 240,000 and 260,000 - 280,000 psi strength ranges was much more stress corrosion susceptible than oil quenched 4340.
- 12) The most stress corrosion susceptible strength ranges of oil quenched 4340 steel are the 220,000 - 240,000 and 260,000 - 280,000 psi ranges. These strength ranges are much more stress corrosion susceptible than the lower strength 200,000 - 220,000 psi level.
- 13) The stress corrosion susceptibility of H-11 steel in the 280,000 - 300,000 psi strength range is much greater than 4340M steel heat treated to comparable strengths.

- 14) The most stress corrosion susceptible heat treat condition of 4330M is the 220,000 - 240,000 psi strength range. This is much more susceptible than the same material heat treated to strengths of 200,000 - 220,000 and 250,000 psi.
- 15) Air melt 4330M is slightly more stress corrosion susceptible than vacuum melt material. This may be due to a higher concentration of inclusions in the air melt 4330M.
- 16) Painting provides much more protection against failure in 3.5 per cent NaCl solution than does cadmium plating.
- 17) The higher heat treat strengths of the low alloy steels failed by a combination of intergranular plus transgranular cracking. At the lower strength levels only intergranular cracking was noted.
- 18) The K_I value (stress intensity factor) could not be precisely calculated for the majority of the low alloy steels due to geometrical limitations of the notch tensile configuration. In the few cases where a meaningful K_I value was obtained there appeared to be shorter time to failure the lower the K_I value.
- 19) The ratio of notched to unnotched ultimate strengths of low alloy steels provides a good indication of the relative stress corrosion susceptibility.
- 20) The appearance of the fracture faces of 4340M could be correlated with the mode of fracture. When there was a difference between the texture of the fracture origin and the fracture face the cracking was intergranular plus transgranular. When the texture of the entire fracture face was the same, cracking was solely intergranular. The above correlation did not hold true for the 4340, 4330M and H-11 steels.
- 21) There were some steels, at particular strength levels, which were much less stress corrosion susceptible than the comparison steels. These more satisfactory steels, at the various strength levels, are:

270,000 - 300,000 psi	4340M (600°F temper)
240,000 - 260,000 psi	4330M (400°F temper)
220,000 - 240,000 psi	H-11 (1100°F temper)

At common stress levels, below 180,000 psi, H-11 was the least stress corrosion susceptible of the above three steels. All comparisons of the steels were made after accelerated testing and no correlation was attempted with actual environmental or service conditions.

- 22) AM 355 SCT 850 and AM 350 DA 850 and SCT 1050 billet specimen and AM 350 CRT 850 sheet specimens were not susceptible to stress corrosion failure during 1000 hours of alternate immersion testing. Except for a lone failure all AM 350 SCT 850 billet specimens passed the 1000 hour test.

VII. RECOMMENDATIONS

As a result of the findings of this study it is recommended that further studies be carried out in the following areas:

1. It is suggested that subsequent stress corrosion testing be done utilizing the more susceptible transverse grain direction rather than the longitudinal grain direction. This would permit a closer correlation with actual service conditions since the majority of airplane part failures occur in the transverse grain directions.
2. In the area of x-ray diffraction stress measurement, the reason for applied and residual stress measurements not being directly additive should be determined.
3. Further studies of stress corrosion and hydrogen embrittlement cracking should be made to determine why additions of silicon to low alloy steels are beneficial.
4. Correlation between stress corrosion susceptibility and a simple notch toughness specimen should be attempted. Perhaps the cracked Charpy impact specimens under study at Watertown Arsenal should be considered for this correlation.
5. The relationships between metallurgical microstructures and stress corrosion susceptibility should be determined using the electron microscope and electron microprobe. These studies should include evaluations of 4330M, 4340, 4340M and H-11 steels using transmission electron microscopy techniques.

VIII. REFERENCES

- 1) Stress Corrosion of High Strength Steels, WADD RFP 98735, Boeing Document D6-5738.
- 2) Symposium on Stress Corrosion Cracking of Metals, ASTM - AIME, Philadelphia, 1945.
- 3) E. H. Phelps and A. W. Loginow, Stress Corrosion of Steels for Aircraft and Missiles, Corrosion, v.16 (1960) p. 325t.
- 4) H. R. Voorhees and J. W. Freeman, Effect of Long-Time Creep on Structural Sheet Materials, Contract AF33(616)-8334, First Progress Report, University of Michigan, November 1961.
- 5) W. E. Quist and D. A. Bolstad, Stress Measurements by X-Ray Diffraction in High Strength Steel and Aluminum, Boeing Document D6-7016.
- 6) S. C. Lawrence, Jr., Detection and Measurement of Sorbed Hydrogen, Hydrogen Embrittlement in Metal Finishing, Reinhold Publishing Co., New York, 1961.
- 7) International Nickel Company, Sales Brochure on 300M (4340M) Steel.
- 8) B. R. Banerjee and J. J. Hauser, Research and Application Engineering to Determine the Effect of Processing Variables on Crack Propagation of High Strength Steels and Titanium, Contract AF33(616)-8156, Fourth Quarterly Progress Report, Crucible Steel Company, May 1, 1961.
- 9) L. J. Klenger, W. J. Barnett, R. P. Frohberg, A. R. Troiano, The Embrittlement of Alloy Steels at High Strength Levels, ASM Transactions, v.46, (1945) p. 1557.
- 10) D. E. Austin and D. D. Goehler, Effect of Non-Coherent Secondary Phases on the Reduction in Area in the Short Transverse Grain Direction, to be published in Metal Progress.
- 11) R. M. N. Pelloux and J. C. McMillan, The Analyses of Fracture Surfaces by Electron Microscopy, Boeing Scientific Research Laboratories, Document D1-82-0169, May 1962.
- 12) H. R. Voorhees and J. W. Freeman, Effect of Long-Time Creep on Structural Sheet Materials, Contract AF33(616)-8334, Second Progress Report, University of Michigan, April 1962.

TABLE I

Chemical Composition of
4330M Steels

Element	Nominal Composition (MIL-S-8699)	Billet L Heat 1594	Billet R Heat 9519	VVB (Vacuum Melt)	VNB (Air Melt)
C	.28 - .33	.33	.32	.31	.32
Mn	.80 - 1.00	.89	.83	.96	.86
P	.025 Max.	.011	.006	.010	.010
S	.025 Max.	.015	.017	.014	.015
Si	.20 - .35	.28	.30	.29	.26
Ni	1.65 - 2.00	1.95	1.90	1.95	1.80
Cr	.75 - .95	.86	.84	.82	.79
Mo	.35 - .50	.45	.44	.45	.44
V	.05 - .10	.09	.085	.070	.075
Cu		.21	.24	.105	.16
Ti			.014		
Al			.012	.075	.040

TABLE II

Heat Treatments of 433OM (Billet L) and
4340 (Billet M) Specimens

Specimen	Austenitizing Temperature (°F)	Austenitizing Time in Atmosphere Furnace (Min)	Tempering Temperature (°F)	Tempering Time (Hr)
433OM				
1L, 2L, 3L 1AL, 1BL, 1CL, 2AL, 2BL, 2CL, 3AL, 3BL, 3CL, 13L through 24L	1550 - 1600	45	400	3 + 3
4340				
1M through 24M	1500 - 1550	45	400	3 + 3
Blocks 3M, 4M, 5M, 7M, 10M, 13M, 16M	1500 - 1550	60	400	4 + 4

TABLE III

Tensile Properties of
4330M (Billet L) and 4340 (Billet M)

Smooth Tensile

		(Average of Three Specimens)			
Material	Designation	Grain Direction	Ultimate Strength (psi x 10 ⁻³)	Yield Strength (psi x 10 ⁻³)	Per Cent Elongation in 1 inch
					Per Cent Reduction in Area
4330M	Billet L	Short Transverse	252.7	217.2	5
					17
4340	Billet M	Short Transverse	280.5	216.6	8
					20.3
4340	Billet M	Long Transverse	279.6	227.2	6
					14.5
4340	Billet M	Longitudinal	280.7	220.2	12
					45.3

TABLE IV

Chemical Composition of
4340 Steels

Element	Nominal Composition (MIL-S-5000)	Billet K Heat 1749	Billet M Heat 512046	Billet N Heat 1630
C	.38 - .43	.40	.42	.39
Mn	.65 - .85	.65	.70	.72
P	.025 Max.	.013	.025	.013
S	.025 Max.	.014	.022	.014
Si	.20 - .35	.21	.27	.22
Ni	1.65 - 2.00	1.86	1.70	1.84
Cr	.70 - .90	.80	.78	.78
Mo	.20 - .30	.25	.28	.25
Cu			.21	.19
Sn				.019
V			.007	.005
Al			.010	

TABLE V

Heat Treatment of 4340 (Billets K and N)

All specimens austenitized at 1500° - 1550°F for 45 minutes and oil quenched. Specimens were tempered in air furnace.

Specimen	Temper Before Grinding Temperature (°F)	Time (Hr)	Temper After Grinding Temperature (°F)	Time (Hr)
1K through 9K, SK1, SK5, SK9, NK1, NK5, NK9, 28N through 54N, 82N through 87N	400	3 + 3	350	1
10K through 18K, SK2, SK6, SK10, NK2, NK6, NK10	600	2-1/2 + 2-1/2	550	1
19K through 27K, SK3, SK7, SK11, NK3, NK7, NK11	800	1-1/2 + 1-1/2	750	1/2
28K through 36K, SK4, SK8, SK12, NK4, NK8, NK12	1000	1-1/2 + 1-1/2	950	1/2

TABLE VI

Chemically Milling, Electropolishing, Sand Blasting,
Shot Peening and Vapor Blasting Procedures

<u>Surface Finish Treatment</u>	<u>Procedure</u>	<u>Specimen</u>
Sand Blasting	Boeing Process Specification 5748 with Al_2O_3 pellets having a size less than 100 mesh	7M, 8M, 9M Block 7M
Shot Peening	Boeing Process Specification 5730 using a shot size of .023 in. and an intensity of .008A2	10M, 11M, 12M Block 10M, 82N 83N, 84N
	Shot size of .023 in. and an intensity of .012A2	85N, 86N, 87N
Electropolished	Sixty per cent (60%) phosphoric acid, 40% butyl alcohol. Current density approximately 6 amperes per square inch	13M*, 14M*, 15M Block 13M
Chemical Milling	Subcontractor proprietary process	4M, 5M, 6M Block 4M
Vapor Blasting	One hundred mesh Pangborite**grit suspended in water. One hundred psi pressure forced suspension over surface of specimens	All low alloy U-bend specimens except those from billets L and M, 11N, 14N, 16N

• Substituted specimens. Original specimens had not received satisfactory surface finish.

•• Trade name of Pangborn Company

TABLE VII

Surface Grounding of Low Alloy Steels

<u>Machine Variables</u>	<u>Machine Constants</u>	
	Tension Surface	Compression Surface*
Wheel Abrasive	Al ₂ O ₃	19A60
Hardness	I	L
Structure	8	5
Bond	Vitrified	Vitrified
Cross Speed	.050"/pass	Hand Adjusted
In-Speed	.0015"/pass	.0005"/pass
Dress of Grinding Wheel	20"/min	Hand Adjusted
Final In-Feed	.001"/pass	.0005"/pass
Coolant	Sultran A20	Air Cooled
Wheel Size	10"	2"
Work Speed	60'/min	Hand Adjusted
Wheel Speed	6000 SFM	3000 SFM

- * The differences between the top and bottom surface finishing treatments were unavoidable owing to the geometrical difficulties introduced by the specimen legs. This was of concern when the U-bend specimens from Billets L and M were being prepared. All subsequent ground U-bend specimens were finished on four surfaces using the procedure outlined under the Tension Surface subheading.

TABLE VIII

Face Milling of Low Alloy Steels
(32 RHR Finish)

Machine Variables

Machining Constants

Tool Type

- (1) Kenemet K4H carbide tips
- (2) +10° axial rake preferred although +5° axial rake is acceptable
- (3) -5° radial rake
- (4) Primary clearance 1/16" to width at 6°; secondary clearance at approximately 45°
- (5) 45° corner chamfer for milling through, corner radius per callout in corners
- (6) Concavity angle 1/2° per quarter inch of width. If set up not rigid, increase this angle.

Speed

165 RPM

Feed

.001 to .002 inches per tooth (1-15/16"/min)

Depth of Cut

.050 inches

Coolant

Soluble oil

TABLE IX

**Face Milling of Low Alloy Steels
(125 RHR Finish)**

Machine Variables

Machining Constants

Tool Type

**C-6 carbide tool, 0° axial rake -15° radial
rake, 8° primary clearance, 45° corner chamfer**

Speed

110 RPM

Feed

0.005 ipt (inch per tooth)

Depth of Cut

0.020 inch min., 0.100 inch max.

Coolant

Soluble oil

TABLE X**Chemical Composition of 4340M Steel**

Element	Nominal Composition (BMS 7-26)	Billet P Heat 23408
C	.38 - .43	.44
Mn	.60 - .90	.79
Si	1.50 - 1.80	1.51
P	.025 Max.	.002
S	.025 Max.	.005
Cr	.70 - .95	1.20
Ni	1.65 - 2.00	1.75
Mo	.30 - .50	.56
V	.05 - .10	.07

TABLE XI

Chemical Composition of H-11 Steels

Element	Nominal Composition (BMS 7-80)	Billet U Heat 195033	Billet V Heat 31177
C	.37 - .43	.405	.425
Mn	.20 - .40	.53	.33
Si	.80 - 1.00	.99	1.18
P	.030 Max.	.030	.010
S	.030 Max.	.015	.011
Cr	4.75 - 5.25	5.03	5.35
Mo	1.20 - 1.40	1.30	1.30
V	.40 - .60	.41	.60

TABLE XII

Heat Treatment of 4340 (Billet N, Martempered)

All specimens austenitized at 1500° - 1550°F for 45 minutes and quenched in salt at 350° - 400°F until stabilized at bath temperatures. Removed from bath, cooled in still air and tempered within one hour.

Specimen	Temper Before Grinding Temperature (°F)	Grinding Time (Hr)	Temper After Grinding Temperature (°F)	Grinding Time (Hr)
1N through 9N, SN4, SN7, SN10, NN4, NN7, NN10	870	2	820	.5
10N through 18N, 68N through 72N, SN5, SN8, SN11, NN5, NN8, NN11	600	2 + 2*	550	1
19N through 27N, 73N, 74N, 77N, SN6, SN9, SN12, NN6, NN9, NN12	450	2 + 2	400	1

* Indicated double tempering

TABLE XIII

Heat Treatment of 4340M
(Billet P)

All specimens austenitized at 1575° - 1625°F for 45 minutes and oil quenched. Specimens tempered in air furnace.

Specimen	Temper Before Grinding Temperature (°F)	Grinding Time (Hr)	Temper After Grinding Temperature (°F)	Grinding Time (Hr)
1P through 9P, SP1, SP5, SP9, NP1, NP5, NP9	400	3 + 3*	350	1
10P through 18P, SP2, SP6, SP10, NP2, NP6, NP10	600	3 + 3	550	1
19P through 27P, SP3, SP7, SP11, NP3, NP7, NP11	800	2.5 + 2.5	750	1
29P through 37P, SP4, SP8, SP12, NP4, NP8, NP12	1000	1.5 + 1.5	950	.5

* Indicates double tempering

TABLE XIV

Heat Treatment of 4330M
(Billet R, Air Melt, Vacuum Melt)

All specimens were austenitized at 1550° - 1600°F for 45 minutes and oil quenched. Specimens were tempered in an air furnace.

Specimen	Temper Before Grinding Temperature (°F)	Grinding Time (Hr)	Temper After Grinding Temperature (°F)	Grinding Time (Hr)
1R through 9R, SR1, SR5, SR9 NR1, NR5, NR9	400	3 + 3	350	1
10R through 18R, SR2, SR6, SR11, NR2, NR6, NR11, IVVB through 3VVB, 1VNB through 3VNB, SVVB1 through SVVB5, NVVB1 through NVVB5, NVNB1 through NVNB5	600	2.5 + 2.5	550	1
19R through 27R, SR3, SR7, SR10, NR3, NR7, NR10	800	1.5 + 1.5	750	.5
28R through 36R, SR4, SR8, SR12, NR4, NR8, NR12	1000	1.5 + 1.5	950	.5

TABLE XV

Heat Treatment of H-11
(Billet V)

All specimens were austenitized at 1825° - 1875°F for 20 minutes and air cooled. Specimens were tempered in an air furnace.

Specimen	Temper Before Grinding Temperature (°F)	Grinding Time (Hr)	Temper After Grinding Temperature (°F)	Grinding Time (Hr)
1V through 9V, SV1, SV5, SV9, NV1, NV5, NV9	600	3 + 3 + 3	550	1
10V through 18V, SV2, SV6, SV10, NV2, NV6, NV10	800	3 + 3 + 3	750	1
19V through 27V, SV3, SV7, SV11, NV3, NV7, NV11	1000	3 + 3 + 3	950	1
28V through 36V, SV4, SV8, SV12, NV4, NV8, NV12	1100	3 + 3 + 3	1050	1

TABLE XVI

Heat Treatment of H-11 Cubes
(Billets U and V)

Parts placed in air furnace at 1450°F. Ninety minutes were required to reach the austenitizing temperature of 1850°F.

All specimens were austenitized at 1850°F for 45 minutes

<u>Specimen A</u> <u>Oil Quenched</u>	<u>Specimen B</u> <u>Oil Quenched</u>	<u>Specimen C</u> <u>Air Cooled</u>	<u>Specimen D</u> <u>Air Cooled</u>
Double Tempered at 1000°F for 6 hours	Double Tempered at 1000°F for 6 hours	Double Tempered at 1000°F for 6 hours	Double Tempered at 1000°F for 6 hours
Redrawn at 1000°F for 6 hours	Redrawn at 1100°F for 4 hours	Redrawn at 1000°F for 6 hours	Redrawn at 1100°F for 4 hours
*R _c - 54.5	R _c - 47.5	R _c - 54.4	R _c - 47.5
Strength level 296,000 psi	Strength level 234,000 psi	Strength level 296,000 psi	Strength level 234,000 psi

* R_c - Rockwell C Hardness

TABLE XVII

Cadmium Plating of 4340 Specimens

- A. Vapor degreased in trichloroethylene
- B. Abrasive blast cleaned with novaculite silica spherical glass beads (180 to 625 grit)
- C. Immersed in cyanide holding bath until ready to plate. Solution composition:

	<u>Original Preparation</u>	<u>Control Concentration</u>
1. Sodium Cyanide	31#/100 gal	4 - 5 oz/gal
2. Sodium Hydroxide	10#/100 gal	1 - 2 oz/gal
3. Operating Temperature		70 - 85°F

- D. Cadmium plated (no rinse after holding bath) using a current density of approximately 40 amp/ft². Solution composition:

	<u>Original Preparation</u>	<u>Control Concentration</u>
1. Sodium Cyanide	146#/100 gal	
2. Cadmium Oxide	47#/100 gal	
3. Cadmium (metal)		6.5 - 7.5 oz/gal
4. Sodium Carbonate		8.0 oz/gal maximum
5. Sodium Hydroxide		3.5 - 5.0 oz/gal
6. Free Sodium Cyanide (total NaCN - 1.75 x Cd)		9 - 15 oz/gal
7. Water, Deionized	Maintain volume	
8. Operating temperature		70 - 85°F

- E. Cold water rinse (5 minute maximum)
- F. Dry
- G. Bake 23 hours at 375° ± 25°F

TABLE XVIII

Painting of 4340 Specimens

<u>BMS* and Type</u>	<u>Vendor's Designation and Material</u>	<u>Mixing Ratio by Volume</u>	<u>Spray Viscosity</u>	<u>Film Thickness (mils)</u>
10-11 Type 1 (primer)	DeSoto Chemical Coatings 1910091 Primer Base 6108148A Primer Converter MEX Primer Thinner	1 part 1 part 1/10 part max.	31 - 40 sec. No. 1 Zahn	0.9 to 1.1
10-11 Type 2 Enamel	Andrew Brown Company A-423 Series Enamel Base T-261 Enamel Catalyst T-262 Enamel Thinner	4 parts 1 part 3 parts max.	17 - 19 sec. No. 2 Zahn	1.6 to 1.8

* Boeing Material Specification

TABLE XIX

Preparation of Center Holes in 4340 Specimens

Drilling

Drill	7/32" solid carbide
Speed	250 rpm
Feed	.001 inch per tooth (ipt)
Cutting Fluid	Richfield, Allkut 45

Reaming

Reamer	.242" 4 flute carbide insert, 45° chamfer
Speed	250 rpm
Feed	.0005 ipt
Depth of Cut	1/32 on the diameter
Cutting Fluid	Richfield, Allkut 45

Honing

Abrasive Stones	220 Al₂O₃ grit roughing 500 Al₂O₃ grit finishing
Cutting Fluid	Richfield, Allkut 45

TABLE XX

Chemical Composition of AM 355

<u>Element</u>	<u>Nominal Composition (QQ-S-763)</u>	<u>.313" Plate</u>	<u>6" x 6" x 6" Billet</u>
C	.10 - .15	.14	.13
Mn	.50 - 1.25	.64	.52
P	.04 Max.	.025	.018
S	.03 Max.	.019	.012
Si	.5 Max.	.34	.22
Cr	15.0 - 16.0	15.09	15.73
Ni	4.0 - 5.0	4.95	4.76
Mo	2.5 - 3.25	2.60	2.60
N	.07 - .13		
Cu			.12
V			.04

TABLE XXI

Heat Treatment of AM 355 to the
SCT 850 Condition

<u>Specimen</u>	<u>Temperature (°F)</u>	<u>Time (min)</u>	<u>Quenching Medium</u>	<u>Type Treatment</u>
A, B, C (billet)	1950	35	Water at R.T.	Modified processing procedures
	Immediately Cool to -100	180	Still air at R.T.	
	1710	30	Still air	
	Immediately cool to -100	180	Still air	
	850	180	Still air	
I, II, III (plate)	1875	35	Water at R.T.	Standard processing procedures
D, E, F (billet)	1375	180	Still air	
	1710	30	Still air	
	Cool to -100	180	Still air	
	850	180	Still air	

TABLE XXII

Milling of AM 355 and AM 350

Machine Variables

Machining Constants

Tool Type	Freshly ground 4-inch slab mill with 8 teeth and a 45° helix
Speed	13 - 16 RPM
Feed	3/8 to 21/32-inch per minute. The speed is varied with the feed.
Depth of Cut	0.040-inch rough finish on flat faces. 0.010-inch final finish on flat faces.
Method of Cut	Conventional mill
Coolant	Soluble oil

TABLE XXIII

Chemical Composition of AM 350

<u>Element</u>	<u>Nominal Composition (QQ-S-763)</u>	<u>Billet Y Heat 93378</u>	<u>Sheet Z Heat 35828</u>
C	.08 - .12	.10	.11
Mn	.50 - 1.25	.54	.65
P	.040 max.	.029	.010
S	.030 max.	.010	.015
Si	.50 max.	.22	.26
Cr	16.00 - 17.00	15.92	16.10
Ni	4.00 - 5.00	4.98	4.90
Mo	2.50 - 3.25	2.68	2.90
N	.07 - .13		
Cu		.14	.21
V		.04	
Al		.065	

TABLE XXIV

Heat Treatment of AM 350 to the
SCT 850, SCT 1050 and DA 850 Conditions
(Billet Y)

<u>Specimen</u>	<u>Temperature (°F)</u>	<u>Time (min.)</u>	<u>Quenching Medium</u>
1Y through 9Y, SY2 SY4, SY10, NY2, NY4, NY10	1900 - 1950	50	Water
	1375	180	Air
19Y through 27Y, SY3 SY7, SY8, NY3, NY7, NY8	1710	30	Air
	-100	180	Air
SCT 850 (1Y through 9Y, etc.)	850	180	Air
SCT 1050 (19Y through 27Y, etc.)	1050	30	Air
DA 850 10Y through 18Y, SY1, SY5, SY9, NY1, NY5, NY9	1900 - 1950	50	Water
	1375	180	Air
	1710	45	Water
	1375	180	Air
	850	180	Air

TABLE XXV

Testing Times of 4330M Specimens
(Billet L)

<u>Specimen</u>	<u>Grain Direction</u>	<u>Surface Finish</u>	<u>Surface Roughness (RHR)</u>	<u>Time to Failure (Hr)</u>
1L	Short Transverse	Ground	10	30 - 34
2L	"	"	6	7 - 22
3L	"	"	12	23.7
13L	"	Chem Milling	160	31 - 45
17L	"	"	160	7 - 22
18L	"	"	85	7 - 22
1AL	"	Face Milled (32RHR)	90	7-1/2 - 22
1BL	"	"	103	7-1/2 - 22
1CL	"	"	110	7-1/2 - 22
2AL	"	Face Milled (32 RHR) and Shot Peened	21	96 - 120
2BL	"	"	21	96 - 120
2CL	"	"	21	96 - 120
3AL	"	Face Milled (125 RHR) and Sand Blasted	55	7 - 22
3BL	"	"	45	30 - 34
3CL	"	"	25	7 - 22
14L	"	Electropolished	250	96 - 120
15L	"	"	80	31 - 45
16L	"	"	70	31 - 45
19L	Long Transverse	Ground	30	35 - 46
20L	"	"	26	52 - 55
21L	"	"	50	22 - 23
22L	Longitudinal	"	38	No failure in two weeks
23L	"	"	50	"
24L	"	"	40	"


TABLE XXVI

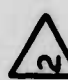
Testing Times of 4340 Specimens (Billet M)

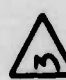
Specimen	Grain Direction	Surface Finish	Surface Finish Processing	Residual Surface Stresses (psi x 10 ⁻³)	Surface Roughness (RHR)	Time to Failure (Hours)
1M	Short	Transverse	Table VII	-71.5	28	38.5
2M	"	"	"	-65.0	23	15
3M	"	"	"	-24.0	26	23
Block 5M	"	"	"	-32.0	20	
Block 4M	"	Chem Milled	Table VI	-2.5	275	
4M	"	"	"	-60.0	300	4
5M	"	"	"	-38.0	300	.67
6M	"	"	"	-38.0	325	2
Block 7Ma	"	Face Milled (125 RHR)	Table IX		150	
7Ma	"	"	"		100	
8Ma	"	"	"		145	
9Ma	"	"	"		85	
Block 7Mb	"	Sand Blasted	Table VI	-94.5	155	45
7Mb	"	"	"	-83.0	115	No failure 1000 hrs.
8Mb	"	"	"	-96.2	165	No failure 1000 hrs.
9Mb	"	"	"	-94.5	100	
Block 10Ma	"	Face Milled (32 RHR)	Table VIII	-28.7	17	
10Ma	"	"	"	-48.0	17	
11Ma	"	"	"	-67.0	30	
12Ma	"	"	"	-65.0	20	
Block 10Mb	"	Shot Peened	Table VI	-89.0	22	No failure 1000 hrs.
10Mb	"	"	"	-76.9	28	845
11Mb	"	"	"	-120.0	24	476
12Mb	"	"	"	-59.0	20	

TABLE XXVI (Cont'd)

<u>Specimen</u>	<u>Grain Direction</u>	<u>Surface Finish</u>	<u>Surface Finish Processing</u>	<u>Residual Surface Stresses (psi x 10⁻³)</u>	<u>Surface Roughness (RHR)</u>	<u>Time to Failure (Hours)</u>
Block 13M	Short Transverse	Electropolish	Table VI	+21.0	110	
13M	"	"	"	- 9.0	69	2
14M	"	"	"	- 5.2	80	2
15M	"	"	"	-26.0	135	5.5
Block 16M	"	Face Milled (32 RHR)	Table VIII	-79.0	32	
16M	"	"	"	-66.0	12	No failure 1000 hrs.
17M	"	"	"	-38.0	14	209
18M	"	"	"	-91.8	15	34
Block 19M	Long Transverse	Ground	Table VII	-51.0	16	9
20M	"	"	"	-73.0	26	38
21M	"	"	"	-68.0	21	-
22M	Longitudinal	"	Table VII	-79.0	29	363
23M	"	"	"	-74.5	21	422
24M	"	"	"	-71.4	19	250

 Negative sign indicates compressive stresses.

 Specimens lettered a and b are the same. The letters indicate different surface finishes.

 Second set of specimens. The original specimens were rejected because of unsatisfactory surface finishes.


 Unsatisfactory specimen, incorrect dimensions.

TABLE XXVII

Testing Times of 4340 Shot Peened Specimens
(Billet N)

<u>Specimen</u>	<u>Surface Finish</u>	<u>Surface Finish Processing</u>	<u>Residual Surface Stress</u> (psi x 10 ⁻³)	<u>Surface Roughness</u> (RHR)	<u>Stress</u> (psi x 10 ⁻³)	<u>Per Cent Yield Strength</u>	<u>Time to Failure</u> (Hr)	<u>Remarks</u>
82N	Ground	Table VII	-79.7					
83N	"	"						
84N	"	"						
85N	"	"	-42.7					
86N	"	"						
87N	"	"						
82N	Shot Peened	Table VI	-101	37	170	75	35	a
83N	"	"		35	170	75	41	b
84N	"	"		45	170	75	125	b
85N	"	"	-63.8		170	75	77	b
86N	"	"		55	170	75	24	b
87N	"	"		30	170	75	10.5	a

a Origin at corner of trailing edge

b Origin near center of tension face

TABLE XXVIII

Smooth Tensile Properties of 4340
(Billet N, Martempered)

<u>Specimen</u>	<u>Hardness Rockwell C</u>	<u>Ultimate Strength (psi x 10⁻³)</u>	<u>Yield Strength 0.2% Offset (psi x 10⁻³)</u>	<u>Per Cent Reduction in Area</u>	<u>Per Cent Elongation in 1 inch</u>
SN4	43	196.3	182.9	13.0	4.0
SN7	43	196.7	182.3	13.3	5.0
SN10	45	196.7	181.7	14.2	6.0
SN5	50	244.0	207.5	9.0	4.0
SN8	50	245.9	213.1	11.9	4.0
SN11	50	244.9	211.9	10.5	4.0
SN6	49	262.4	213.5	7.8	5.0
SN9	48	269.4	223.7	6.4	3.0
SN12	50	279.1	230.4	11.0	4.0

TABLE XXIX

Notched Tensile Properties of 4340
(Billet N, Martempered)

<u>Specimen</u>	<u>Hardness Rockwell C</u>	<u>Notch Radius (in.)</u>	<u>Ultimate Strength (psi x 10⁻³)</u>	<u>K_{Ic} (psi in^{1/2})</u>	<u>Notched Unnotched</u>
NN4	42.0	.001	245.6	> 37.7	1.27
NN7	42.0	.0009	237.7	> 37.6	1.21
NN10	41.5	.0008	246.6	> 37.5	1.25
					Avg. 1.24
NN5	49.5	.0009	222.4	> 42.7	0.91
NN8	48.5	.0009	197.6	40.7	0.81
NN11	47.5	.001	207.7	42.8	0.85
					Avg. 0.86
NN6	43.0	.001	187.8	38.6	0.72
NN9	42.0	.0009	189.9	39.1	0.71
NN12	48.5	.001	185.3	38.3	0.66
					Avg. 0.70

$$K_{Ic} \approx 0.233 \sigma_u \sqrt{\pi D}$$

TABLE XXX

Smooth Tensile Properties of 4340
(Billet K)

<u>Specimen</u>	<u>Rockwell C</u>	<u>Ultimate Strength (psi x 10⁻³)</u>	<u>Yield Strength 0.2% Offset (psi x 10⁻³)</u>	<u>Per Cent Reduction in Area</u>	<u>Per Cent Elongation in 1 inch</u>
SK1	52.3	275.4	225.7	14.3	6
SK5	53.0	277.7	230.7	9.8	5
SK9	52.7	277.0	224.2	12.1	5
SK2	49.0	240.3	211.2	12.9	3.5
SK6	48.5	239.4	207.1	16.6	5
SK10	49.0	241.4	211.1	7.2	4
SK3	44.5	206.6	190.2	14.9	4.4
SK7	44.7	204.5	185.8	24.0	6.5
SK11	43.7	205.8	187.4	17.1	5.5
SK4	37.0	178.4	163.0	22.7	8
SK8	38.7	173.7	158.3	25.3	9
SK12	38.2	172.1	154.5	31.2	10

TABLE XXXI

Notched Tensile Properties of 4340
(Billet K)

<u>Specimen</u>	<u>Rockwell C</u>	<u>Notch Radius (inch)</u>	<u>Ultimate Strength (psi x 10⁻³)</u>	<u>K_{Ic} (psi in^{1/2}) (x 10⁻³)</u>	<u>Notched Unnotched (NK1 etc.) S_{KI}</u>
NK1	53.0	.0015	237.7	> 46.4	.86
NK5	53.5	.0014	231.3	> 47.5	.836
NK9	53.7	.0016	228.0	> 46.1	.824
					Avg. .840
NK2	49.0	.0012	161.7	--	--
NK6	47.3	.0013	218.7	> 42.6	.91
NK10	48.7	.0011	212.0	> 43.5	.88
					Avg. .90
NK3	44.0	.0011	249.9	> 39.2	1.20
NK7	43.1	.0010	248.2	> 38.2	1.21
NK11	42.7	.0013	245.4	> 38.6	1.19
					Avg. 1.20
NK4	39.2	.0015	236.4	> 33.6	1.32
NK8	37.7	.0015	233.4	> 32.6	1.34
NK12	39.0	.0013	240.5	> 31.8	1.38
					Avg. 1.35

$$K_{Ic} \geq 0.233 \sigma_u \sqrt{\pi D}$$

TABLE XXXII

Testing Times of 4340 Specimens
(Billet N, Martempered)

Specimen	Nominal H.T. Strength (psi x 10 ⁻³)	Strength Level (psi x 10 ⁻³)	Per Cent Yield Strength	Surface Roughness (RHR)	Residual Surface Stress (psi x 10 ⁻³)	Time to Failure Avg. Hr.	Avg. Min.	Remarks
1N	196	90	50	17				a
2N	"	135	75	18				a
3N	"	165	90	17				a
4N	"	135	75	16	-112.8			a
5N	"	90	50	18				a
6N	"	165	90	30				a
7N	"	165	90	32				a
8N	"	135	75	16				a
9N	"	90	50	28				a
10N	244	105	50	16		199.0	11,900	f
11N	"	160	75	18		14.0	840	d, g
70N	"	160	75	40		4.5	270	f
12N	"	105	50	16		443.0	26,500	e
13N	"	190	90	17	-134.2	1.25	75	d, e
14N	"	160	75	19		2.0	120	d, g
71N	"	160	75	32		2.0	120	d
15N	"	105	50	17		5.5	330	e
69N	"	105	50	34		623.0	37,380	f
16N	"	160	75	18		3.3	210	g
72N	"	160	75	32		2.6	156	d
17N	"	190	90	21		13.0	780	e
18N	"	190	90	17		22.5	1,350	d
68N	"	190	90	45		1.5	90	d

TABLE XXXII (Cont'd)

<u>Specimen</u>	<u>Nominal H.T. Strength (psi x 10⁻³)</u>	<u>Strength Level (psi x 10⁻³)</u>	<u>Per Cent Yield Strength</u>	<u>Surface Roughness (RHR)</u>	<u>Residual Surface Stress (psi x 10⁻³)</u>	<u>Time to Failure Avg. Hr. Avg. Min.</u>	<u>Remarks</u>
19N	269	110	50	35		2.0	e
20N	"	165	75	45		1.0	e
21N	"	200	90	40		---	b
73N	"	200	90	35		4.5	d
22N	"	165	75	40		1.0	e
23N	"	110	50	45		703.0	f
24N	"	200	90	40		---	b
77N	"	200	90	30		---	b
25N	"	200	90	35	-138.4	1.0	d, e, f
26N	"	165	75	45		---	b
74N	"	165	75	38		4.7	f
27N	"	110	50	40		850	c
						51,300	

a No failure in 1,000 hours of testing.

b Failed while stressed but before testing.

c Failed outside test area but more than 1.50-inch from specimen end.

d Failure originated at trailing edge of tension surface.

e Failure originated at center of tension surface.

f Failure originated at leading edge of tension surface.

g Specimens were not vapor honed.

TABLE XXIII

Testing Times of 4340 Specimens
(Billet K)

Specimen	Nominal H.T. Strength (psi x 10 ⁻³)	Stress Level (psi x 10 ⁻³)	Per Cent Yield Strength	Surface Roughness (RHR)	Residual Surface Stresses (psi x 10 ⁻³)		Time to Failure		Remark
					BVB	AVB	Avg.Hr.	Avg.Min	
1K	276	115	50	33	-40.0	-85.5	817	49,020	b
2K	"	170	75	24			3	180	c
3K	"	205	90	25			0.75	45	b
4K	"	170	75	29	-68.0	-73.1	1.0	60	b
5K	"	115	50	43			727	43,500	b
6K	"	205	90	32			0.67	40	b
7K	"	205	90	26			9.0	540	b
8K	"	170	75	35			25.0	1,500	d
9K	"	115	50	23			479	28,740	b
10K	240	105	50	33	-85.5	-98.0	85	5,100	c
11K	"	160	75	28			1.5	90	b
12K	"	105	50	37			684	41,040	b
13K	"	190	90	25	-61.9	-143.0	5.5	330	b
14K	"	160	75	26			15	900	b
15K	"	105	50	30			721	43,260	b
16K	"	160	75	29		-147.0	5.5	330	b
17K	"	190	90	30			0.8	48	b
18K	"	190	90	38			----	----	e
19K	205	95	50		-28.6	-90.5			a
20K	"	145	75						a
21K	"	170	90	28			943	56,580	c
22K	"	145	75	35	-41.2	-91.0			a
23K	"	95	50						a
24K	"	170	90	30			131	7,860	b
25K	"	170	90			-67.0	36	2,160	c
26K	"	145	75						a
27K	"	95	50						a

TABLE XXXIII (Cont'd)

Specimen	Nominal H.T. Strength (psi x 10 ⁻³)	Stress Level (psi x 10 ⁻³)	Per Cent Yield Strength	Surface Roughness (RHR)	Residual Surface Stresses (psi x 10 ⁻³)		Time to Failure Avg.Hr.	Remarks
					BVB	AVB		
28K	175	80	50	37	-40.0	-74.0		a
29K	"	120	75					a
30K	"	145	90					a
31K	"	120	75	27	-35.0	-67.0		a
32K	"	80	50					a
33K	"	145	90					a
34K	"	145	90	33		-60		a
35K	"	80	50					a
36K	"	120	75					a

BVB Before Vapor Blasting

AVB After Vapor Blasting

- a No failure in 1,000 hours
b Failure originated at the trailing edge of specimen
c Failure originated in center section of specimen
d Failure originated at leading edge of specimen
e Failed while stressed but before testing

TABLE XXXIV

Smooth Tensile Properties of 4340M
(Billet P)

<u>Specimen</u>	<u>Hardness Rockwell C</u>	<u>Ultimate Strength (psi x 10⁻³)</u>	<u>Yield Strength 0.2% Offset (psi x 10⁻³)</u>	<u>Per Cent Reduction in Area</u>	<u>Per Cent Elongation in 2 inches</u>
SP1	52.9	299.6	244.9	27.6	8
SP5	50.3	296.9	240.2	26.7	10
SP9	43.2	295.7	236.6	23.9	8
SP2	49.0	290.3	246.4	24.7	8
SP6	53.2	288.4	244.4	31.7	9
SP10	49.2	289.1	245.8	24.1	8
SP3	46.6	252.8	205.2	28.0	9
SP7	44.1	252.1	206.6	30.9	10
SP11	44.7	250.5	207.0	27.1	8
SP4	44.8	223.0	204.0	35.4	10
SP8	44.3	224.3	204.7	27.4	9.5
SP12	39.7	224.9	204.5	24.8	11

TABLE XXXV

Notched Tensile Properties of 4340M
(Billet P)

Specimen	Hardness Rockwell C	Notch Radius (in.)	Ultimate Strength (psi x 10 ⁻³)	K _{Ic} ^o (psi in ^{1/2}) (10 ⁻³)	Notched Unnotched
NP1	46.5	.0012	249.0	> 51.4	.84
NP5	46.0	.0011	270.8	> 49.6	.91
NP9	46.5	.0009	268.8	> 48.8	.91
					Avg. = .89
NP2	46.2	.0010	249.0	> 50.8	1.03
NP6	47.2	.0009	256.0	> 50.4	.88
NP10	46.0	.0009	251.7	> 50.6	.87
					Avg. = .93
NP3	44.0	.0009	221.5	> 42.3	.87
NP7	43.2	.0009	216.7	> 42.6	.86
NP11	43.5	.0008	217.9	> 42.7	.88
					Avg. = .87
NP4	42.5	.0010	261.1	> 42.0	1.17
NP8	40.5	.0009	263.2	> 42.4	1.17
NP12	42.0	.0009	204.5	42.3	.92
					Avg. = 1.09

$$K_{Ic}^o \geq 0.233 \sigma_u \sqrt{\pi D}$$

TABLE XXXVI

Testing Times of 4340M Specimens
(Billet P)

Specimen	Nominal H.T. Strength (psi x 10 ⁻³)	Stress Level (psi x 10 ⁻³)	Per Cent Yield Strength	Surface Roughness (RHR)	Residual Surface Stresses (psi x 10 ⁻³)		Time to Failure Avg.Hr. Avg.Min.	Remarks
					BVB	AVB		
1P	297	115	50	23	-72.0			a
2P	"	175	75	30			87 5,220	b
3P	"	210	90	30			19 1,140	c
4P	"	175	75	30	-80.6		16 960	b
5P	"	115	50	30				a
6P	"	210	90	29			9 540	b
7P	"	210	90	21	-78.9		445 26,700	b,f
8P	"	175	75	24			350 21,000	b,f
9P	"	115	50	20				a
10P	290	115	50	22	-56.2	-120.0		a
11P	"	175	75	33			252 15,120	b
12P	"	115	50	20				a
13P	"	210	90	25	-60.0		136 8,160	c
14P	"	175	75	21			278 16,680	b,f
15P	"	115	50	20				a
16P	"	175	75	32	-63.7		448 26,880	d
17P	"	210	90	29			101 6,060	b
18P	"	210	90	21			11 660	b
19P	250	105	50	25	-54.6	-116.3	649 38,940	e
20P	"	155	75	27			177 10,620	b
21P	"	185	90	30			91 5,460	c
22P	"	155	75	20	-55.0		78 4,680	b
23P	"	105	50	32			565 33,900	d,f
24P	"	185	90	31			5 300	c
25P	"	185	90	30			36 2,160	b
26P	"	155	75	31			91 546	c
27P	"	105	50	21	-50.3			a

TABLE XXXVI (Cont'd)

Specimen	Nominal H.T. Strength (psi x 10 ⁻³)	Stress Level (psi x 10 ⁻³)	Per Cent Yield Strength	Surface Roughness (RHR)	Residual Surface Stresses (psi x 10 ⁻³)		Residual Surface Stresses (psi x 10 ⁻³)		Time to Failure Avg.Hr.	Avg.Min.	Remarks
					BVB	AVB	BVB	AVB			
29P	224	95	50	31					924	55,440	a
30P	"	150	75	21					403	24,180	d
31P	"	175	90	22	-47.9	-82.3			1,000	60,000	d
32P	"	150	75	33							d
33P	"	95	50	30							a
34P	"	175	90	33	-46.5				671	40,260	d
35P	"	175	90	34					660	39,400	c
36P	"	95	50	20					884	53,040	a
37P	"	150	75	24	-55.7						e

BVB Before Vapor Blasting

AVB After Vapor Blasting

- a No failure in 1,000 hour test
b Failure originated at trailing edge of tension surface
c Failure originated in center section of tension surface
d Failure originated at leading edge of tension surface
e Not possible to determine origin of failure
f Failed outside test area but more than 1.50 inches from specimen ends

TABLE XXXVII

Smooth Tensile Properties of H-11
(Billet V)

<u>Specimen</u>	<u>Hardness Rockwell C</u>	<u>Ultimate Strength (psi x 10⁻³)</u>	<u>Yield Strength 0.2% Offset (psi x 10⁻³)</u>	<u>Per Cent Reduction in Area</u>	<u>Per Cent Elongation in 1 inch</u>
SV1	57	310.8	249.3	4.1	4
SV5	56.5	294.4	231.5	16.5	6
SV9	57	304.3	281.6	21.1	7
SV2	57	282.1	269.3	3.1	1
SV6	57.5	299.2	249.9	6.8	4
SV10	57	298.4	275.7	1.6	2
SV3	57	303.1	247.4	9.6	4
SV7	57	306.7	254.6	10.3	5
SV11	57	308.9	280.0	14.6	6
SV4	49	233.7	200.8	27.4	8
SV8	51	234.6	202.7	33.1	10
SV12	51	237.1	201.7	31.6	5

TABLE XXXVIII

Notched Tensile Properties of H-11
(Billet V)

Notched Specimen	Rockwell C	Notched Radius (in.)	Ultimate Strength (psi x 10 ⁻³)	K _{Ic} ^a (psi in. ^{1/2}) (x 10 ⁻³)	Notched Unnotched (NV1 etc.) SV1
NV1	55.5	.001	215.0	44.4	.694
NV5	55.7	.0022	180.7	37.2	.612
NV9	54.0	.0007	205.3	42.3	.674
					Avg. = .660
NV2	56.5	.0021	179.0	36.9	.635
NV6	55.5	.0009	189.0	39.1	.634
NV10	56.5	.001	160.6	33.1	
					Avg. = .635
NV3	55.0	.0009	201.6	41.6	.664
NV7	56.0	.0008	202.5	41.8	.660
NV11	57.0	.0008	155.1	32.0	
					Avg. = .662
NV4	47.5	.0011	255.7	>41.5	1.09
NV8	49.0	.0015	294.8	>41.5	1.25
NV12	48.7	.0009	290.8	>41.9	1.24
					Avg. = 1.19

$$K_{Ic}^a \geq 0.233 \sigma_u \sqrt{\pi D}$$

TABLE XXXIX

Testing Times of H-11 Specimens
(Billet V)

Specimen	Nominal H.T. Strength (psi x 10 ⁻³)	Stress Level (psi x 10 ⁻³)	Per Cent Yield Strength	Surface Roughness (RHR)	Residual Surface Stresses (psi x 10 ⁻³)	Time to Failure		Remarks
						Avg. Hr.	Avg. Min.	
1V	300	125	50	26	-168.5	128	7,680	a
2V	"	185	75	27		3	180	a, d
3V	"	225	90	30		2	120	c
4V	"	185	75	28	-155.2	3	180	a, c, d
5V	"	125	50	28		79	4,740	c, e
6V	"	225	90	27		1	60	c
7V	"	225	90	33	-130.5	6	360	c
8V	"	185	75	26		5	330	a
9V	"	125	50	26		160	9,600	a
10V	290	125	50	25	-146.0	17	1,020	c
11V	"	185	75	27		3	180	c
12V	"	125	50	27		47	2,820	a
13V	"	225	90	29	-173.9	3	210	a
14V	"	185	75	28		3	180	c
15V	"	125	50	32		11	660	c
16V	"	185	75	32	-149.7	18	1,080	a
17V	"	225	90	32		1	60	a
18V	"	225	90	27		2	90	a
19V	306	125	50	32	- 97.1	131	7,860	a
20V	"	185	75	26		82	4,920	a
21V	"	225	90	30		10	600	a
22V	"	185	75	32	-136.3	50	3,000	c
23V	"	125	50	32		195	11,700	a
24V	"	225	90	32		18	1,080	a
25V	"	225	90	32	-111.1	13	780	a
26V	"	185	75	32		37	2,220	a
27V	"	125	50	32		323	19,380	a

TABLE XXXIX (Cont'd)

Specimen	Nominal H.T. Strength (psi x 10 ⁻³)	Stress Level (psi x 10 ⁻³)	Per Cent Yield Strength	Surface Roughness (RHR)	Residual Surface Stresses (psi x 10 ⁻³)	Time to Failure Avg. Hr.	Avg. Min.	Remarks
28V	235	100	50	27	-141.7			f
29V	"	150	75	32				f
30V	"	180	90	28				f
31V	"	150	75	32	-123.6			f
32V	"	100	50	35				f
33V	"	180	90	32		957	57,100	b
34V	"	180	90	27	- 94.2			f
35V	"	100	50	32				f
36V	"	150	75	32				f

- a Origin located in trailing edge of specimen
 b Origin located in leading edge of specimen
 c Origin located in center of specimen
 d Two origins formed
 e Three origins formed
 f No failure in 1,000 hours of testing

TABLE XL

Smooth Tensile Properties of 4330M
(Billet R)

<u>Specimen</u>	<u>Hardness Rockwell C</u>	<u>Ultimate Strength (psi x 10⁻³)</u>	<u>Yield Strength 0.2% Offset (psi x 10⁻³)</u>	<u>Per Cent Reduction in Area</u>	<u>Per Cent Elongation in 2 inches</u>
SR1	49.5	250.3	205.5	19.2	9
SR5	49.2	249.6	204.9	10.0	6
SR9	48.2	250.9	205.1	12.2	8
SR2	46.5	227.8	195.1	7.8	6
SR6	45.7	228.2	196.0	24.9	8
SR11	46.0	226.1	193.5	13.7	7
SR3	43.4	202.5	185.0	15.8	5
SR7	43.0	202.7	185.4	27.9	9
SR10	42.8	202.3	184.4	30.4	10
SR4	41.3	188.4	173.5	17.8	9
SR8	42.0	188.9	175.3	27.0	11
SR12	42.2	186.9	174.0	14.3	7

TABLE XLI

Notched Tensile Properties of 4330M
(Billet R)

Specimen	Rockwell C	Notch Radius (in.)	Ultimate Strength (psi x 10 ⁻³)	K _{IC} ^a (psi in ^{1/2})	Notched Unnotched (NPL etc.) SPL
NR1	48.5	.0009	271.1	> 42.3	1.08
NR5	48.5	.001	274.8	> 42.2	1.10
NR9	48.2	.0009	271.6	> 42.3	1.08
					Avg. = 1.09
NR2	46.5	.0009	246.9	> 40.4	1.08
NR6	46.2	.0013	257.6	> 40.6	1.12
NR11	44.5	.0009	265.3	> 40.0	1.17
					Avg. = 1.12
NR3	43.5	.0012	227.6	> 38.3	1.14
NR7	42.5	.001	243.9	> 38.4	1.20
NR10	42.5	.0011	242.0	> 38.2	1.19
					Avg. = 1.18
NR4	40.5	.0008	256.1	> 35.8	1.36
NR8	41.2	.0011	254.5	> 36.1	1.36
NR12	40.5	.0011	256.4	> 35.8	1.37
					Avg. = 1.36

$$K_{IC}^a \geq 0.233 \sigma_u \sqrt{\pi D}$$

TABLE XLII

Testing Times of 4330M Specimens
(Billet R)

Specimen	Nominal H.T. Strength (psi x 10 ⁻³)	Stress Level (psi x 10 ⁻³)	Per Cent Yield Strength	Surface Roughness (RHR)	Residual Surface Stresses (psi x 10 ⁻³)		Time to Failure Avg.Hr. Avg.Min.	Remarks	
					BVB	AVB			
1R	250	105	50	22	-74.6			a	
2R	"	155	75	15				a	
3R	"	185	90	17			529	31,740	b, d
4R	"	155	75	23	-58.4	-119.7			a
5R	"	105	50	22					a
6R	"	185	90	22			720	43,200	b, d
7R	"	185	90	24	-54.1	- 76.8	720	43,200	b, d
8R	"	155	75	25			816	48,960	b, d
9R	"	105	50	24					a
10R	227	95	50	22		-107.6			a
11R	"	140	75	25			487	29,220	b
12R	"	95	50	21					a
13R	"	170	90	25		-130.3	144	8,650	c
14R	"	140	75	21			76	4,560	b
15R	"	95	50	25					a
16R	"	140	75	22		-119.9	770	46,200	b
17R	"	170	90	23			480	28,800	b
18R	"	170	90	21			434	26,000	c
19R	202	90	50	23		-114.7			a
20R	"	135	75	18					a
21R	"	165	90	21			876	52,560	b
22R	"	135	75	25		-120.0			a
23R	"	90	50	21					a
24R	"	165	90	22			335	20,100	b
25R	"	165	90	22		-116.0	940	56,400	c
26R	"	135	75	23					a
27R	"	90	50	23					a

TABLE XLII (Cont'd)

Specimen	Nominal H.T. Strength (psi x 10 ⁻³)	Stress Level (psi x 10 ⁻³)	Per Cent Yield Strength	Surface Roughness (RHR)	Residual Surface Stresses (psi x 10 ⁻³)		Time to Failure Avg.Hr.	Remarks
					BVB	AVB		
28R	188	85	50	22		-108.0		a
29R	"	130	75	20				a
30R	"	155	90	22				a
31R	"	130	75	20		-130.0		a
32R	"	85	50	22				a
33R	"	155	90	20				a
34R	"	155	90	20		-105.0		a
35R	"	85	50	18				a
36R	"	130	75	25				a

BVB Before Vapor Blasting

AVB After Vapor Blasting

- a No failure in 1,000 hours
b Failure origin near trailing edge of tension surface
c Failure origin near leading edge of tension surface
d Failed outside test area but more than 1.50 inch from specimen end

TABLE XLIII

Testing Times of Cadmium Plated or
Painted Center Hole 4340 Specimens
(Billet N)

Specimen	Nominal H.T. Strength (psi x 10 ⁻³)	Stress Level (psi x 10 ⁻³)	Per Cent Yield Strength	Residual Surface Stresses* (psi x 10 ⁻³)	Protective Coating	Time to Failure Avg. Hr. Avg. Min.	Remarks
28N	276	200	90	-128.0	a, c	146	e, f
29N	"	165	75		a, c	90	e, f
30N	"	110	50		a, c		k
31N	"	110	50		a, c		k
32N	"	200	90		a, c	430	e, f
33N	"	165	75		a, c	310	e, g, j
34N	"	110	50		a, c		k
35N	"	200	90		a, c	810	f
36N	"	165	75		a, c		k
37N	276	110	50		a, d		k
38N	"	165	75		a, d	528	h
39N	"	200	90	-115.0	a, d	918	g, h
40N	"	110	50		a, d		k
41N	"	165	75		a, d		k
42N	"	200	90		a, d	167	f
43N	"	110	50		a, d		k
44N	"	165	75		a, d	960	i, j
45N	"	200	90	-122.0	a, d	84	e, f, j
46N	276	110	50		b, d		k
47N	"	200	90		b, d	210	f
48N	"	165	75		b, d	310	g, h
49N	"	200	90		b, d		k
50N	"	110	50		b, d		k
51N	"	165	75	-106.0	b, d		k
52N	"	110	50		b, d		k
53N	"	200	90		b, d		k
54N	"	165	75		b, d		k

TABLE XLIII (Cont'd)

•	Before plating or painting
a	Cadmium plated surface
b	Painted surface
c	Center hole empty
d	Cadmium plated bolt through hole
e	Origin not outlined by rust ring
f	Failure originated at interface between base metal and protective coating.
g	Origin at trailing edge
h	Failed outside test area
i	Due to rust coating not possible to determine fracture origin point
j	Failed in test area but not through bolt hole
k	No failure in 1000 hours

TABLE XLIV

Smooth Tensile Properties of
Air Melt (VNB) and Vacuum Melt (VVB) 4330M

<u>Specimen</u>	<u>Hardness Rockwell C</u>	<u>Ultimate Strength (psi x 10⁻³)</u>	<u>Yield Strength 0.2% Offset (psi x 10⁻³)</u>	<u>Per Cent Reduction in Area</u>	<u>Per Cent Elongation in 2 inches</u>
SVVB1	45.5	225.1	190.6	47.2	12
SVVB2	45.5	227.3	192.0	49.4	12
SVVB3	45.0	226.0	191.2	46.7	12
SVVB4	45.5	225.6	189.4	46.4	12
SVVB5	45.5	224.9	190.9	51.3	12
SVNB1	45.0	226.3	194.7	53.2	13
SVNB2	45.5	228.9	195.5	54.5	13
SVNB3	45.5	225.6	195.3	54.3	13
SVNB4	46.0	224.0	192.6	55.1	13
SVNB5	45.0	224.9	192.6	54.8	13

TABLE XLV

Notch Tensile Properties of
Air Melt (VNB) and Vacuum Melt (VVB) 4330H

Specimen	Hardness Rockwell C	Notch Radius (inches)	Ultimate Strength (psi x 10 ⁻³)	K _{Ic} [°] (psi in ¹ / ₂) (x 10 ⁻³)	Notched Unnotched (NVVB1 etc.) SVVB1
NVVB1	46	.0004	297.2	> 39.5	1.32
NVVB2	45.5	.0005	298.2	> 40.2	1.31
NVVB3	45.5	.0007	294.8	> 39.6	1.30
NVVB4	46.0	.0006	299.8	> 39.2	1.31
NVVB5	45.5	.0005	299.3	> 39.5	1.33
NVNB1	45.5	.0005	297.6	> 40.4	1.31
NVNB2	46	.0006	298.4	> 40.5	1.30
NVNB3	46	.0005	302.8	> 40.5	1.34
NVNB4	46	.0006	288.1	> 40.0	1.28
NVNB5	45.5	.0005	298.4	> 40.0	1.33

$$K_{Ic}^{\circ} \geq 0.233 \sigma_u \sqrt{\pi D}$$

TABLE XLVI

Testing Times of Air Melt (VNB) and Vacuum Melt (VVB)
4330M Specimens

Specimen	Nominal H.T. Strength (psi x 10 ⁻³)	Stress Level (psi x 10 ⁻³)	Per Cent Yield Strength	Surface Roughness (RHR)	Residual Surface Stresses (psi x 10 ⁻³)		Time to Failure		Remarks
					AVB*		Avg. Hr.	Avg. Min.	
1VNB	225	170	90	35	-123.0		655	39,300	a
2VNB	225	170	90	35			480	28,800	a
3VNB	225	170	90	30			480	28,800	a
1VVB	225	170	90	30	- 85.6		800	48,000	b
2VVB	225	170	90	35			625	31,500	a, b
3VVB	225	170	90	34			840	50,400	a

* AVB After Vapor Blasting

- a Failure originated at leading edge
- b Failure originated at trailing edge

TABLE XLVII

Testing Times of AM 355 Specimens

Specimen	Condition	Nominal Heat Treat Strength (psi x 10 ⁻³)	Stress Level (psi x 10 ⁻³)	Per Cent Yield Strength	Surface Roughness (RHR)	Residual Surface Stresses (psi x 10 ⁻³)	Time to Failure (Hr.)	Remarks
1 (plate)	SCT 850 a	215	160	90	30		7½ - 22	c
2 "	" a	"	"	"	40		29 - 48	c
3 "	" a	"	"	"	53		7½ - 22	c
A (billet)	SCT 850 b	220	120	75	22	-23.6		d
B "	" b	"	"	"	16	-26.0		d
C "	" b	"	"	"	17	-22.0		d
D "	" a	"	"	"	18	-10.3		d
E "	" a	"	"	"	18	-44.3		d
F "	" a	"	"	"	21	-30.0		d

a Standard heat treat procedure

b Modified heat treat procedure

c Failure originated at corner of tension surface

d No failure in 1000 hours

TABLE XLVIII

Tensile Properties of AM 355

<u>Specimen</u>	<u>Ultimate Strength (psi x 10⁻³)</u>	<u>Yield Strength (psi x 10⁻³)</u>	<u>Per Cent Elongation in 1 inch</u>	<u>Per Cent Reduction in Area</u>
Plate 1-1	214.8	174.8	14	3
" 1-2	217.2	177.2	14	3.3
" 1-3	217.3	177.0	14	2.9
Billet A1	220.4	184.4	13	45.1
" A2	221.3	186.9	16	44.3
" A3	222.9	190.2	14	43.4
" D1	221.3	183.6	14	41.8
" D2	222.4	189.8	13	43.9
" D3	219.0	178.5	15	40.5

TABLE XLIX

Smooth Tensile Properties of AM 350
(Billet Y)

<u>Specimen</u>	<u>Material Condition</u>	<u>Hardness Rockwell C</u>	<u>Ultimate Strength (psi x 10⁻³)</u>	<u>Yield Strength 0.2% Offset (psi x 10⁻³)</u>	<u>Per Cent Reduction in Area</u>	<u>Per Cent Elongation in 2 inches</u>
SY1	DA 850	38.6	168.7	140.7	30.0	17
SY5	"	39.0	169.3	140.1	16.8	13
SY9	"	37.0	168.0	138.1	18.5	14
SY2	SCT 850	44.6	200.5	160.9	12.7	7
SY4	"	44.1	200.1	161.5	8.2	6
SY10	"	43.0	203.7	158.8	7.9	7
SY3	SCT 1050	35.7	169.6	148.0	36.5	15
SY7	"	37.0	173.9	154.7	42.6	16
SY8	"	37.8	170.7	148.3	36.5	15

TABLE I

Notched Tensile Properties of
AM 350 (Billet Y)

Specimen	Condition	Rockwell C	Notch Radius (inches)	Ultimate Strength (psi x 10 ⁻³)	K _{Ic} [°] (psi in ^{1/2})	Notched Unnotched (NY1 etc.) SYL
NY1	DA 850	37.2	.0008	198.4	> 29.0	1.17
NY5	"	37.0	.0009	171.3	> 28.9	1.01
NY9	"	37.4	.0013	169.4	> 28.5	1.01
						Avg. = 1.06
NY2	SCT 850	43.5	.0009	164.2	> 33.2	.82
NY4	"	44.0	.0013	160.8	> 33.3	.80
NY10	"	44.2	.001	166.0	> 32.7	.83
						Avg. = .82
NY3	SCT 1050	35.7	.0011	208.9	> 30.6	1.23
NY7	"	37.0	.0011	217.9	> 31.9	1.25
NY10	"	37.8	.0011	220.9	> 30.8	1.29
						Avg. = 1.25

$$K_{Ic} \geq 0.233 \sigma_u \sqrt{\pi D}$$

TABLE LI

Testing Times of AM 350 Specimens
(Billet Y)

<u>Specimen</u>	<u>Nominal H.T. Strength (psi x 10⁻³)</u>	<u>Stress Level (psi x 10⁻³)</u>	<u>Per Cent Yield Strength</u>	<u>Surface Roughness (RHR)</u>	<u>Residual Surface Stress (psi x 10⁻³)</u>	<u>Time to Failure Avg. Hr. Avg. Min.</u>	<u>Remarks</u>
1Y	200	80	50	30	-56.7		b
2Y	"	120	75	27			b
3Y	"	145	90	35		310 18,600	a
4Y	"	120	75	32	-72.4		b
5Y	"	80	50	41			b
6Y	"	145	90	32			b
7Y	"	145	90	32	-69.0		b
8Y	"	120	75	32			b
9Y	"	80	50	35			b
10Y	168	70	50	30	-62.3		b
11Y	"	105	75	35			b
12Y	"	70	50	35			b
13Y	"	125	90	30	-67.0		b
14Y	"	105	75	32			b
15Y	"	70	50	30			b
16Y	"	105	75	40	-73.0		b
17Y	"	125	90	30			b
18Y	"	125	90	32			b
19Y	170	75	50	15	-57.4		b
20Y	"	115	75	16			b
21Y	"	135	90	15			b
22Y	"	115	75	15	-50.7		b
23Y	"	75	50	14			b
24Y	"	135	90	14			b
25Y	"	135	90	13	-24.2		b
26Y	"	115	75	12			b
27Y	"	75	50	12			b

a Origin located at trailing edge

b No failure in 1000 hours

TABLE LII

Smooth Tensile Properties of AM 350
(Sheet Z)

<u>Specimen</u>	<u>Rockwell C</u>	<u>Ultimate Strength[•] (psi x 10⁻³)</u>	<u>Yield Strength 0.2% Offset (psi x 10⁻³)</u>	<u>Per Cent Elongation in 1 inch</u>
SZ1	44	212.2	171.9	21.5
SZ2	44	204.7	174.0	20.5
SZ3	44	202.7	172.7	19.5
SZ4	44	196.1	166.9	20.5

• Transverse grain direction of 0.060" sheet

TABLE LIII

Notch Tensile Properties of AM 350 CRT 850
(Sheet Z)

<u>Specimen</u>	<u>Hardness Rockwell C</u>	<u>Notch Radius (inches)</u>	<u>Ultimate Strength* (psi x 10⁻³)</u>	<u>Notched Unnotched (NZ1 etc.) SZ1</u>
NZ1	45	.0003 - .0006	152.3	.719
NZ2	45	.0006 - .0007	170.8	.836
NZ3	45	.0003 - .0004	150.7	.745
NZ4	45	.0005 - .0007	157.8	.805
				Avg. = .776

* Transverse grain direction of 0.060" sheet

TABLE LIV

Testing Times of AM 350
(Sheet Z)

<u>Specimen</u>	<u>Nominal H.T. Strength (psi x 10⁻³)</u>	<u>Stress Level (psi x 10⁻³)</u>	<u>Per Cent Yield Strength</u>	<u>Surface Roughness (RHR)</u>	<u>Residual Surface Stress (psi x 10⁻³)</u>	<u>Time to Failure Avg. Hr. Avg. Min.</u>	<u>Remarks</u>
1Z	203	155	90	10			a
2Z	"	155	90	10			a
3Z	"	155	90	10	-46.2		a
4Z	"	130	75	10			a
5Z	"	130	75	10			a
6Z	"	130	75	10			a
7Z	"	85	50	10			a
8Z	"	85	50	10	-20.9		a
9Z	"	85	50	10			a

a No failure in 1000 hours

TABLE LV

Residual Surface Stress Levels in Surface Ground
Low Alloy Steel U-Bend Specimens

<u>Steel</u>	<u>Billet Designation</u>	<u>Residual Surface Stress (psi x 10⁻³)</u>	
		<u>Before Vapor Blasting</u>	<u>After Vapor Blasting</u>
4340	N	-20 to -40	-90 to -140
	K	-25 to -70	-70 to -150
4340M	P	-45 to -80	-80 to -120
H-11	V		-90 to -170
4330M	R	-55 to -75	-75 to -130

TABLE LVI

Average Times to Failure of Low Alloy Steels

Time to Failure
(avg. min.)

Heat Treat Strength (psi x 10 ⁻³)	4340										4330M				
	Martempered			Oil Quenched				4340M			H-11				
Above 300	90°	75°	50°	90	75	50	90	75	50	90	75	50	90	75	50
										(1000°F Temper)					
										800	3500	11,000			
										(600°F Temper)					
										174	250	6600			
280 - 300										(400°F Temper)			(800°F Temper)		
										1260	2150	b	126	500	1260
										(600°F Temper)					
										5000	20,000	b			
260 - 280	a	126	a	200	500	40,000									
250							2500	6800	b				a	b	b
220 - 240	a	250	a	200	500	27,600	35,500	50,000	b	b	b	b	21,150	26,660	b
200 - 220				22,200	b	b							43,030	b	b
175 - 200	b	b	b	b	b	b							b	b	b

• Stress level expressed as a percentage of the yield strength

a Not possible to determine an average time to failure

b Complete failure of all three specimens did not occur in 1000 hours of testing

TABLE LVII

Mode of Cracking in Low Alloy Steels
(Determined From Optical Microscopic Examination)

	Tempering Temperature (°F)					
	<u>400°</u>	<u>450°</u>	<u>600°</u>	<u>800°</u>	<u>870°</u>	<u>1000°</u> <u>1100°</u>
4340• Billet N		I+T	I		a	
4340 Billet K	I+T		I	I	a	
4340M Billet P	I+T		I+T	I		I
4330M Billet R	I+T		I+T	I	a	
H-11			I+T	I+T		I+T a.

a No Failures in 1000 hours

I Intergranular cracking

T Transgranular cracking

• Martempered

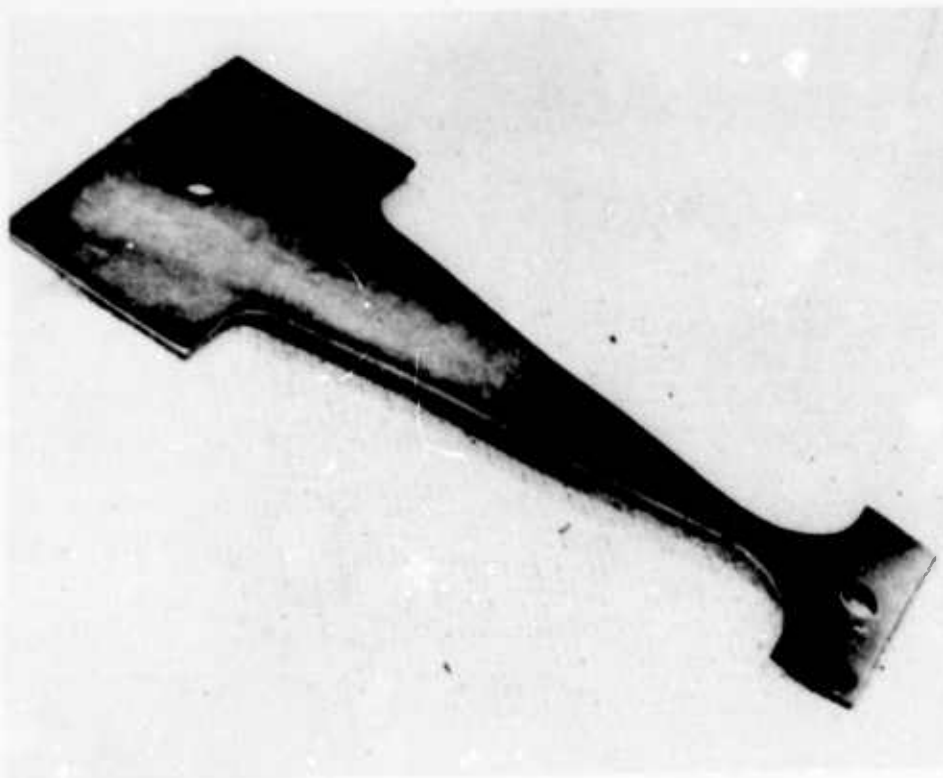


FIGURE 1
Cantilever Bend Specimen

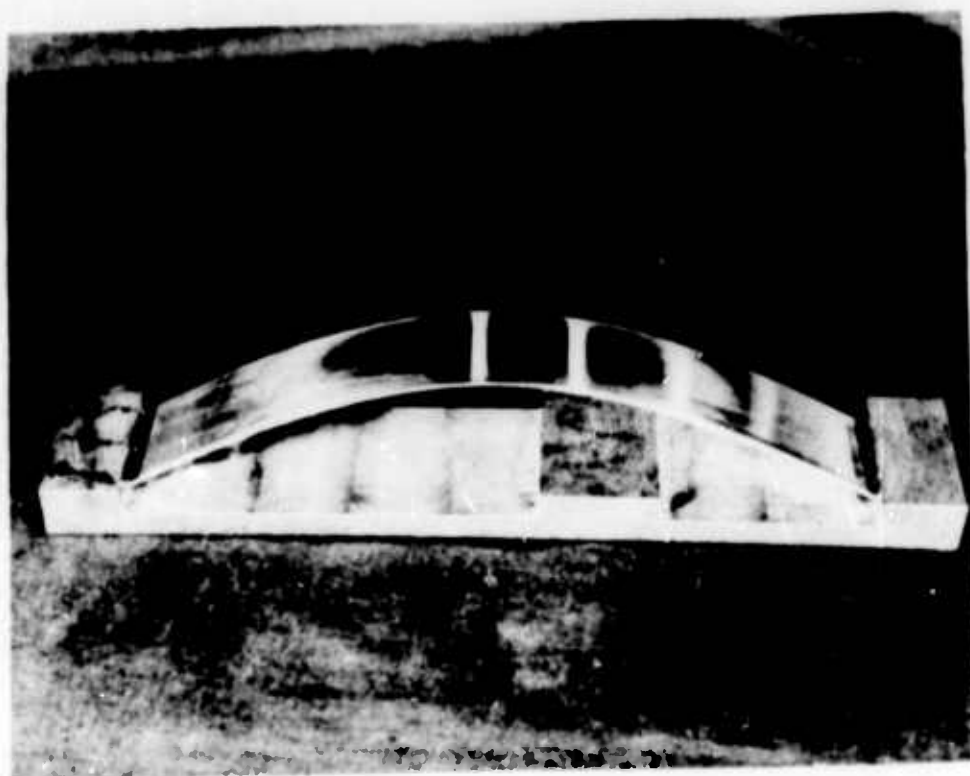


FIGURE 2
Phelps-Loginow Specimen

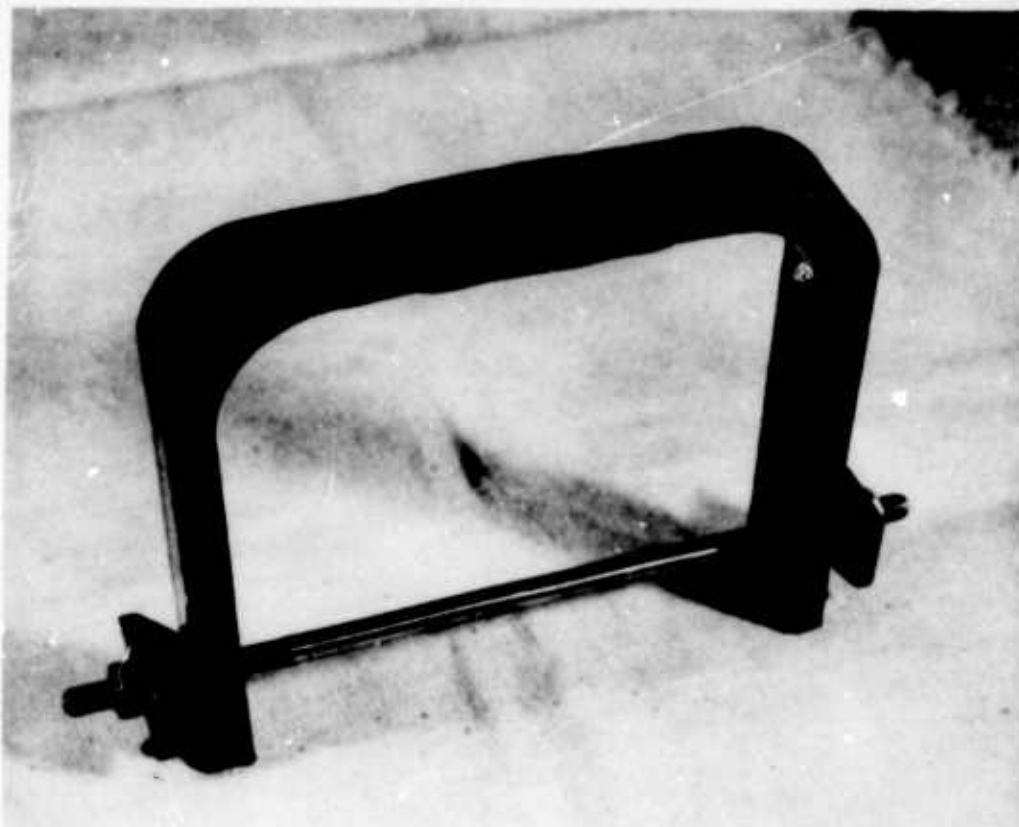


FIGURE 3
Boeing U-Bend Specimen-Original Configuration

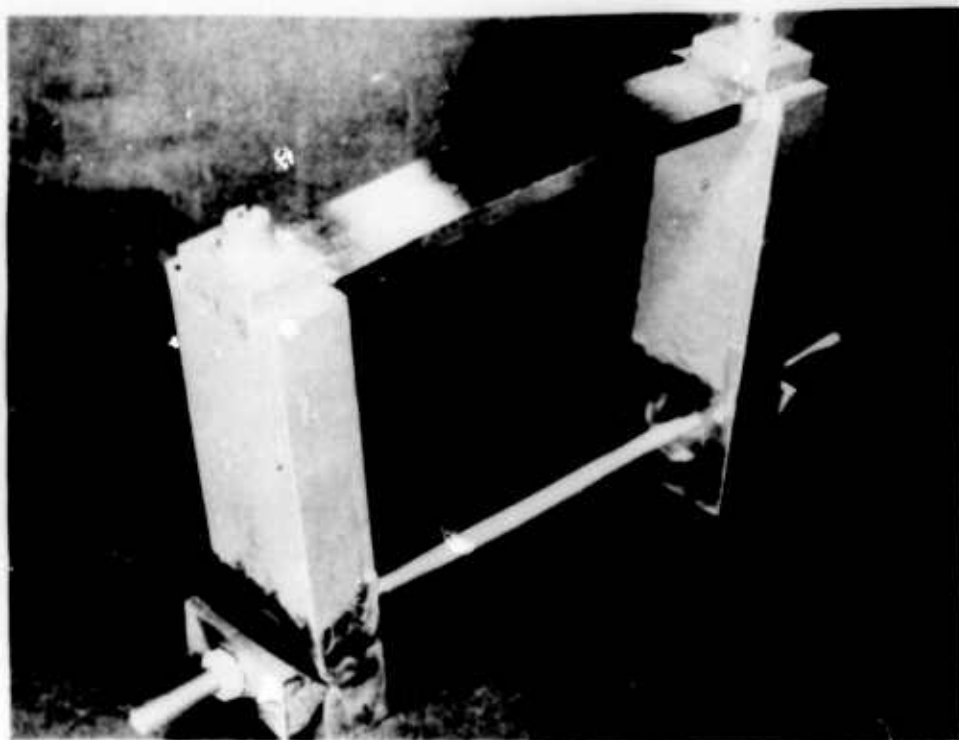


FIGURE 4a
Boeing U-Bend Specimen-Modified Configuration

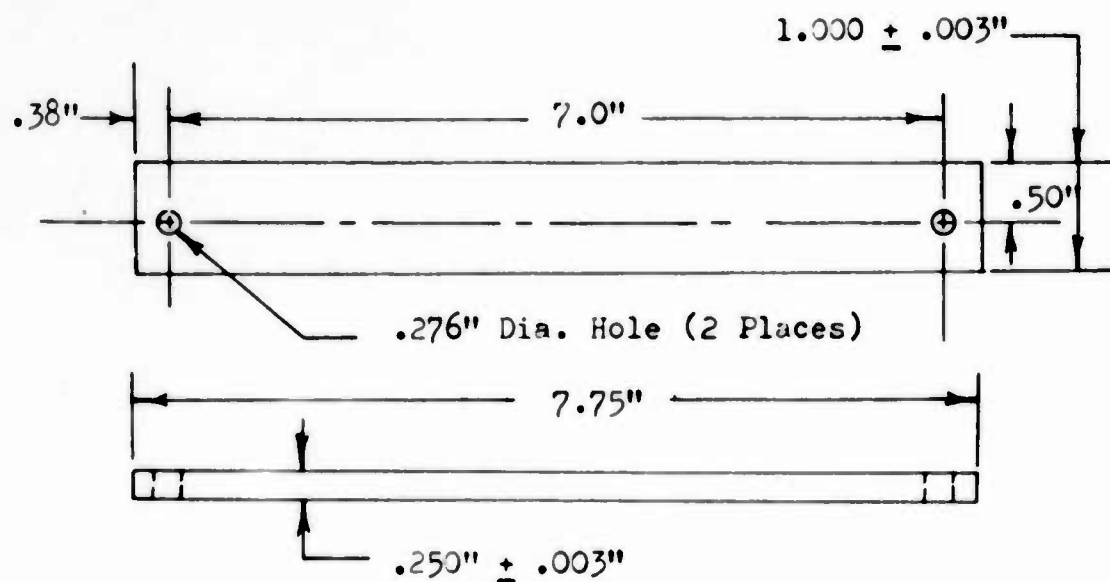


FIGURE 4b
Schematic of Modified Boeing U-Bend Specimen

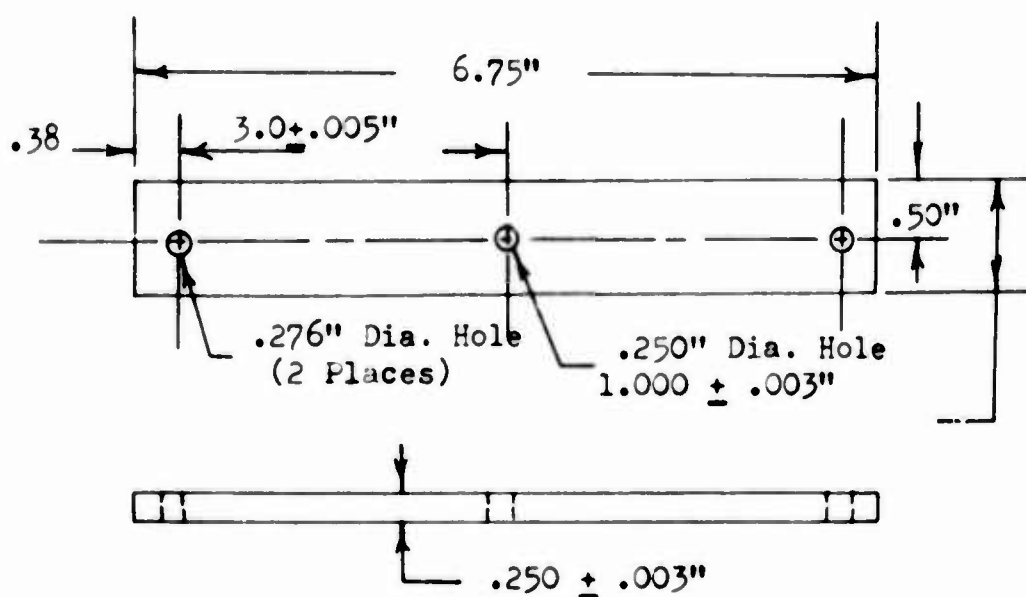


FIGURE 5
Boeing U-Bend Specimen with Center Hole

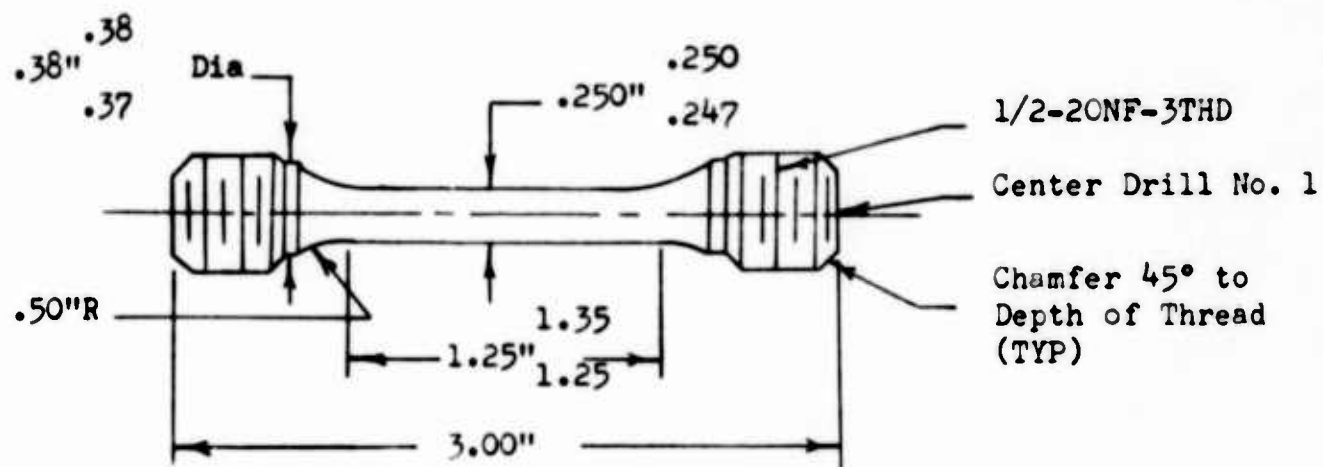


FIGURE 6
Billet Smooth Tensile Specimen (Round)

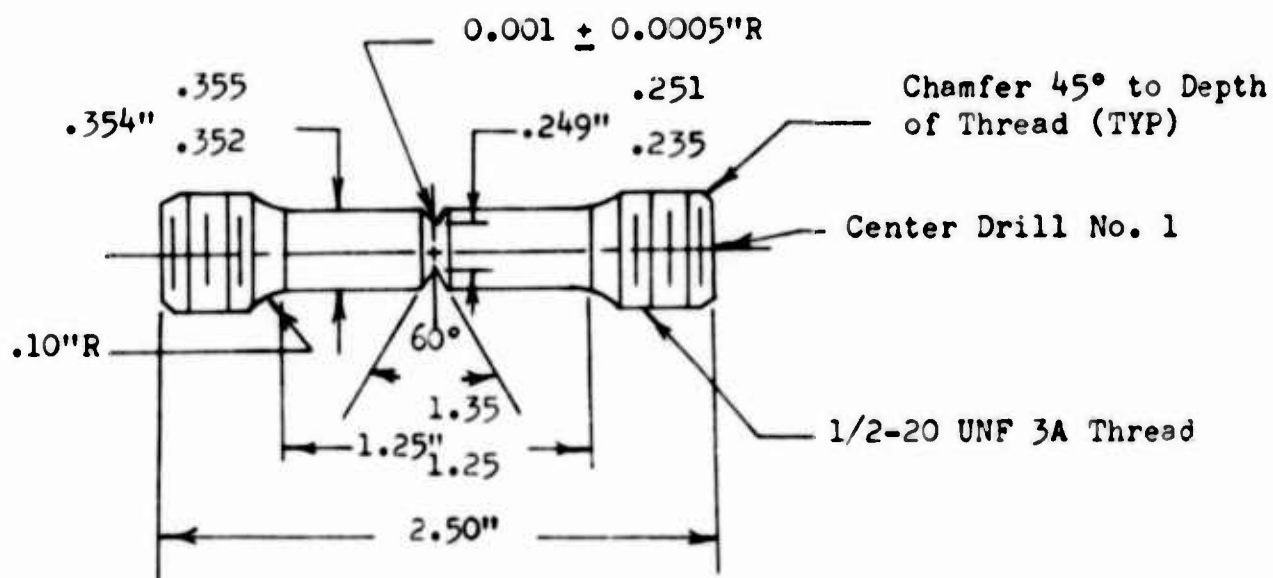


FIGURE 7
Billet Notched Tensile Specimen (Round)

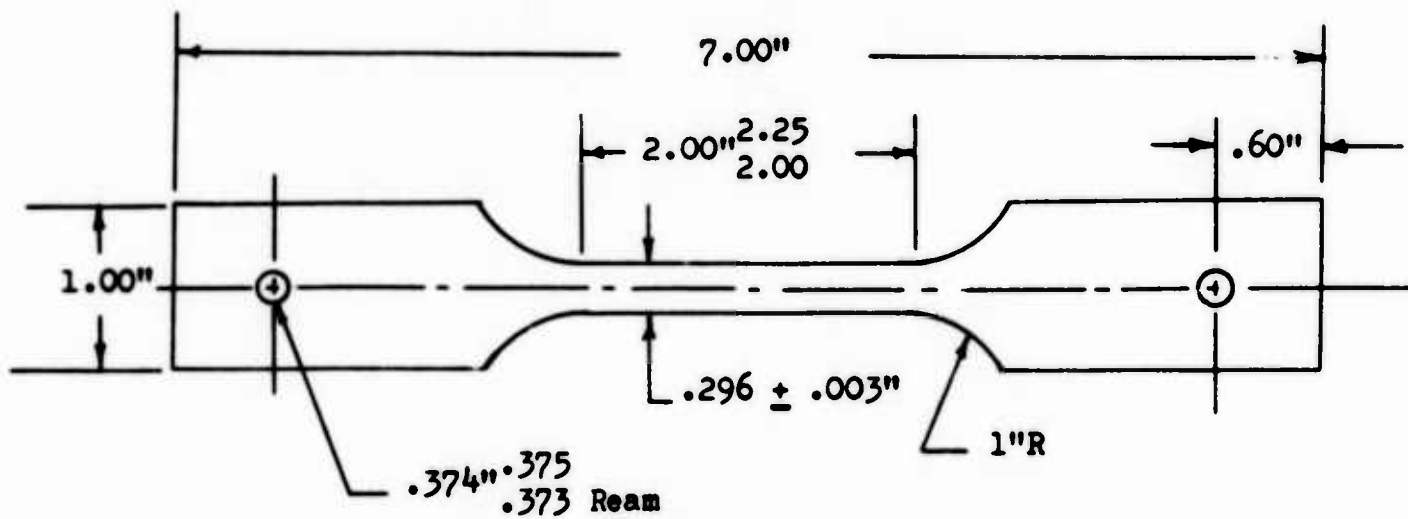


FIGURE 8
Sheet Stress Corrosion Specimen



FIGURE 9
Sheet Stress Corrosion Test Jig

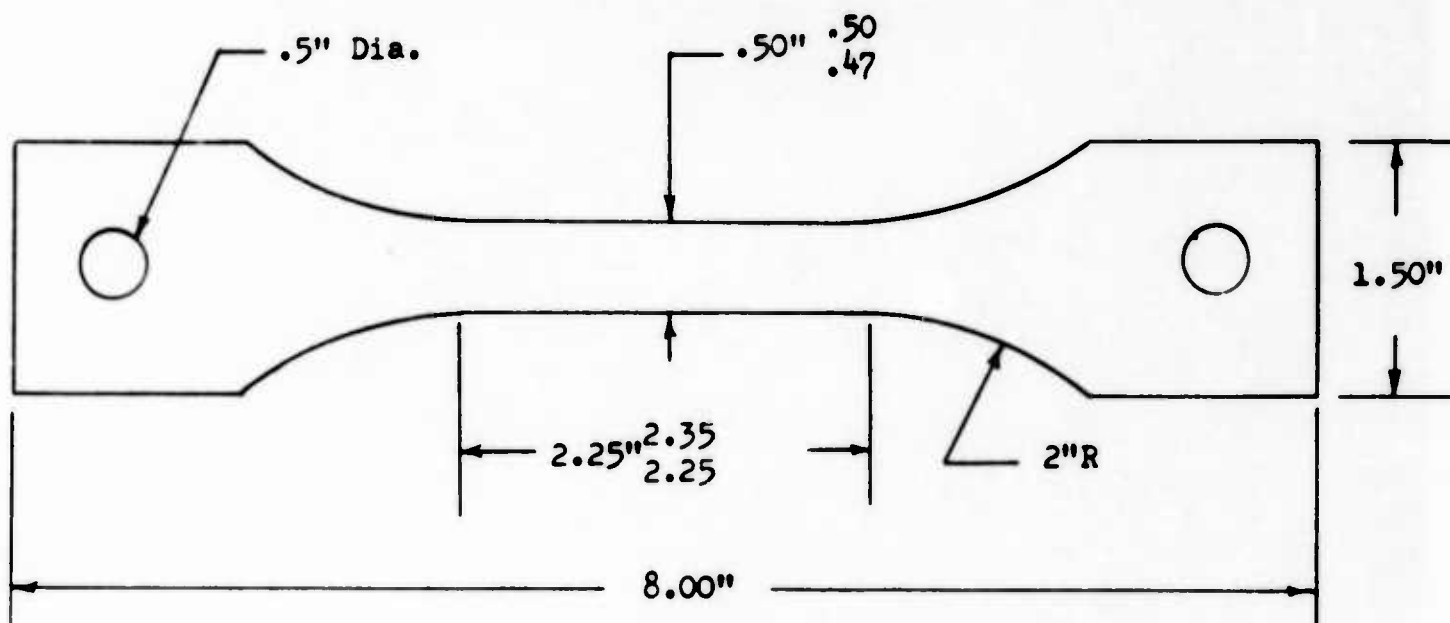


FIGURE 10

Sheet Smooth Tensile Specimen

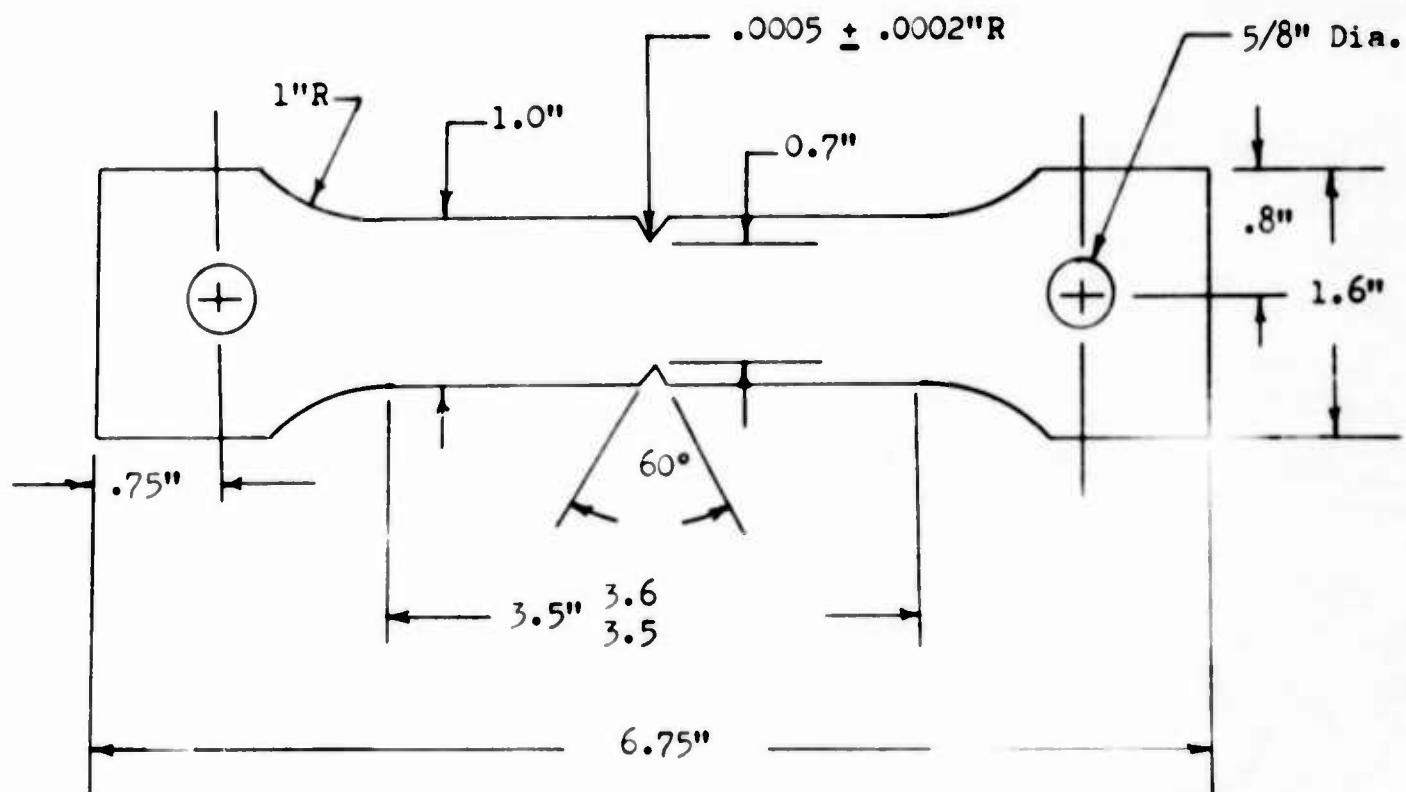


FIGURE 11

Sheet Notched Tensile Specimen

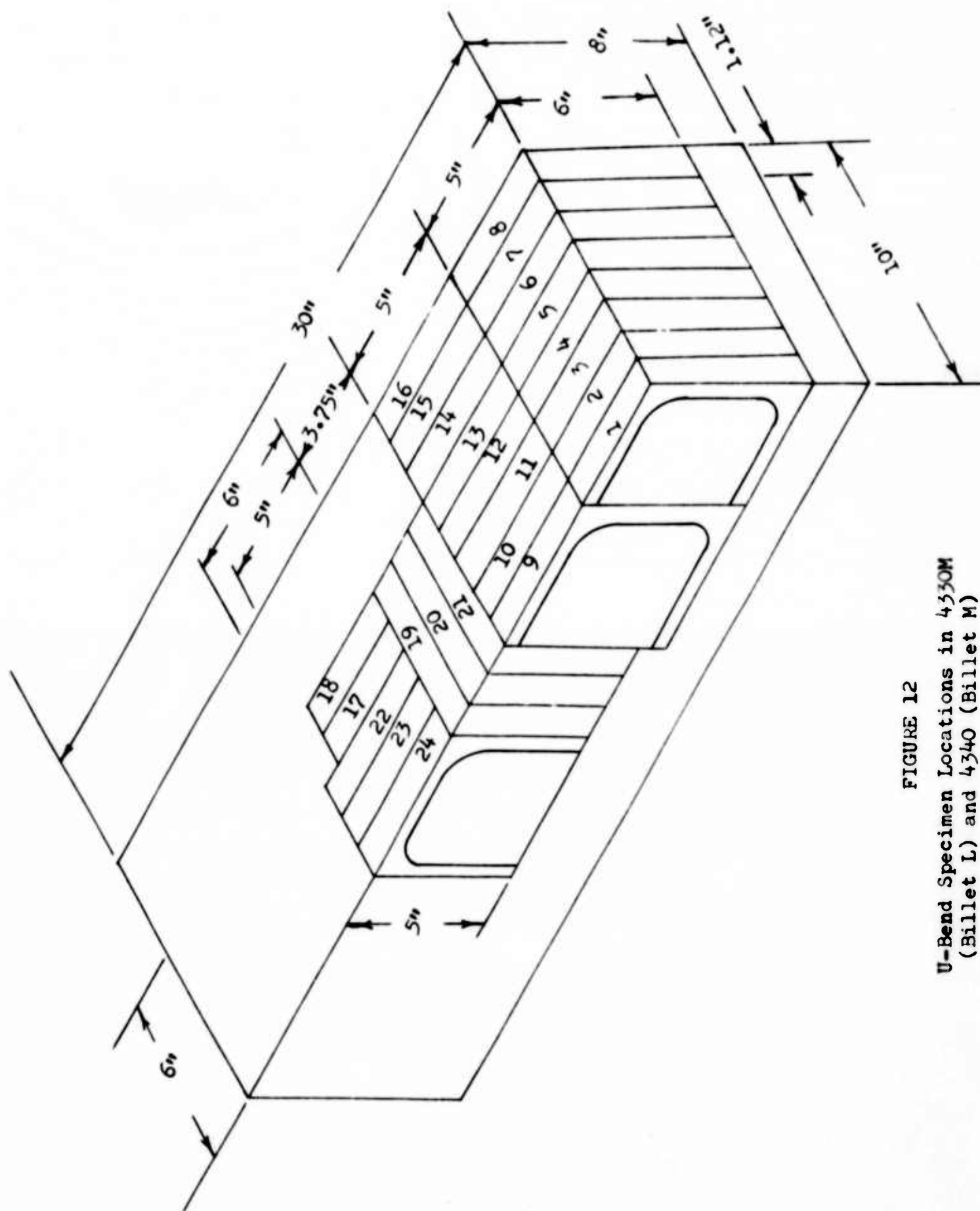


FIGURE 12
U-Bend Specimen Locations in 4330M
(Billet L) and 4340 (Billet M)

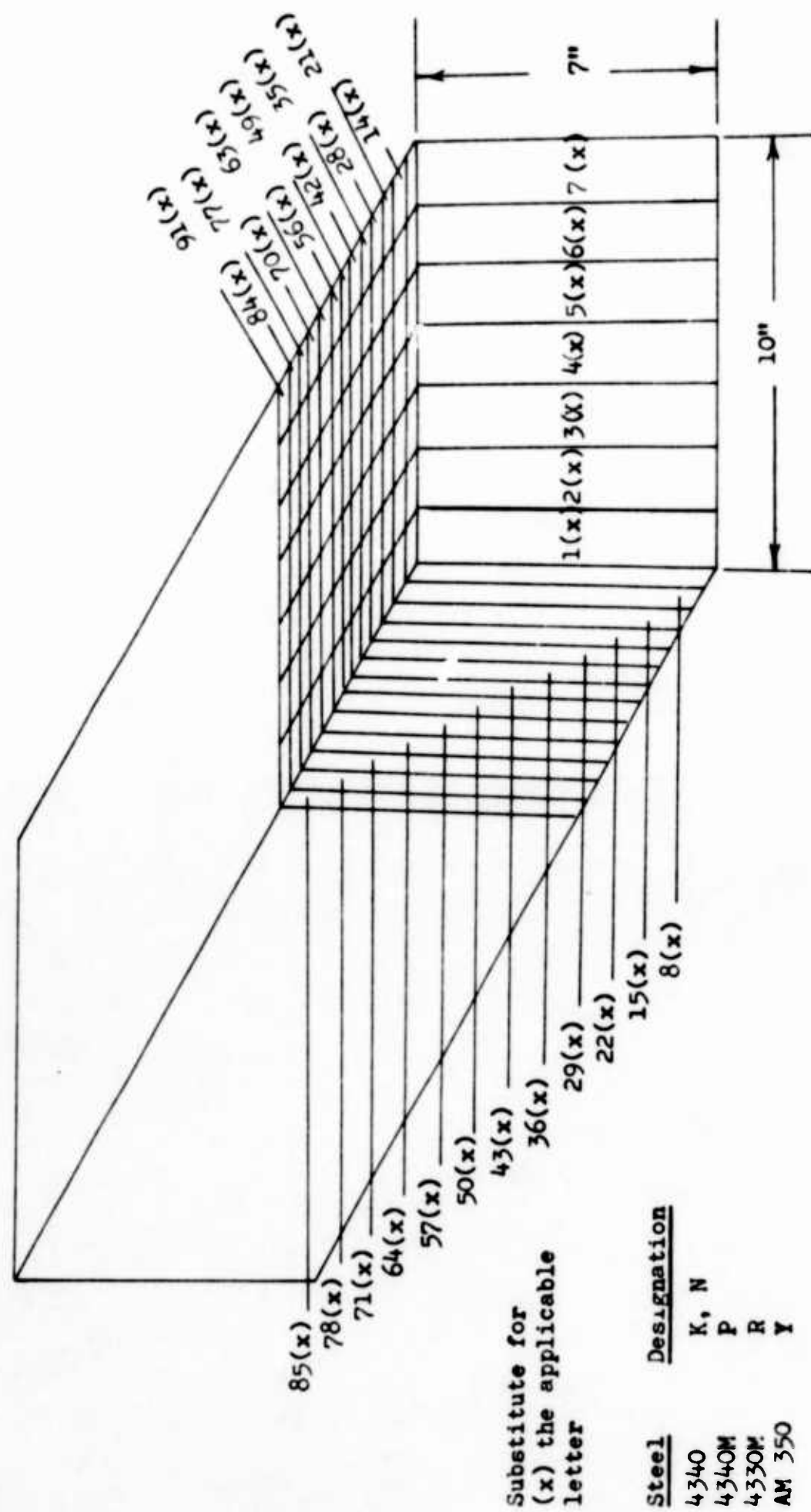


FIGURE 13. U-Bend Specimen Locations in 4340 (Billets K and N), 4340M (Billet P), 4330M (Billet R) and AM 350 (Billet Y)

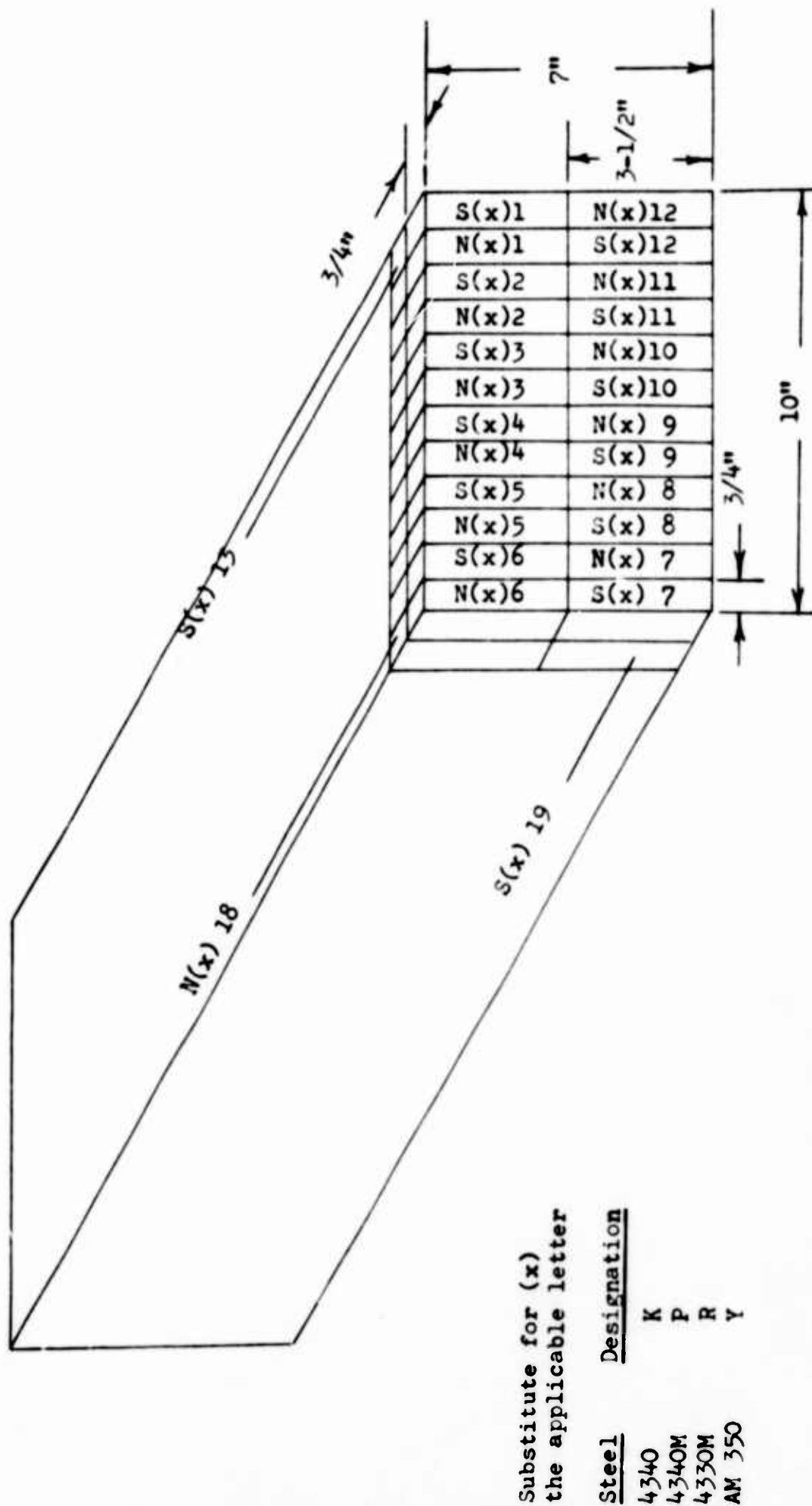


FIGURE 14. Tensile Specimen Locations in 4340 (Billet K), 4340M (Billet P), 4330M (Billet R), AM 350 (Billet Y)

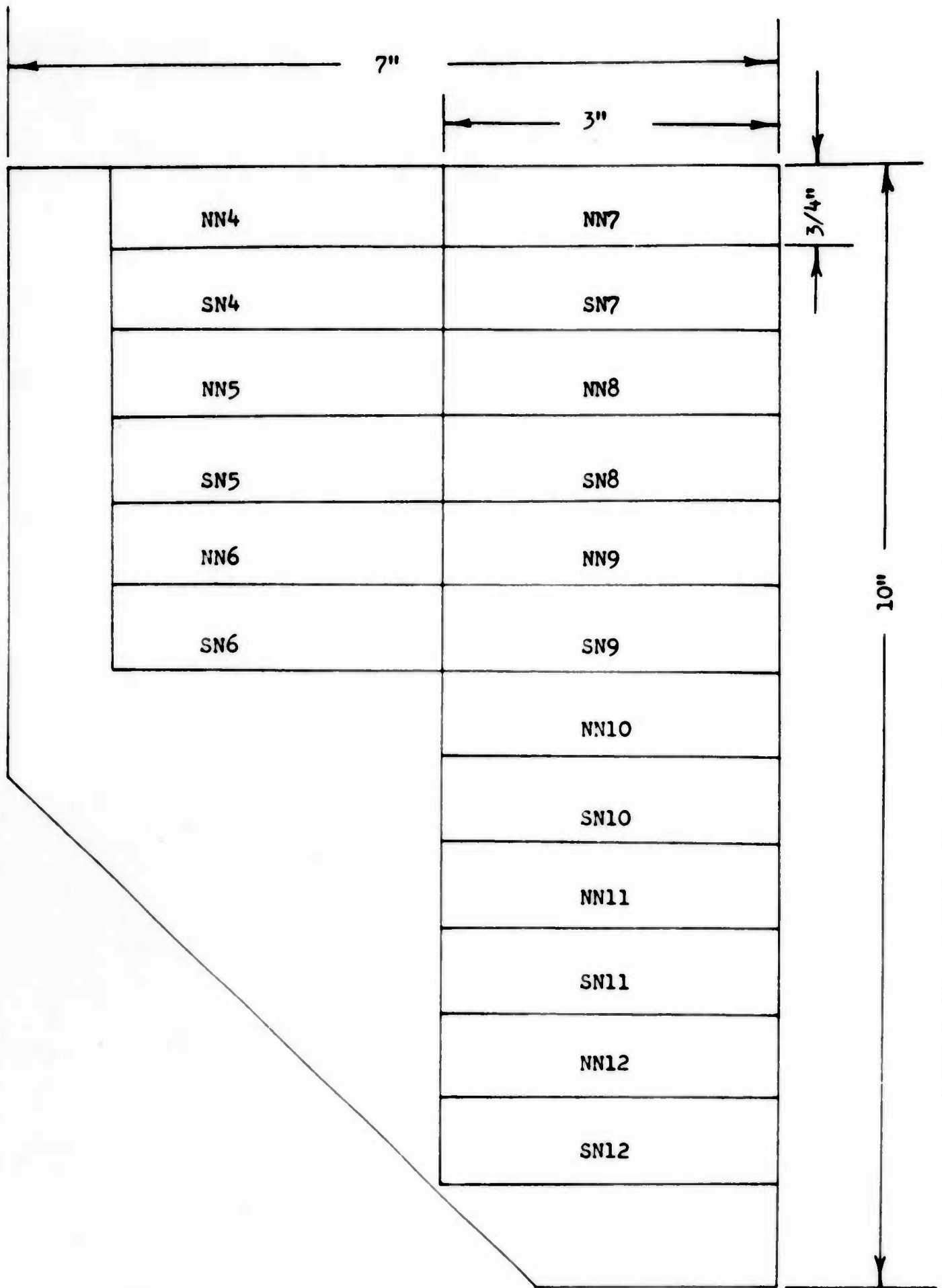


Figure 15. Tensile Specimen Locations in 4340 (Billet N)

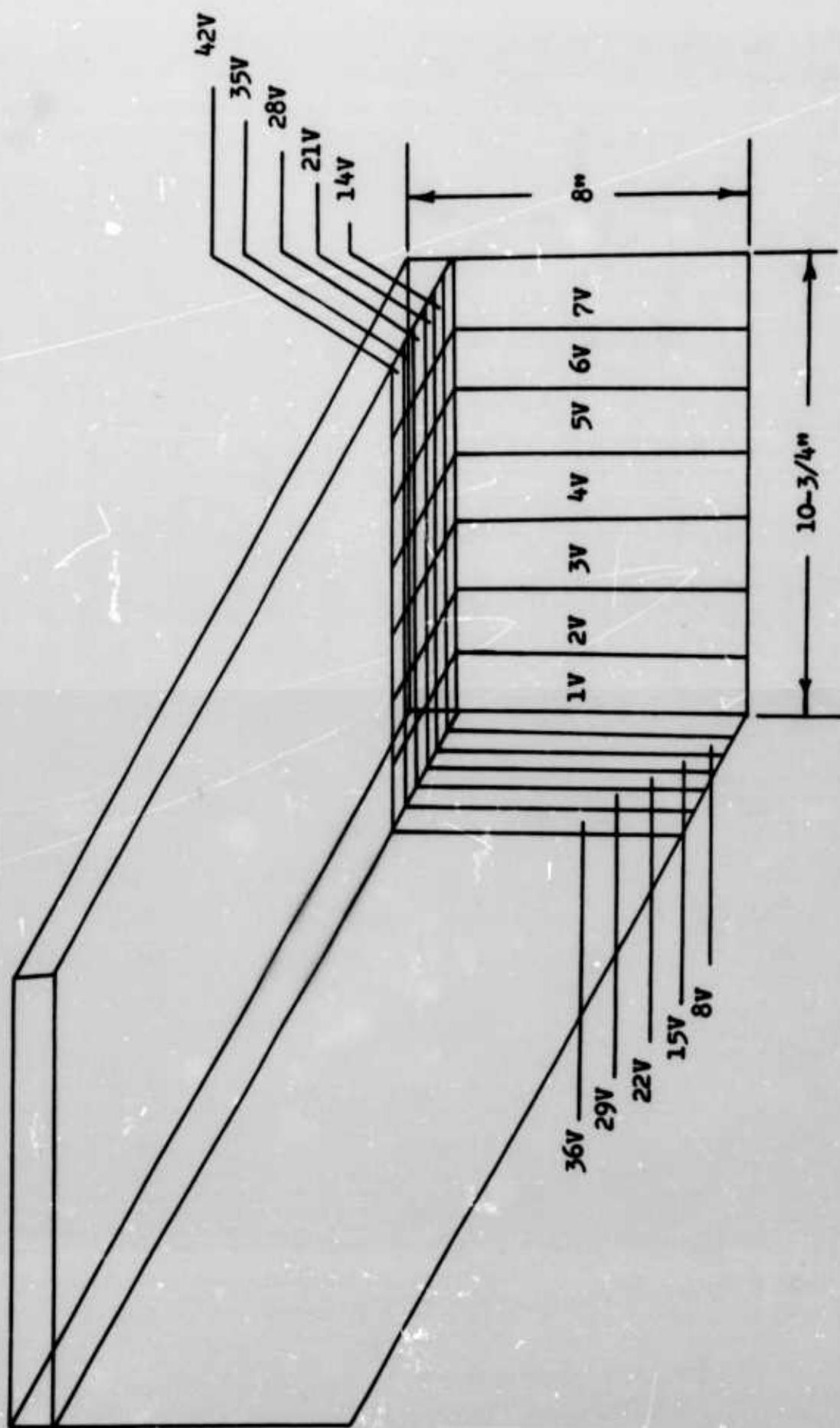


FIGURE 16. U-Bend Specimen Locations in H-11 (Billet V)

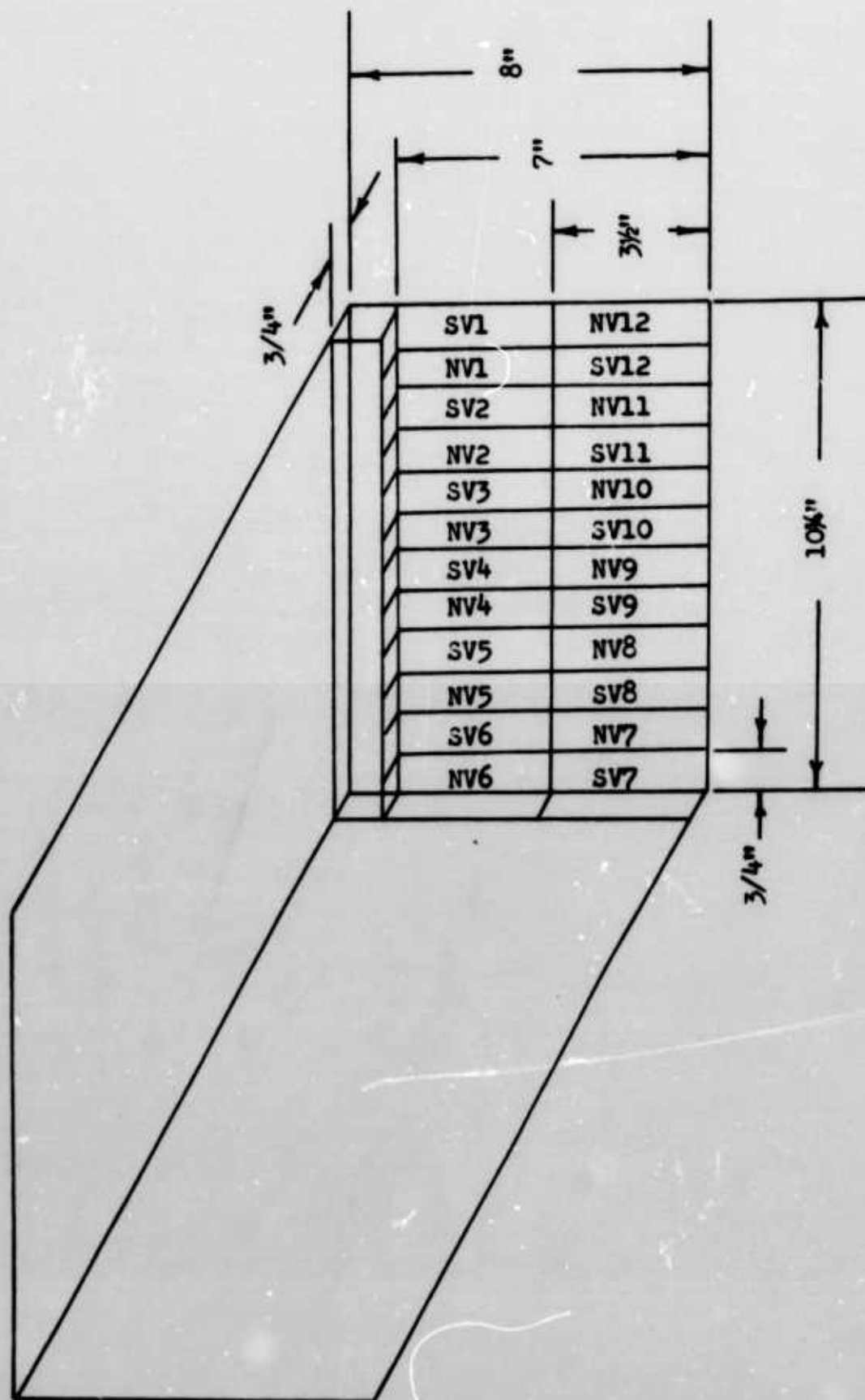


FIGURE 17. Tensile Specimen Locations in H-11 (Billet V)

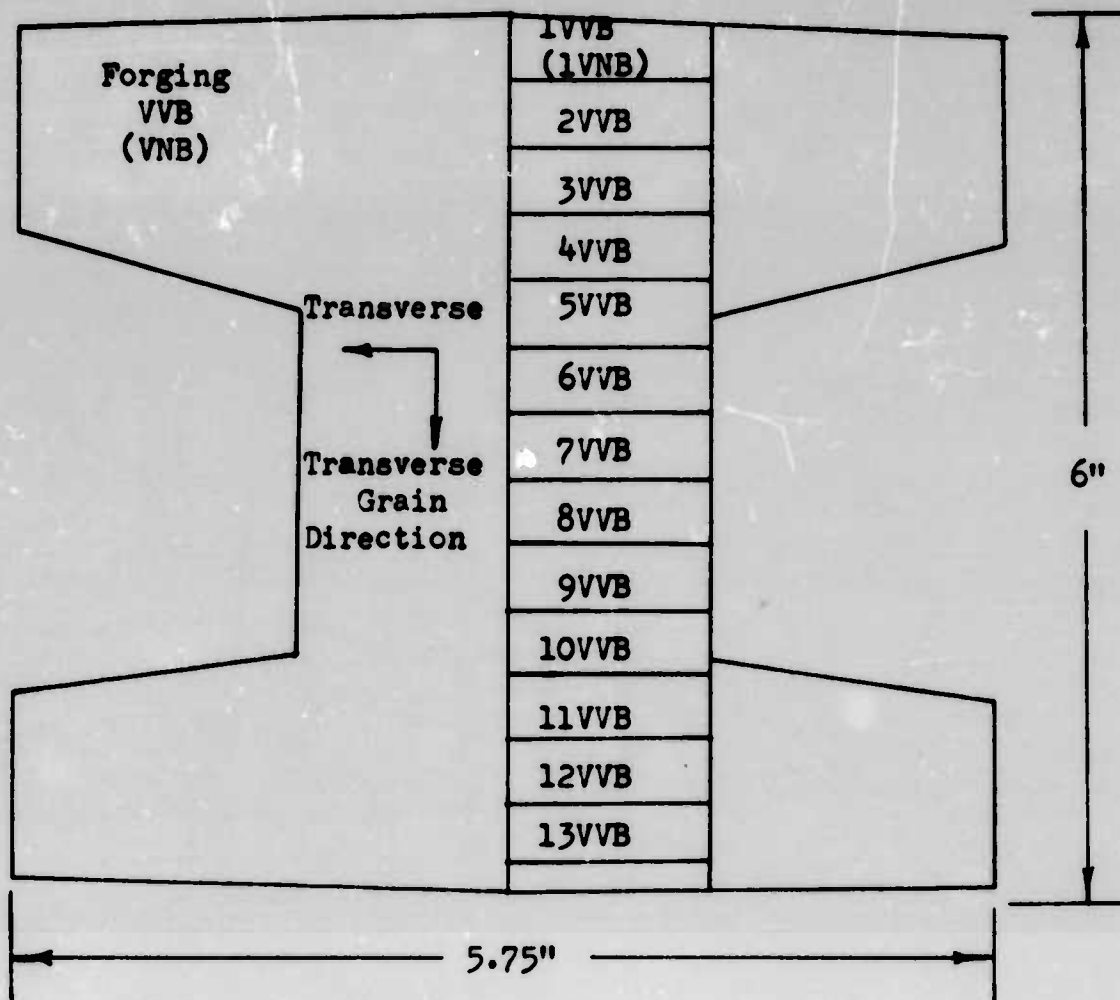


FIGURE 18

U-Bend Specimen Locations in Vacuum Melt
(VVB) and Air Melt (VNB) 4330M

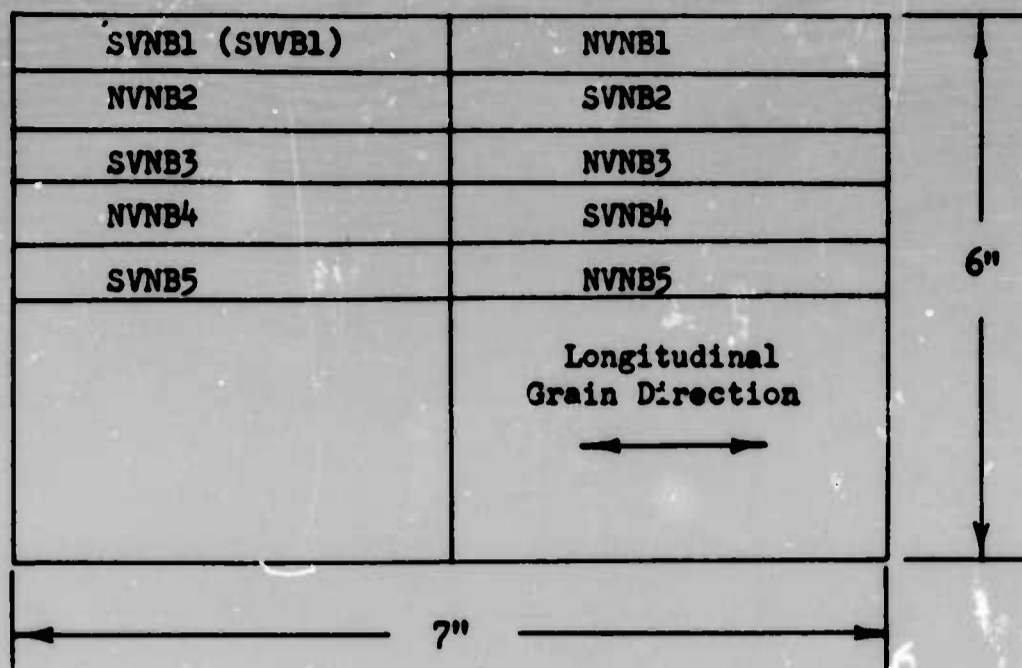


FIGURE 19

Tensile Specimen Locations in
Vacuum Melt and Air Melt 4330M

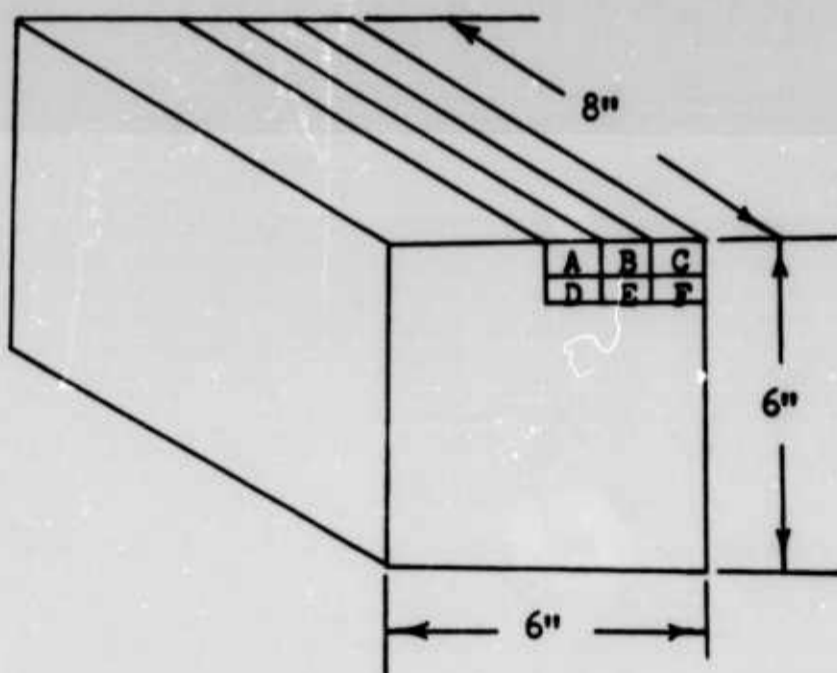


FIGURE 20. U-Bend Specimen Locations in AM 355 Billet

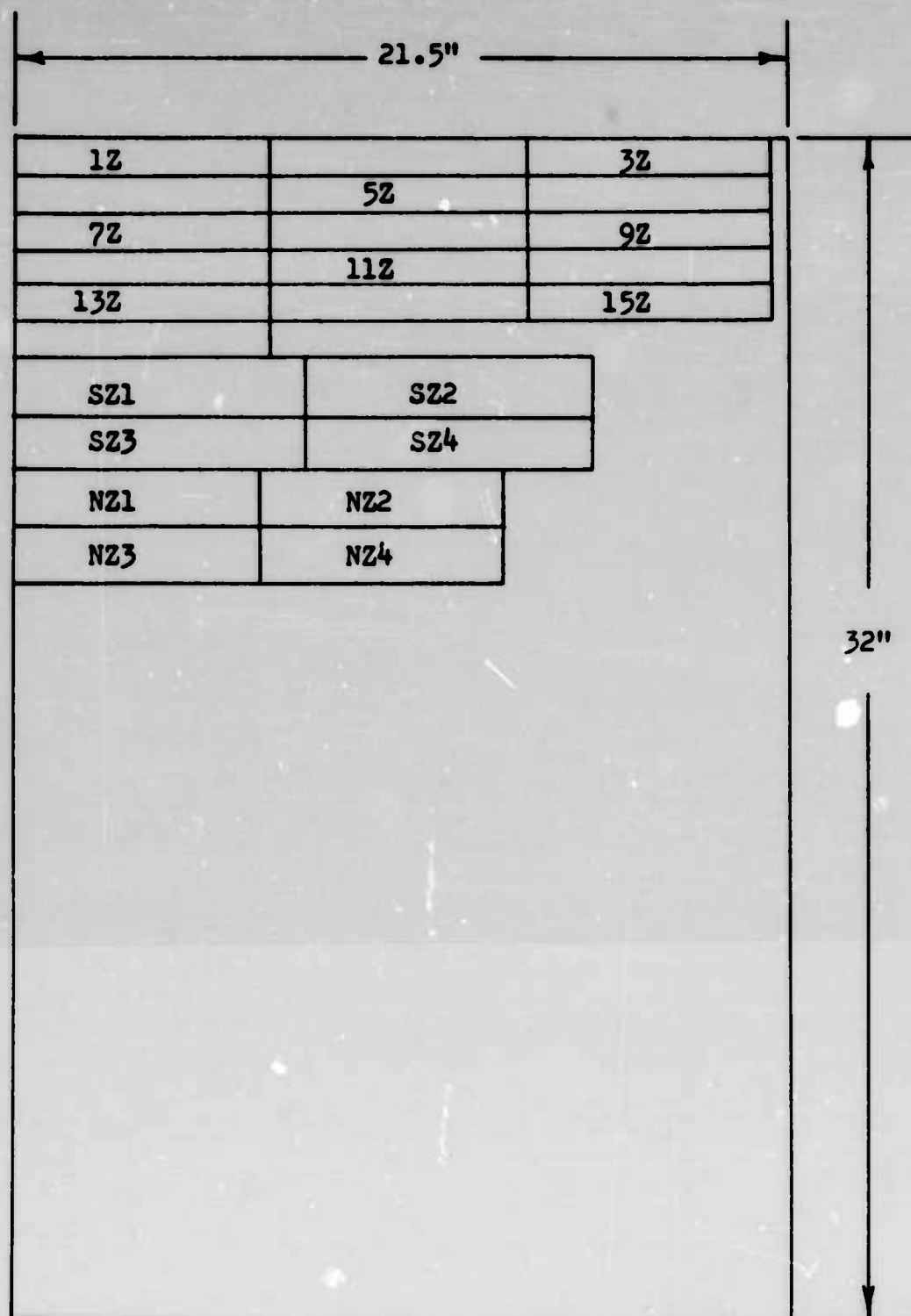


FIGURE 21
Stress Corrosion and Tensile Specimen
Locations in AM 350 (Sheet 2)

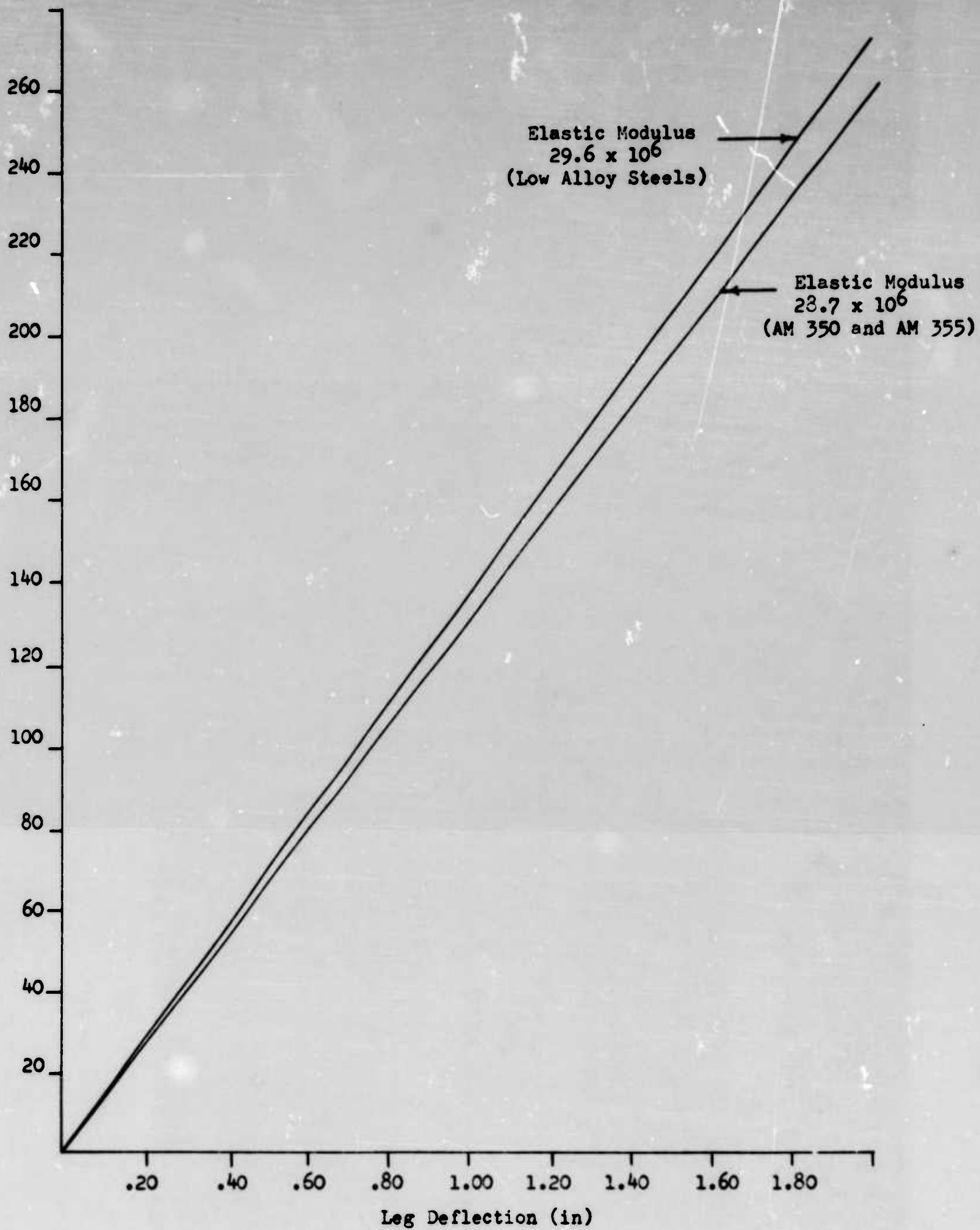


FIGURE 22. Stress Level as Function of U-Bend Specimen Leg Deflection

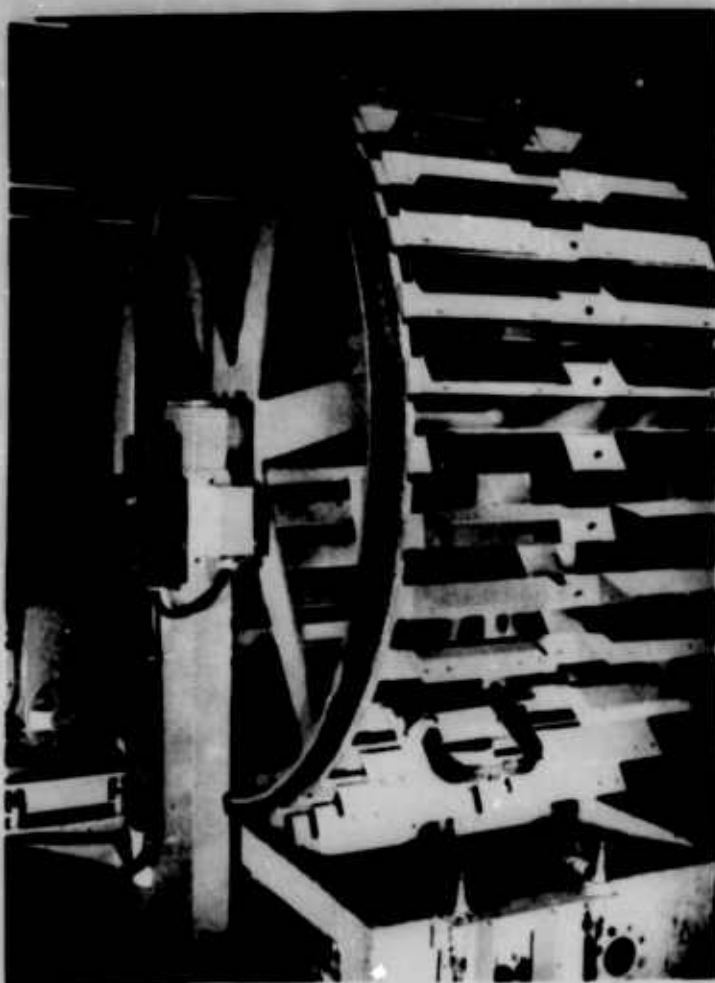


FIGURE 23
Ferris Wheel
Alternate Immersion Testing Apparatus



FIGURE 24
Chemically Milled Surface (with inclusion)
Nital 750X

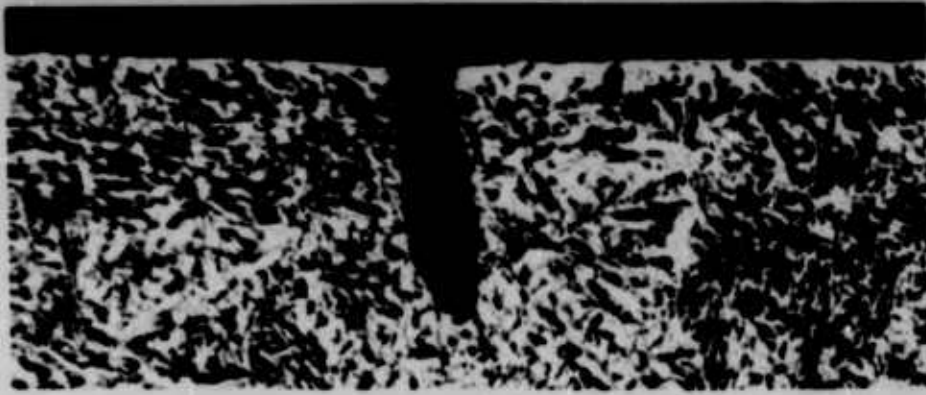


FIGURE 25
Electropolished Surface (with inclusion)
Nital 750X

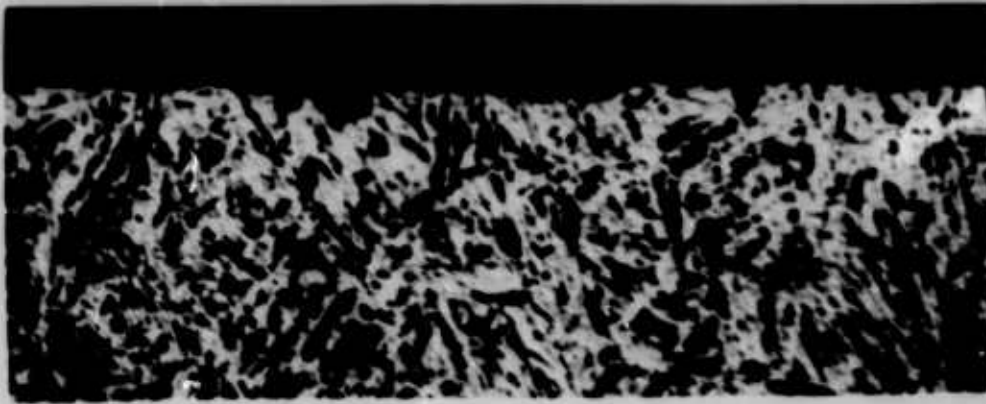


FIGURE 26
Ground Surface
Nital 750X

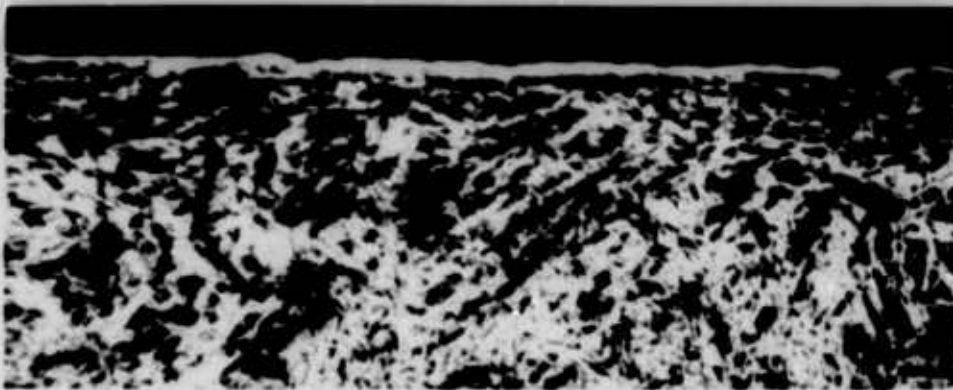


FIGURE 27
Face Milled (32 RHR) Surface
Nital 750X



FIGURE 28
Face Milled (125 RHR) and Sand Blasted Surface
Nital 750X



FIGURE 29
Face Milled (32 RHR) and Shot Peened Surface
Nital 750X

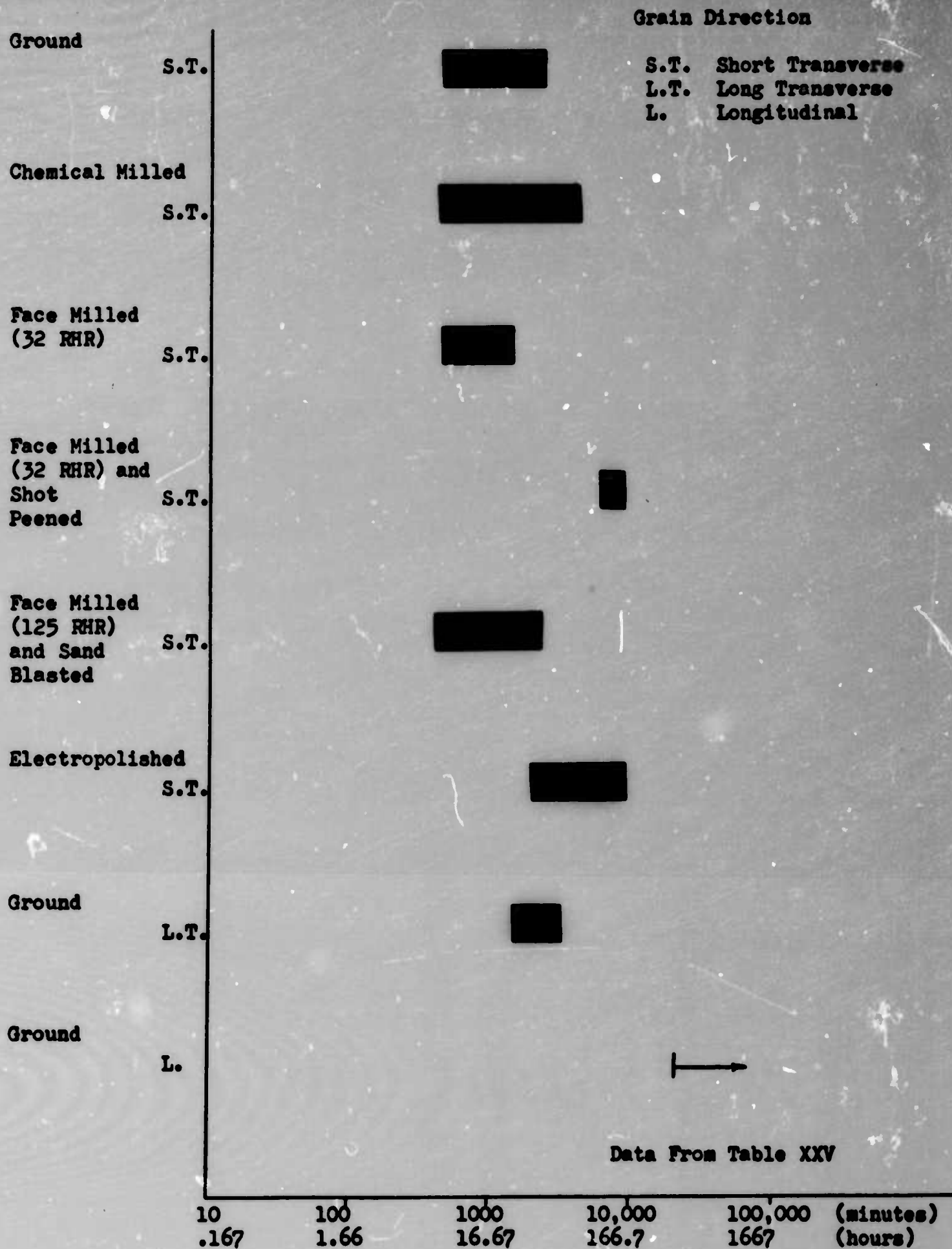


FIGURE 30. Range of Failure Times of 4330M (Billet L) U-Bend Specimens After Receiving Various Surface Finishes

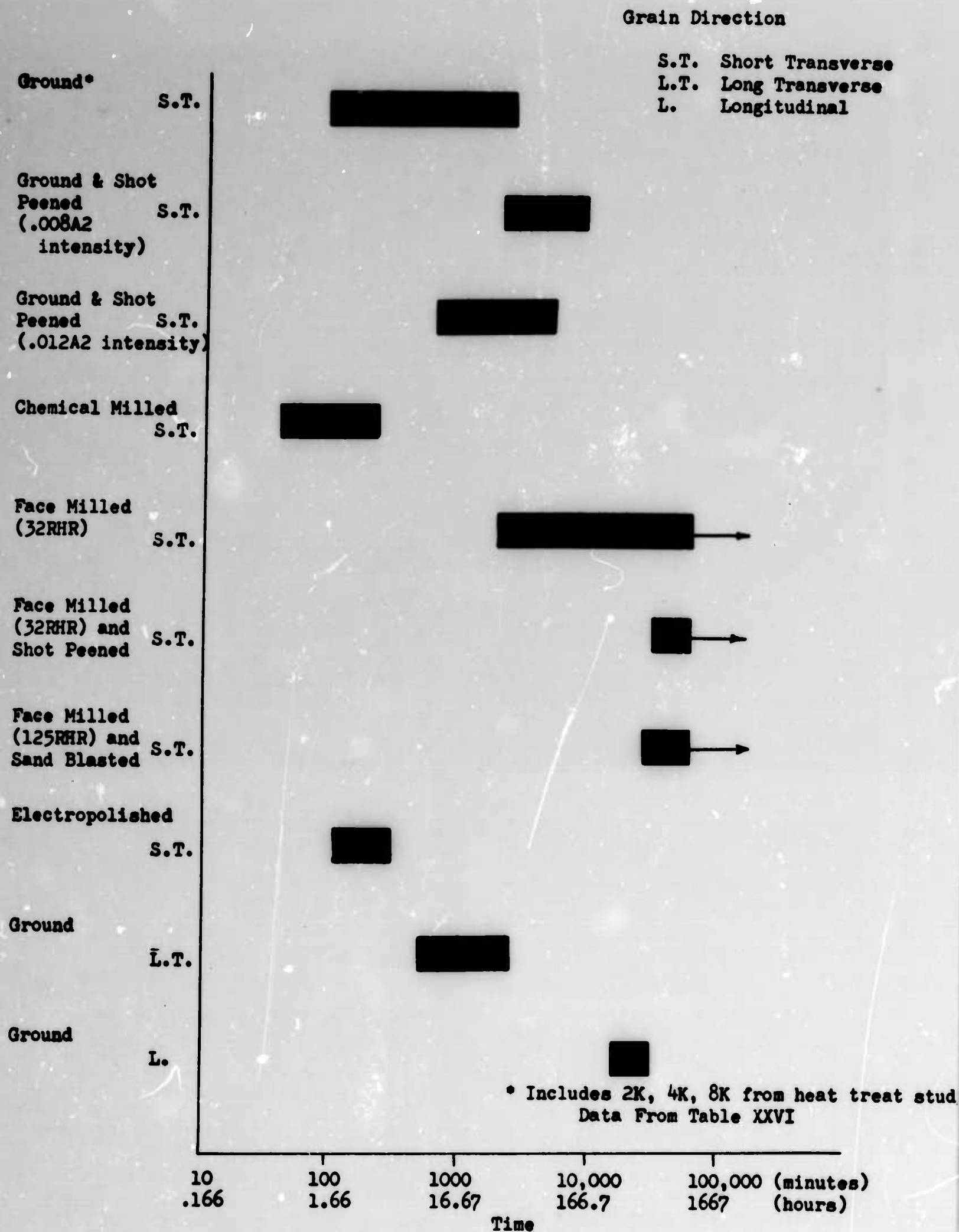


FIGURE 31. Range of Failure Times of 4340 U-Bend Specimens After Receiving Various Surface Finishes

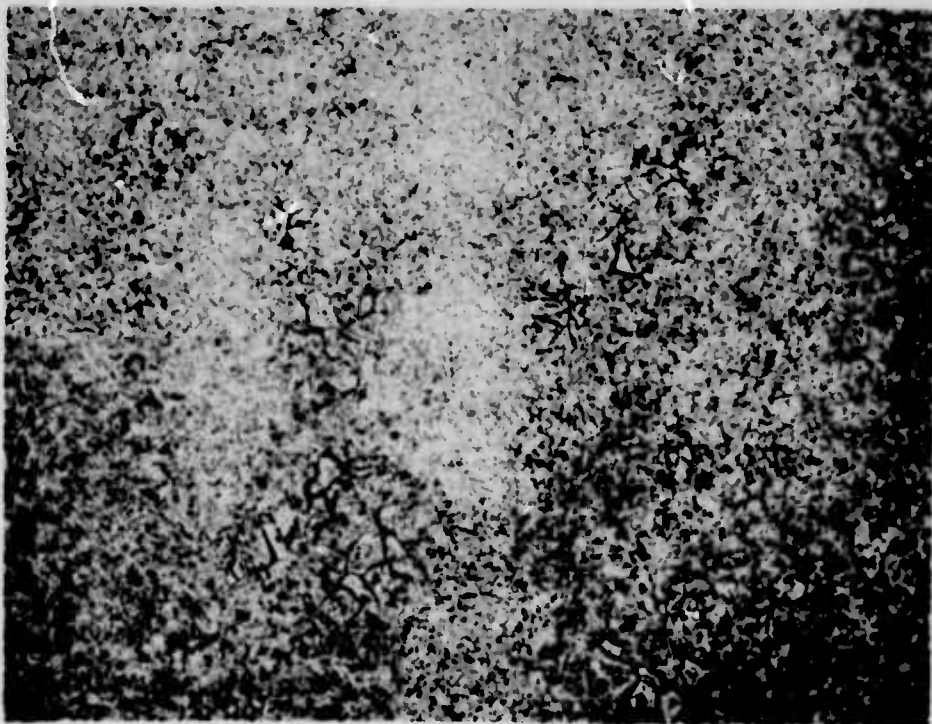


FIGURE 32
Banding in Specimen U B (Billet U, H-11) After 1100°F Temper
Nital plus Zephrian Chloride 50X

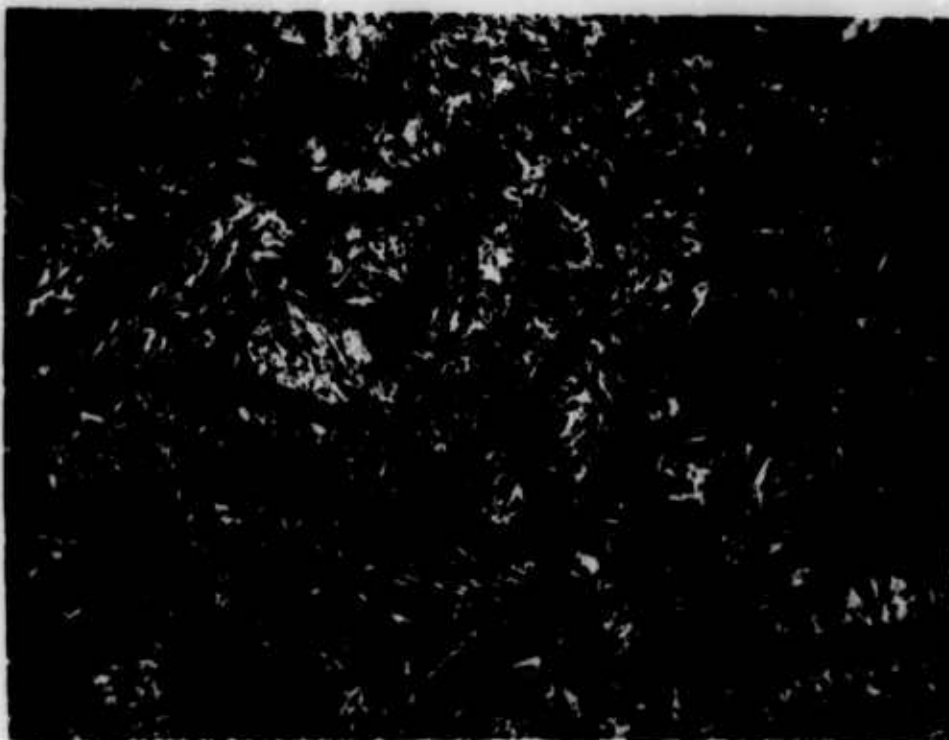


FIGURE 33
Precipitation in Specimen U B (H-11) After 1100°F Temper
Nital plus Zephrian Chloride 500X

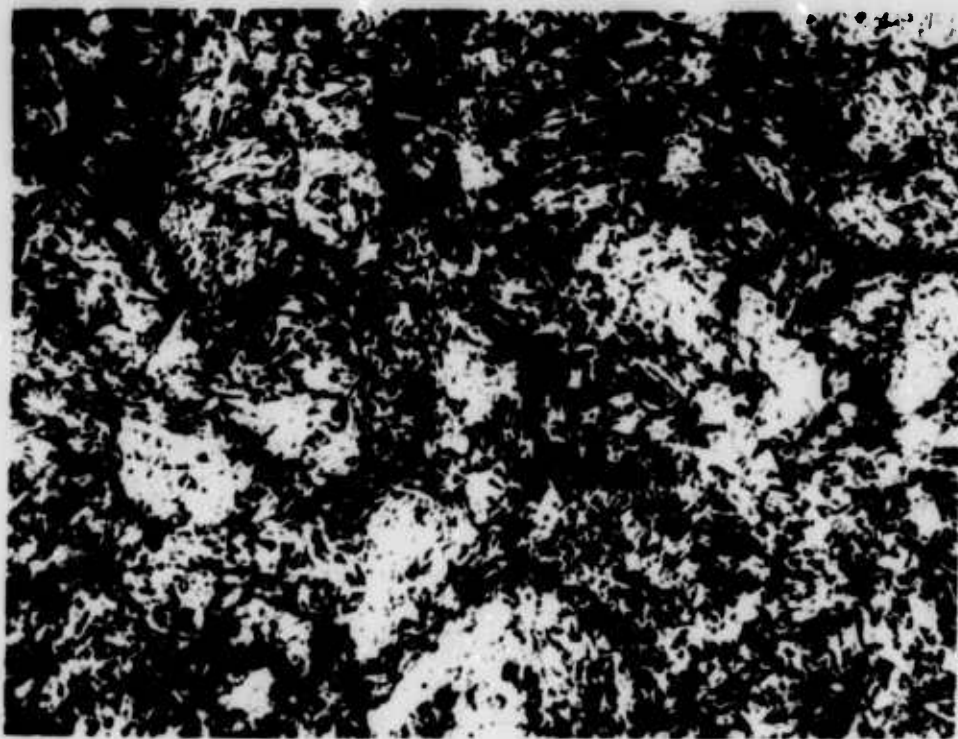


FIGURE 34
Precipitation in Specimen U A (H-11) After 1000°F Temper
Nital plus Zephrian Chloride 500X

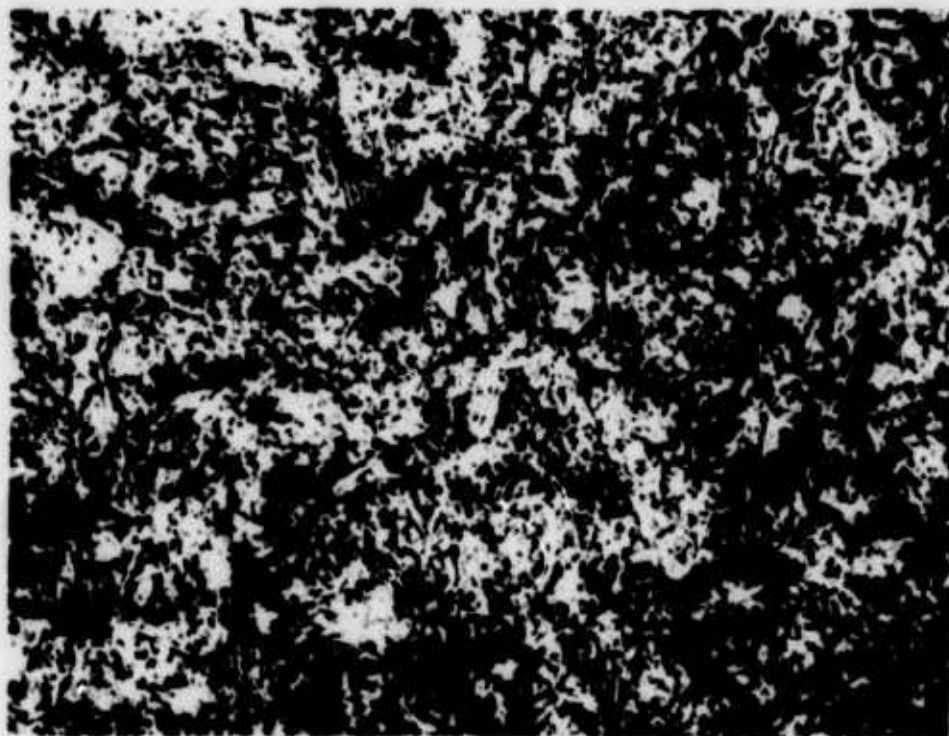


FIGURE 35
Precipitation in Specimen V D (H-11, Billet V) After 1000°F
Temper. Nital plus Zephrian Chloride 500X

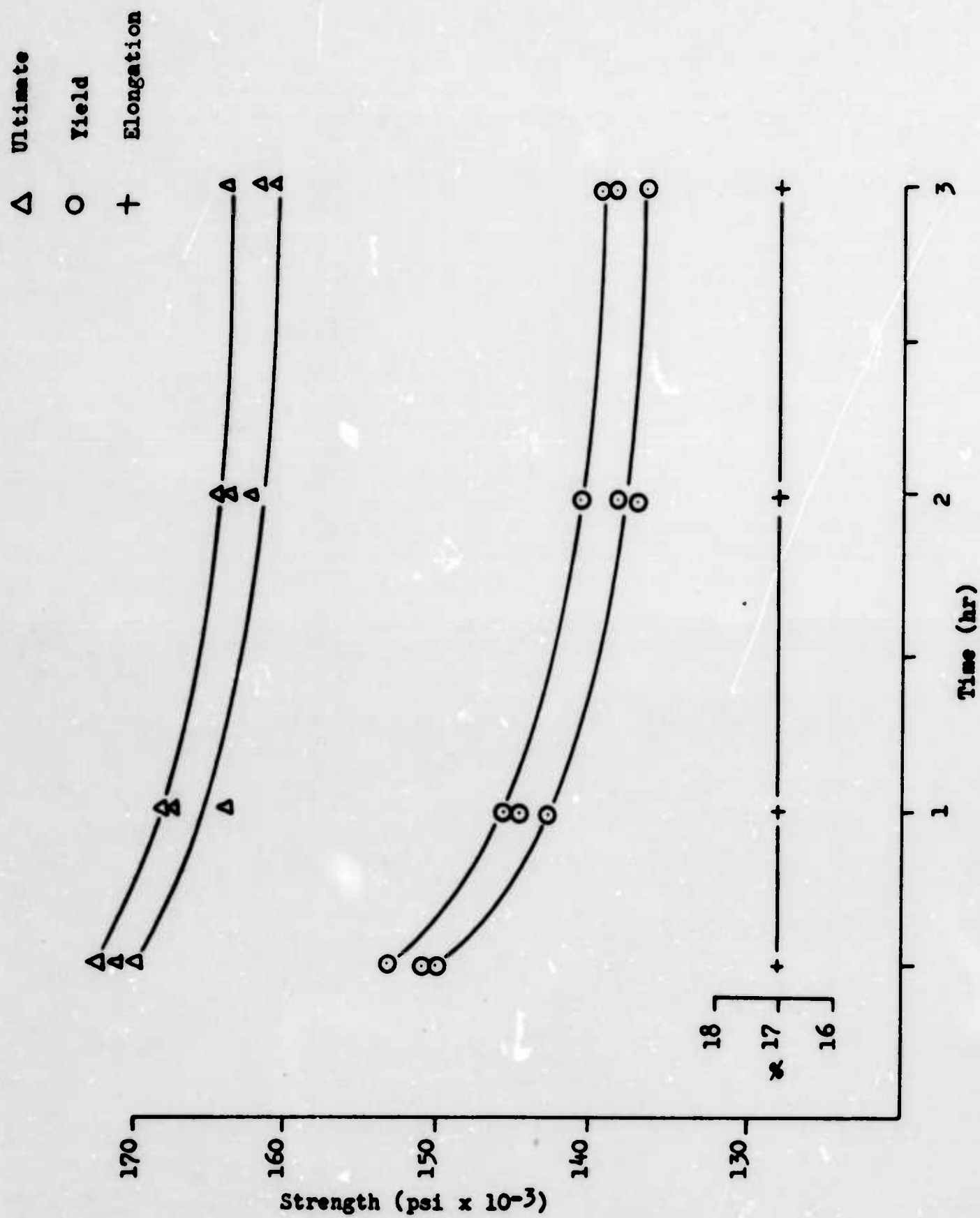


FIGURE 36. Smooth Tensile Properties As A Function of Tempering Time
At 1050°F of AM 350 SCT 1050 Condition

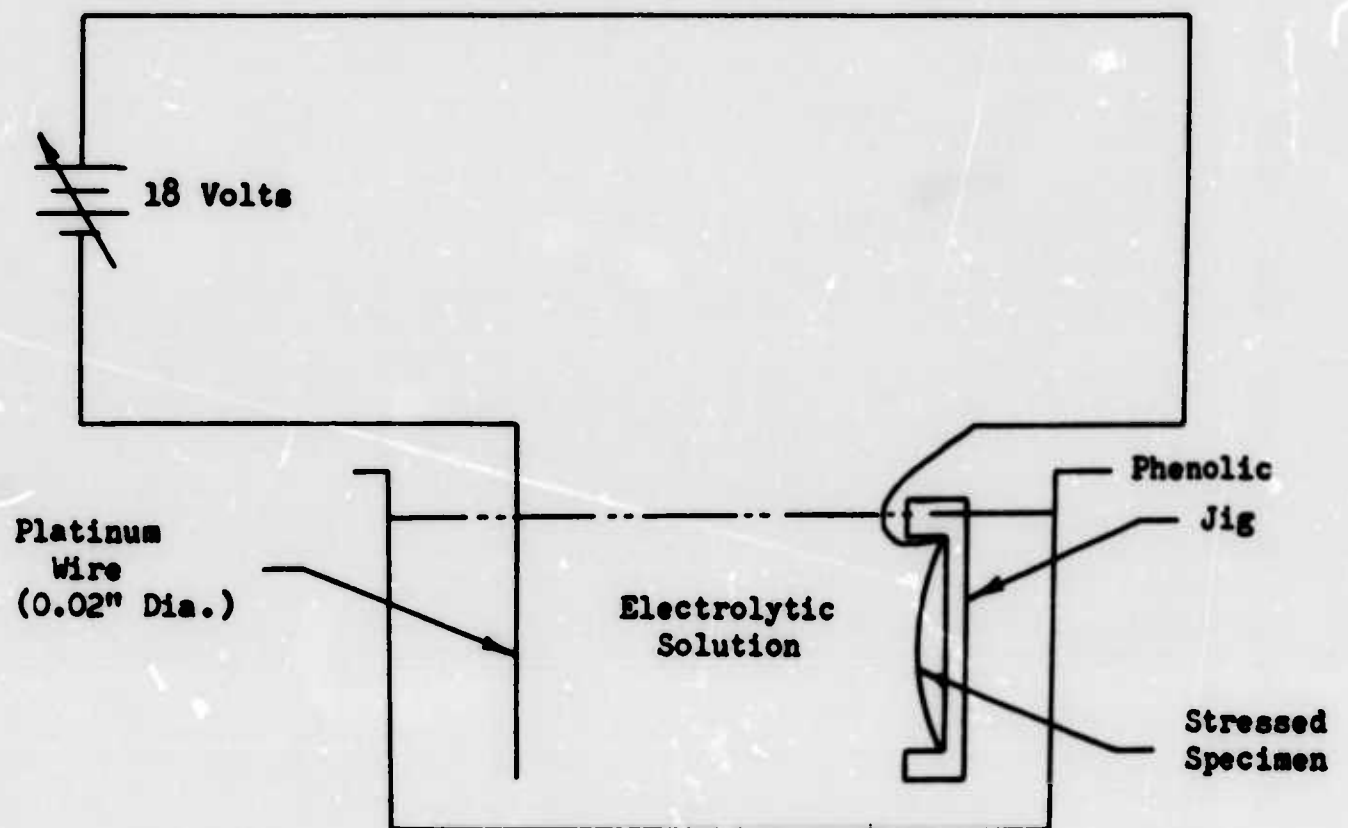


FIGURE 37. Electrolytic Cell Arrangement Used in Hydrogen Embrittlement and Stress Corrosion Crack Shape Studies

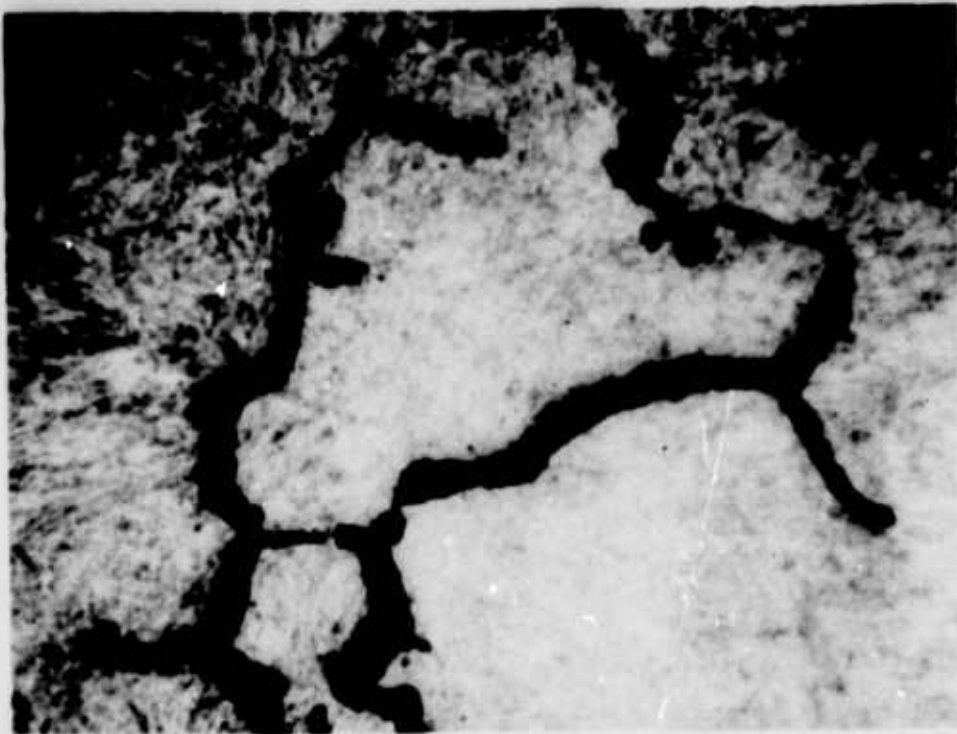


FIGURE 38
Cracking in 4340M Specimen Anodic in 3% NaCl Solution
Nital 1200X

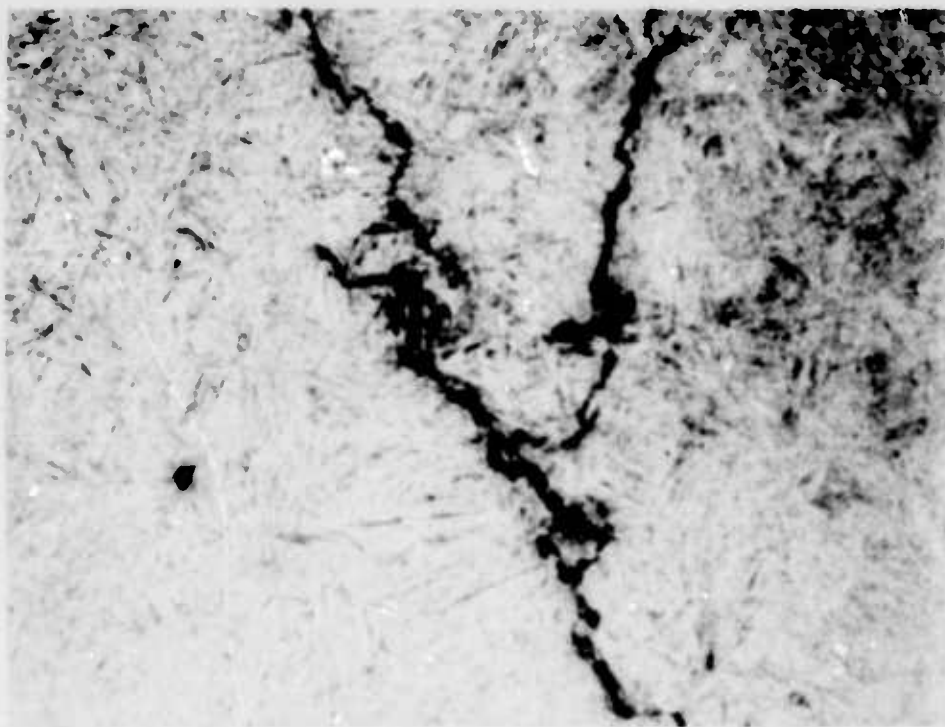


FIGURE 39
Cracking in 4340M Specimen Cathodic in 3% NaCl Solution
Nital 1200X

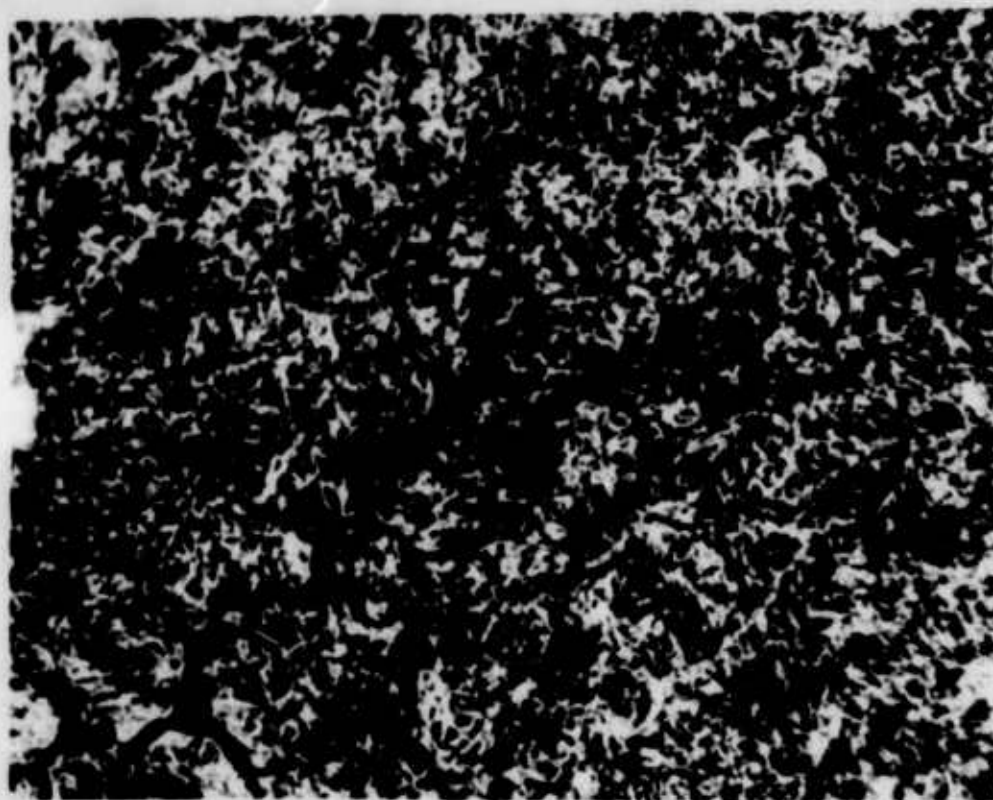


FIGURE 40
Cracking in 4340 Specimen Anodic in 3% NaCl Solution
Cu Cl₂ 500X

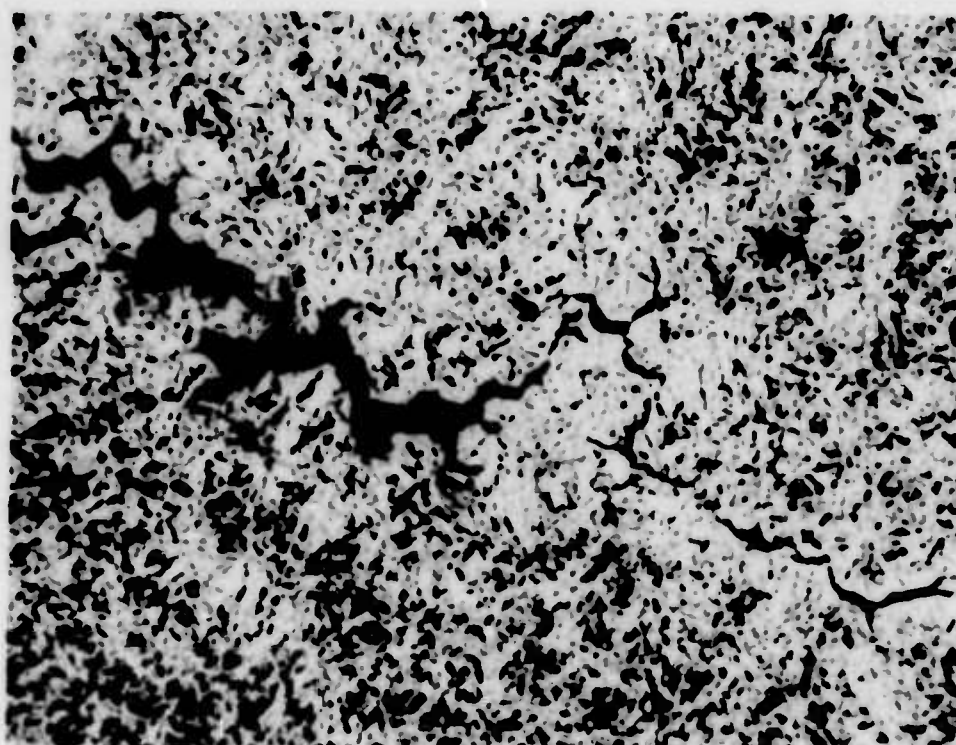


FIGURE 41
Cracking in 4340 Specimen Cathodic in 0.125 N Na₂S Solution
Cu Cl₂ 500X

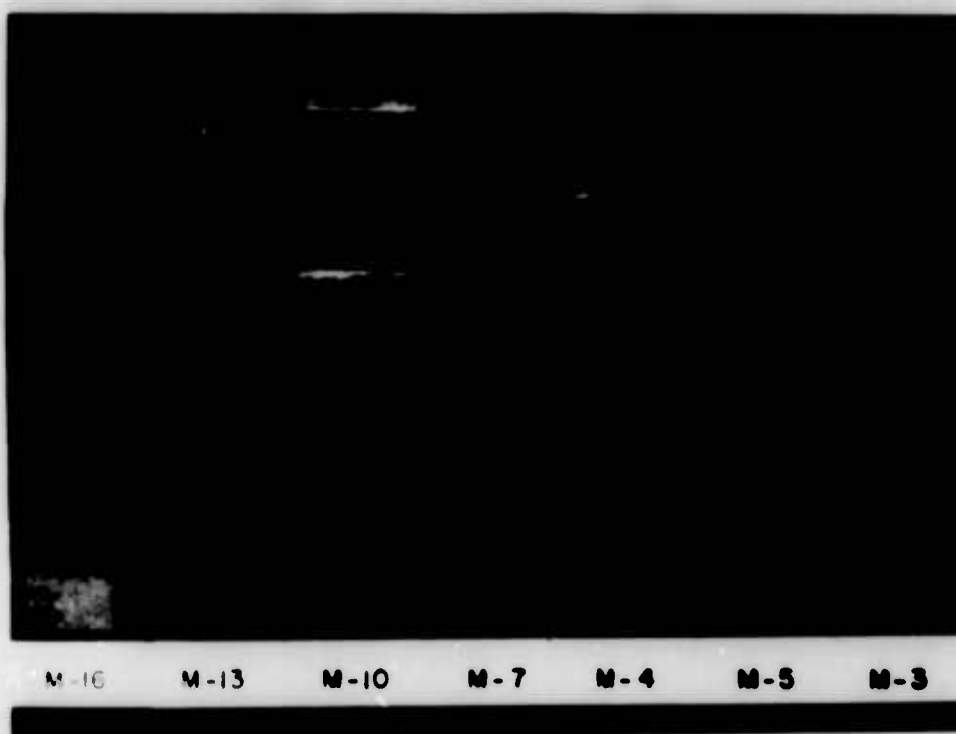


FIGURE 42
Rust on 4340 (Billet M) Test Blocks
280,000 psi Strength



FIGURE 43
Fractured 4340 (Billet M) Surface Ground Specimens
280,000 psi Strength



FIGURE 44. Fracture Faces of 4340 (Billet M)
Surface Ground Specimens

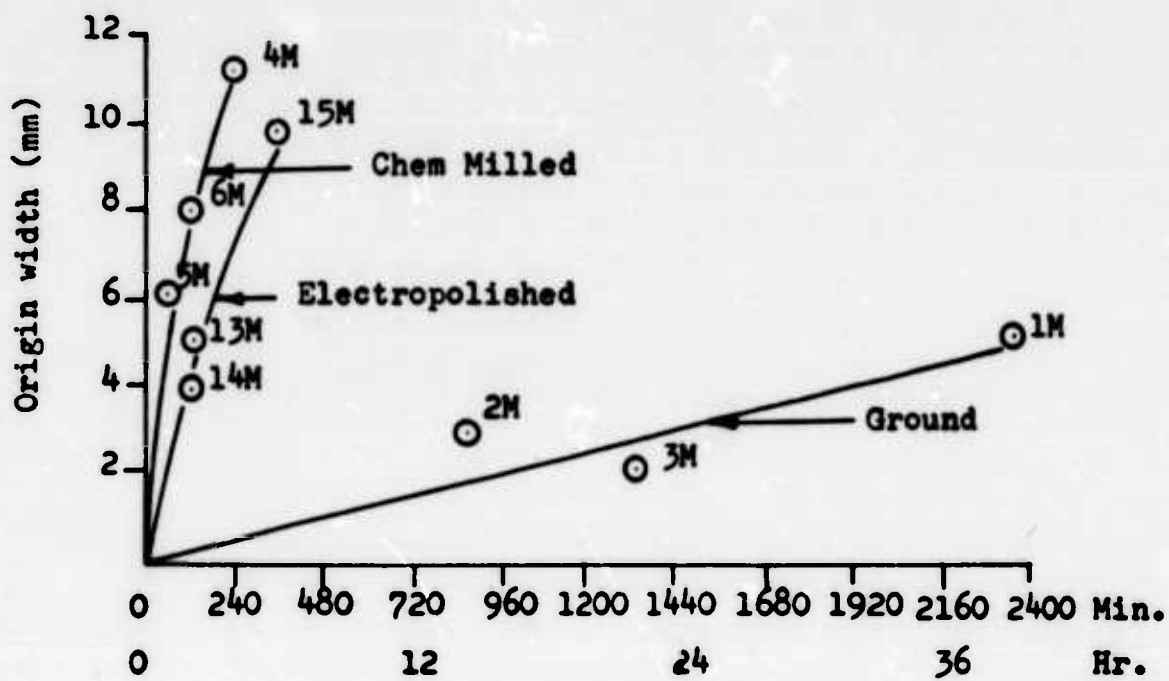


FIGURE 45. Fracture Origin Width Versus Time to Failure
4340 (Billet M)

a 90% Yield Strength
b 75% Yield Strength
c 50% Yield Strength

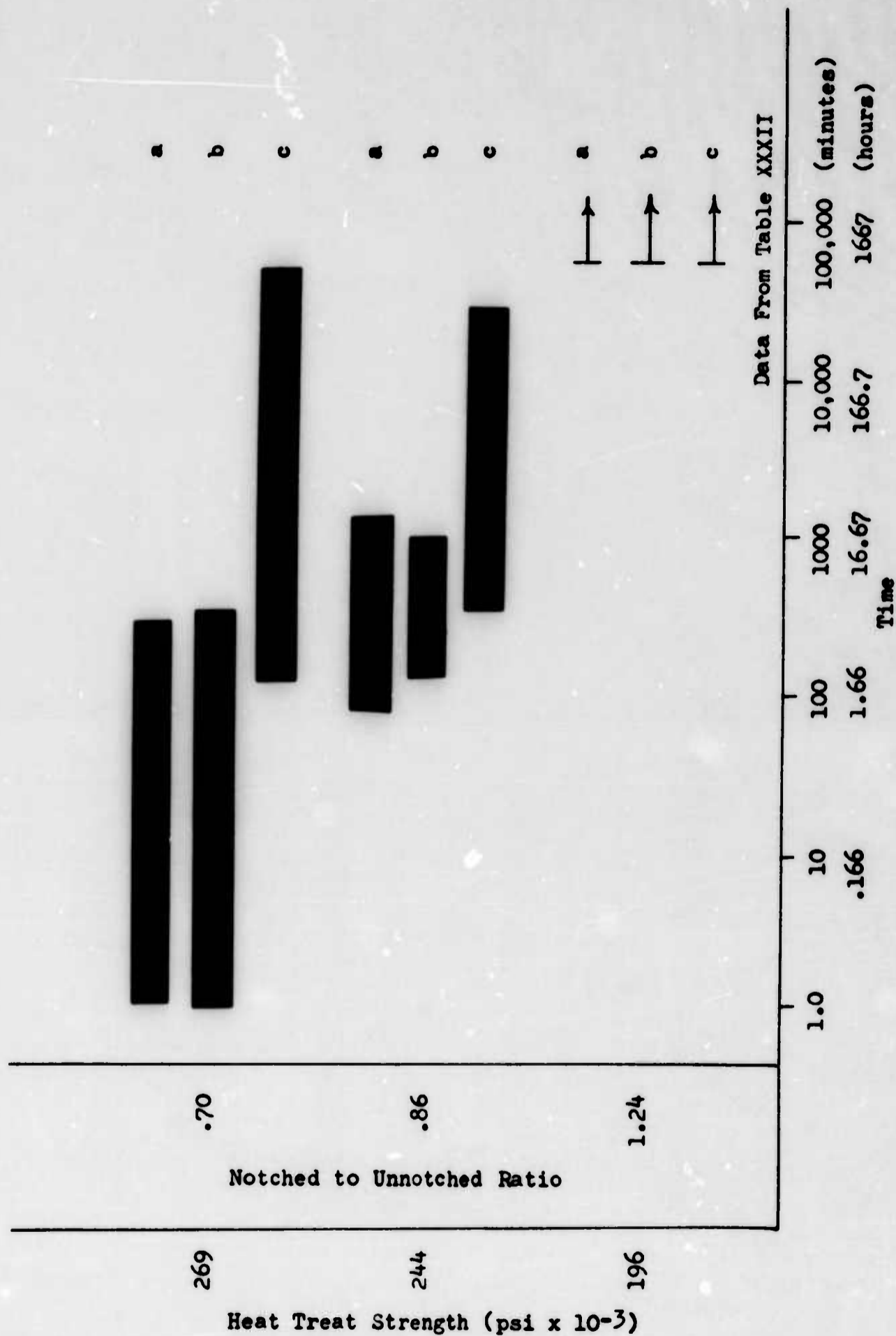


FIGURE 46. Range of Failure Times of Martempered 4340 (Billet N)

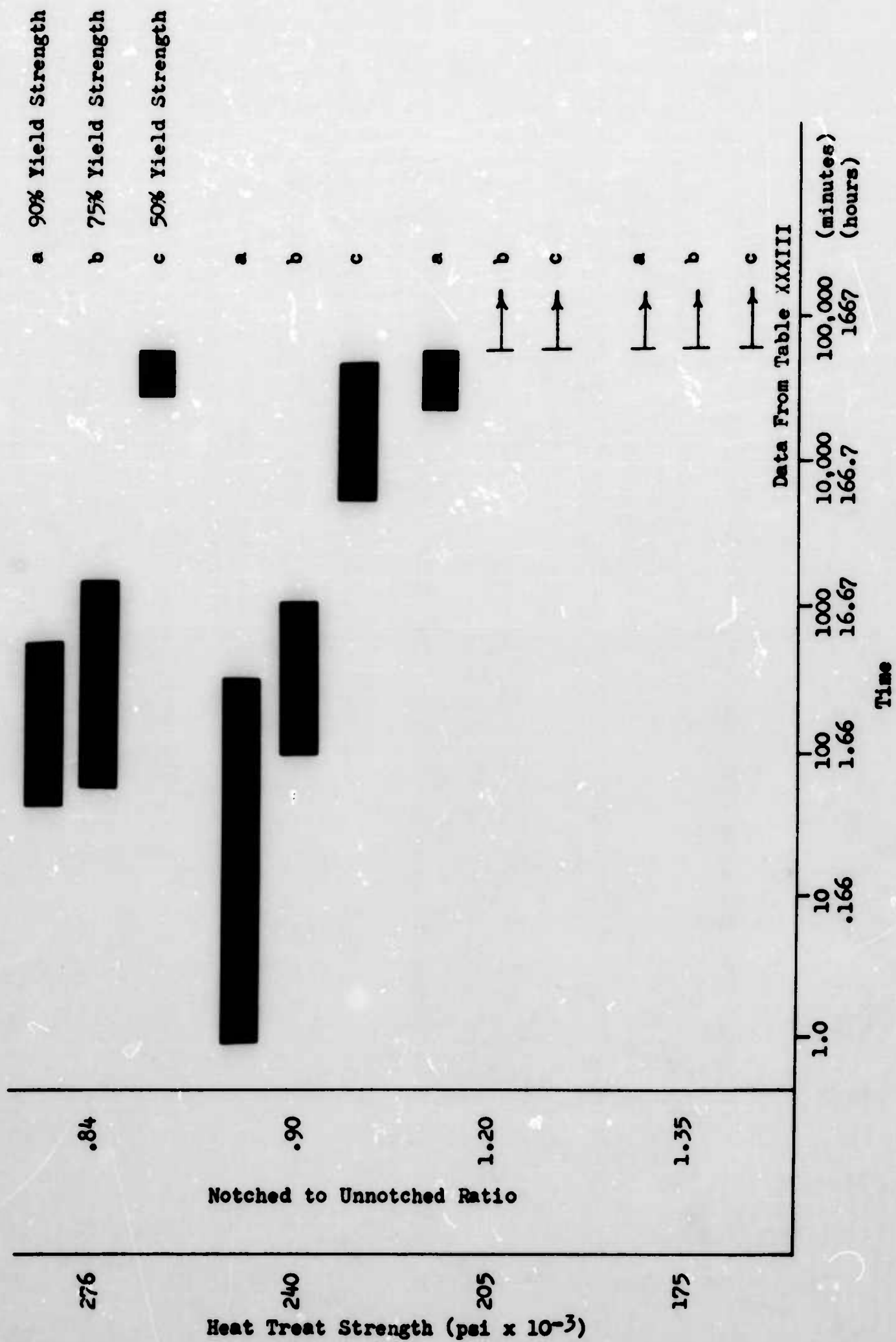


FIGURE 47. Range of Failure Times of 4340 (Billet K)

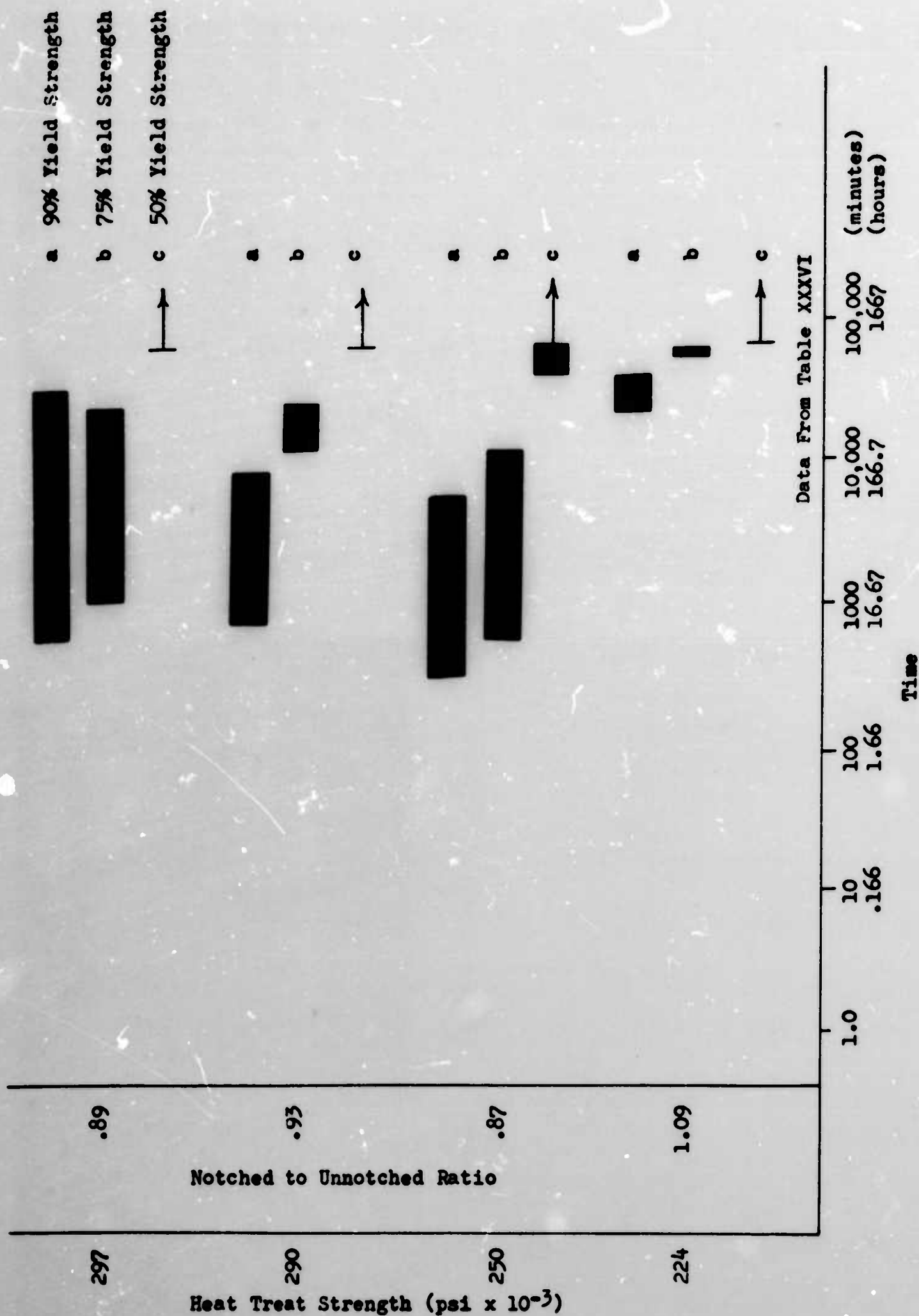


FIGURE 48. Range of Failure Times of 4340M (Billet P)

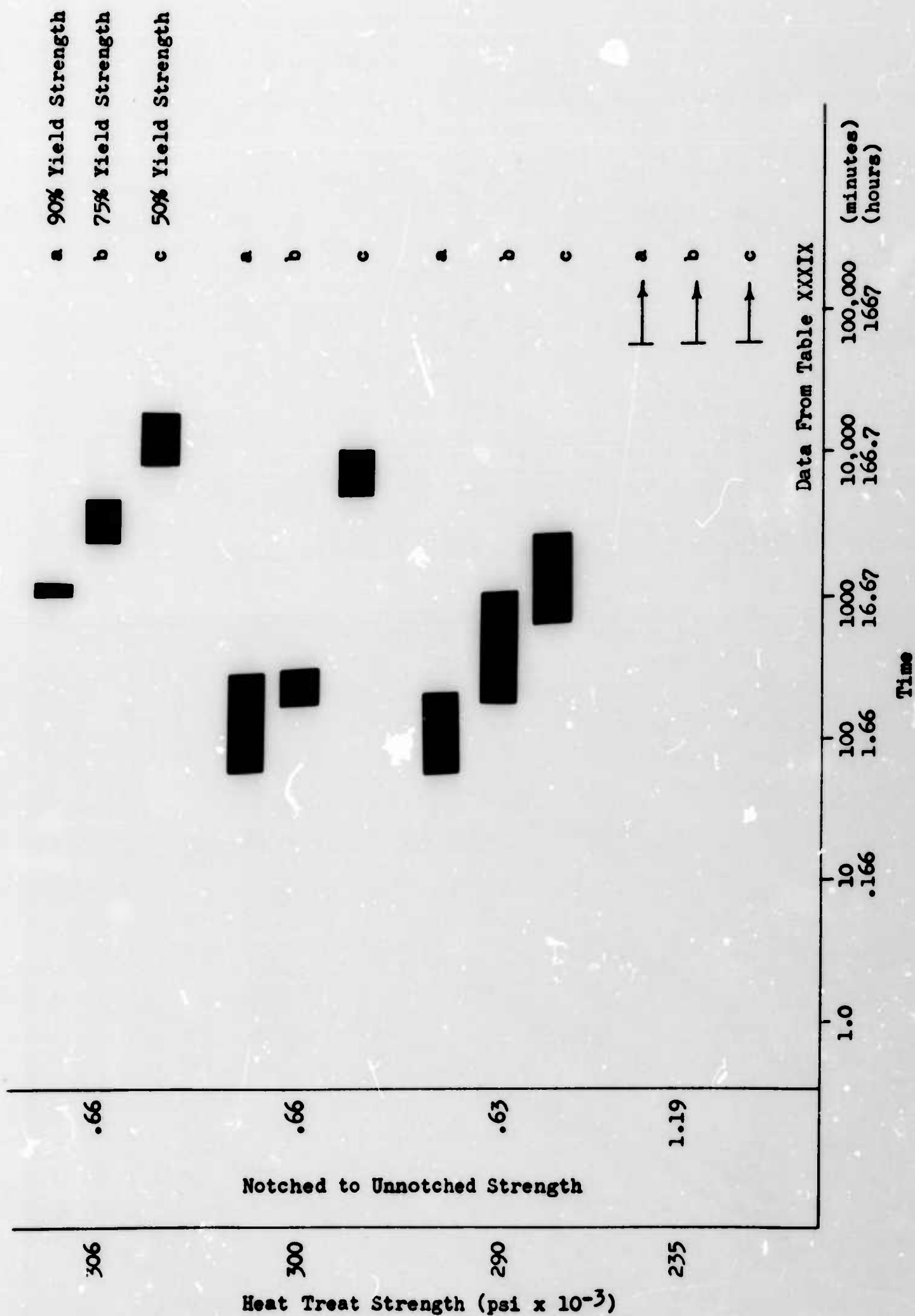


FIGURE 49. Range of Failure Times of H-11 (Billet V)

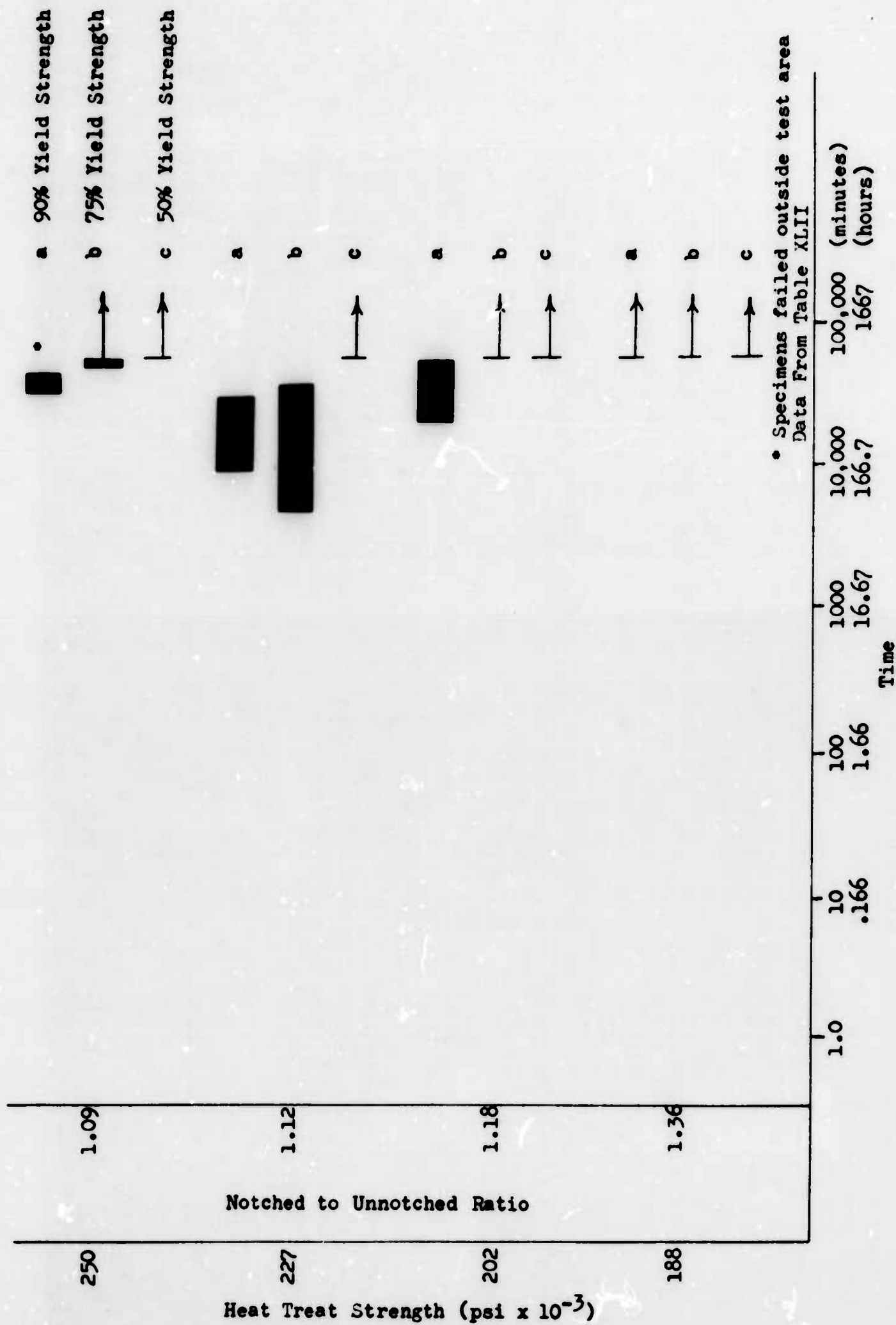


FIGURE 50. Range of Failure Times of 4330M (Billet R)

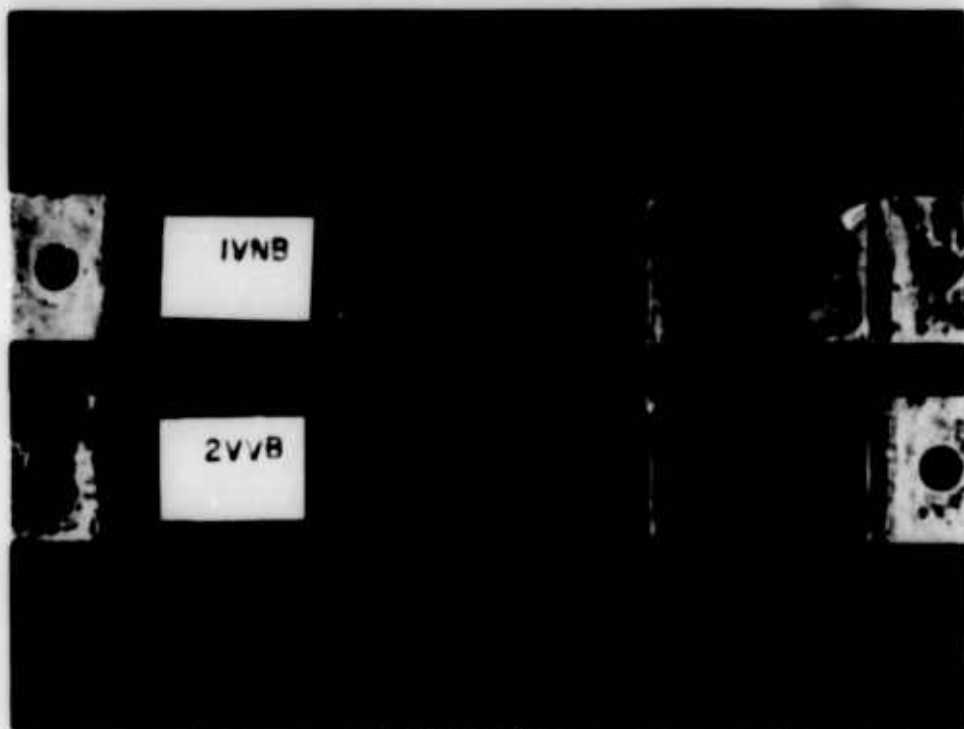


FIGURE 51
Fractured Air Melt (VNB) and Vacuum Melt (VVB) 4330M Specimens
225,000 psi Strength



FIGURE 52
Fracture Faces of Air Melt and Vacuum Melt 4330M Specimens
225,000 psi Strength



FIGURE 53
Fracture Origin of 4340 Specimen (Martempered 21N) Which Failed
While Stressed But Before Testing 10X - 269,000 psi Strength

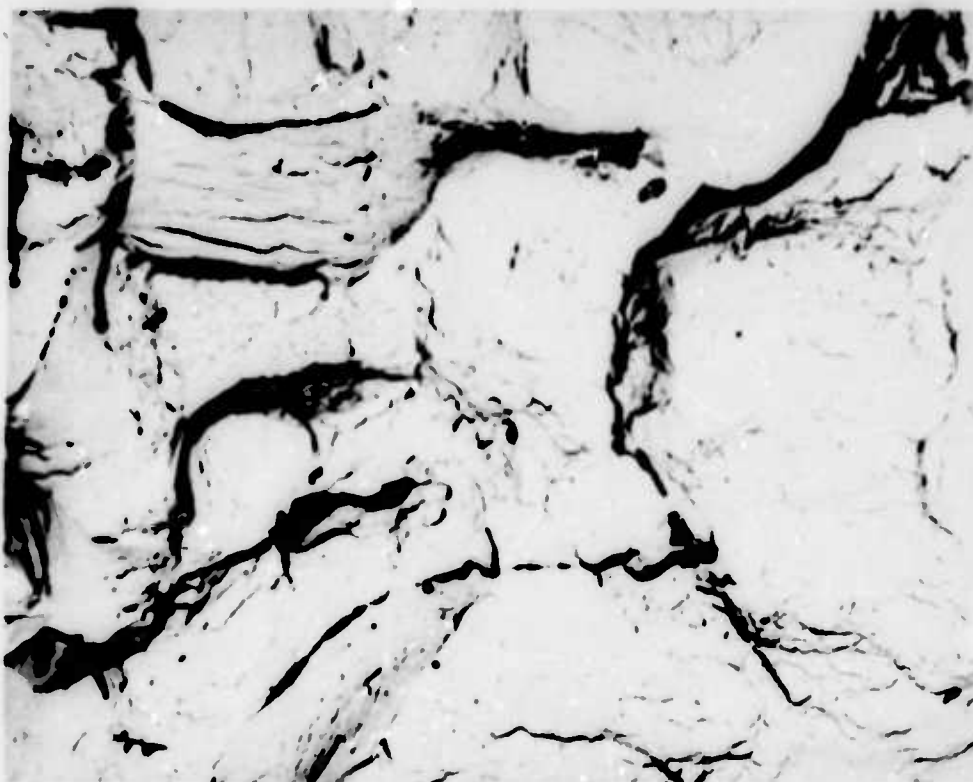


FIGURE 54
Electron Micrograph of Fracture Origin of 21N. 4340 (Martempered)
269,000 psi Heat Treat Strength 5800X



FIGURE 55
Electron Micrograph of Hydrogen Embrittlement Failure 4340
269,000 - 280,000 psi Heat Treat Strength Range
4600X

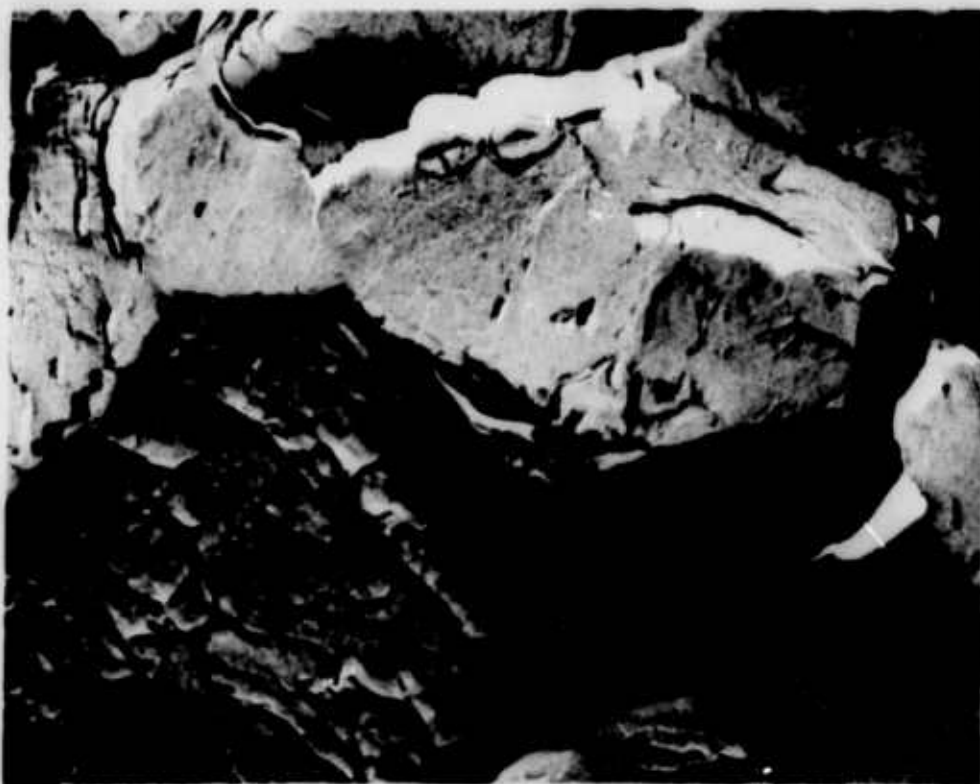


FIGURE 56
Electron Micrograph of Stress Corrosion Failure.
Specimen 3M 4340 280,000 psi Heat Treat Strength 8700X

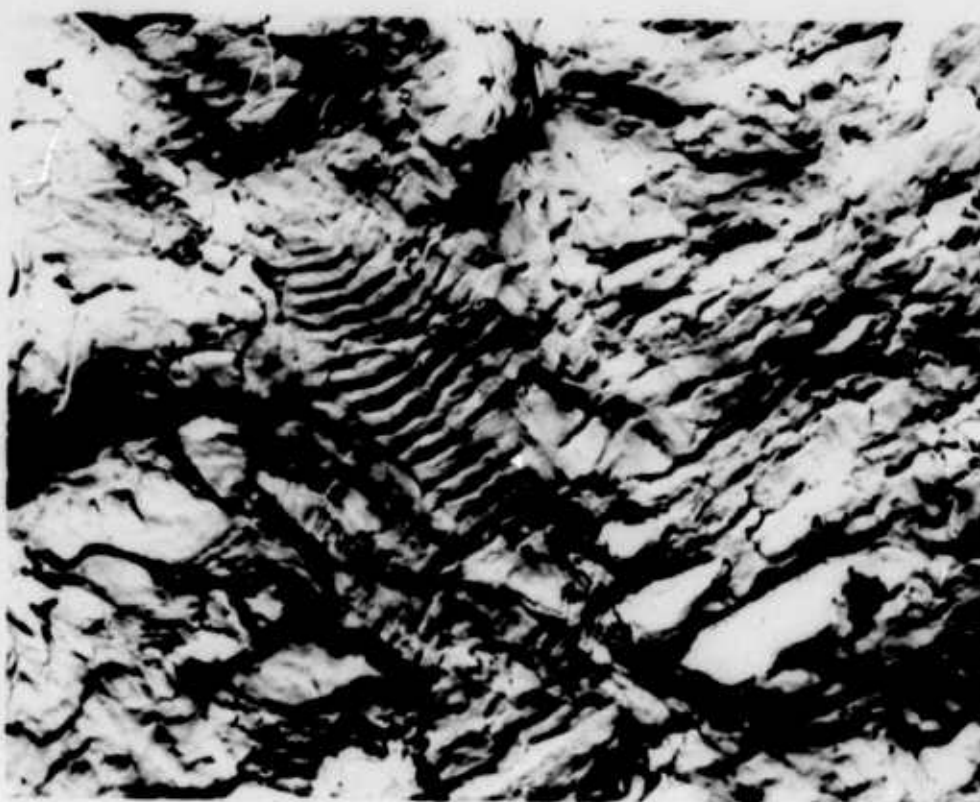


FIGURE 57
Electron Micrograph of Fatigue Failure.
4330M 220,000-240,000 psi Heat Treat Strength Range 6600X



FIGURE 58
Electron Micrograph of Ductile Fracture Failure
4340 260,000-280,000 psi Heat Treat Strength Range
7800X



FIGURE 59
Electron Micrograph of Quench Crack Fracture Face.
4340 Water Quenched from 1575°F
4200X

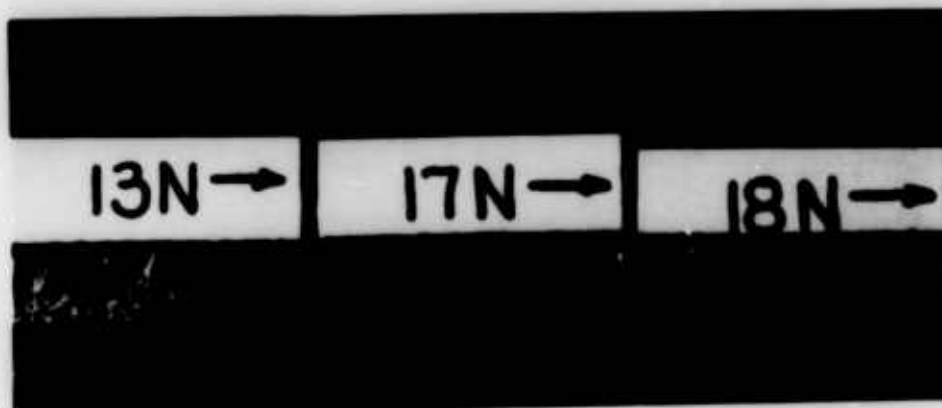


FIGURE 60
Fracture Faces of 4340 (Billet N, Martempered) Specimens
Arrows Indicate Edge First to Enter Test Solution
244,000 psi Strength



FIGURE 61
Fracture Faces of 4340 (Billet K, Oil Quenched) Specimens
275,000 psi Strength

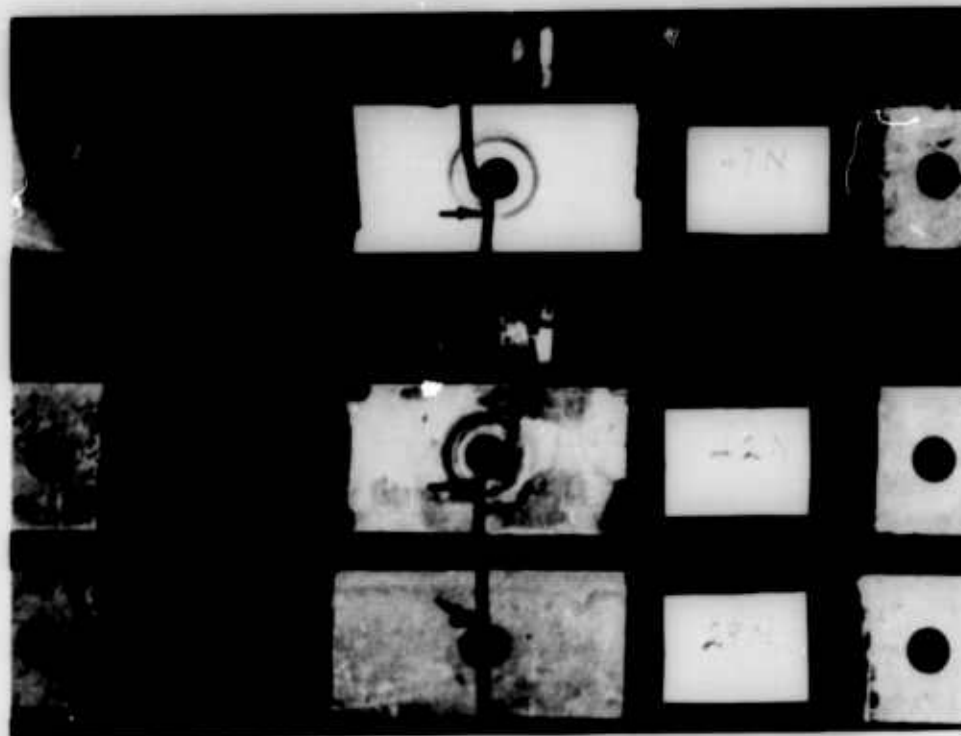


FIGURE 62
Fractured Painted and Cadmium Plated 4340 Specimens. Small
Arrows Indicate Failure Origins - Large Arrows Indicate Edge
First to Enter Test Solution 275,000 psi Strength



FIGURE 63
Fracture Faces of Painted and Cadmium
Plated Specimens. Arrows Indicate Failure Origins
275,000 psi Strength

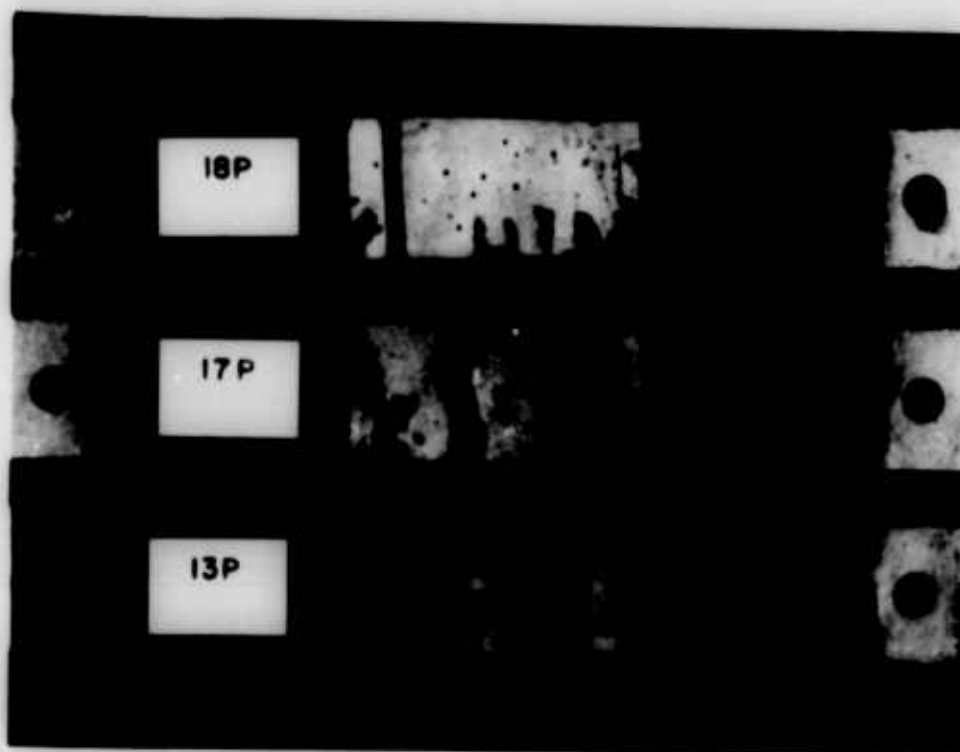


FIGURE 64
Fractured 4340M (Billet P) High Strength Specimens
290,000 psi Strength

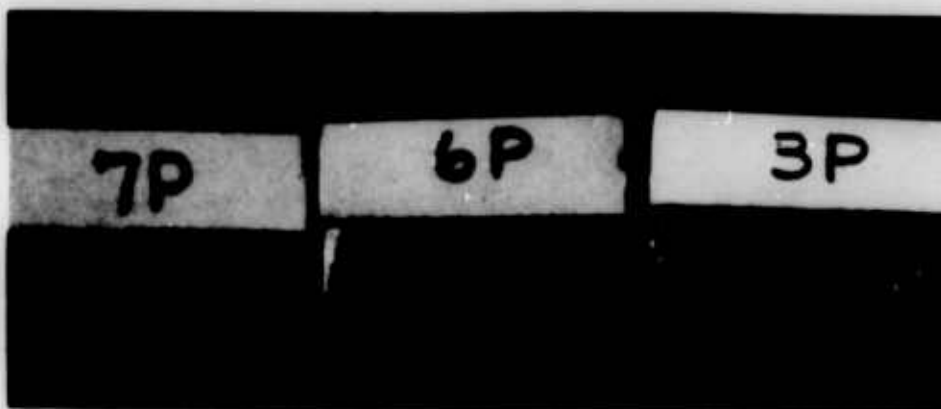


FIGURE 65
Fracture Faces of High Strength 4340M (Billet P) Specimens
297,000 psi Strength



FIGURE 66

Fracture Faces of Low Strength 4340M (Billet P)
Specimens 250,000 psi Strength



FIGURE 67

Fracture Faces of H-11 (Billet V) Specimens
306,000 psi Strength



FIGURE 68

Fracture Faces of 4330 (Billet R) Specimens
227,000 psi Strength

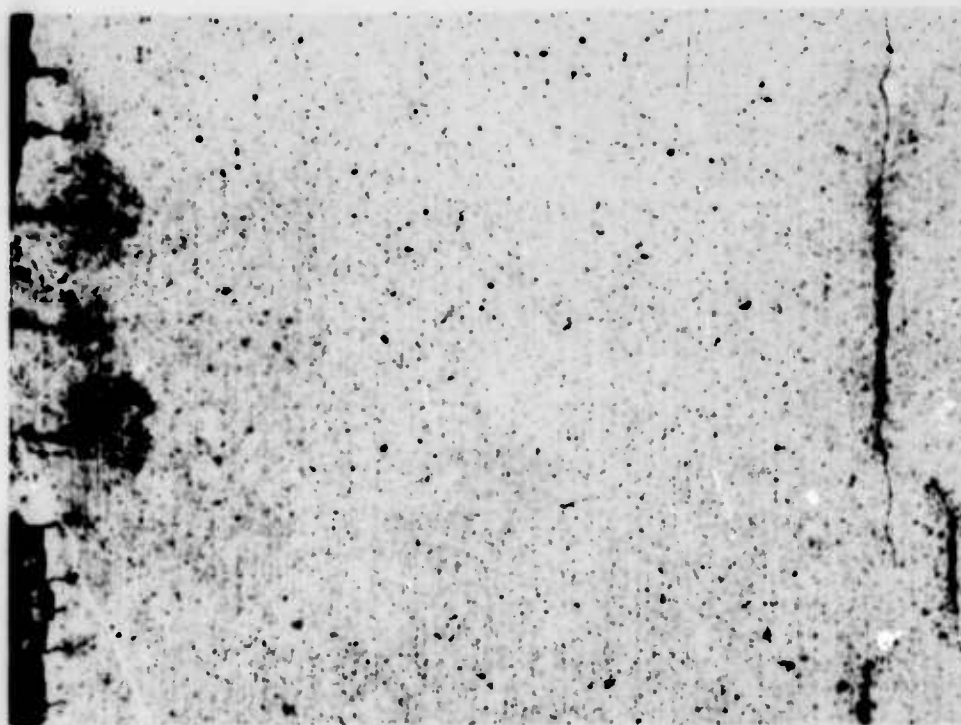


FIGURE 69

Cracking on Tension Surface of Failed H-11 (Billet V) Steel Specimen. Similar Cracking was Found on Other Low Alloy Steel Samples. Surface Revealed by Lightly Polishing and Macroetching in 50% HCl. 10X

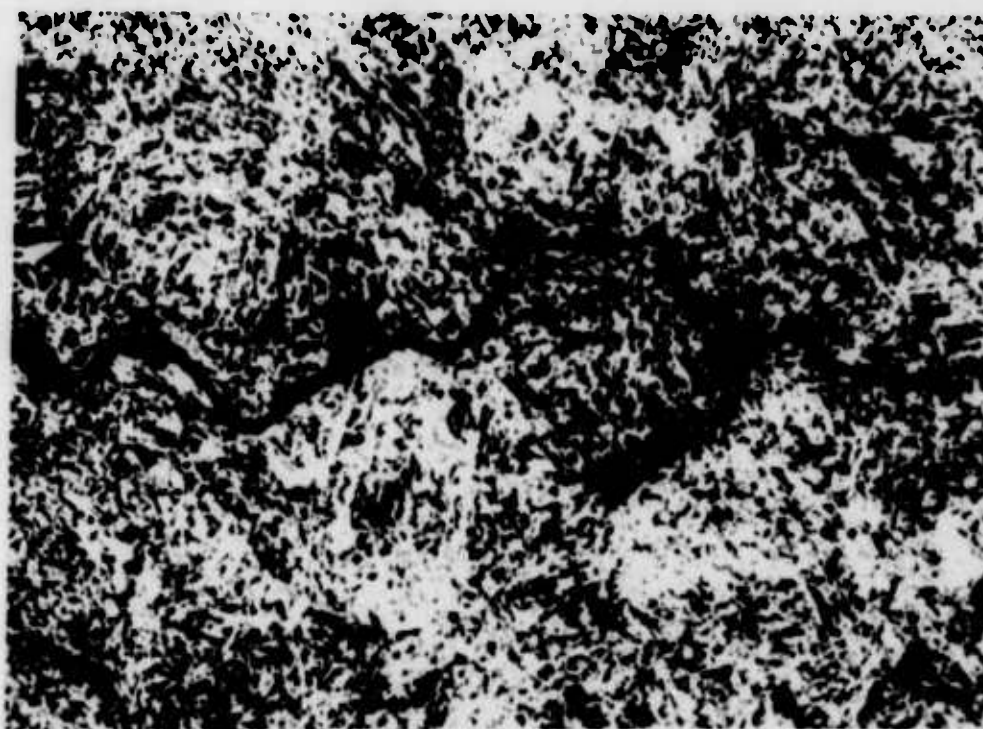


FIGURE 70

Stress Corrosion Cracking in 4340 Heat Treated to 240,000 psi Strength. Picral plus Cu Cl₂ 750X

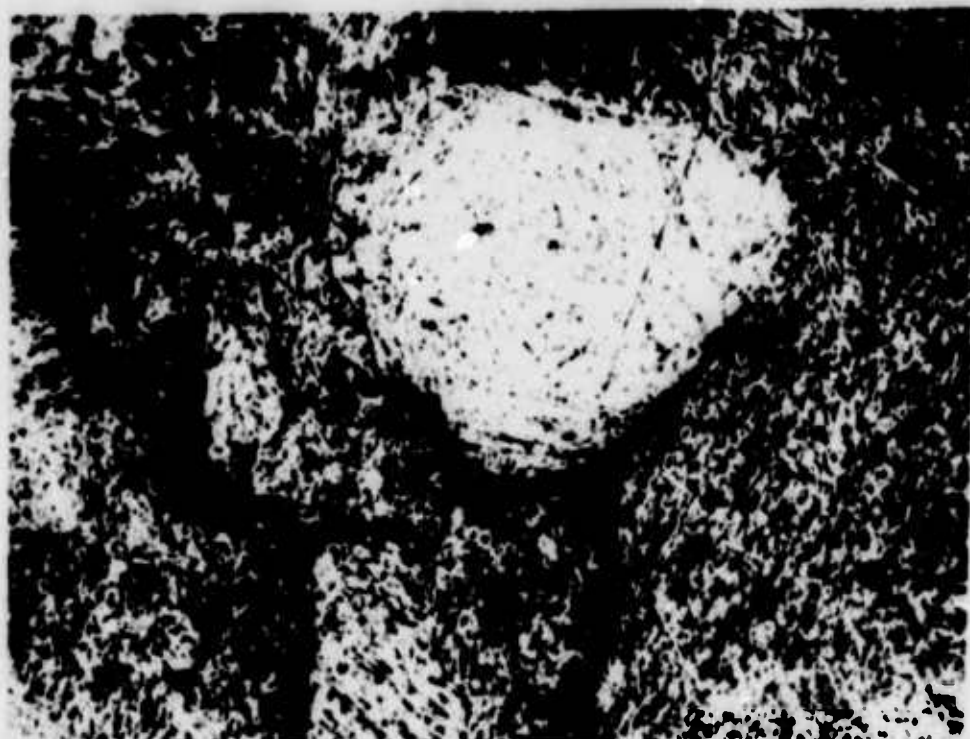


FIGURE 71
Stress Corrosion Cracking in 4340M
Heat Treated to 290,000 psi Strength
Picral plus Cu Cl₂ 750X

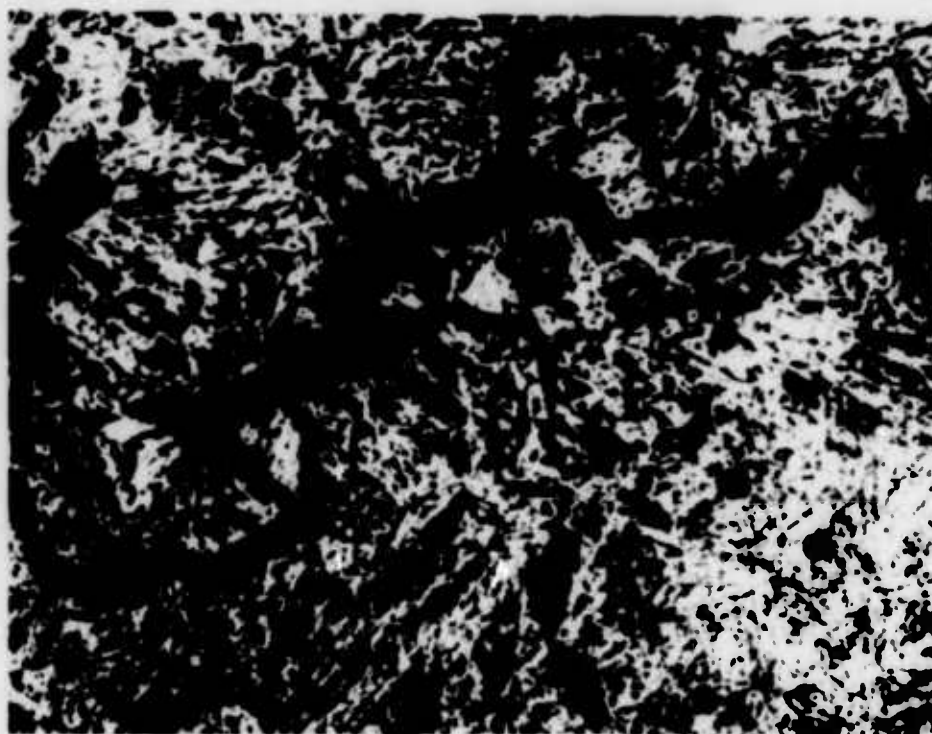


FIGURE 72
Stress Corrosion Cracking in 4330M
Heat Treated to 227,000 psi Strength
Picral plus Cu Cl₂ 750X

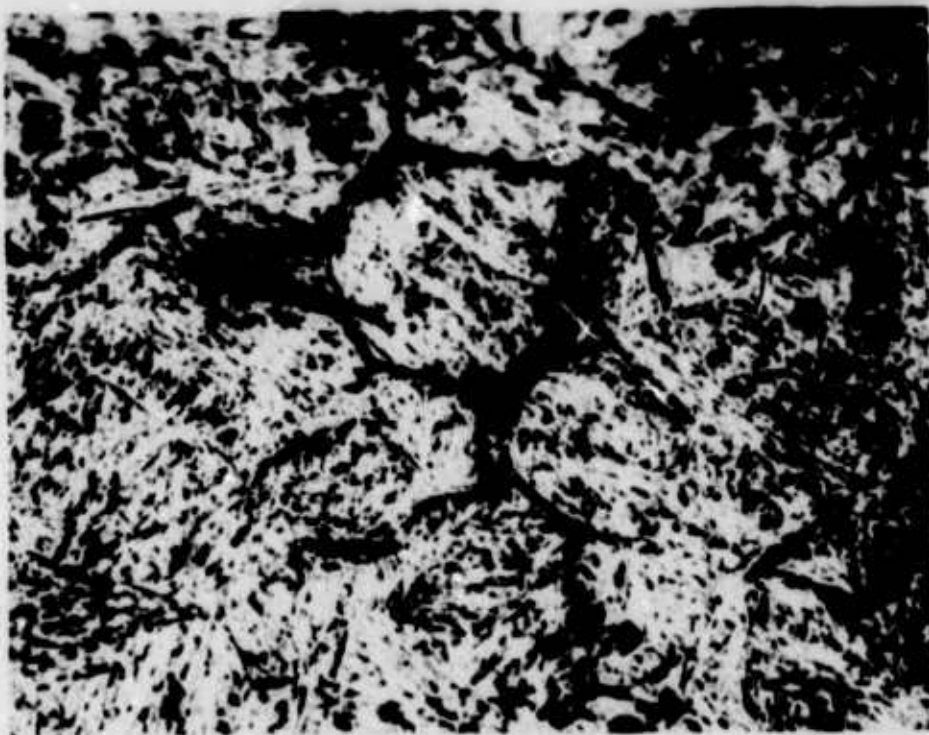


FIGURE 73
Stress Corrosion Cracking in H-11
Heat Treated to 293,000 psi Strength
Picral plus Cu Cl₂ 750X

FIGURE 74
Inclusions Surrounded by Corrosion Products.
Microstructure Revealed by Lightly Polishing Away
Rust Cover on Ground Tension Surface 250X

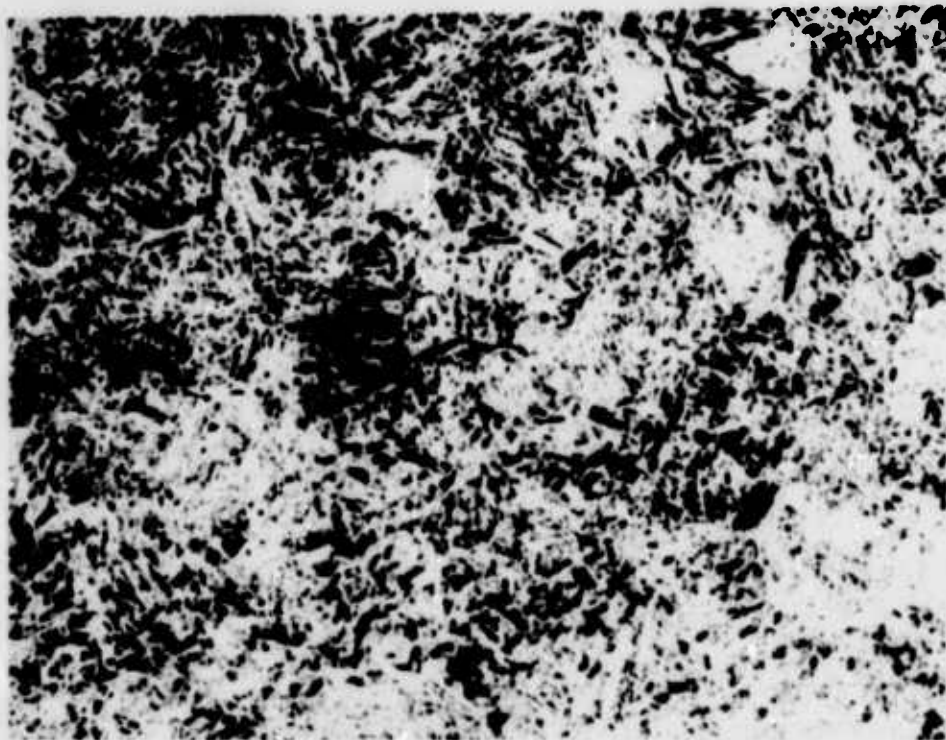


FIGURE 75
Crack Originating From Inclusion Pit and
Traveling Parallel to Fracture Face Nital 500X

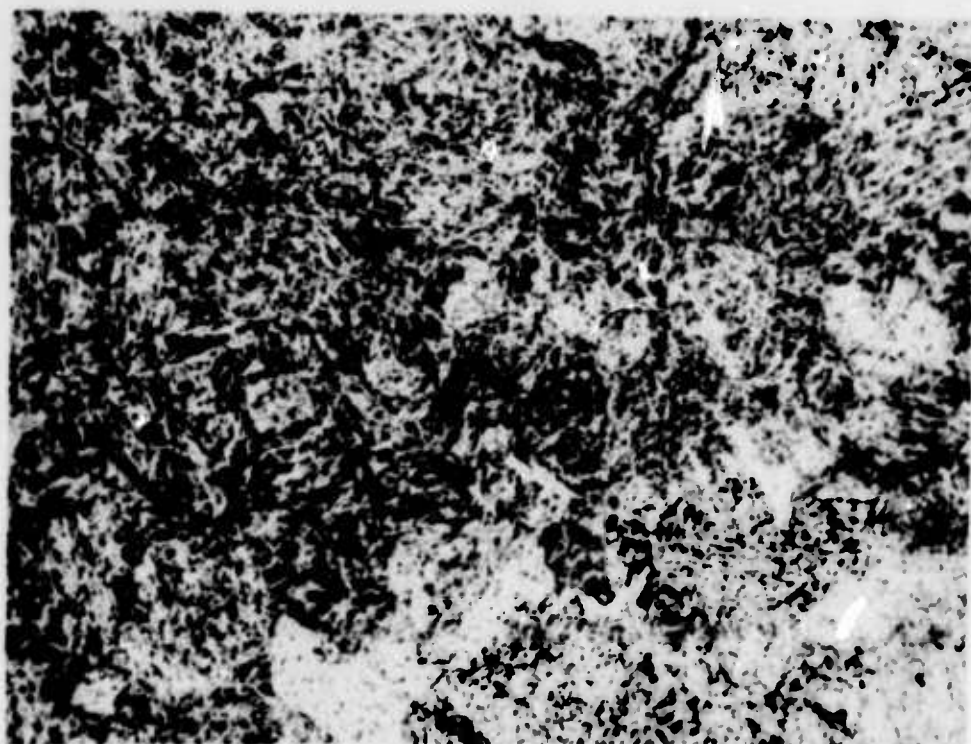


FIGURE 76
Microstructure of 4340 (Billet K) Heat Treated to
174,000 psi Strength Cu Cl₂ 400X



FIGURE 77
 Microstructure of 4330M (Billet R)
 Heat Treated to 188,000 psi Strength. Picral plus Cu Cl₂
 750X

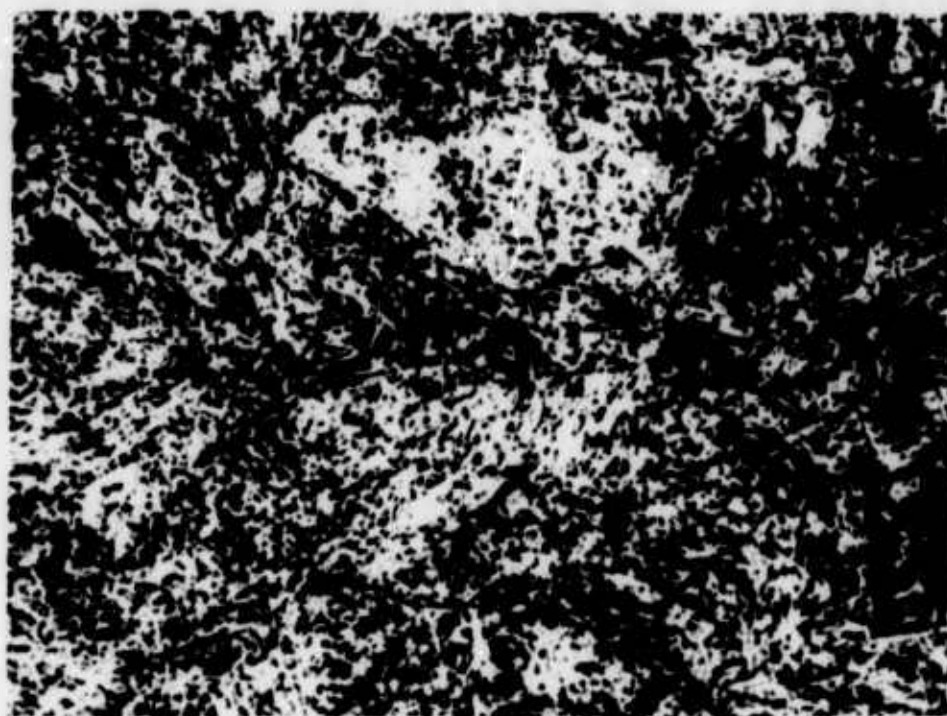


FIGURE 78
 Microstructure of H-11 (Billet V) Heat Treated to
 235,000 psi Strength. Picral plus Cu Cl₂
 750X

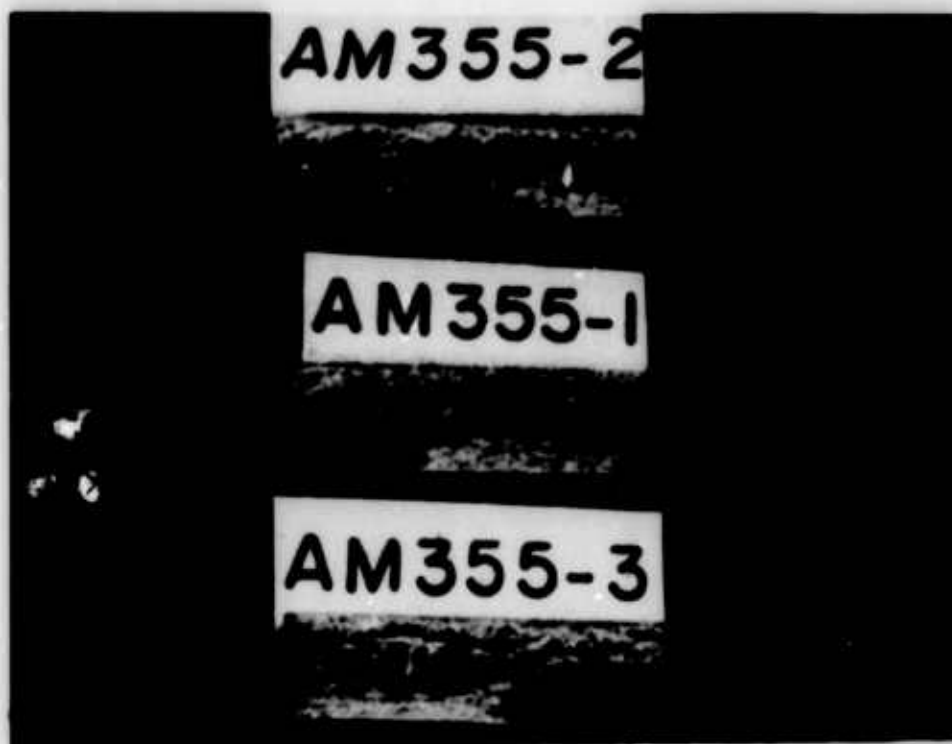


FIGURE 79
Fracture Faces of AM 355 SCT 850
Plate Specimens
216,000 psi Strength



FIGURE 83
Fracture Face of AM 350 SCT 850
Specimen
200,000 psi Strength

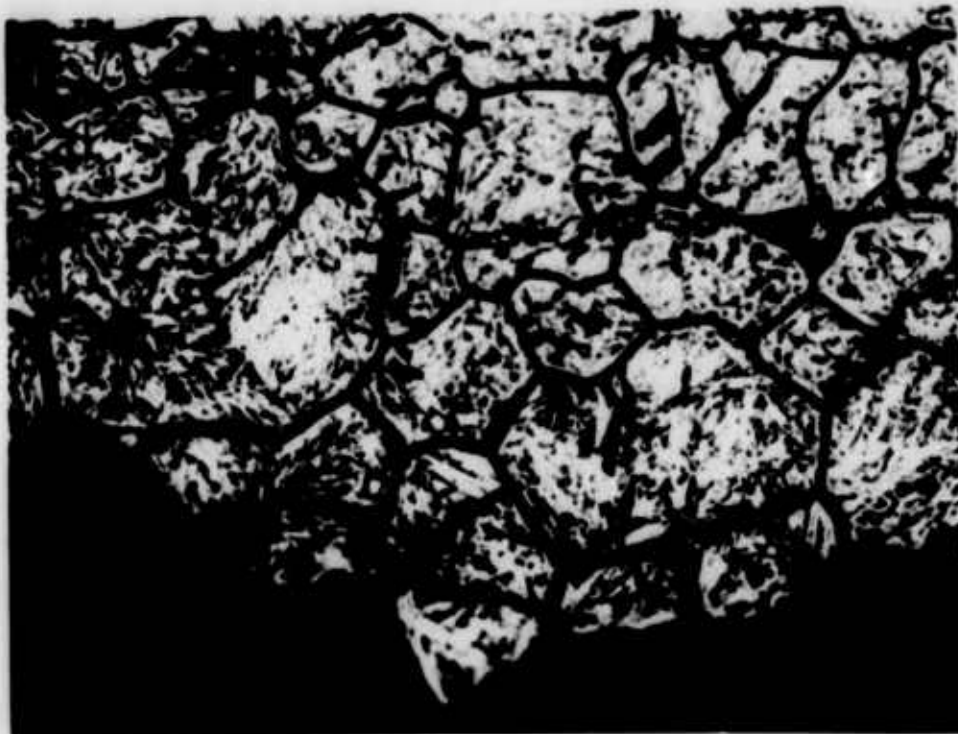


FIGURE 80
Microstructure of AM 355 Plate Near Fracture Origin
Ammonium Persulphate 400X



FIGURE 81
AM 355 Billet Material Heat Treated to the SCT 850
Condition Using Standard Procedure. Ammonium Persulphate
400X

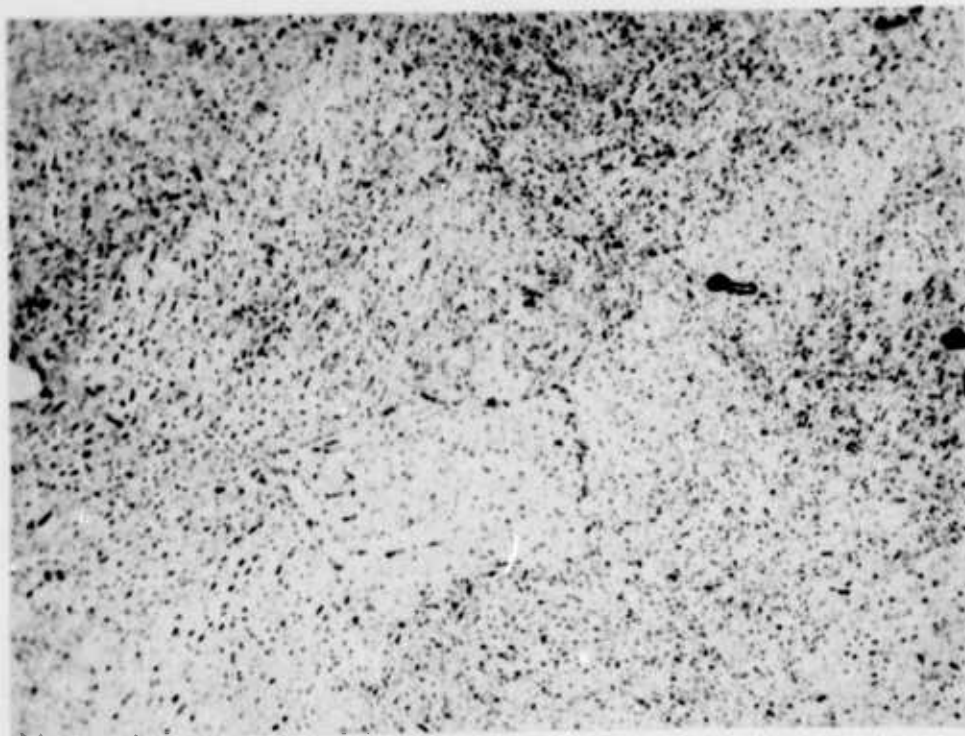


FIGURE 82
AM 355 Billet Material Heat Treated to the SCT 850 Condition
Using Modified Procedure. Ammonium Persulphate 400X

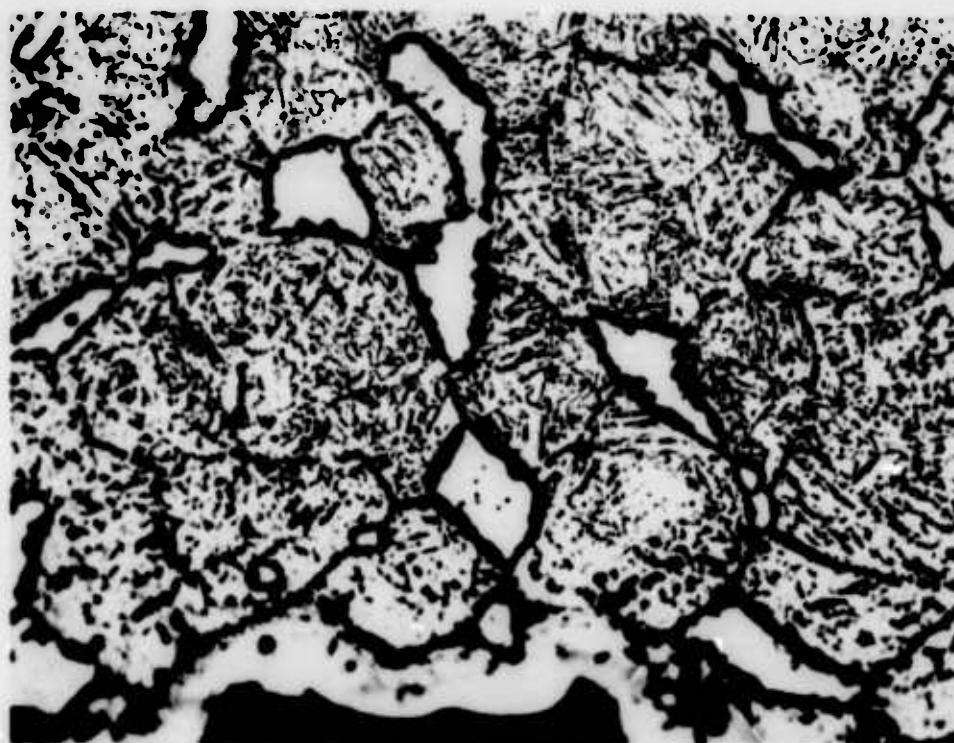


FIGURE 84
Microstructure of AM 350 SCT 850 Specimen 3Y Near
Fracture Origin. White Areas are Delta Ferrite
Ammonium Persulphate 400X

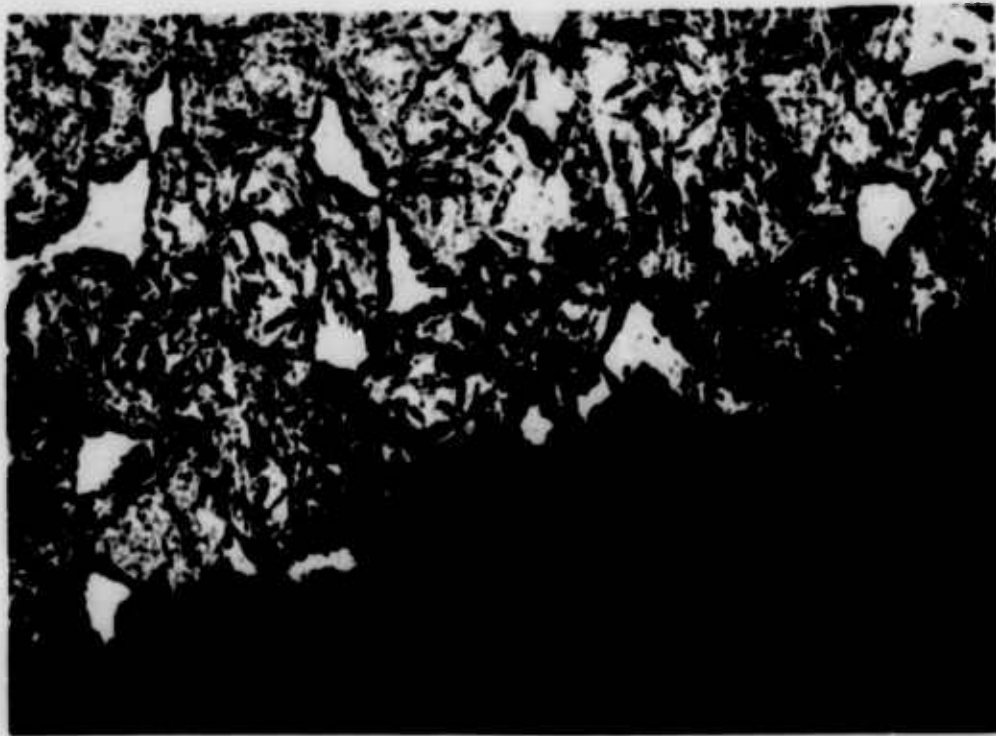


FIGURE 87
Tensile Fracture Face of AM 350 DA 850 Specimen
Ammonium Persulphate 250X

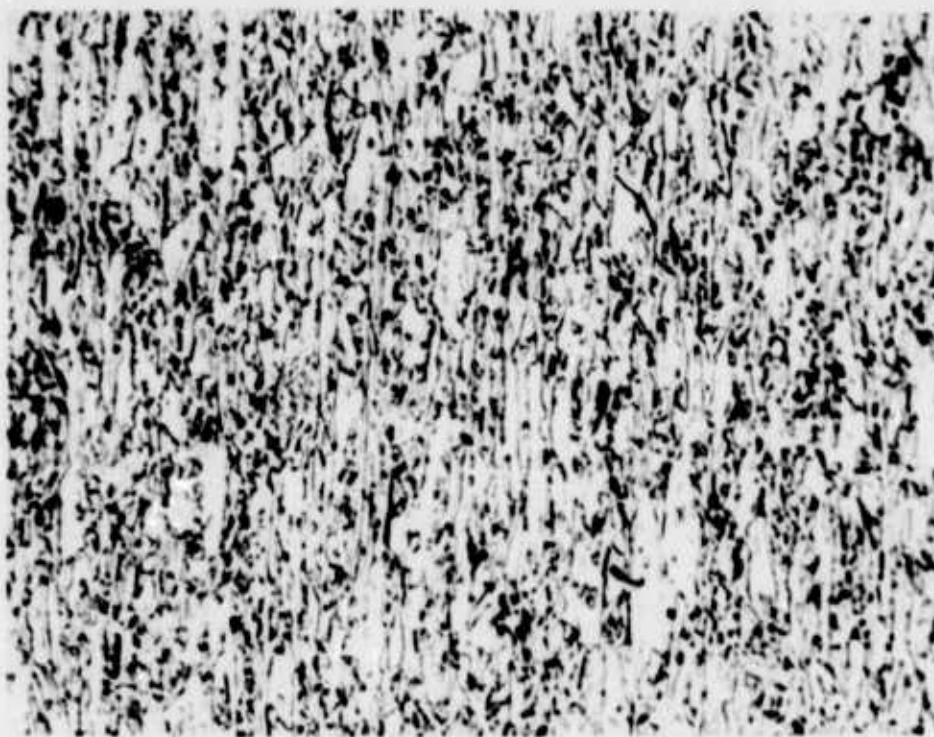


FIGURE 88
Microstructure of AM 350 CRT 850
0.060" Sheet in the Longitudinal Grain Direction
Ammonium Persulphate 400X



FIGURE 89
Microstructure of AM 350 CRT 850
0.060" Sheet in the Transverse Grain Direction
Ammonium Persulphate 400X

APPENDIX I

STRESS CORROSION SPECIMEN

CONFIGURATIONS

STRESS CORROSION SPECIMEN CONFIGURATIONS

I. THE TAPERED CANTILEVER SPECIMEN

A. Analytical Stress Analysis

Figure 90 shows the tapered cantilever specimen with coordinate axes and load P.

The bending moment at any point x is $M = P (l-x)$.

The longitudinal bending stress σ_x at any point x is

$$\sigma_x = \frac{M_c}{I} = \frac{P(l-x) \frac{t}{2}}{\frac{bt^3}{12}} = \frac{6P(l-x)}{bt^2}$$

From trigonometry

$$\frac{b_1}{l} = \frac{b}{l-x} \quad \text{or} \quad b = b_1 \left(\frac{l-x}{l} \right)$$

Hence, $\sigma_x = \frac{6Pl}{b_1 l^2}$ and is theoretically constant for any section along the beam. There is a complicating factor, however, arising at the specimen edge because of the taper of the specimen. At the free boundary no normal or shear stresses exist. Hence, the longitudinal stress σ_x cannot be parallel to the center line of the specimen at the tapered boundary. Between the centerline of the specimen and the tapered edge, the longitudinal stress must change its direction from the x-direction to become parallel with the tapered edge.

The stresses generated in the transverse direction depend upon the width to thickness ratio b/t of the specimen. At low values of b/t , e.g., $b/t < 5$, no transverse stresses are developed. At high values of b/t , e.g., $b/t > 12$, transverse stresses are produced which approach a maximum of one-third the longitudinal stress. This variation in σ_z the transverse stress is shown in Figure 91.

The variation in shear stresses is parabolic through the thickness dimension of the specimen. The maximum shear stress varies with the distance along the x-axis.

Since $b = b_1 \left(\frac{l-x}{l} \right)$,

$$\tau_{xy} = \frac{3}{2} \frac{P}{b_1 t} \left(\frac{l}{l-x} \right)$$

For the specimen geometry shown $b_1 = 1.5$ inches and

$$\tau_{xy_{max}} = \frac{P}{t} \left(\frac{1}{1-x} \right)$$

This variation in shear stress through the thickness dimension is shown in Figure 92.

B. Experimental Stress Analysis

A tapered cantilever specimen was cut from 4340M steel sheet and heat treated to a hardness of Rockwell C 52 to 55. The final thickness dimension of the specimen after machining was 0.053 inches. Photo stress plastic was applied to the surface to be loaded in tension. Loads of 4000, 6000, and 7000 grams were applied and stress readings were made at the positions shown in Figure 93. A color photograph of the photo stress plastic under load is shown in Figure 94.

Strain gage rosettes were applied at the two positions shown in Figure 93 after removal of the photo stress plastic. Readings were made under similar loading conditions. Table LVIII contains the computed photo stress and strain rosette data.

II. THE PHELPS - LOGINOW SPECIMEN

A. Analytical Stress Analysis

A stress analysis of the Phelps-Loginow specimen is best approached by assuming the specimen behaves as a pin-loaded column. Wang (1) has carried out such an analysis. Figure 95 shows the coordinate axes and variables used to assess the deflection and hence, bending moment M of such a column.

The bending moment M at any cross section is $-PW$ and the differential equation of the deflection curve is

$$\frac{EI}{R} = -PW$$

The exact expression for curvature of the beam is

$$\frac{1}{R} = \frac{d\theta}{ds}$$

Combining these two expressions yields the differential equation

$$EI \frac{d\theta}{ds} + PW = 0$$

Wang (1) solves this equation and applies boundary conditions to obtain an expression for δ , the deflection at midspan and L , the length of the column

$$L = \frac{2}{k} \int_0^{\pi/2} \frac{d\phi}{\sqrt{1-p^2 \sin^2 \phi}} = \frac{2K}{k}$$

where $K = \int_0^{\pi/2} \frac{d\theta}{\sqrt{1-p^2 \sin^2 \theta}}$

and $K^2 = \frac{P}{EI}$

and $\sin \frac{\theta}{2} = p \sin \phi$

For the deflection δ , at midspan where $\theta = 0$

$$\delta = \frac{1}{2k} \int_0^{\alpha} \frac{\sin \theta d\theta}{\sqrt{\sin^2(\frac{\alpha}{2}) - \sin^2(\frac{\theta}{2})}}$$

and in terms of ϕ

$$\delta = \frac{2p}{k} \int_0^{\pi/2} \sin \phi d\phi = \frac{2p}{k}$$

Wang shows that

$$\frac{\delta}{L} = \frac{2p}{\pi \sqrt{P/P_{CR}}} = \frac{P}{K}$$

It can be shown that evaluation of the foregoing expressions with a table of elliptical integrals yields results shown graphically in Figure 96.

For the specimen dimensions used by Phelps and Loginow, a longitudinal stress can be derived from Figure 96 and the formula

$$\sigma_x = - \frac{P}{A} + \frac{Mc}{I}$$

The specimen geometry used by Phelps and Loginow was as follows:

Length $L = 7$ inches

Width $B = 1$ inch

Thickness $= 0.050$ inches

A bending jig with a span H of 6.51 inches was constructed at Boeing to evaluate a specimen with dimensions described above.

For this specimen $H/L = 0.935$

For this value of H/L , Figure 96 shows that $\delta/L = 0.16$. Hence $\delta = 0.16(7) = 1.12$ inches. Also from Figure 96 for $\delta/L = 0.16$, $P/P_{CR} = 1.034$.

P_{CR} can be calculated from the Euler column buckling formula

$$P_{CR} = \frac{\pi^2 E I}{L^2} \quad \text{where } I \text{ is the moment of inertia of the cross section.}$$

$P_{CR} = 63$ pounds and hence, $P = (1.034)(63) = 65$ pounds.

With this value of P , one is able to calculate σ_x the longitudinal stress.

$$\begin{aligned} \sigma_x &= - \frac{P}{A} + \frac{Mc}{I} = - \frac{P}{A} + \frac{6Ps}{Bt^2} \\ &= - \frac{65}{0.05} + \frac{6(65)(1.12)}{1(0.005)^2} \end{aligned}$$

$$\therefore \sigma_x = -1300 \pm 175,000$$

For the tensile surface $\bar{\sigma}_x = 173,700$ psi.

In summary, the solution for the deflection of a pin-ended column as outlined by Wang(1), may be used to calculate a stress level (longitudinal) for the Phelps-Loginow bend specimen. Numerical calculations for a specimen at dimensions used by Phelps and Loginow and bending jig 6.5 inches long yield a tensile stress level of 173,700 psi.

B. Experimental Stress Analysis

A Phelps-Loginow specimen was cut from a piece of 4340M sheet and heat treated to Rockwell C 50 to 53. The final dimensions after machining were 7 inches x 1 inch x 0.050 inch. The specimen was coated with photostress plastic and loaded in bending between supports 6.51 inches apart. Figure 97 shows a color photograph (of the stressed specimen) taken with polarized light. Photostress readings taken normal to the plastic surface are depicted graphically in Figure 98. Only longitudinal stresses were evaluated with this specimen.

Two strain gages were applied at the maximum stress area of a second identically processed specimen. Both gages measured longitudinal strain except that one was at the center of the specimen and one at the edge. It was virtually impossible to attain a consistent reading on either gage because of relaxation of the specimen under load. However, at any one time the outer gage read approximately 15 per cent higher than the central gage. These readings corroborate approximately those made with the photostress analysis.

One complicating factor in this analysis was that of permanent set in the specimen after unloading. Even though strain readings were well below the yield point of the 4340M steel permanent set was appreciable (approximately 1/4 inch at mid span). No explanation for this phenomenon was readily apparent.

II. BOEING U-BEND SPECIMEN

A. Analytical Stress Analysis

The analysis of the Boeing U-bend specimen can be approached very simply. A beam as depicted in Figure 99 is subjected to pure bending by two end moments. These moments are applied by closing the two legs of the U-specimen.

The longitudinal bending stress can be calculated from

$$\sigma = \frac{Mc}{I}$$

A typical bending moment for use with this specimen is 2000 in-lbs. For this value of M, and for the dimensions shown in Figure 100

$$\sigma = \frac{6M}{bt^2} = \frac{6(2000)(16)}{1} = 192,000 \text{ psi}$$

B. Experimental Stress Analysis

Two specimens of the configuration shown in Figure 100 were machined from 4340M steel and heat treated to Rockwell C 51 to 53. One specimen was coated with photostress plastic and loaded to three different nominal stress levels of 60,000, 120,000 and 140,000 psi. Figure 101 shows the variation in longitudinal bending stress along the test section of the specimen. Figure 102 shows a photograph under polarized light of the U-bend specimen stressed to 140,000 psi.

Strain gages were applied to the second specimen as shown in Figure 100. The specimen was then loaded to three nominal stresses of 140,000, 210,000 and 250,000 psi and strain gage readings taken at each level. The results of this testing are shown in Table LIX.

The modification of the U-bend configuration to a simple bar and jig combination (Figure 103) was analyzed using photostress and strain gauges. The only difference was the use of 4340 (Rockwell C 53 to 55) instead of 4340M steel.

Strain gauge locations on a modified U-bend specimen are given in Figure 104 and the photostress reading points in Figure 105. The uniformity after loading to 185,000 psi (and agreement with prior stress analysis) in the stress level across the tension surface is illustrated in Figures 106 and 107.

The stress distribution in a modified U-bend specimen with a 0.250 inch diameter center hole was measured experimentally. Locations of the photostress reading points are shown in Figure 105. In the longitudinal direction, along the center axis the stresses were uniform (65,000 psi) 1.50 inches from the specimen end to within 0.5 inch of the center hole. At this point the stresses gradually decrease to the center hole edge (Figure 108). The maximum stresses (150,000 psi) occur at the edges of the hole closest to the specimen sides (transverse to the longitudinal direction). These latter stresses gradually decrease to a constant level (75,000 psi) .08 inch from the hole edge (Figure 109).

When loading a U-bend specimen of the center hole configuration the maximum stresses could be determined from the ratio of the stresses at the edge of the center hole and in the area of uniform stress ($\frac{150,000}{65,000}$ or 2.30), since the stresses in the uniform stress area

between the center hole and specimen end are known from either strain gauge or by deflection measurements.

The stress variation in the modified Boeing U-bend specimen after a bolt had been placed in the center hole is illustrated in Figures 110, 111, and 112. The stresses at the edge of the washer on the tension side, near the specimen sides, were approximately 1.4 times the stresses in the area of uniform loading. The stress distribution at the edge of the center hole could not be determined.

REFERENCE

- (1) C. Wang, Applied Elasticity, McGraw-Hill 1953, p. 217

TABLE LVIII

Strain Gauge and Photostress Readings
on Tapered Cantilever Specimen

Photostress Stress Analysis

<u>Reading Position</u>	<u>Load Grams</u>	<u>(long) (psi x 10⁻³)</u>	<u>(trans) (psi x 10⁻³)</u>
1	4000	63.8	14.3
	6000	94.6	23.1
	7000	111.1	25.3
2	4000	75.9	1.1
	6000	112.2	3.3
	7000	132.0	3.3
3	4000	78.1	5.5
	6000	116.6	6.6
	7000	136.4	8.8
4	4000	68.2	13.2
	6000	103.4	18.7
	7000	119.8	22.0
5	4000	66.0	13.2
	6000	95.7	22.0
	7000	111.1	26.4

Strain Gauge Stress Analysis

1	4000	65.1	23.8
	6000	99.4	37.1
	7000	118.3	44.8
2	4000	68.4	20.1
	6000	105.0	31.0
	7000	129.5	38.6

TABLE LIX

Strain Gauge Test Results from U-Bend Stress Corrosion
Specimen of M300 Steel
(R_c 52 Hardness)

Nominal Stress Level (psi x 10 ⁻³)	Strain Readings Micro inches/inch				Calculated Stresses (psi x 10 ⁻³)			
	ϵ_t Gauge 1	ϵ_l Gauge 2	ϵ_l Gauge 3	ϵ_t Gauge 4	σ_l Gauge 2	σ_t Gauge 1	σ_l Gauge 3	σ_t Gauge 4
139	-1260	4500	4680	-1030	136.0	2.9	144.0	12.2
210	-1890	6700	7050	-1500	202.0	3.9	218.0	2.0
250*	-2320	8100	8420	-1770	244.0	3.6	260.0	2.5

Formulas Used for Calculation:

$$\sigma_l = \frac{(\epsilon_l + \mu \epsilon_t)}{1 - \mu^2} E; \quad \sigma_t = \frac{(\epsilon_t + \mu \epsilon_l)}{1 - \mu^2} E$$

Where σ_l = Longitudinal stress; σ_t = Transverse stress;
 ϵ_l = Longitudinal strain; ϵ_t = Transverse strain; μ = Poisson's ratio;
 E = Young's modulus

* In excess of Yield Strength

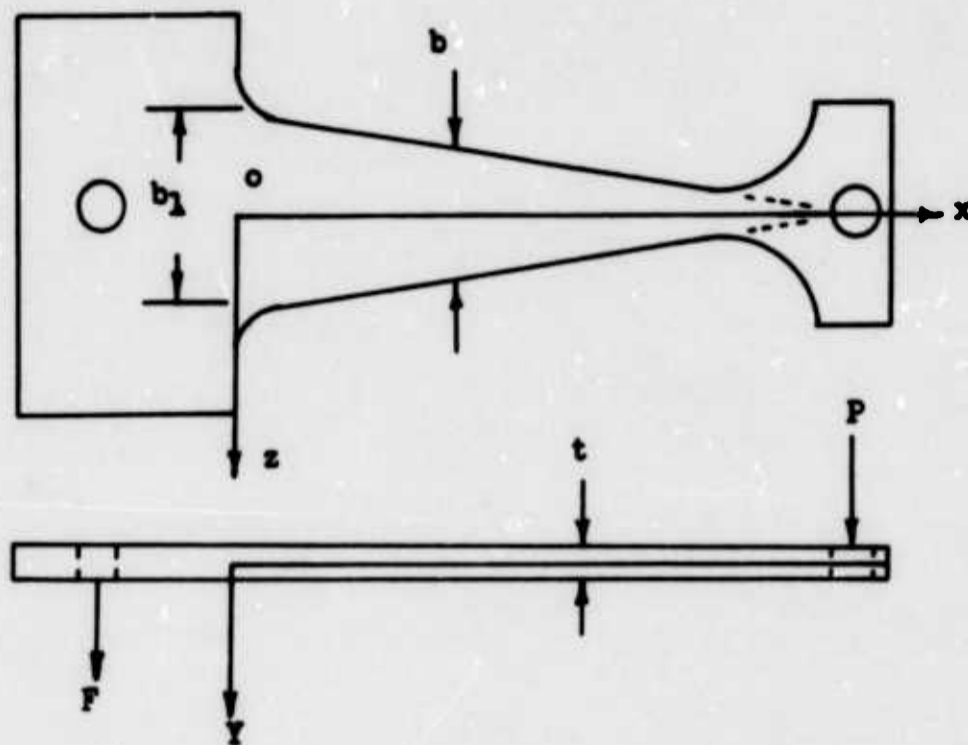
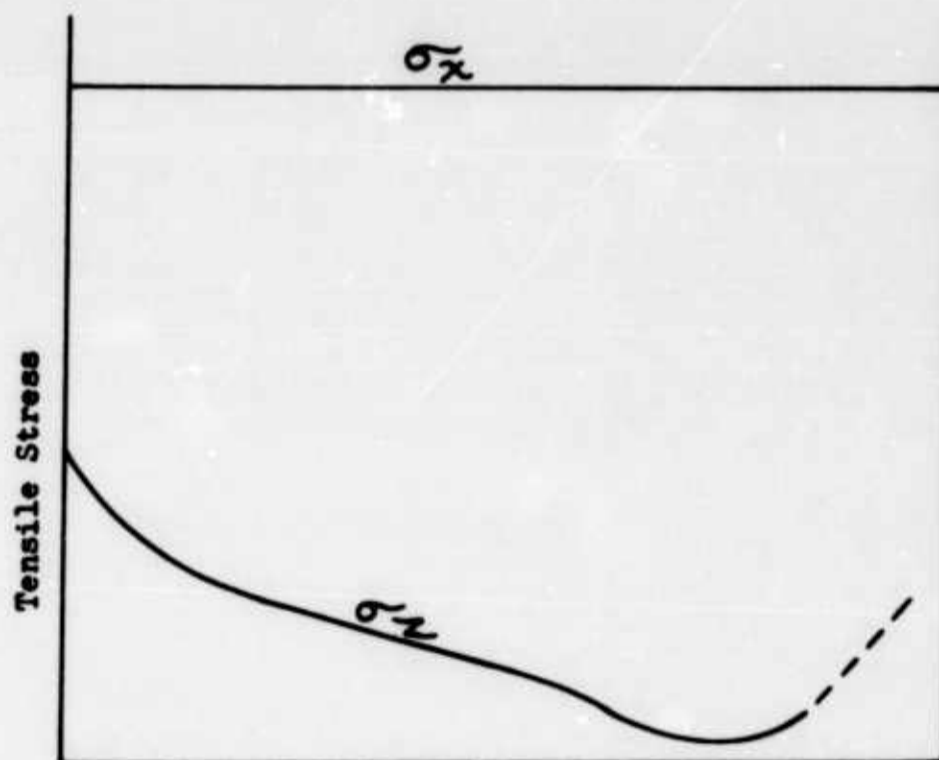


FIGURE 90. Tapered Cantilever Specimen



0 Distance Along x -Axis

FIGURE 91

Variation in Longitudinal and Transverse
Tensile Stresses in Tapered Cantilevered Specimen

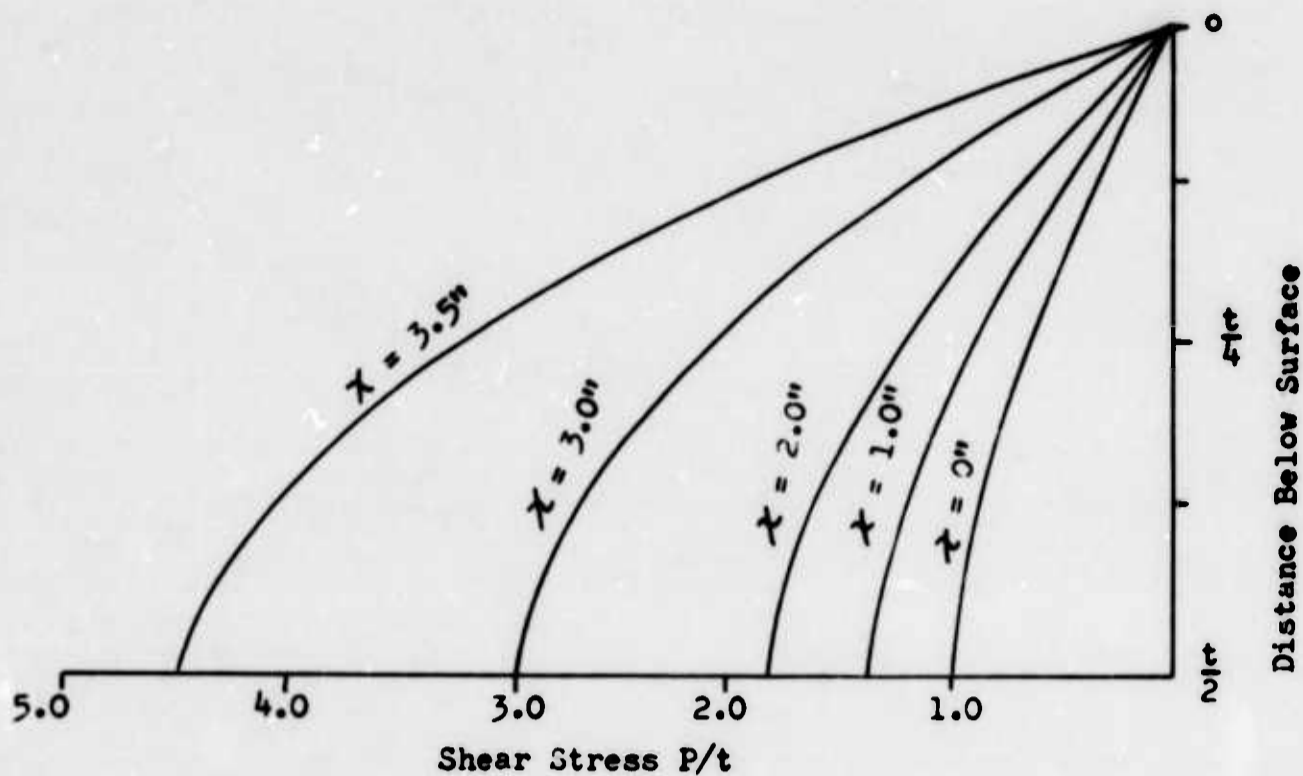


FIGURE 92
Variation in Shear Stresses Through the
Thickness of the Tapered Cantilevered Specimen

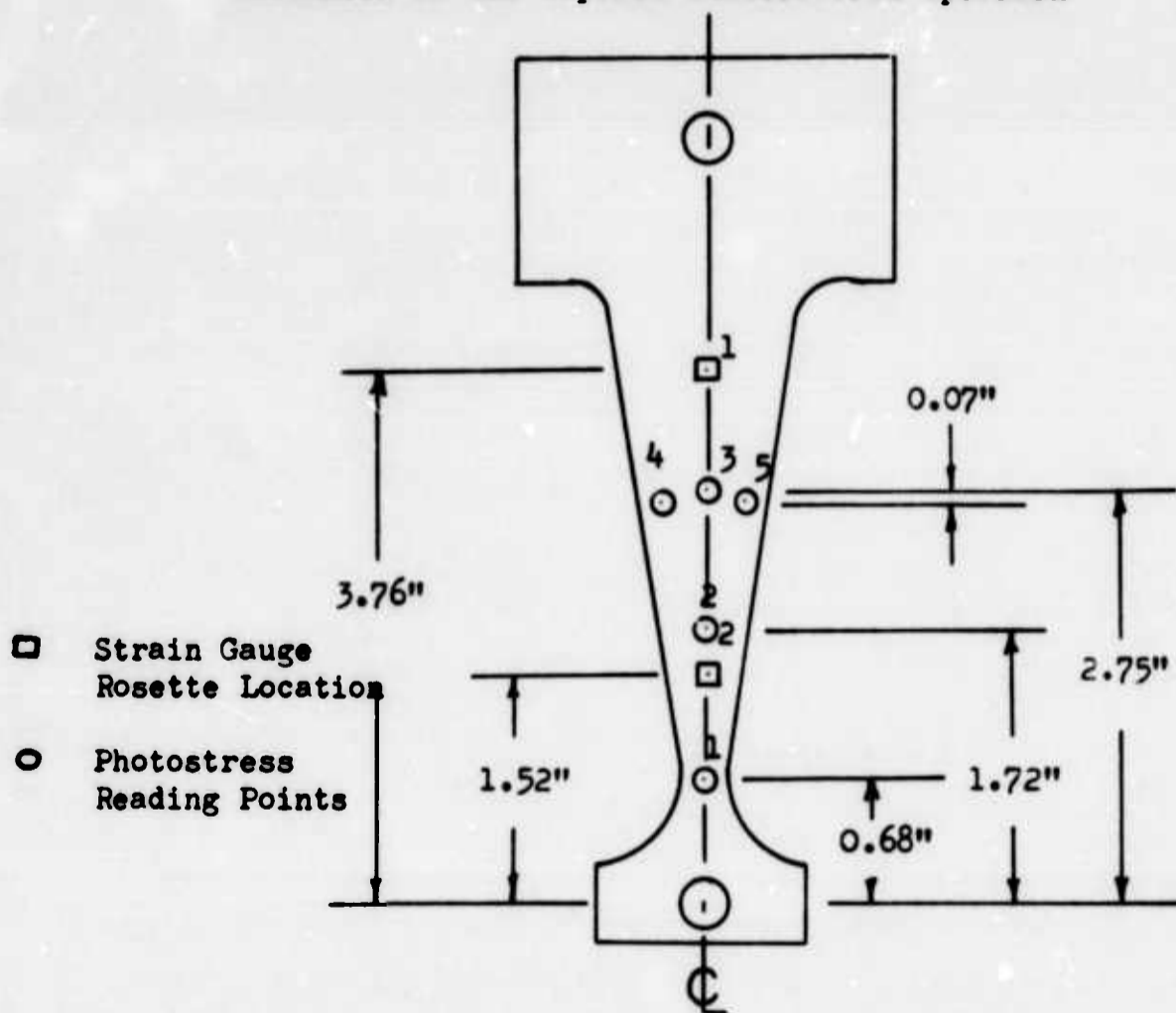


FIGURE 93. Location of Stress Readings on Tapered
Cantilever Specimen

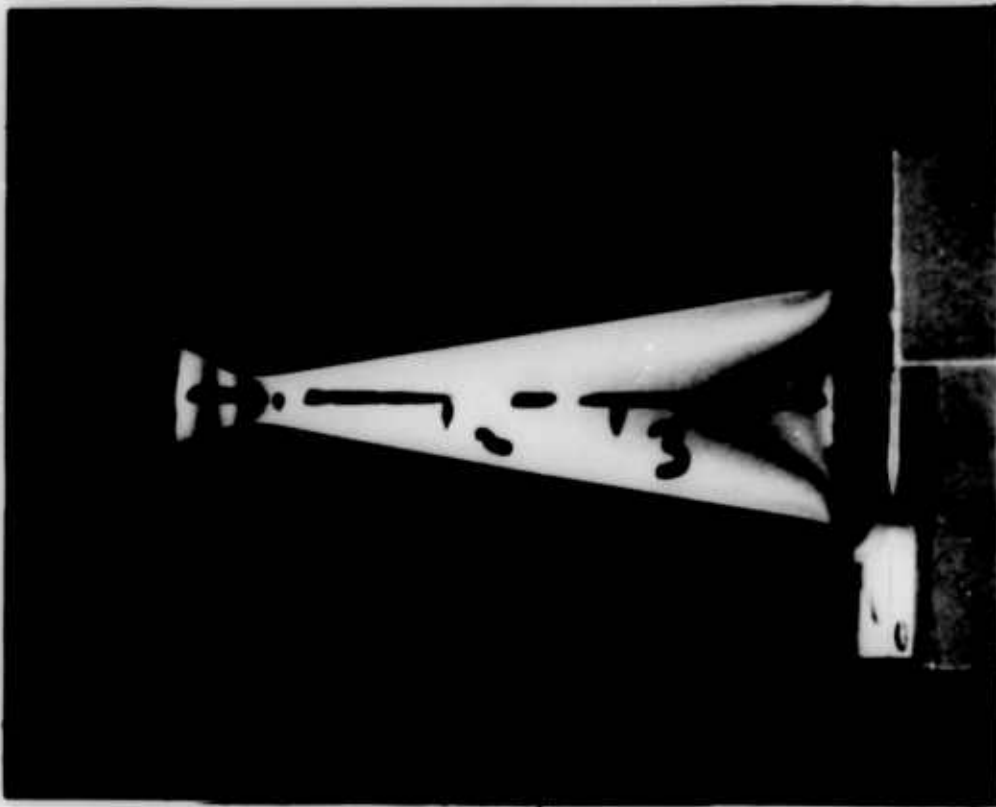


FIGURE 94

Photograph Under Polarized Light of
Stressed Cantilever Specimen with Photostress

6A 40087-1

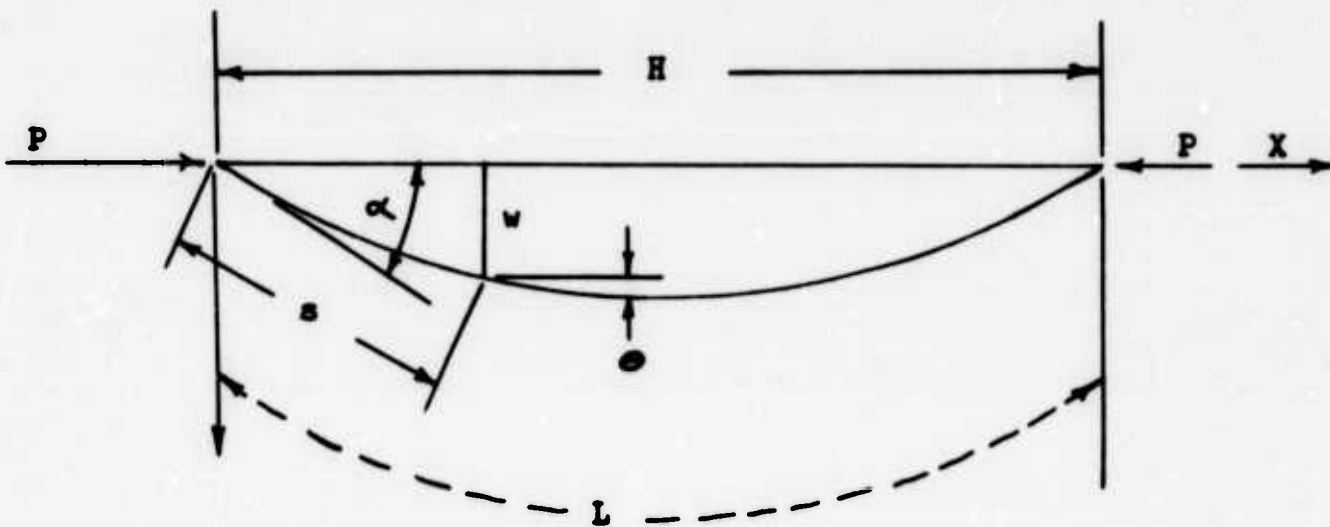


FIGURE 95

Deflection Variables in a Pin Loaded Column

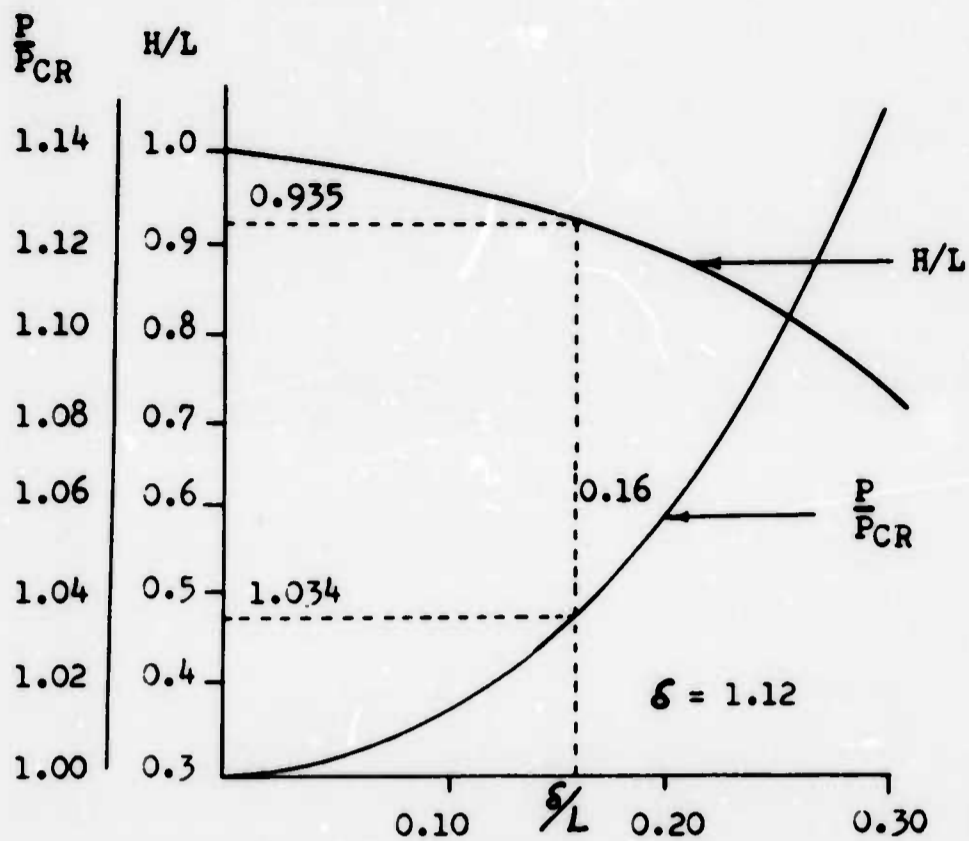


FIGURE 96

Relationship Among P/P_{CR} , H/L and δ/L for Phelps-Loginow Specimen



FIGURE 97

Photograph Under Polarized Light of Stresses
Phelps-Loginow Specimen with Photostress

6A 40087-3

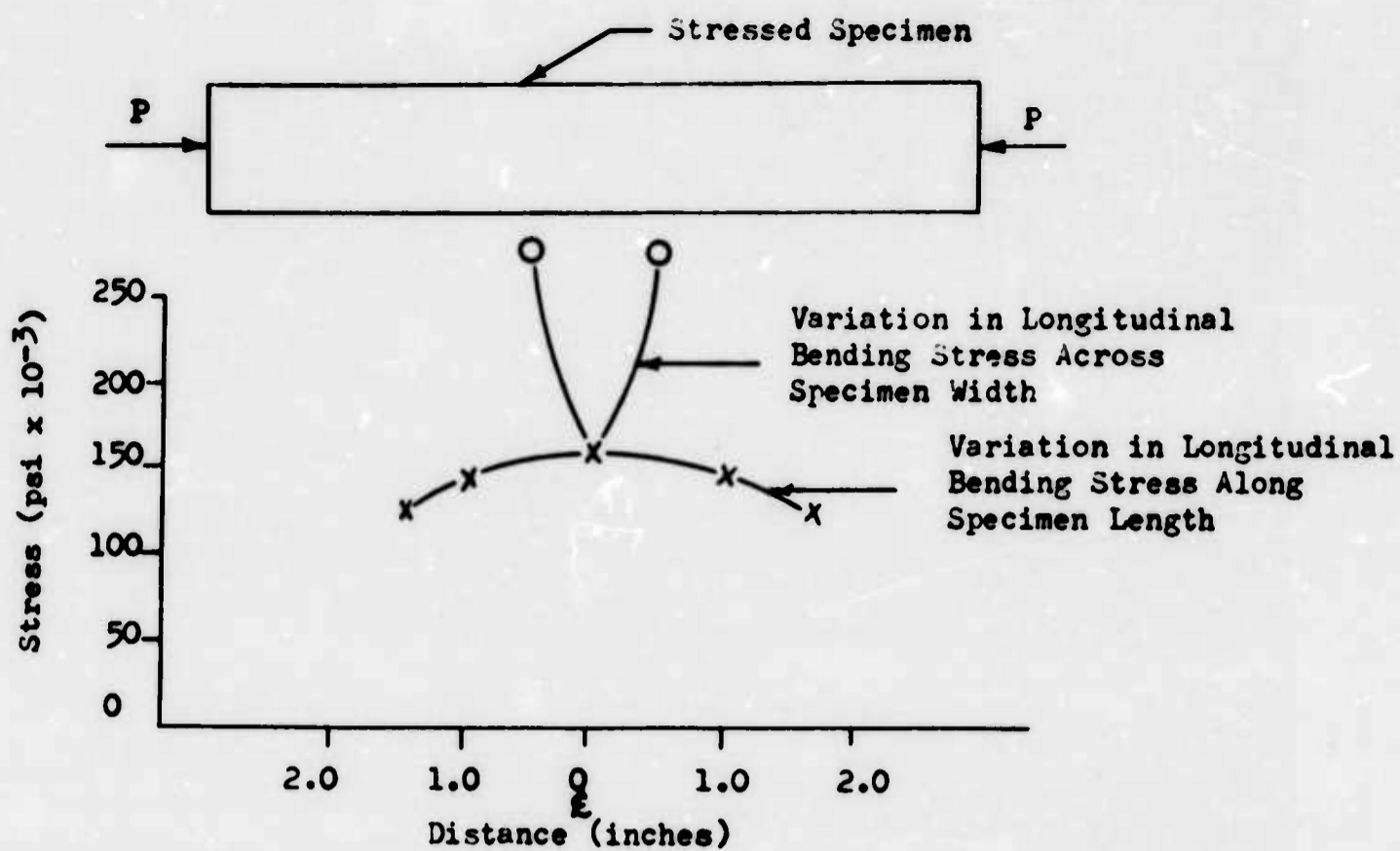


FIGURE 98. Photostress Readings from Stressed Phelps-Loginow Specimen

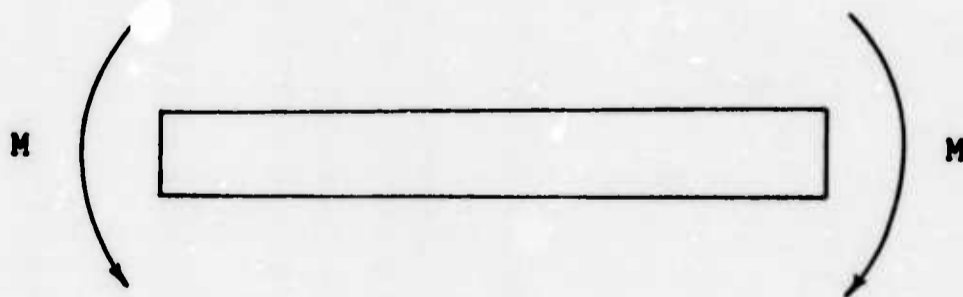


FIGURE 99
Simple Beam in Pure Bending

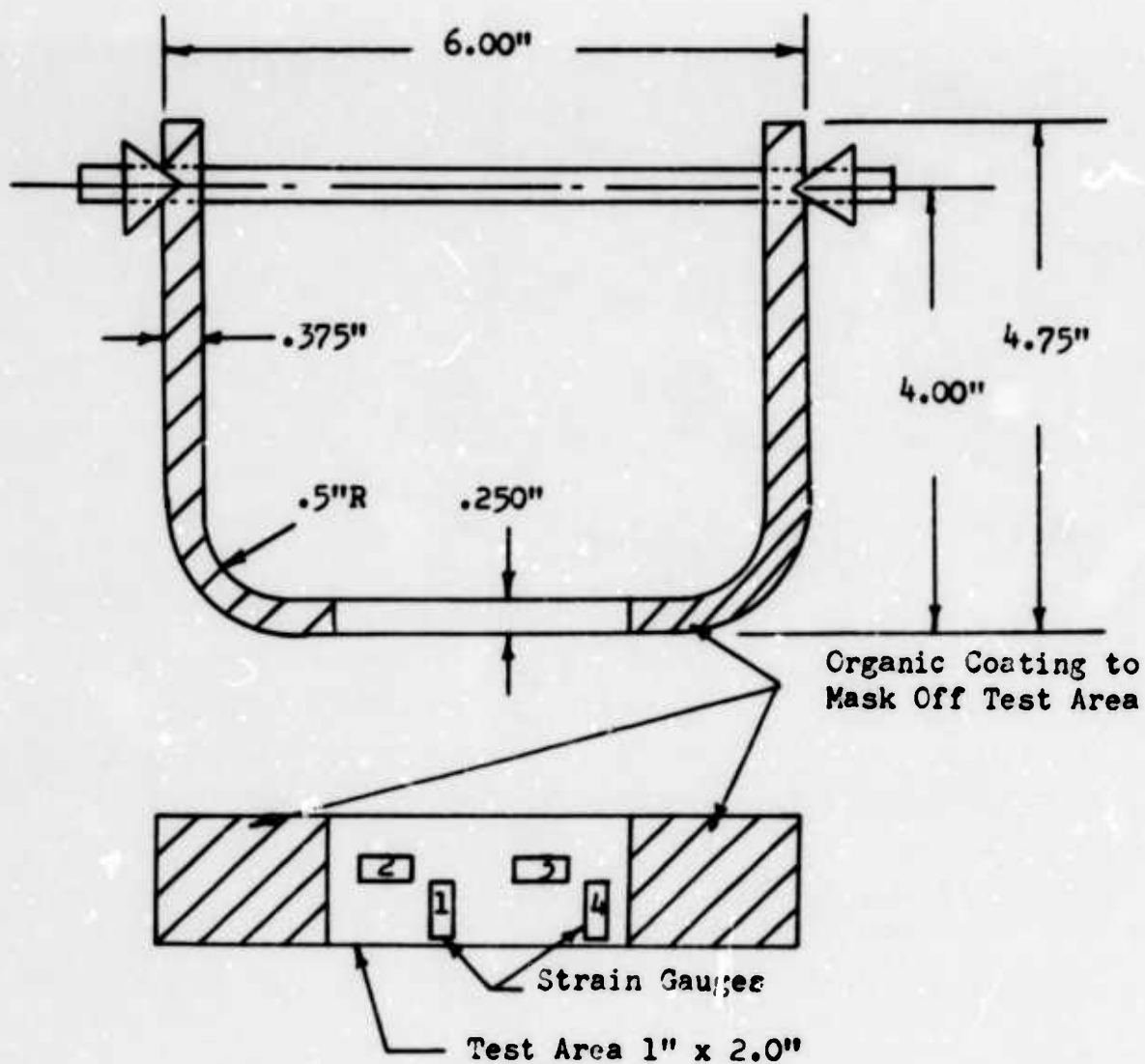


FIGURE 100. U-Type Stress Corrosion Specimen Showing Strain Gauge Locations

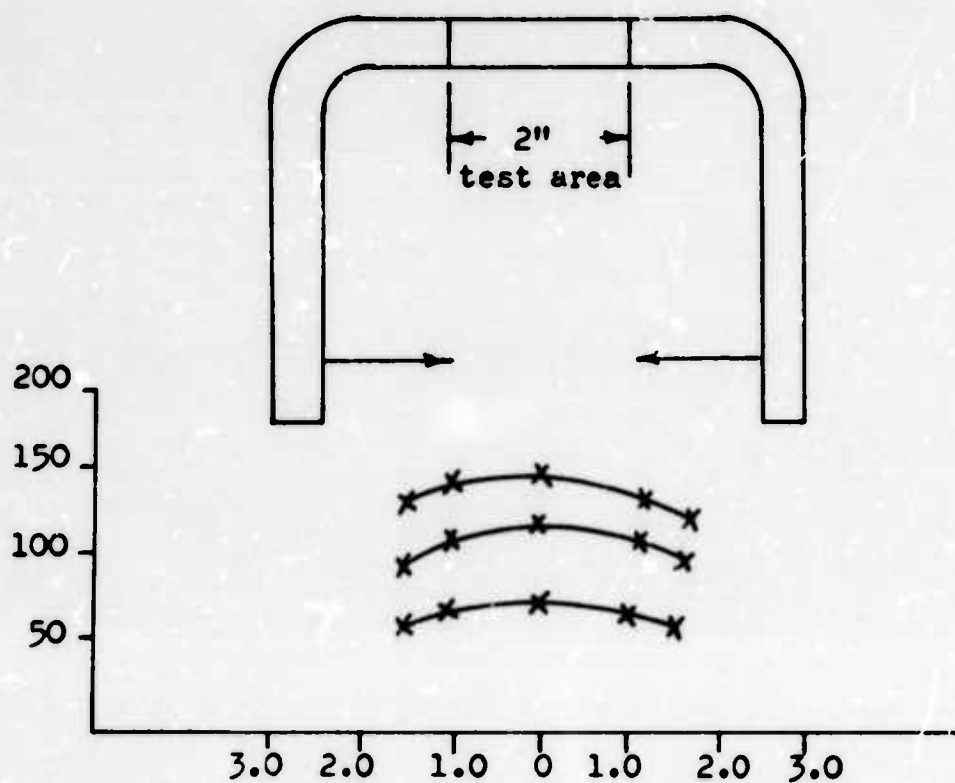


FIGURE 101. Variation in Longitudinal Bending Stress in Boeing U-Bend Specimen

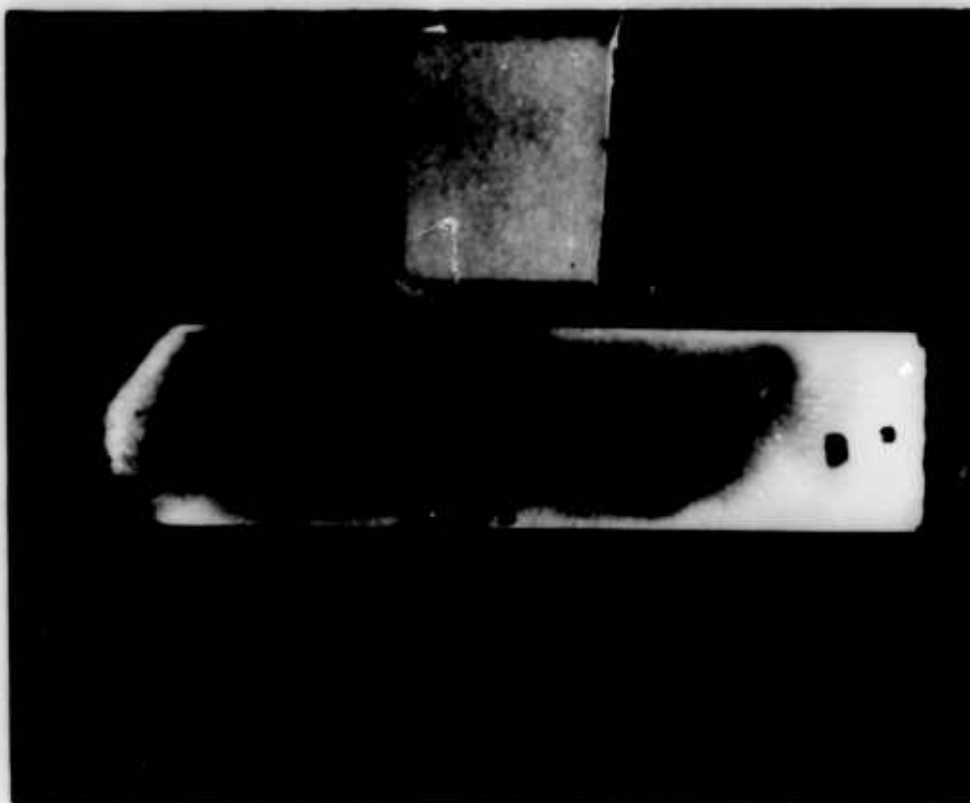


FIGURE 102

Photograph Under Polarized Light of
Stressed Boeing U-Bend Specimen
6A 40087-2

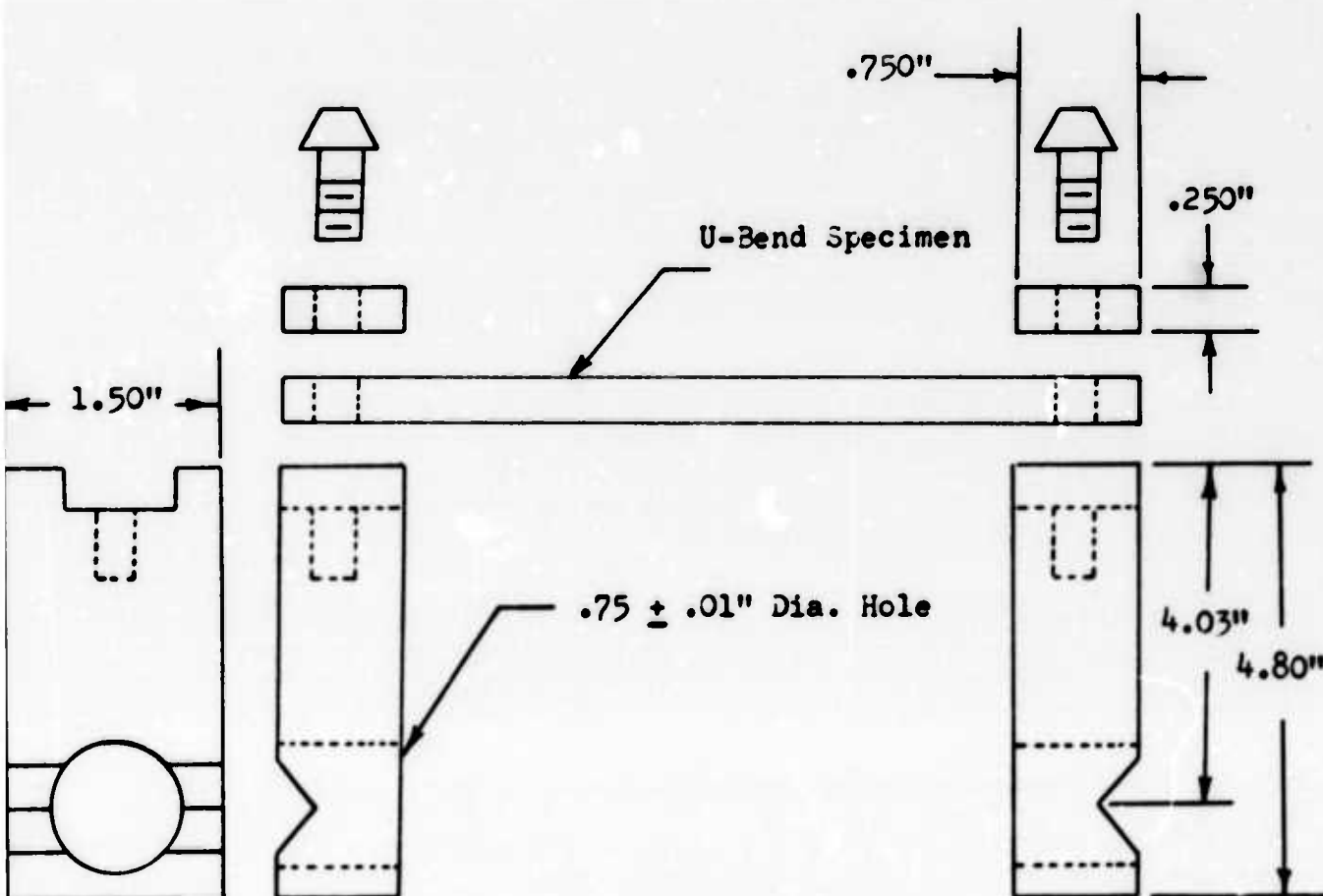


FIGURE 103

Schematic of Modified Boeing U-Bend Assembly

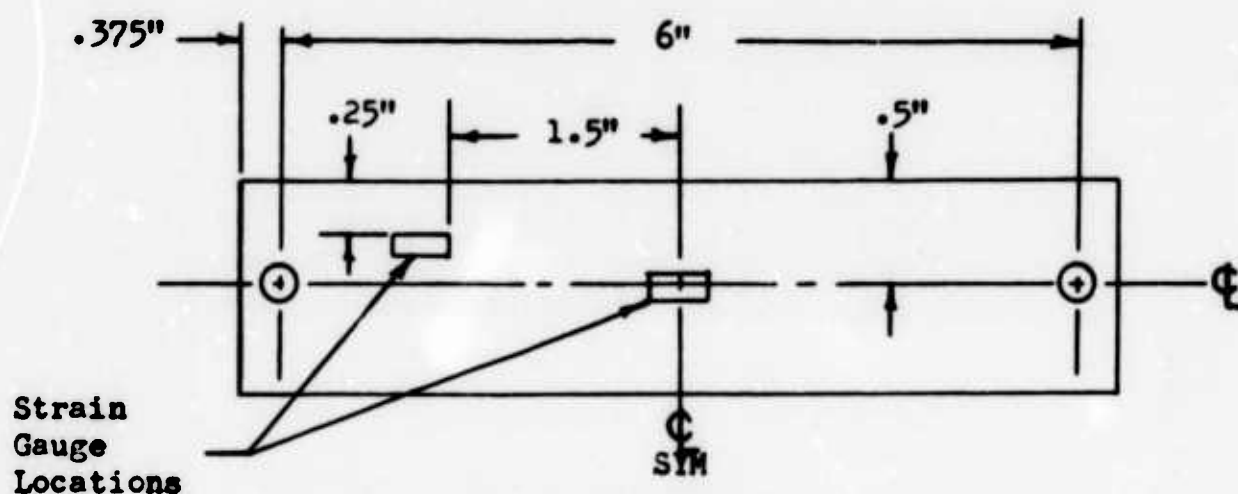


FIGURE 104

Strain Gauge Locations on Modified
Boeing U-Bend Specimen

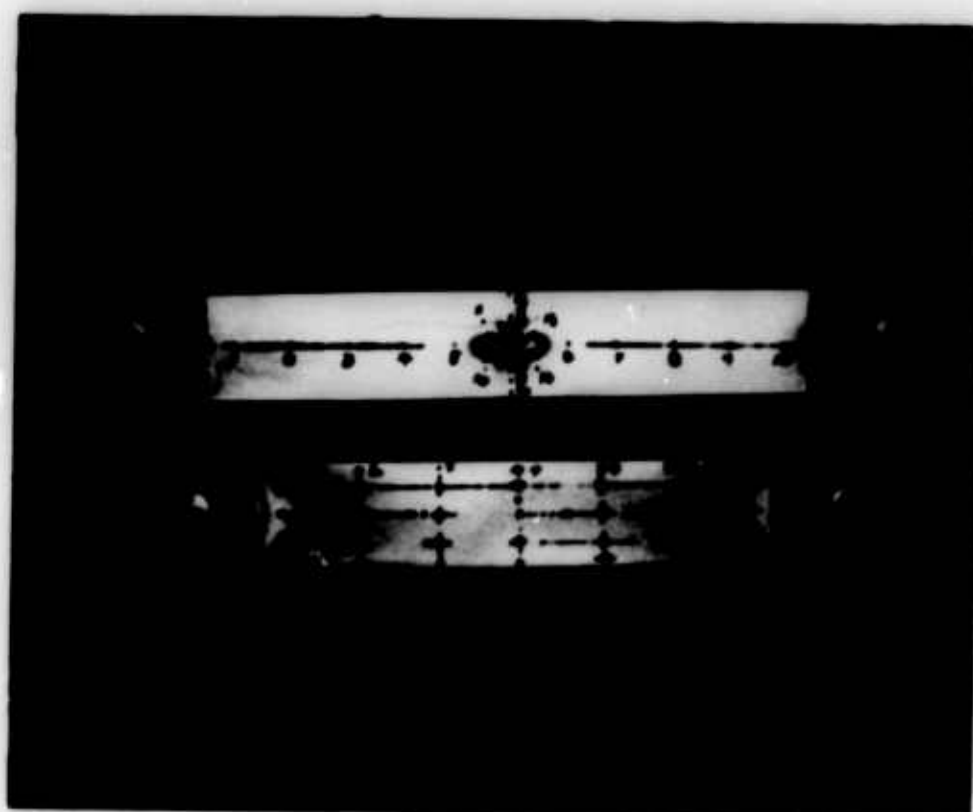


FIGURE 105

Photostressed Boeing U-Bend Specimens with
and without Center Holes. Numbers Refer
to Photostress Reading Points

6A 40236-2

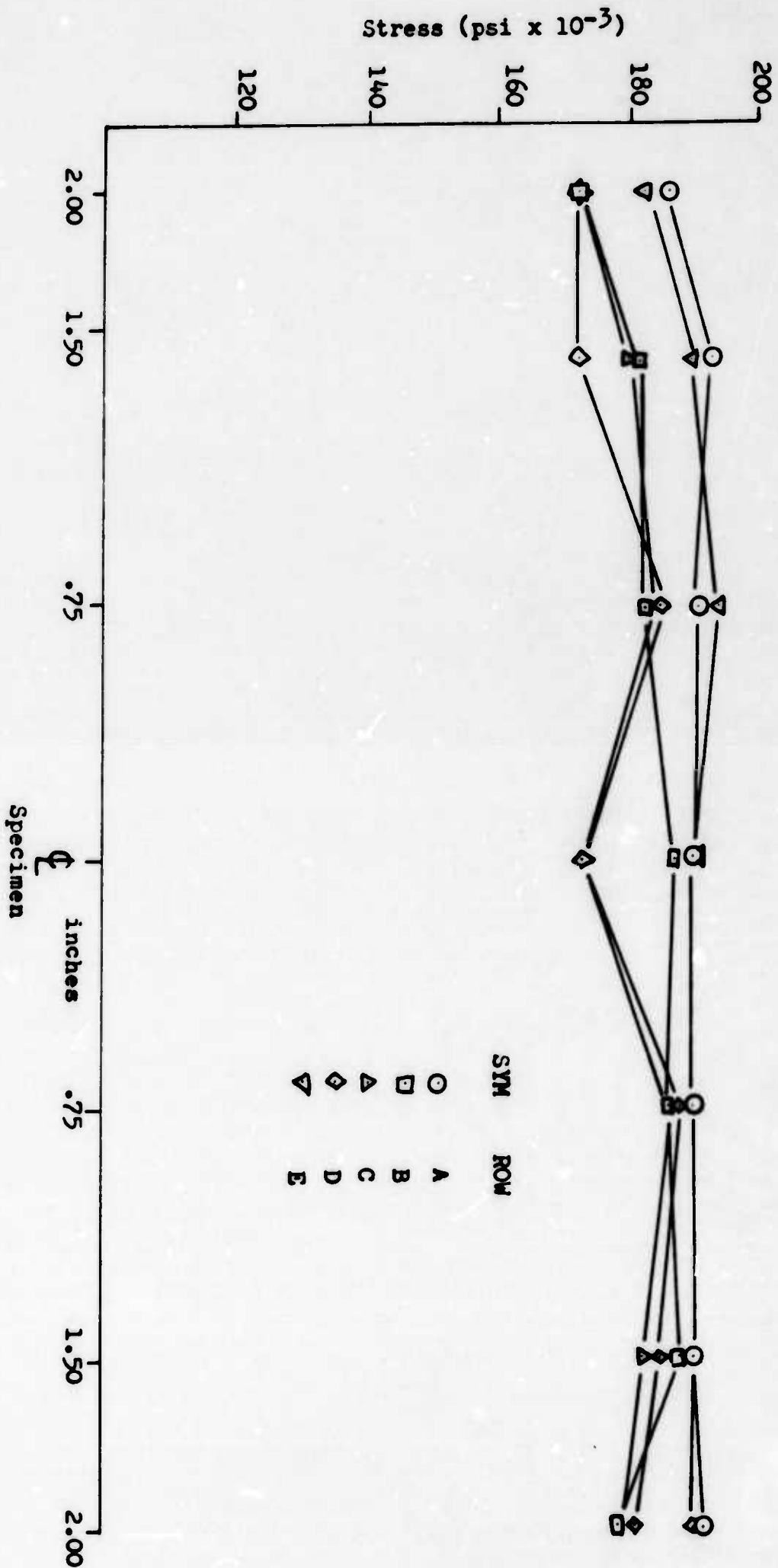


FIGURE 106. Stress Distribution Parallel to the Longitudinal Axis of the U-Bend Specimen. Symbols Refer to Locations Shown in Figure 105.

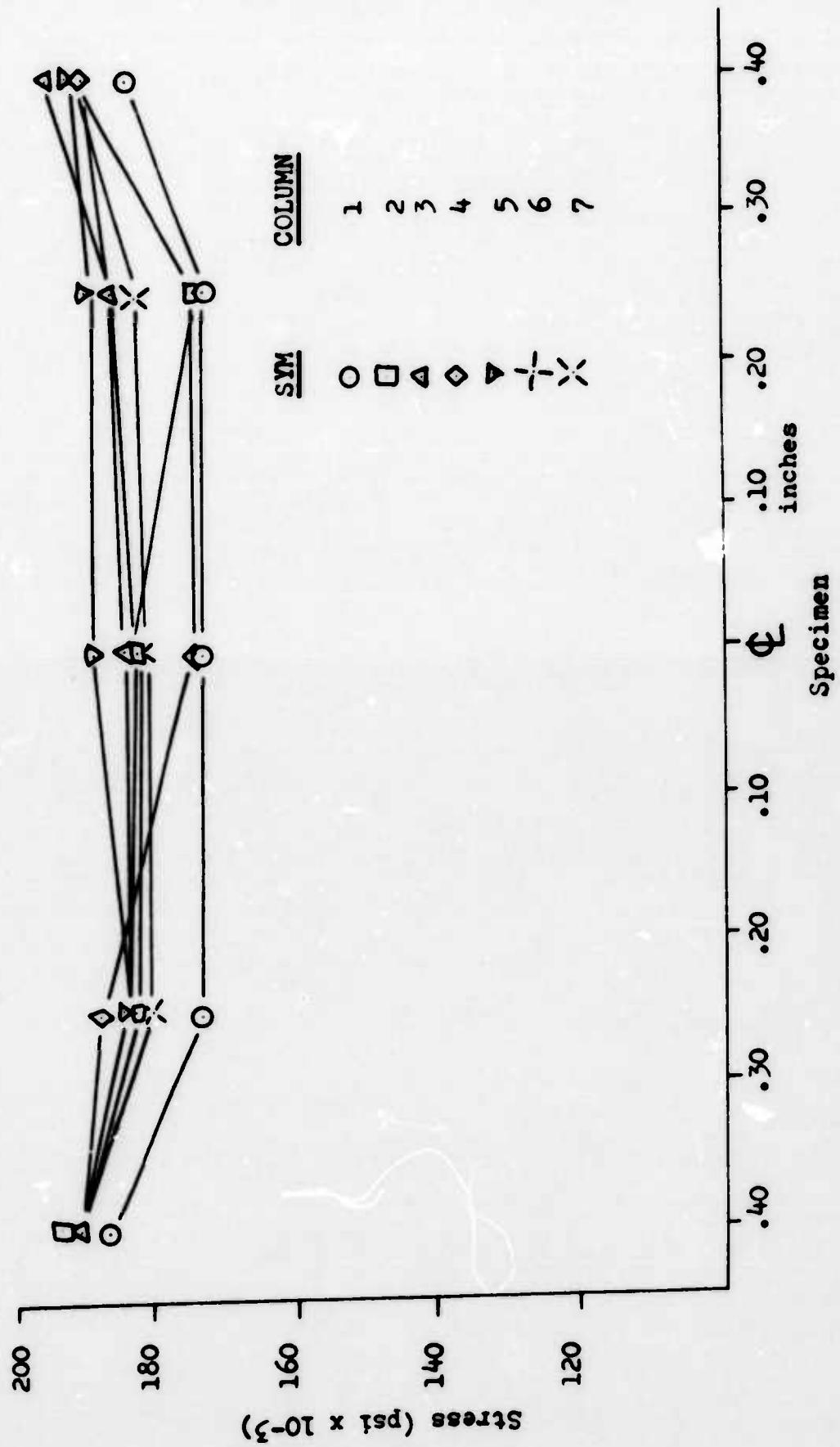


FIGURE 107. Stress Distribution Transverse to the Longitudinal Axis of the U-Bend Specimen. Symbols Refer to Locations Shown in Figure 105.

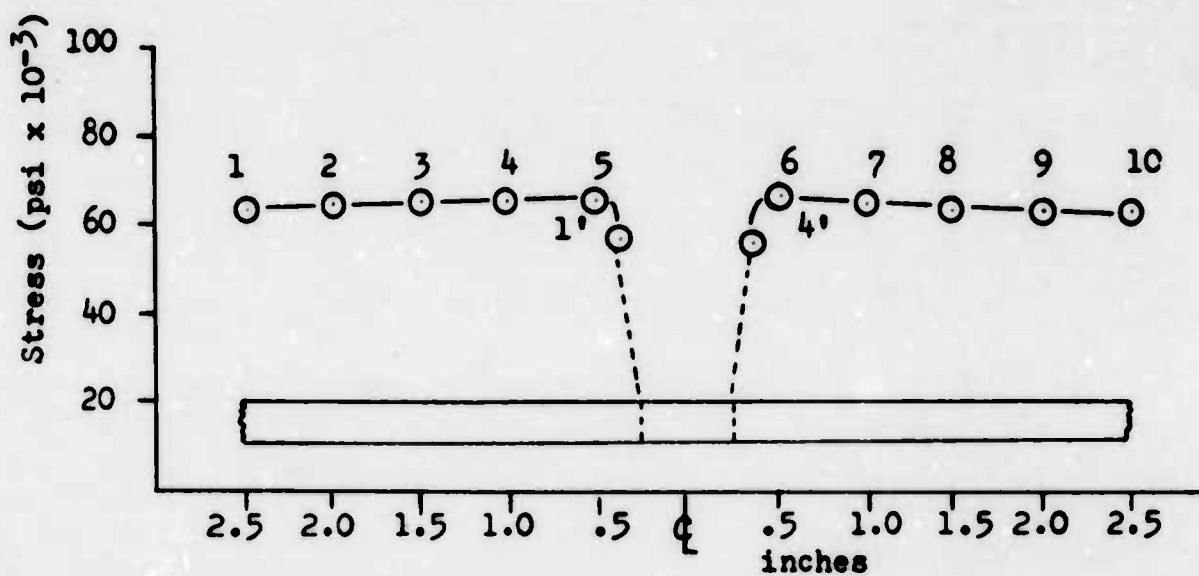


FIGURE 108

Stress Variation Parallel to the Longitudinal Axis of U-Bend Specimen with Center Hole. Numbers Refer to Locations Given in Figure 105

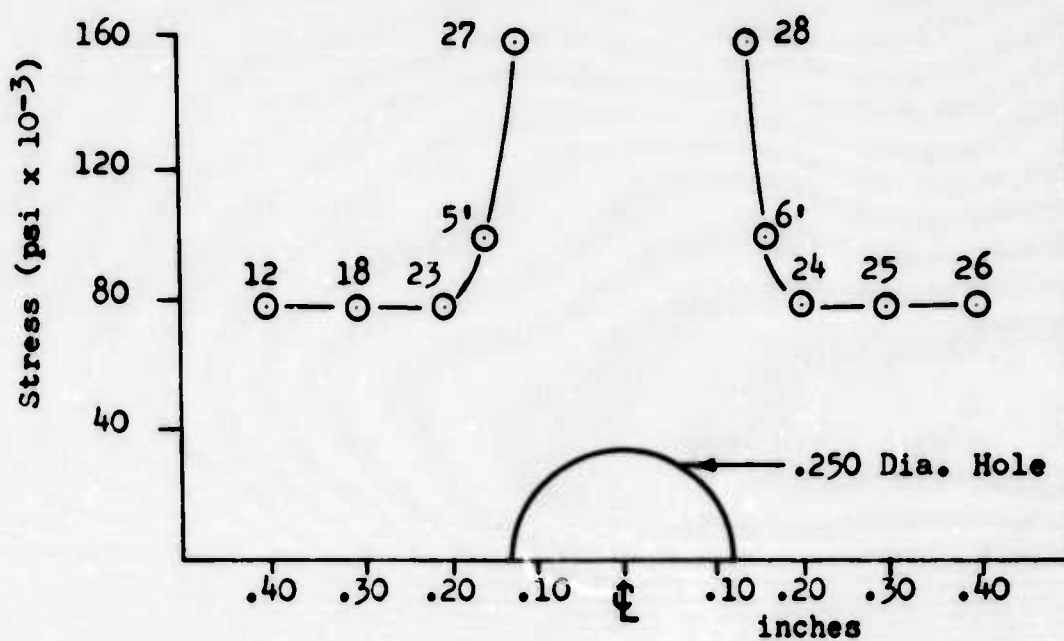


FIGURE 109

Stress Variation Transverse to Longitudinal Axis of U-Bend Specimen with Center Hole. Numbers Refer to Locations Given in Figure 105.

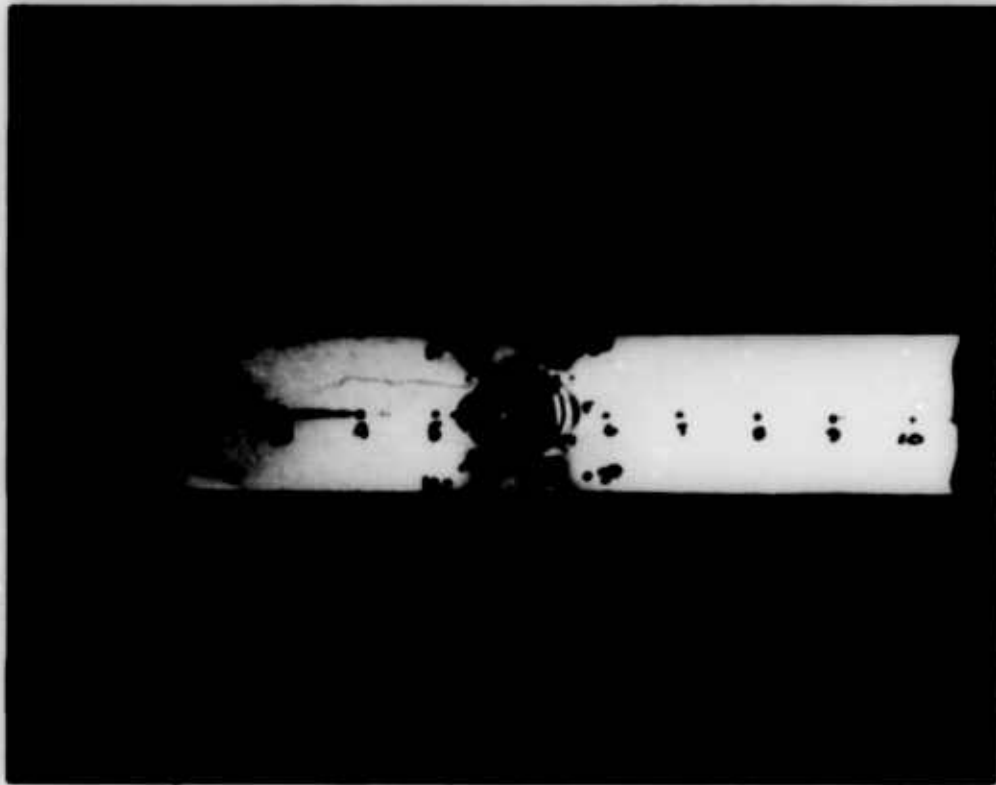


FIGURE 110

Stress Distribution in Stressed U-Bend Specimen with Bolt Through the Center Hole. Photograph of Photostress with Polarized Light.

6A 40248

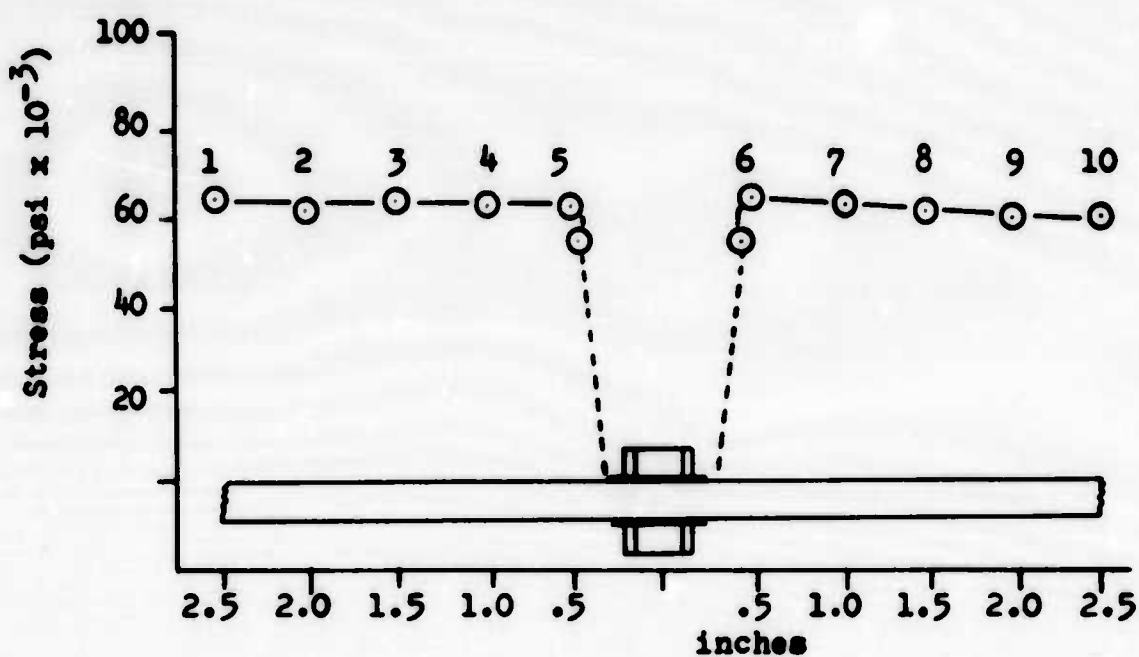


FIGURE 111

Stress Distribution Parallel to Longitudinal Axis of U-Bend Specimen with Bolt Through the Center Hole. Numbered Points Refer to Photostress Reading Locations in Figure 110.

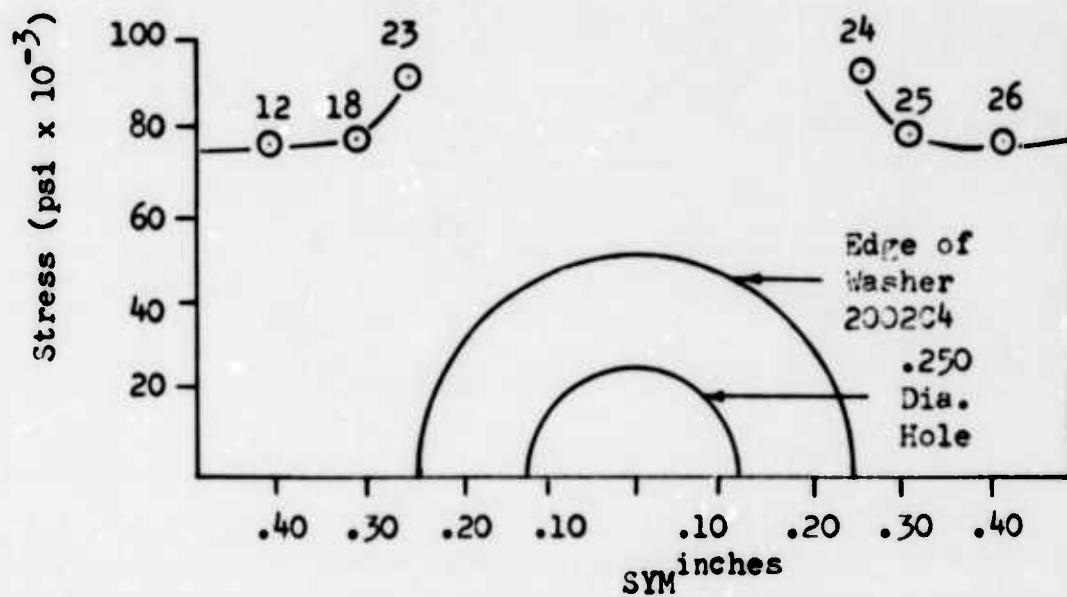


FIGURE 112

Stress Distribution Transverse to the Longitudinal Axis of U-Bend Specimen with Bolt Through Center Hole. Numbered Points Refer to Photostress Reading Locations in Figure 110

APPENDIX II

ROUND NOTCHED TENSILE SPECIMEN

CONFIGURATION

ROUND NOTCHED TENSILE SPECIMEN CONFIGURATION

I. ORIGINAL CONFIGURATION

In many instances fatigue cracks, which act as stress risers, are formed in thick forgings and thick plate materials mainly under conditions of plane strain. These fatigue crack conditions cannot be duplicated by a blunt notch, such as a 0.010" notch radius, because of the amount of plastic deformation required before brittle fracture.

The condition of plane strain can best be approximated by making a very sharp notch in a round notched tensile coupon. In a report by Irwin (1) a notch radius of .0005" was found to satisfy the above requirements. The stress intensity parameter can then be calculated using the relationship:

$$K_{Ic} = 0.233 \sigma_m \sqrt{\pi} D, \text{ where}$$

σ_m = average tensile stress across the net section,

D = net section diameter

K_{Ic} = plane strain stress intensity factor

It has been possible to obtain this notch radius (0.0005") in aluminum alloys but extremely difficult to do so with any consistency in steel alloys. Experimental results indicate that for comparative purposes a notch radius of 0.001" (which was the nominal radius of the majority of U-bend specimens tested in this program) was nearly as effective as a 0.0005" radius. This indicates that though precise tear resistance data cannot be obtained a meaningful comparison could be made relating the notch sensitivity of steels heat treated in different ways.

The dimensions of the notched tensile specimen used in this study, in addition to the nominal notch radius of 0.001", were:

Net section diameter	.250 inch
Gross section diameter	.354 inch
Length between grips	1.25 inch
Total length	2.50 inch

II. MODIFIED CONFIGURATION

After testing of the notched tensile specimens (original configuration) it was noted that much of the data could not be used since the notched tensile ultimate strengths exceeded the smooth tensile yield limit, causing net section yielding. A new notched tensile configuration was designed that would theoretically provide more useful K_{Ic} values.

The dimensions of the new (modified) notched tensile configuration were determined from a consideration of the Irwin formula,

$$K_{Ic} = 0.233 \bar{\sigma}_m \sqrt{\pi D}$$

By rearrangement,

$$D = \frac{K_{Ic}^2}{.054 \bar{\sigma}_m^2 \pi}$$

A value of K_I (60,000 psi in^{-1/2}) was selected that was greater than that calculated using any of the billet notched tensile ultimate strengths. The lowest yield strength (150,000 psi) of any of the billets tested in this program (for which K_{Ic} could not be determined) was substituted for $\bar{\sigma}_m$, the average tensile stress across the net section. Inserting these two values into the formula provided the net section diameter or,

$$D = \frac{(60,000)^2}{.054 (150,000)^2 (3.14)} \approx 1.0 \text{ in.}$$

Since	Area (gross)	=	2 Area _(net)	(2)
	Area (gross)	=	2 (.78)	= 1.56 sq. in.
	Diameter (gross)	=	1.4 in.	

The length between the specimen grips should be at least 5 times the net section diameter or,

$$\text{Length between grips} = (5) (1) = 5 \text{ in.}$$

$$\text{Total length, with grips, } 7.0 \text{ in.}$$

REFERENCES

- (1) G. R. Irwin Crack Toughness Evaluation Using Circumferentially Notched Round Bars, U. S. Naval Research Laboratories, May 1961 Meeting of ASTM Committee on Fracture Testing of High Strength Metallic Materials.
- (2) P. C. Paris Short Course in Fracture Mechanics, Lecture series given in Structures Research Unit, Transport Division, The Boeing Company, Copywrite 1960.

APPENDIX III

THE NATURE OF STRESS CORROSION CRACKING

W. C. Gallagher

**THE BOEING COMPANY
Transport Division
Renton, Washington**

THE NATURE OF STRESS CORROSION CRACKING IN STEELS

1.0 Introduction

Stress corrosion cracking involves the complex interplay of tensile stress, corrosion, and crack-sensitive paths through a metal or alloy. It has been defined as the combined action of static tensile stress and corrosion which leads to the cracking of metals. This definition makes a distinction from the term stress corrosion which is the effect of any state of stress and corrosion(1)*. Many authors do not make this distinction, therefore, both terms will be used with the understanding that only static tensile stresses are considered. Stress corrosion cracking causes a spontaneous failure, normal to applied stress, that results after a definite time interval in which a ductile metal or alloy fails in a brittle manner (2, 3). Tensile stresses (residual or applied) are a basic requirement for promotion of stress corrosion cracking (1, 2, 3, 4, 5, 6, 7, 8, 9, 10, 11, 12). Each metal and alloy has its own particular corrosive environment which initiates cracking by a primarily electrochemical mechanism in the presence of stress (3, 5, 13, 14, 15, 16, 17, 18).

Alloys of steel and titanium have a special embrittling problem which is different from other alloys, i.e., hydrogen embrittlement. The separation between stress corrosion and hydrogen embrittlement in these two alloys systems is a difficult task. Their mechanisms are not known in all cases nor are their identifications clear. Generally, body-centered-structures are the basic requirement for hydrogen embrittlement while there is no definite structure dependence for stress corrosion.

The scope of the survey is limited to the factors of stress corrosion associated with low alloy steels and stainless steels with other alloys mentioned to illustrate a particular point. The majority of work found in the literature has been primarily on austenitic stainless steels which have consequently received the greatest amount of work on checking the effect of experimental variables on stress corrosion. Only a small amount of information was available for low alloy steels and so some of the proposed theories may not be applicable

1.1 Mechanisms of Stress-Corrosion Cracking

The most widely accepted theory of stress corrosion is the electrochemical mechanism based on the phenomena of cathodic protection which is explained in section 3.0. Many feel that a mechanical mechanism is the prime means of stress corrosion cracking. The basic problem in applying a general mechanism is due to the large number of variables, both inherent and experimental, encountered in various systems. In steels there seems to be two modes of thought, (a) basically an electrochemical mechanism with the addition of mechanical aspects and (b) a cooperative action of both the electrochemical and mechanical mechanisms. Van Rooyen (19) has pointed out that the mechanism cannot be purely electrochemical

since there are only a few electrolytes that create stress corrosion susceptibility for a given alloy.

A general description of the mechanisms of stress corrosion cracking was given by Roberts (3) and will be reiterated here for continuity.

"The Electrochemical Theory calls for susceptibility to selective corrosion along more or less continuous paths and a high stress tending to pull the metal apart along these paths. These continuous paths could be along grain boundaries where a precipitated anodic phase, or an anodic depleted zone resulting from precipitation, may exist. Trenching or pitting results, causing stress raisers or notches where cracks begin to form and then propagate because of corrosion and stress at the point of the crack. Differences in potential between the grain boundary area and the grains have been observed. This theory explains the intergranular cracking observed in some systems.

"The Mechanical Theory states briefly that localized corrosion forms the notch or stress raiser; but the propagation of the crack is then caused by mechanical effects and corrosion does not play a continuous role.

"According to the Strain Accelerated Decomposition Theory, an anodic phase is formed because of stress. In other words a site that is not susceptible becomes susceptible because of a phase decomposition or formation caused by stress.

"The Anodic Shift Theory explains the propagation of a crack by stating that when a certain stress concentration is brought about by corrosive attack (pitting or trenching) some plastic deformation takes place and the electrode potential of the metal is shifted in an anodic direction at the crack base because of the latent energy produced by the deformation. The anodic area produced in this manner is attacked and the crack again produces a stress concentration sufficient for plastic behavior. This process can be visualized as a continuous shifting in potential and simultaneous metal removal.

"The Film Theory, another form of the electrochemical theory of corrosion, suggests a different driving force than composition differences. Stress corrosion is started by the usual electrochemical attack, and stress concentration at the base of the incipient crack is propagated by the simultaneous corrosion of the exposed metal and tearing of the film that may form. The fact that potential differences do exist between filmed and film-free metal surfaces has been confirmed many times. In one case the potential at the base of notches in alloys subject to tensile stretching was found to be as much as 0.7 volts anodic to the remainder of the specimen. Attack in these bare areas becomes permanently faster than on the filmed surface and preferential corrosion occurs."

The mechanical theory is related to the dislocation model of fracture which has been pointed out by Evans (22). When the time to failure versus stress was plotted for 18-8 stainless steel, a "knee" exists at approximately 0.1 per cent proof stress with is in the vicinity of the engineering yield point (See Figure 113). If crack growth requires a large number of dislocations, then the effect of stress in the plastic range should be more effective. This is shown in Figure 113.

Whenever stress is applied some plastic deformation always occurs, consequently a number of glide dislocations are produced in a glide system. When barriers are encountered by the dislocations, a pile-up occurs in which two things can happen: (22)

- a. A Frank-Read source can operate to relieve stress concentration and produce a ductile fracture.
- b. The glide dislocations can be converted into cavity dislocations which grow in the form of a crack thereby producing a brittle fracture.

The obstacles in face-centered-cubic material are not as strong as in body-centered-cubic material and therefore cannot alone generate a brittle-type fracture. Consequently the effect of environment on surface energy must be considered (22).

"Cottrell has shown, theoretically, that cracks formed by dislocations coalescence will begin to spread when $\sigma n b \geq 2\gamma$ where σ is the shear stress on a glide plane, n is the number of dislocations in a pile-up of Burgers vector b , and γ is surface energy term. Environmental conditions can sometimes lead to a lowering of γ when the energy of a chemical reaction γ_g can contribute to the propagation of a crack. Thus, if γ_g is large, then γ will be small and the force required to advance a crack may become very small (22)." This is felt by some to be a very important factor in stress corrosion cracking in body-centered-cubic metals.

Nelson (20) has proposed that solid corrosion products deposited within active cracks in steel exert a wedging action which develop lateral tensile forces. When these forces are added to residual and applied stresses, there is sufficient force to cause spontaneous crack propagation by mechanical fracture. This theory does not explain the time dependence of stress corrosion cracking.

1.2 Mode of Cracking

The mode of cracking is either transgranular or intergranular or a composite of both types depending on the physical aspects of the material and the environment. Intergranular corrosion is due mainly to potential differences between differently orientated grains or electrochemical differences at the grain boundaries due to precipitation

or segregation in alloys and in pure metals (9). Transgranular corrosion remains a mystery as to the exact cause; many alloy systems have been investigated but no direct evidence has been initiated to give a general hypothesis for this phenomena. Preist, Beck and Fontana (21) have proposed an electrochemical mechanism for transgranular corrosion in a magnesium base alloy. Cracking occurred along (0001) planes of the hexagonal-close-packed material where an anodic phase preferentially precipitated.

The effect of grain size on the mode of cracking in steel has not been investigated to any great extent. It has been observed in a magnesium-base alloy that specimens of small grain size, furnace cooled from solution temperature, cracked intergranularly. Water quenching of small grain size specimens resulted in transgranular failure. Specimens with grain size larger than ASTM No. 7 failed transgranularly regardless of heat treatment. Preist, et al, (21) also found that the pH of corroding solution had no effect on the mode of cracking.

From the well established correlation of impact tests and embrittlement, it could be possible to predict the mode of failure in steels since grain size affects impact energy values (23). The aspect was not found in the literature.

Lula, Lena and Kiefer (24) looked into the theory of intergranular corrosion of Type 430 stainless steel. They reported that austenite in ferritic stainless steels was not necessary for intergranular corrosion and that titanium stabilization does not prevent intergranular attack. When the carbon content was as low as 0.05 per cent by weight, intergranular corrosion still prevailed. The minimum temperature for intergranular corrosion (sensitizing temperature) was found to be independent of the chromium content. The theory of intergranular corrosion in ferritic stainless steels is therefore based on cooling rate, since slow cooling produces carbide or nitride precipitation in the grain boundaries which causes excess strain in the material. This strained area is anodic resulting in it being preferentially attacked.

Intergranular corrosion in general occurs in aluminum-base alloys, copper-base alloys, carbon and low alloy steels, martensitic straight-chromium stainless steels and PH stainless steels. Transgranular cracking is related to magnesium base alloys and austenitic stainless steels. (25)

1.2.1 Crack Initiation

The times to failure data reported in the literature consists of a crack initiation period followed by propagation period. The induction period corresponds to the probability of crack initiation. It is generally conceived that cracks initiate at pits formed on the surface due to local electrochemical reactions. The probability of pit formation depends on the surface condition which is related to fabrication procedures and internal condition of the material. Pit creations consequently depend on the intersection of the surface with grain boundaries,

sub grain boundaries, dislocations, slip bands and grain boundaries of heterophases along with heterogeneous surface strains (1, 7, 9, 19, 26). Van Rooyen (19) claims that both transgranular and intergranular cracking originate at pits.

Hines and Hoar (7) believe that the probability of crack initiation depends on the amount of exposed bare metal, since, the greater the area, the greater the chance for exposure of regions of proper susceptibility. Uhlig and Sava (10) feel that the probability of crack initiation is related to metallurgical and compositional factors accompanying plastic behavior and low temperature treatments (these variables are discussed in later sections).

Uhlig and Sava exposed 18-8 stainless steel to $MgCl_2$ as did Hoar and Hines; the former pickled the specimens intermittently but with no change in the time to failure with the number of picklings. Consequently, this throws doubt on the role of oxide film in determining the time to failure. They conclude that the induction time consists in the time "for slow plastic deformation to occur and for nitrogen to diffuse to dislocation arrays in the alloy produced by deformation."

A number of investigators have followed the process of stress corrosion cracking through solution potential measurements. The curves of potential versus failure time for steels have a general form (7):

- a. The potential falls when the solution penetrates into pores and cracks and comes in contact with imperfections.
- b. The solution potential rises gradually during the induction period and reaches a peak at the initiation of a crack.
- c. A decrease in potential results as cracking occurs (See Figure 114).

These curves have been used to check the effect of various experimental variables on stress corrosion cracking such as testing temperature, stress, surface oxide films, composition of corroding medium, and microstructure. Discussion of the parameters are in later sections.

Hoar and Hines (7) followed the variation of mechanical properties of 18-8 stainless steel with exposure time in a $MgCl_2$ solution. During the induction period the ultimate tensile stress did not vary while the elongation revealed an initial decrease followed by no variation. The induction period is influenced by environment, temperature, stress and amount of plastic deformation. The low stress required for failure after long induction periods is described as having stress raisers becoming more effective with time or more stress raisers developing with time. Cold working increases the number of imperfections and practically eliminate the induction period. The testing temperature is directly related to the induction period, i.e., the higher the temperature the

shorter the induction period. The temperature dependence is greater in the induction period than in the propagation period (7). The composition of the environment determines the reaction rate which in turn affects the induction period.

1.2.2 Crack Propagation

The mechanism of crack propagation in steels is very complex and difficult to analyze. Cracking has always been found to occur normal to the applied tensile stress and propagates at a rate approximately 1 millimeter per hour (7, 19). The manner of cracking in steels has been theorized to fall in one of three groups:

- a. Gradual growth with no detectible jumps in electrochemical potentials or specimen (Dix's theory) (30).
- b. Growth in alternating slow and relatively rapid steps with discontinuous drops in potential (Logan's theory) (27).
- c. Cracking in steps of instantaneous mechanical failures alternating with a slow stage. Characterized by sudden negative jumps in potential and acoustical sounds (proposed by Keating) (31).

Experimental work supports the concept of gradual growth of cracks in stainless steels (7, 19). The cracking in steps over a limited distance of instantaneous mechanical failures alternating with a slow step has also been postulated for stainless steels; this theory can also account for gradual penetration of metals and elimination of cracking by removal of corrosive atmosphere. The high current density required for maintaining stress corrosion cracking in many stainless steels has more or less eliminated the theory of instantaneous jumps. Hoar and Hines (40) have observed discontinuous extension and potential changes in 18-8 stainless steel, but this does not conclusively mean that stress corrosion cracking occurs in this manner for it has been revealed that local yielding of grains can vary, which would give sudden changes. This is found in the stressing of steels without cracks. If the discontinuous theory holds, Dix (30) concludes that the steps must be too small for detection. In most low alloy and stainless steels the growth rate has been considered to be of the gradual form (32).

The susceptible paths that a corrosion crack can follow has been theorized to be dependent on many things for various alloys. One of the most important factors is the distribution and composition of precipitated particles. Austenitic stainless steels have failed transgranularly even when grain boundary precipitation is present and pure metals have failed intergranularly without grain boundary precipitates. The grain boundary precipitation is the predominate factor in determining the mode of stress corrosion cracking in low alloy steels.

C. Edeleanu (32) has shown that in austenitic stainless steels, austenite can transform in a strain induced diffusionless manner to "quasi-martensite" which provides a susceptible path for stress corrosion cracking in hot magnesium chloride solution. Hoar and Hines (28) have concluded that quasi-martensite is important only in the initiation of cracks for they found no preferential cracking along quasi-martensite when it was within the bulk of the material.

P. Lillys and A. E. Nehrenberg (2) investigated the stress corrosion susceptibility of martensitic stainless steels Types 410, 420, 422 and 436. They found that cracks would only propagate intergranularly when a nearly continuous grain boundary network of carbide precipitates existed.

Uhlig and Sava (10) have determined that the crack sensitive paths in stable austenitic stainless steels are formed by the association of nitrides or nitrogen atoms and dislocations. The interstitials form arrays along the dislocations produced by plastic deformation. "The segregated nitrogen atoms mark paths for electrochemical action, or paths for preferred absorption of the environment leading to the reduction of surface energy."

C. Edeleanu and A. J. Forty (33) postulated that cracking in brass which occurs in steps was due to a crack propagating at the rate of approximately one third the speed of sound until a slip band, which has soft material at its interface, was intersected. Fracture was again initiated after an incubation period.

Leu and Helle (34) found that the initiation of cracking of 18-8 steel in $MgCl_2$ was along slip bands. This is in agreement with the concept of increased imperfection density and resulting in preferred concentration of interstitials of such slip bands.

The exact mechanisms by which a crack propagates is still in the experimental stage. The large number of variables in laboratory accelerated tests plus the variables inherent in materials cause a large number of speculations. Generally, the distribution of precipitates determines where a crack will most likely propagate but the detailed explanation of how it propagates is still not fully understood.

2.0 Experimental Variables

The controllable variables in an investigation affect stress corrosion cracking both in effectiveness and degree. The most effective factors are stress, environment, alloy composition and heat treatment. Other factors such as specimen configuration and size, grain size and direction, and testing temperature only change the degree of stress corrosion susceptibility. The following sections present a composite picture of the experimental variables investigated by various authors.

2.1 Specimen Configurations

The possibility of correlating published data is very difficult, partially because of the variety of specimen configurations which cause a difference in the effect of other variables. Some of the types of specimens employed are illustrated in the following:

- a. U-bend specimens used mainly in the testing of billet material.
 - (1) Phelps-Loginow (8), this type utilizes a bending moment and is also used when utilizing sheet material. An analysis of this specimen is in a preceding section of this document.
 - (2) Horseshoe (9), this specimen configuration is used in the testing of cold worked material.
 - (3) Split ring (35), a recent development.
 - (4) Boeing U-bend is also analyzed in a preceding section.
 - (5) Cantilever, *ibid*
- b. Tensile specimens when using thin material such as wire and sheet.
- c. Special specimen configurations for studying particular aspects.
 - (1) Hollow specimen (36), used in high temperature work.
 - (2) Notched specimens (37, 38), used for studying notch sensitivity in stress corrosion tests.

All types have both advantages and disadvantages; usage varies according to the inherent properties of the material and equipment available to the investigator.

The Phelps-Loginow specimen has had the greatest universal acceptance due to its simplicity and ease of mass testing. Its major drawback is the lack of a uniformly stressed area and the problem of producing the desired stress level.

The horseshoe type of configuration is produced by bending flat specimens into a "U" shape, using tension bolts at the open end of the "U" to maintain the applied stress. This type of specimen has an inherent handicap in estimating or measuring the stress caused by the complex stress distribution.

The tensile specimens can be uniformly stressed but are limited because of the size of apparatus needed in stressing the material. The hollow tension specimen designed by Logan (36) has apparently been successfully used with Type 304 stainless steel. It is especially applicable to high temperature testing.

The split ring configuration has only been recently adapted to stress corrosion tests and comparative data is not available (35).

When correlating U-bend and tensile specimens in stress corrosion tests, a factor exists which is extremely difficult to analyze. As stress corrosion occurs, which involves the removal of material, the cross-sectional area decreases. In a tensile specimen of constant load, the stress increases while in a U-bend specimen the bending moment decreases which in turn decreases the load (7).

Small tensile specimens minimize the period for crack propagation to produce fracture and therefore may be a better susceptibility test for various steels, since there is no stress relief. In a U-bend specimen a small crack may exist for a long time before detection (7).

Ault (38) investigated the notch sensitivity of 0.060 AM 350 sheet in the SCT 850 heat treated condition. All the tensile specimens were alternately immersed in 3.5 per cent NaCl at room temperature. The unnotched specimens all failed within 150 hours while the notched specimens were still intact after 800 hours. He concluded that stress raisers do not have a noticeable effect on the stress corrosion susceptibility of AM 350 (SCT 850), of greater importance are the local defects or in homogenities in the material.

Brown (37) has pointed out the misleading concept of stress corrosion susceptibility that can arise because a material is notch sensitive. "For the materials user, rupture of a given material after short exposure appears sufficient for the practical purpose of rejecting the material without distinguishing between stress corrosion and brittle fracture; it should be noted however, that this could sometimes lead to rejection because of extreme notch sensitivity, of material which cracks by stress-corrosion only very slowly and which in other geometries and other stress configurations might not be susceptible to brittle fracture. If the materials user observes absence of cracking in specimens of a given material, this would suffice for tentative acceptance from the standpoint of stress-corrosion cracking although, of course, it says nothing about notch sensitivity."

These two modes of fracture (stress corrosion and brittle failure) are affected differently by heat treatment and alloy composition. Since the metallurgical variables controlling them are not fully understood, the improvement of a given material will be more expedient if one assesses the two properties separately (37).

2.2 Stress Factor

It has been generally accepted that stress corrosion cracking develops after some local plastic deformation has occurred (2, 7, 10, 19, 25, 39, 40, 41); therefore, any tensile stress that is sufficient to cause creep is adequate in time to cause stress corrosion cracking. Also specimens stressed in the elastic range can crack after an induction period (42).

Many authors have published threshold stresses for various alloys. The results are not consistent because of the number of variables and the limit of time of exposure to which the specimens are held. For example, some of the available data are as follows:

<u>Material</u>	<u>Threshold Stress</u>
18-9 and 17-7 Cr - Ni steels (43) annealed condition	38,500 psi
Cold rolled condition (43)	50,000 psi
Fully softened condition (28)	25,000 psi

Logan (39) has observed that the threshold stress was procedure-sensitive when working with a magnesium-base alloy. He also found the strain rate in air after loading had a critical value of $500 \pm 100 \times 10^{-6}/\text{min.}$ below which stress corrosion cracking did not occur. The strain rate increased markedly when the applied stress was greater than the threshold stress (approximately 95-1/2 per cent of the yield strength). A high strain rate involves dislocations escaping at the specimen edges. There was no change in the strain rate after the corrodant was added.

Because of the many variables which have not been completely evaluated, it has been suggested that establishing any threshold stress values is not practical at this time (44).

Several researchers have said that stress plays a minor role in stress corrosion cracking; its major effect occurs during the crack propagation period (7, 9, 19). The primary effect of stress during the induction period is to provide localized corrosion centers, i.e., anodic sites. The stress has a two-fold purpose during this period according to those who concur on the Film Theory. First the stress can cause dislocation pile-ups at the surface and increase the stress concentrations at inclusion, grain boundaries, etc.; secondly, the stress ruptures the film by producing comparatively small amounts of plastic deformation of the underlying material (27). Others believe that only the first effect is applicable to the stress factor (10).

During the crack propagation period the stress is the factor which tends to tear the metal apart and finally produce catastrophic failure.

Hoar and Hines (7) expresses the effect of stress as follows:

"Increase in stress has little influence on the preliminary corrosion process except slightly to increase the corrosion currents throughout, probably through cracks produced in the surface oxide film by mechanical strain and through a small stimulation of anodic electrode process proper. High applied stress shortens the induction period before the rapid potential fall, the form of the potential time curve before the fall being unaltered. Crack propagation begins before film-breakdown conditions have been established. This means that at high applied stresses only a very small amount of attack at the metal surface that occurs during the film-repair process is sufficient to initiate cracking.

"At lower stresses, film-breakdown conditions become established before crack propagation starts and a period of steady potential occurs between the maximum and the final potential fall. The decrease in stress has no effect on the period of film-repair and only a slight effect on duration and extent of rapid potential fall (crack propagation), but is associated with a considerable increase of steady potential. The low stress requires a relatively large attack after film-breakdown for crack initiation."

The mechanism by which a crack propagates is based on stress inducing a phase transformation. William (1) and Hoar and Hines (7) conclude that stress can create a sensitive path after the film is ruptured by forming surface pits. The resulting stress concentration develops another phase which is anodic to the matrix and can thus cause more corrosion which increases the stress concentration. The cycle is then repeated.

Logan's (26) work on Type 304 stainless steel using $\text{NaCl} - \text{K}_2\text{CrO}_4$ corroding medium enhances Hoar and Hines observations of a cathodic layer along the sides of cracks. Logan found "copious quantities of gas (probably hydrogen) escaping from stress corrosion cracks" which indicates that cathodes were located primarily along crack sides.

2.2.1 Internal Stress

Before any reliability is placed on threshold stress values one must consider the internal stress of the material. The general term "stress" in stress corrosion cracking refers to the total stress acting at the time of failure, i.e., summation of applied and internal stress. Internal stresses or strains cannot be directly measured with a great amount of assurance. The production of internal strain is through any inhomogenities in the material, phase transformations, compositional or thermal gradients and plastic deformation.

The volume change associated with a phase transformation creates internal strains; the amount depends on the type of bounding between matrix and precipitates phase, i.e., coherent, semicoherent and noncoherent. This aspect is related to precipitate hardenable steels and should require more consideration with respect to susceptibility to stress corrosion cracking.

Thermal gradients are not of great concern since most tests are under constant temperature conditions. If an extensive thermal gradient occurred during the fabrication of the material, this could result in a compositional gradient.

Compositional gradients are a major problem not only from the internal strain standpoint but from mechanical properties and reactivity viewpoint. A susceptibility test can give erroneous results because of variation of reactivity within a sample and also inhomogeneity of notch sensitivity. Dislocations and imperfections can add to the problem of compositional gradients.

A major contribution to internal strain is cold working which creates a highly imperfect structure. Normally stress corrosion cracking increases with the amount of cold working since the increase in internal stress is additive to the applied stress. Severely cold rolled iron in its pure state has the same stress corrosion susceptibility as annealed iron but if carbon or nitrogen are added, the susceptibility of cold rolled iron greatly increases (10). Consequently, the compositional gradient produced by the dislocation is the critical factor.

The investigation of the effect of cold working on fully softened 18-8 type stainless steel by Hoar and Hines (28) has shown that " - - failures are unlikely in heavily cold-worked material at applied stresses less than one-half of 0.1 per cent proof stress. With intermediate amounts of cold work the situation is more complex. The best interpretation of all the data is probably that the stress S_c - which corresponds very roughly to an apparent threshold stress - falls and then rises with increasing amounts of cold work; with some compositions, e.g., those with a pronounced duplex structure in the fully softened condition, or those that form large quantities of quasi-martensite on slight straining, it may decrease sufficiently with quite small amounts of cold work for fracture at zero applied stress to occur." Perryman (45) has pointed out that materials become saturated with dislocations at 20 per cent deformation with no change until 80 per cent deformation is reached. Consequently, stress corrosion susceptibility could be increased by compositional gradients associated with dislocations up to 20 per cent deformation and with greater amounts of cold work the dislocation pile-ups and interactions, i.e., work hardening, could decrease the susceptibility because of a decrease in notch sensitivity.

The internal strains produced during heat treatment have a very noticeable effect on the stress corrosion susceptibility in steels. Many authors have noted failures with zero applied stresses. Bloom (9)

checked the effect of martempering (low quenching stresses) vs oil quenching of various martensitic stainless steels. Types 410 and 431 cracked when exposed to 1/2 per cent H_2SO_4 - 6 per cent NaCl - H_2S after oil quenching but specimens martempered at 600°F in a salt bath resisted fracturing. Type 440A did not fail by either heat treating process.

The effect of stress on the specimen potentials makes both ferrous and non-ferrous material slightly less noble (more anodic) and it increases to lesser nobility with increasing stress. The minimum of nobility occurs at the yield point (5, 7).

2.3 Environment

Every alloy has a maximum stress corrosion susceptibility in a particular environment. This environment produces the greatest amount of pitting corrosion in the absence of stress over a long period of time. A corrosive medium which gives a high rate of general corrosion is not usually very good for stress corrosion (3). The number of electrolytes that cause susceptibility are very limited for every alloy.

The composition or degree of purity of the corrosive medium plays a significant role in stress corrosion. Steels are most susceptible in chloride solutions in which MgCl_2 or NaCl are the principle compounds. The addition of an acid reduces the time to failure as shown by Hoar and Hines (7) and Van Rooyen (19). This is due primarily to a decrease in induction time caused by rapid film breakdown, also the specimen potential in the acid solution was more noble than in the non-acid solution.

If 3 per cent MgNO_3 is added to boiling MgCl_2 solution the nucleation rate of crack formation in Type 304 stainless steel is decreased while the rate of crack propagation is increased. The results have not been completely analyzed and so explanations are not explicit (46). Indications are that the induction period is affected more by the testing temperature than by the composition of the MgCl_2 solution. The reason for the greater rate of crack propagation is most likely caused by the effect of increased reactivity or surface energy lowering by the nitrate ions along crack sides or with dislocations.

The form of cracking of austenitic stainless steels varies with the type of chloride solution used (12). Transgranular failure occurred in 18-8 stainless steel when exposed to both chloride and caustic alkali solutions. High temperature testing using NaCl and KOH caused intergranular failures (47). The effect of solution composition on the mode of cracking in other materials is illustrated in Table LX.

The PH of a 3 per cent NaCl solution saturated with oxygen affects the stress corrosion susceptibility of 12MoV steel as follows (16):

- a. At pH 1 stress corrosion cracking occurred relatively rapidly with the evolution of hydrogen. Failure times increased as pH changed from 3 to 11. At pH 11.5 or greater there was no stress corrosion cracking.
- b. Anodic polarization of specimens caused stress corrosion cracking at pH 1, 6.5 and 12.5.
- c. Cathodic polarization at relatively high current densities caused hydrogen embrittlement at pH 1, 6.5 and 12.5.
- d. Without applied current at pH 6.5 the mechanism of failure was stress corrosion.
- e. Without applied current at pH 1 the mechanism of failure could be either stress corrosion or hydrogen embrittlement.

Many stress corrosion tests are performed in atmospheric environments. The variables which affected the amount of corrosion were temperature, relative humidity, temperature fluxations, moisture condensation, drying of moisture films and solar radiation (48, 49). The atmospheric conditions have varied from marine, semi-industrial to industrial environments.

Logan (26) has observed that most weather-exposure specimens failed during or just after rainfall. His explanation is that the collected water "dissolves the oxide film over some areas which allows the escape of block dislocations. This allows slip on certain microscopic areas and microscopic extension at a sufficiently high rate to initiate stress corrosion cracking in the rainwater solution."

There is apparently no known case of stress corrosion cracking in an aqueous medium which cannot be arrested by stopping the corrosion reaction (19).

2.4 Heat Treatment and Microstructure

The tempering temperature controls the microstructure which in turn affects the stress corrosion susceptibility. A general trend has been observed that extreme high tempering temperatures for most steels have relatively high resistance to stress corrosion in chloride solutions. Phelps and Loginow (8) tested 12 MoV stainless steel and Airsteel X200. They performed both weather-exposure at Kure Beach and laboratory accelerated tests. The 12 MoV was most susceptible at 800° - 900°F tempering temperature range for the lab tests. When it was tempered in 400° - 600°F range no failure occurred in the lab but failures were reported in 40 days in the atmosphere at Kure Beach. The difference was explained as being due to the type of exposure, one was complete immersion and the other was rain droplets. The atmospheric

test also showed that the presence of untempered martensite did not change the susceptibility of the specimens tempered in the 400° - 600°F range. Airsteel X200 was reported to have maximum resistance in the 1100° - 1200°F tempering range while in the atmosphere the specimens showed complete resistance in range of 400° - 1100°F.

Lillys and Nehremberg (2) investigated martensitic stainless steels such as 410, 420, 422 and 436. They found these steels to be most susceptible after tempering at 900°F (50), while specimens in the as-quenched condition, those tempered at 700°F or less and those tempered at 1100°F or higher, did not fail in 75 days. Failures were predominantly intergranular in the tempering range of 950° - 1100°F. These steels revealed carbides precipitated in the prior austenitic grain boundaries after tempering at 850°F. Intergranular failure occurred only when there was a nearly continuous network of carbides. When tempered just below the immunity temperature general corrosion occurred along with stress corrosion.

It was also noted (2) that the presence of 5 to 10 per cent ferrite minimized the stress corrosion susceptibility. Types 422 and 436 were not as sensitive to the protective effect of delta ferrite as Type 410. Types 410 and 420, the latter containing no delta ferrite, failed after tempering in the range of 800° to 1000°F. With the presence of 5 to 10 per cent delta ferrite in Type 410, failure only occurred after tempering at 900°F with the time to failure being much greater. This increased time delay is explained on the basis that delta ferrite interrupts crack propagation, observing that a crack changed direction when it approached a grain of delta ferrite. This would most likely affect the rate of crack propagation.

Bloom (9) investigated the immunity tempering temperature for stainless steels Type 410 and 431 after quenching from 1800°F. Cracking was prevented in 410 and 431 by tempering above 1050° and 950°F respectively. The difference in tempering is due to the initial stress levels produced during the quench and also the amount of retained austenite which is greater in Type 431.

Trozso and McCartrey (51) investigated the stress corrosion susceptibility of AISI 410 stainless steel in high purity water. They used electron microscopy and x-ray diffraction to study the microstructural effects. They reported that at 650°F temper, corrosion was along continuous networks of untempered martensite in prior austenitic grain boundaries. At a 1175°F temper the network was broken up which increased the resistance to stress corrosion.

The most susceptible heat treat strength for low alloy steels was investigated by Robinson and Uzdarwin (32); they reported data only for Vascojet 1000 in which the ultimate strength heat treat range was 212,000 to 238,000 psi for environments of tap and distilled water, salt water and a high humidity atmosphere. In other environments the ultimate strength level was 242,000 psi.

Welded panels of 4130 were tested by Briggs (15) in which the corrosion was different from welded zones and base metal. A slow cooling rate from the austenite temperature allows more chromium to diffuse to cementite leaving ferrite more anodic. Increasing the cooling rate increases the resistance to corrosion. Riabehinkov, Nikiforova and Akoamove (5) have reported that in cast irons, cementite was cathodic to ferrite and graphite plus pearlite was cathodic to graphite. Kiefer (24) reported that martensite is anodic to ferrite in steels and will thus preferentially corrode when the two constituents are present.

The relation between mode of cracking and microstructure is not a uniform picture for each class of steel. The large number of variables controlling the microstructure along with the variables encountered in the various tests creates a situation that does not permit a simple uniform explanation. In the case of low alloy steels the problem of producing a satisfactorily etched microstructure showing the grain boundary outlines has handicapped metallurgists in observing the microstructural effects. General theories may develop with time.

2.4.1 Aging

The time required for a failure can occur simultaneously with aging time in stainless steel. It has been observed that steels not susceptible to stress corrosion cracking in cold worked or heat treated condition will become susceptible following a 6 month to a year aging at room temperature. Elevated aging temperatures can be used to duplicate the aging effects but caution must be employed so as not to change the mode of cracking by changing the microstructure. Aging generally increases the susceptibility of the material (30).

2.5 Composition of Material

Although every steel alloy has its particular susceptibility for a given corrosive medium, there are some generalities that need consideration. Alloy additions to steel affect the susceptibility of stress corrosion cracking in the following manner (49):

- a. Increased carbon increases susceptibility
- b. Increased chromium decreases susceptibility
- c. Increased nickel decreases susceptibility

Magnesium and low alloy steels have approximately the same resistance in the same solution. Upp, et al (52) experimented with the nickel content in 18 per cent chromium steel, Type 304. They found that the heat treatment for maximum resistance to intergranular corrosion of 18-8 also made Type 430 susceptible to intergranular corrosion. The transition point in nickel content was 2.4 to 3 per cent by weight;

above this percentage, material should be heat treated like austenitic steels and steel of lower percentages should be treated like ferritic steels.

Snowden (47) also has noted similar heat treat behaviors in stainless steels. He reported that under conditions which lead to rapid stress cracking of the austenitic steels, high chromium ferritic alloys are immune to cracking or suffer a much less catastrophic type of attack.

3.0 Stress Corrosion Cracking Prevention

Stress corrosion cracking is a major problem in high strength steel applications. Many situations will not permit using an alternate material; therefore, other means are used such as change in design, elimination of surface tensile stresses, elimination of corrosive attack through use of inhibitors, use of protective layers and application cathodic protection. Redesign and use of inhibitors are applicable in only specific cases.

3.1 Removal of Surface Tensile Stresses

This can be obtained through shot peening, sand blasting and vapor honing. The former is the most effective and is employed to a great extent. The result of shot peening is to produce compressive surface stresses. Suss (53) reported that hardened stainless steel AISI 410 had greater resistance to stress corrosion cracking in high purity water at 300°F after the shot peening operation. Prior to the shot peening the specimens failed within a week while afterwards there were no failures in 8 weeks. He concluded that at 45,000 psi (1/3 yield point of AISI 410) shot peening will eliminate stress corrosion indefinitely and at 60,000 psi only for a definite period.

The effectiveness of shot peening depends on the material, environment, and applied stress. Generally, it increases the resistance to stress corrosion cracking without excessively increasing the cost of a part.

3.2 Coatings

Coatings may or may not delay the time to failure depending on the polarization of the coating. Phelps and Loginow (8) tested 12 MoV steel and a hot-worked die steel type A. After tempering the specimens at 1000°F prior to coating, they were placed in both marine and semi-industrial environments. The delay time was increased in both locations when the coating was anodic to the base material such as zinc-dust dibutyl titanate primers, sprayed aluminum and nickel-cadmium electroplate. The coatings which were cathodic to the underlying steel, i.e., electroplated chromium and electroless nickel on both steels and electroplated nickel on the die steel, did not prevent or delay cracking. One exception occurred in which the cathodic coating of electroless nickel on 12 MoV steel did delay the time to failure.

Many coatings can delay the time to failure of stress corrosion cracking, yet at the same time may induce hydrogen embrittlement as is in the case with some porous cadmium plating. The selection of a proper coating requires a great deal of knowledge about the parameters related to a particular situation or application.

3.3 Cathodic Protection

It is this process through which stress corrosion cracking has been defined as a basically electrochemical mechanism. In all reported tests the application of a cathodic current has stopped the process of stress corrosion cracking except in the very latter part of the cracking period where mechanical failure occurs.

Logan's (26) work with a magnesium alloy demonstrated very clearly that cathodic protection will stop cracking right up to the time of failure. His specimens did not retain the polarization, which is normal; in fact, after release of the protection, the specimens were 400 mv more positive than before the protection was applied. It soon changed to a potential value of 1.5 volts which was the initial value. Many other authors have done similar work producing similar results.

A large cathodic charge can induce hydrogen embrittlement in steels. A big problem that has become evident when working with high strength steels is the separation of stress corrosion cracking and hydrogen embrittlement. The mechanisms are similar which makes it difficult to separate when the two processes are occurring simultaneously.

4.0 Conclusions

There are a few basic points listed below that apply to all stress corrosion cracking mechanisms.

- a. Stress-corrosion cracking is primarily an electrochemical phenomena.
- b. Specific environments are required for each alloy or metal.
- c. Tensile stresses, applied or internal, are required for promotion of stress-corrosion cracking.
- d. Intergranular corrosion occurs only in the presence of a continuous network of an anodic phase at the grain boundary.
- e. The exact effect of many variables is not known.
- f. Stress-corrosion cracking can be stopped with the application of a sacrificial anodic coating or external electric current.
- g. There is no direct method of separating stress-corrosion cracking and hydrogen embrittlement.
- h. There is no known case of stress corrosion cracking in an aqueous medium which cannot be arrested by stopping the corrosion reaction.

TABLE LX

**Corrosives Which Induce Stress Corrosion Cracking
In Certain Metals (54)**

**I Intergranular Cracks
T Transgranular Cracks**

**IT Intergranular and/or
Transgranular Cracks**

<u>Corrosive</u>	<u>+ Steel</u>	<u>xl8-8</u>	<u>Brass</u>	<u>Monel</u>	<u>Titanium</u>
Aluminum Chloride	IT				
Aluminum Sulfate		IT			
Amines			T		
Ammonia (Dilute)			IT		
Ammonium Chloride		IT			
Ammonium Nitrate	I	I	I		
Barium Chloride		IT	T		
Butane + Sulfur Dioxide			T		
Calcium Chloride		IT			
Calcium Nitrate	I				
Chromium Chloride		T			
Cobalt Chloride		T			
Dichlorophenol		T			
Epicklocohydrien		T			
Ethyl Benzene		T			
Ethyl Chloride		IT			
Fatty Acids Containing Chloride		T			
Fluosilicic Acid		T		I	
Hydrogen Chloride	T	T	T*		
Hydrogen Cyanide	T				
Hydroflouric Acid		IT	T*		

<u>Corrosive</u>	<u>+ Steel</u>	<u>xl8-8</u>	<u>Brass</u>	<u>Monel</u>	<u>Titanium</u>
HNO ₃ , HCl, HF Pickling Acids		T			
Lithium Chloride		IT			
Manganese Chloride	IT				
Magnesium Chloride		T			
Mercuric Chloride		IT			
Mercurious Nitrate			IT	IT	
Mercury			IT	IT	
Methyl Chloride (Wet)		T			
Monoethanolamine	IT		T		
Nickel Nitrate	I				
HNO ₃ + Manganese Chloride	I				
Nitric Acid (Red Fuming)					I
Nitric Acid Vapors			T		
Organic Acids & Chlorides		T			
Organic Chlorides		T	I*		
Potassium Chloride		IT			
Potassium Hydroxide	I	T			
Potassium Permanganate	I				
Sodium Aluminate	IT	IT			
Sodium Chloride		T			
Sodium Hydroxide	I	IT			
Sodium Hydroxide + Lead Oxide	I				
NaOH + Manganese Chloride	I				
Sodium Hydroxide + Sodium Nitrate	I				
Sodium Hydroxide + Sodium Silicate	I				

<u>Corrosive</u>	<u>+ Steel</u>	<u>x18-8</u>	<u>Brass</u>	<u>Monel</u>	<u>Titanium</u>
Sodium Nitrate + Manganese Sulfate	I				
Sodium Sulfate		IT			
Steam			Al Bronze Bronze		
Steam Condensate + SppNH ₃	T	I			
Sulfate Liquor**		IT			
Sulfite Liquor		IT			
Sulfurous Acid Cont. Metal Chlorides (100 opm)		IT			
Vinyl Chloride		T			
Zinc Ammonium Chloride		T			
Zinc Chloride		T			

+ (C 0.10 to 0.30
(Mn 0.50 to 0.80
(Si 0.10 min.

x 18-8 refers to type 302, 304, 321
and 347

- Does not crack unless nitrogen compounds are also present.
- ** White liquor containing over 10g/l Na₂S and 30g/lNaOH 350°F and 100 - 150 psi.

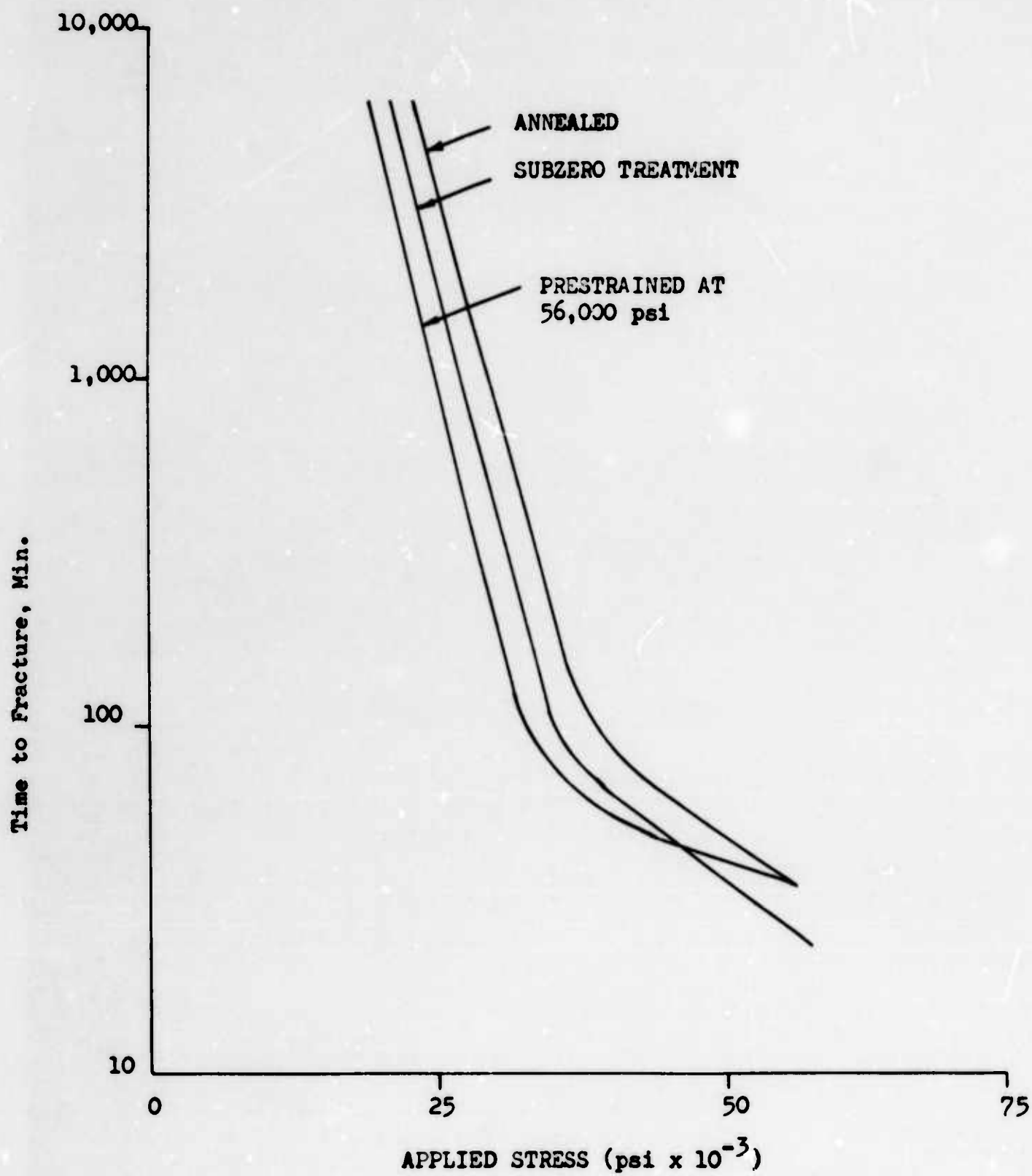


FIGURE 113. Variation of Time to Fracture with Applied Stress for 18-8 Stainless Steel

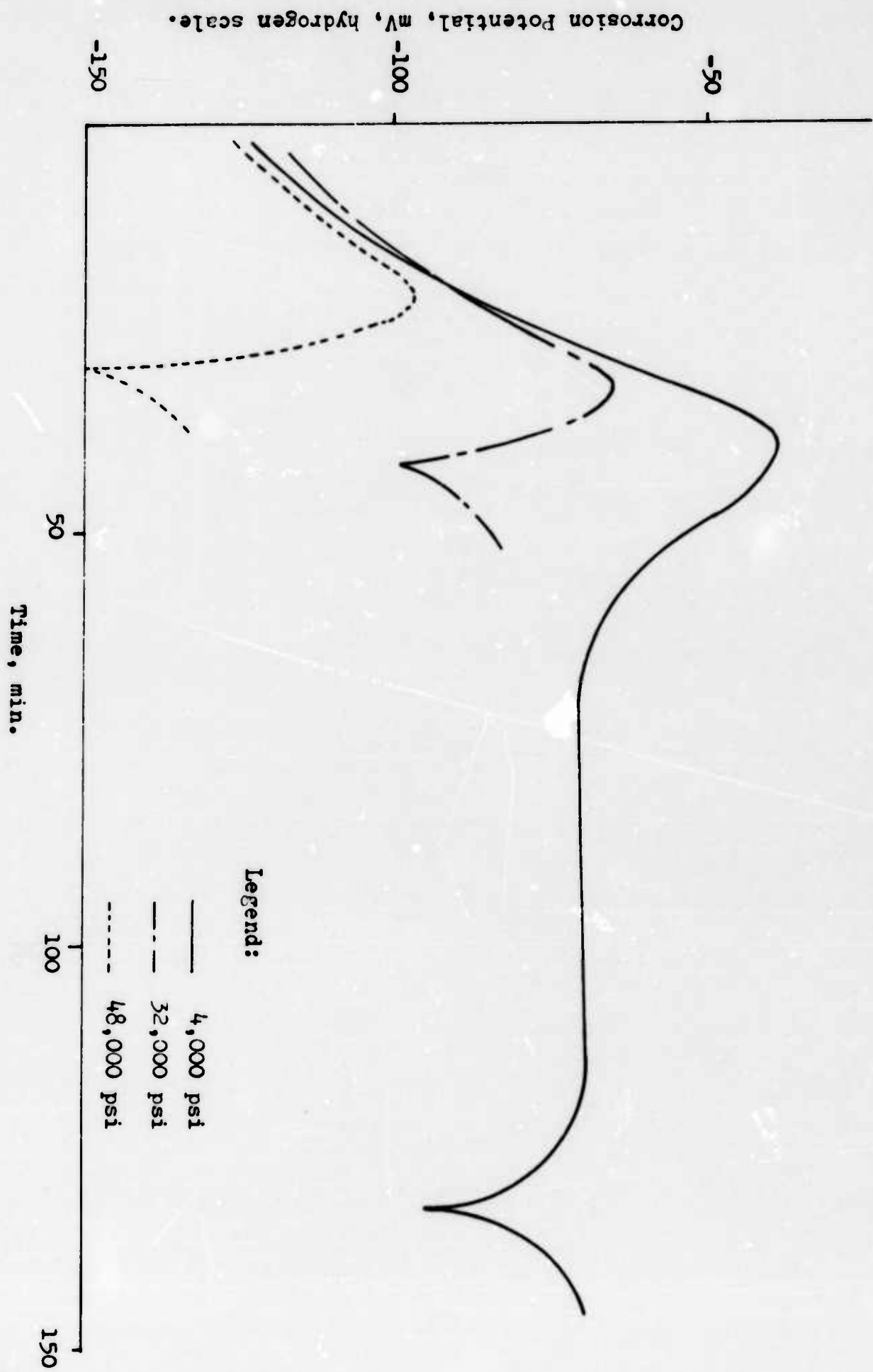


FIGURE 114. Specimen Potential Curves for 18-8 Stainless Steel

REFERENCES

- (1) Williams, W. L., "Stress-Corrosion Cracking--A Review of Current Status," Corrosion, v. 17, July 1961, pp 92.
- (2) Lillys, P. and Nehrenberg, A. E., "Effect of Tempering Temperature on Stress Corrosion Cracking and Hydrogen Embrittlement of Martensitic Steels," ASM Transaction, v. 48, 1956, pp 327.
- (3) Roberts, E. C., "A Review of Stress Corrosion Cracking," Boeing Document D6-7502, Contract AF33(616)-7839, June 30, 1961, Appendix II.
- (4) Schafer, G. J. and Foster, P. K., "The Role of the Metal-Ion Concentration Cell in Crevice Corrosion," Electrochemical Society Journal, v. 106, May 1959, pp 468.
- (5) Riabehinkov, A. V., Nikiforova, V. M. and Akoamova, V. F., "Microchemical Method for Investigating the Corrosion of Metal Under Stress," Industrial Laboratory (Russian), v. 24, February 1959, pp 171.
- (6) Mears, R. B., Brown, R. H. and Dix, E. H. Jr., "A Generalized Theory of Stress-Corrosion of Alloys," Symposium on Stress-Corrosion Cracking of Metals, ASTM - AIME, 1944, pp 323.
- (7) Hoar, T. P. and Hines, J. G., "The Stress-Corrosion Cracking of Austenitic Stainless Steels," Part I - "Mechanism of the Process in Hot Magnesium-Chloride Solutions," J. of the Iron and Steel Institute, v. 176, February 1956, pp 124.
- (8) Phelps, E. H. and Loginow, A. W., "Stress-Corrosion of Steels for Aircraft and Missiles," Corrosion, v. 16, 1960, pp 325t.
- (9) Bloom, F. K., "Stress-Corrosion Cracking of Hardenable Stainless Steels," Corrosion, v. 11, 1955, pp 351t.
- (10) Uhlig, H. H. and Sava, J. P., "Origin of Delay Time in Stress Corrosion Cracking of Austenitic Stainless Steels," M.I.T. Report No. 16-E, Contract No. DA-19-020-ORD-5247.
- (11) Treuting, R. G., "Residual Stress Measurements," ASM Symposium, 1952, Cleveland.
- (12) Edeleanu, C., J. of the Iron and Steel Institute, v. 173, 1953, pp 140.
- (13) Schwerdtfeger, W. J., "Current and Potential Relations for the Cathodic Protection of Steel in Salt Water," Corrosion, v. 14, October 1958, pp 446t.

- (14) Marsh, G. A. and Schasehl, E., "Effect of Dissolved Oxygen on Corrosion and on Cathodic Protection Requirements," Corrosion, v. 13, November 1957, pp 695t.
- (15) Briggs, D. C., MacEwan, J. U. and Yates, H. H., "The Corrosion Behavior of Welded Low Alloy Steel," Corrosion, v. 16, April 1960 pp 141.
- (16) Bhatt, H. J. and Phelps, E. H., "Effect of Solution pH on the Mechanism of Stress-Corrosion Cracking of Martensitic Stainless Steel," Corrosion, v. 17, September 1961, pp 98.
- (17) Fitzgerald-Lee, G., "Sacrificial Corrodibility and the Relative Corrodibility of Metals," Corrosion Technology, v. 6, August 1959, pp 245.
- (18) Gilbert, P. T. and Hadden, S. E., "A Theory of the Mechanism of Stress Corrosion in Aluminum -7% Manganese Alloy," J. of the Institute of Metals, v. 77, 1950, pp 237.
- (19) Van Rooyen, D., "Qualitative Mechanism of Stress Corrosion Cracking of Austenitic Stainless Steels," Corrosion, v. 16, 1960, pp 421t.
- (20) "Physical Metallurgy of Stress Corrosion Fracture," Edited by Thor N. Rhodin, Interscience Publishers, New York, 1959.
- (21) Preist, D. K., Beck, F. H. and Fontana, M. G., "Stress-Corrosion Mechanism in a Magnesium-base Alloy," ASM Transactions, v. 47, 1955 pp 473.
- (22) Evans, U. R., "A Mechanism for Stress Corrosion Embrittlement," Final Report No. ARF 2152-18, Contract No. Nonr-2602(00), 1961.
- (23) Mardirosian, M. M., "Metallurgical Evaluation of Ultrahigh-Strength Vacuum-Melted and Air-Melted Steel Tubular Extrusions," Technical Report No. WAL TR 320.2/1, November 1961, Watertown Arsenal.
- (24) Lula, R. A., Lena, A. J., and Kiefer, G. C., "Intergranular Corrosion of Ferritic Stainless Steels," ASM Transactions, v. 46, 1954, pp 197.
- (25) Slunder, C. J. and Boyd, W. K., "Environmental and Metallurgical Factors of Stress-Corrosion Cracking in High Strength Steels," D'IC Report 151, April 14, 1961.
- (26) Logan, H. L., "Mechanism of Stress-Corrosion Cracking in AZ31B Magnesium Alloy," J. of Research of the National Bureau of Standards, v. 16, No. 6, December 1958, Research Paper 2919, pp 503.
- (27) Logan, H. L., "Film-Rupture Mechanism of Stress-Corrosion," J. of Research of the National Bureau of Standards, v. 48, No.2, February 1952, Research Paper 2291, pp 99.

- (28) Hoar, T. P. and Hines J. G., "The Stress-Corrosion Cracking of Austenitic Stainless Steels." Part II - "Fully Softened, Strain-Hardened and Refrigerated Material," J. of the Iron and Steel Institute, v. 176, October 1956, pp 166.
- (29) Van Rooyen, D., "Stress Corrosion Cracking," J. of the Electrochemical Society, August 1960.
- (30) Dix, E. H., "Acceleration of the Rate of Corrosion by High Constant Stresses," AIME Transactions, IMD Lecture, v. 137, 1940, pp 11.
- (31) Keating, F. H., "Symposium on Internal Stresses in Metals and Alloys," J. of the Institute of Metals, London, 1948, pp 311.
- (32) Robinson, R. B. and Uzdarwin, R. J., "Stress-Corrosion Cracking of High-Strength Alloys," Report No. 2092, Contract DA-04-495-CRD-3069, Aerojet General Corporation, June 30, 1961.
- (33) Edeleanu, C. and Forty, A. J., "Some Observations on the Stress-Corrosion Cracking of Brass and Similar Alloys," Philosophical Magazine, October 1960, pp 1029.
- (34) Leu, K. and Helle, J., Corrosion, v. 14, 1958, pp 59.
- (35) Savage, C. H., "Verification of Test Procedure for Evaluation of Stress-Corrosion of Ph Semi-Austenitic Steels," ARTC 10-59 Project, Report No. TM-346-311, 1962.
- (36) Logan, H. L., "A Specimen for Use in Investigating the Stress-Corrosion Cracking of Metals at Elevated Temperatures," Materials Research and Standards, February 1962, pp 98.
- (37) Brown, B. F., "Notch Sensitivity Effects in Stress-Corrosion and Hydrogen Embrittlement Tests on High Strength Steels," Corrosion, v. 15, August 1959.
- (38) Ault, R. T., "Stress-Corrosion of Notched and Unnotched AM 350 Alloy," Progress Report for September - December 1959, WADD TR: 60-95.
- (39) Mears, R. B., "The Ubiquity of Localized Corrosion," Electrochemical Society Journal, v. 106, May 1959, pp 467.
- (40) Slunder, C. J., "Stress-Corrosion Cracking of High-Strength Stainless Steels in Atmospheric Environments," DMIC Report 158, September 15, 1961.
- (41) Graf, L., "The Investigation of Stress Corrosion Susceptibility of Homogeneous Alloys," Ministry of Supply, Thames House, Millbank, London, SW1, June 1947.
- (42) Uhlig, H. and White, A., "Austenitic Cr-Fe-Ni Alloys Resistant to Stress Corrosion Cracking in Magnesium Chloride," Acta Metallurgica, v. 5, August 1957, pp 473.

- (43) Copson, H. R., "The Influence of Corrosion on Cracking of Pressure Vessels," Corrosion, v. 10, 1954, pp 124.
- (44) Suss, H., "Practicality of Establishing Threshold Values to Eliminate Stress Corrosion Failures in Metals and Alloys," Corrosion, v. 17, February 1961, pp 83.
- (45) Perryman, E. C. W., "Observations on the Structural Changes Accompany Recovery in Super Purity Aluminum," Acta Metallurgica, v. 2, January 1954, pp 26.
- (46) Eckel, J. F., "Relation of Nitrogen to Stress-Corrosion Cracking," Virginia Polytechnic Institute, Troy, N. Y.; Summary Reports on Current Research Projects, Project No. 5, Corrosion Research Council, New York, N. Y.
- (47) Snowden, P. P., "Comparative Stress Corrosion Behavior of Some High-Alloy Steels," J. of the Iron and Steel Institute, v. 181, February 1961, pp 136
- (48) Copson, H. R., "Design and Interpretation of Atmospheric Corrosion Tests," Corrosion, v. 15, October 1959, pp 533t.
- (49) Babakov, A. A. and Tufanov, D. G., "Corrosion of Steels Under Atmospheric Conditions," J. of Applied Chemistry of the U.S.S.R. (Translation), v. 33, No. 6, June 1960.
- (50) "Developments in Stainless Steel," Mechanical World, June 1961.
- (51) Trozzo, P. S. and McCartney, R. F., "The Relationship of Microstructure and Stress Corrosion Cracking of Type 410 Stainless Steel," Corrosion, v. 16, March 1960, pp 26.
- (52) Upp, J. R., Beck, F. H. and Fontana, M. G., "Influence of Nickel on Intergranular Corrosion of 18% Chromium Steels," RF Project 682, Technical Report No. 3, Contract Nonr-495-(11), Ohio State University Research Foundation, July 23, 1958.
- (53) Suss, H., "Shot Peening for Protection Against Stress Corrosion Cracking," Report KAPL-M-HOS-9, Knolls Atomic Power Laboratory, General Electric Company, September 1959.
- (54) From Corrosion Data Survey, Shell Development Company, 1960 ed.

<p>Aeronautical Systems Division Dir/Materials and Processes, Applications Lab, Wright-Patterson AFB, Ohio.</p> <p>Rpt No. ASD-TDR-62-876. INVESTIGATION OF SUSCEPTIBILITY OF HIGH STRENGTH MARTENSITIC STEEL ALLOYS TO STRESS CORROSION. Final report, Sept. 62, 205p. incl illus., tables, 54 refs.</p> <p>Unclassified Report</p> <p>The stress corrosion cracking susceptibility of several high strength steels has been evaluated by alternate immersion testing in a 3.5 per cent salt solution. The variables studied were material, grain direction, heat treatment, stress level, surface preparation,</p>	<ol style="list-style-type: none"> 1. High strength martensitic steels 2. Stress corrosion I. AFSC Project 7381, Task 738103 II. Contract AF 33 (616) 7839 III. The Boeing Co. Renton, Wash. IV. Gary A. Dreyer V. Avail fr CTS VI. In ASTIA collection 	<p>Aeronautical Systems Division Dir/Materials and Processes, Applications Lab, Wright-Patterson AFB, Ohio</p> <p>Rpt No. ASD-TDR-62-876. INVESTIGATION OF SUSCEPTIBILITY OF HIGH STRENGTH MARTENSITIC STEEL ALLOYS TO STRESS CORROSION. Final report, Sept. 62, 205p. incl illus., tables, 54 refs.</p> <p>Unclassified Report</p> <p>The stress corrosion cracking susceptibility of several high strength steels has been evaluated by alternate immersion testing in a 3.5 per cent salt solution. The variables studied were material, grain direction, heat treatment, stress level, surface preparation,</p>	<ol style="list-style-type: none"> 1. High strength martensitic steels 2. Stress corrosion I. AFSC Project 7381, Task 738103 II. Contract AF 33 (616) 7839 III. The Boeing Co. Renton, Wash. IV. Gary A. Dreyer V. Avail fr CTS VI. In ASTIA collection
<p>protective coatings and variations from holes and fasteners. The test materials were 4330M, 4340, 4340M, H-11, AM350, and AM355 steels. Notch tensile testing and x-ray diffraction measurements of residual surface stresses were also carried out.</p>		<p>protective coatings and variations from holes and fasteners. The test materials were 4330M, 4340, 4340M, H-11, AM350, and AM355 steels. Notch tensile testing and x-ray diffraction measurements of residual surface stresses were also carried out.</p>	

<p>Aeronautical Systems Division Dir/Materials and Processes, Applications Lab, Wright-Patterson AFB, Ohio.</p> <p>Rpt No. ASD-TDR-62-876. INVESTIGATION OF SUSCEPTIBILITY OF HIGH STRENGTH MARTENSITIC STEEL ALLOYS TO STRESS CORROSION. Final report, Sept. 62, 203p. incl illus., tables, 54 refs.</p> <p>Unclassified Report</p> <p>The stress corrosion cracking susceptibility of several high strength steels has been evaluated by alternate immersion testing in a 3.5 per cent salt solution. The variables studied were material, grain direction, heat treatment, stress level, surface preparation.</p>	<p>1. High strength martensitic steels</p> <p>2. Stress corrosion</p> <p>I. AFSC Project 7381, Task 738103</p> <p>II. Contract AF 33 (616) 7839</p> <p>III. The Boeing Co. Renton, Wash.</p> <p>IV. Gary A. Dreyer</p> <p>V. Avail fr CTS</p> <p>VI. In ASTIA collection</p>	<p>Aeronautical Systems Division Dir/Materials and Processes, Applications Lab, Wright-Patterson AFB, Ohio</p> <p>Rpt No. ASD-TDR-62-876. INVESTIGATION OF SUSCEPTIBILITY OF HIGH STRENGTH MARTENSITIC STEEL ALLOYS TO STRESS CORROSION. Final report, Sept. 62, 203p. incl illus., tables, 54 refs.</p> <p>Unclassified Report</p> <p>The stress corrosion cracking susceptibility of several high strength steels has been evaluated by alternate immersion testing in a 3.5 per cent salt solution. The variables studied were material, grain direction, heat treatment, stress level, surface preparation.</p>	<p>1. High strength martensitic steels</p> <p>2. Stress corrosion</p> <p>I. AFSC Project 7381, Task 738103</p> <p>II. Contract AF 33 (616) 7839</p> <p>III. The Boeing Co. Renton, Wash.</p> <p>IV. Gary A. Dreyer</p> <p>V. Avail fr CTS</p> <p>VI. In ASTIA collection</p>	<p>protective coatings and variations from holes and fasteners. The test materials were 4330M, 4340, 4340M, H-11, AM350, and AM355 steels. Notch tensile testing and x-ray diffraction measurements of residual surface stresses were also carried out.</p>		
--	--	---	--	---	--	--